University of Southampton

FACULTY OF MEDICINE

Cancer Sciences Unit

Investigating the role of vacuolar-ATPase (V-ATPase) in cancer

by

Bradleigh Whitton

BSc (Hons)

Thesis for the degree of Doctor of Philosophy

September 2019

UNIVERSITY OF SOUTHAMPTON

ABSTRACT

FACULTY OF MEDICINE

Cancer Sciences Unit

Thesis for the degree of Doctor of Philosophy

INVESTIGATING THE ROLE OF VACUOLAR-ATPASE (V-ATPASE) IN CANCER

By Bradleigh Whitton

Overexpression of V-ATPase subunits is linked to cancer cell migration, invasion and metastasis in a number of cancer types including prostate cancer (PCa). Due to expression of androgen receptor (AR) variants, drug resistance is a significant problem in PCa. Various strands of data suggest that the V-ATPase may influence AR function and therefore represents a novel target for which to treat PCa. The central hypothesis addressed in this project is that V-ATPase dysregulation is directly linked to cancer via alterations in activity, and that V-ATPase inhibition influences AR function in prostate cancer.

Somatic missense mutations, glutamine (Q), valine (V) and lysine (K) at glutamate (E) 61 in the human V-ATPase V_1E2 isoform were first identified in the COSMIC database (v81). A V-ATPase ΔE null mutant yeast model was complemented with wild-type or mutant forms of human V_1E1 or E2 subunits to determine whether the mutations altered V-ATPase activity and function. The results indicated that V-ATPase catalytic activity was significantly increased in the V-ATPases with E61 to V and Q substitutions in the V_1E2 subunit compared to the wild-type subunit. The E61Q mutation also substantially increased V-ATPase proton-coupling rate. These results show that cancer-associated V-ATPase mutations can increase enzyme catalytic activity and function.

Inhibition of V-ATPase reduced AR function in wild-type and mutant AR luciferase models. These results were supported by experiments in hormone sensitive PCa cell lines (LNCaP and DuCaP) and mutant AR cell lines (22Rv1 and LNCaP-F877L/T878A), which showed that V-ATPase inhibition reduced AR expression, and expression of AR target genes, at mRNA and protein levels. To investigate the role of individual subunit isoforms, siRNA and CRISPR-Cas9 were used to silence the V_1C1 subunit in LNCaP and 22Rv1 cells. Results showed that transfection with ATP6V1C1 siRNA significantly reduced AR protein levels and function in 22Rv1 cells. Conversely, CRISPR-Cas9 mediated knockout of V_1C1 showed a small increase in AR in both cell lines, which was accompanied by a compensatory increase in protein levels of the alternate V_1C2 isoform. Overall, these results are consistent with the hypothesis that V-ATPase dysregulation is directly linked to cancer via alterations in activity. In particular, this work revealed that somatic mutations identified in tumour samples can increase V-ATPase activity, and that V-ATPase inhibition can reduce AR signalling regardless of mutant AR expression.

Table of Contents

Table of Tables

Table of Figures

Research Thesis: Declaration of Authorship

Print name: BRADLEIGH WHITTON

Title of thesis: INVESTIGATING THE ROLE OF VACUOLAR-ATPASE (V-ATPASE) IN CANCER

I declare that this thesis and the work presented in it are my own and has been generated by me as the result of my own original research.

I confirm that:

1. This work was done wholly or mainly while in candidature for a research degree at this University;
2. Where any part of this thesis has previously been submitted for a degree or any other qualification at this University or any other institution, this has been clearly stated;
3. Where I have consulted the published work of others, this is always clearly attributed;
4. Where I have quoted from the work of others, the source is always given. With the exception of such quotations, this thesis is entirely my own work;
5. I have acknowledged all main sources of help;
6. Where the thesis is based on work done by myself jointly with others, I have made clear exactly what was done by others and what I have contributed myself;
7. Parts of this work have been published as:

Whitton B, Okamoto H, Packham G, Crabb SJ. Vacuolar ATPase as a potential therapeutic target and mediator of treatment resistance in cancer. Cancer Medicine. 2018;7(8):3800-11

Signature: Date:

Acknowledgements

Firstly, I would like to thank my supervisors Prof. Graham Packham, Dr. Simon Crabb and Dr. Haruko Okamoto for their guidance throughout my PhD as well as giving me the opportunity to carry out this research.

Furthermore, I am grateful to members of the Packham, Crabb and Okamoto lab groups (both past and present) for their support throughout my PhD. Particularly to Dr. Sergio Regufe Da Mota for training and mentoring me at the beginning of my PhD.

In addition, I would like to thank Jocelyn Ceraline (University of Strasbourg, France) for the AR-V7, AR-Q641X and AR-F877L expression plasmids, as well as the LNCaP vector only and LNCaP F877L/T878A mutant AR cell lines.

Finally, thank you to The Gerald Kerkut Charitable Trust, Wessex Medical Research and The Urology Foundation for funding this research.

I would like to give special thanks to my friends and family for their support over the past four years. I would especially like to thank my partner, Sarah, for her encouragement and never-ending patience.

A final thank you to my mum, Julie, for her belief in me. Without her support, this PhD would not have been possible.

Definitions and Abbreviations

5-FU	5-Fluorouracil
ADT	Androgen deprivation therapy
AF-1	Activation function-1
AKT (PKB)	Protein kinase B
AMPK	5'-adenosine monophosphate-activated protein kinase
ANOVA	Analysis of variance
APS	Ammonium persulphate
AR	Androgen receptor
ARA	Androgen receptor associated protein
ARE	Androgen response element
ARF	ADP-ribosylation factor
AS	Active surveillance
ATG5	Autophagy related 5
ATM	Ataxia-telangiectasia mutated
ATP	Adenosine tri-phosphate
Baf-a1	Bafilomycin-A1
BMI	Body mass index
BNIP3	BCL2/adenovirus E1B 19 kDa protein-interacting protein 3
BRCA1/2	Breast cancer type 1/2
BSA	Bovine serum albumin
Cas	CRISPR associated protein
cDNA	Complementary DNA
CHEK2	Checkpoint kinase 2
CMV	Cytomegalovirus
CO_2	Carbon dioxide
Con-a	Concanamycin-A
COSMIC	Catalogue Of Somatic Mutations In Cancer
CRISPR	Clustered regularly interspaced short palindromic repeats
CRPC	Castration-resistant prostate cancer
CSS	Charcoal stripped serum
Ct	Cycle threshold

5-FU	5-Fluorouracil
CTLA4	Cytotoxic T-lymphocyte-associated protein 4
Cyclic AMP; cAMP	3’,5’-cyclic adenosine monophosphate
CYP	Cytochrome P-450
DBD	DNA-binding domain
ddH_2O	Double de-ionised water
DHT	Dihydrotestosterone
DMEM	Dulbecco's modified eagle medium
DMOG	Dimethyloxaloylglycine
DMSO	Dimethyl sulfoxide
DNA	Deoxyribonucleic acid
dNTP	Deoxy nucleotide
DRE	Digital rectal examination
DSB	Double-stranded break
EAU	European Association of Urology
EBRT	External beam radiotherapy
ECL	Enzyme linked chemiluminesence
EDTA	Ethylenediaminetetraacetic acid
EGF	Epidermal growth factor
EGTA	Ethylene glycol tetraacetic acid
ERG	ETS-related gene
ERK	Extracellular signal–regulated kinases
ESCC	Oesophageal squamous cell carcinoma
FBS	Fetal bovine serum
FL	Follicular lymphoma
Fz	Frizzled
GAPDH	Glyceraldehyde 3-phosphate dehydrogenase
GFP	Green fluorescent protein
Glu	Glutamic acid
GTP	Guanosine-5’-triphosphate
GWAS	Genome-wide association study
H_2O	Water
HCC	Hepatocellular carcinoma

5-FU	5-Fluorouracil
HDR	Homology directed repair
HER	Human epidermal growth factor receptor
HF	High-Fidelity
HIF-1α	Hypoxia inducible factor 1 alpha
HRG	Histidine rich glycoprotein
HRP	Horse radish peroxidase
Hrs	Hours
HSP	Heat shock protein
IF	Immunofluorescence
IGFR	Insulin-like growth factor receptor
IHC	Immunohistochemistry
IL-6R	Interleukin 6 Receptor
IMRT	intensity-modulated radiation therapy
JAK	Janus kinase
JNK	c-Jun N-terminal kinase
Kb	Kilobase
KDa	Kilodalton
Km	Michaelis-Menten constant
LASS2	Homo sapiens longevity assurance homologue 2 of yeast LAG1
LB	Luria-Bertani
LBD	Ligand-binding domain
LHRH	Luteinizing hormone-releasing hormone
LiAC	Lithium acetate
LN	Lymph node
LNM	Lymph node metastasis
LOH	Loss of heterozygosity
LRP	Low density lipoprotein receptor-related protein
MAPK	Mitogen-activated protein kinase
mCRPC	Metastatic castration-resistant prostate cancer
MEK/MAPKK	Mitogen-activated protein kinase kinase
MES	2-(N-Morpholino)ethanesulfonic acid
Mins	Minutes

5-FU	5-Fluorouracil
MIP	Macrophage Inflammatory Proteins
MLH1	MutL homolog 1
MLV	Murine leukaemia virus
MMP	Matrix metalloproteinase
MMR	Mismatch repair
mRNA	Messenger ribonucleic acid
MSH2	MutS Homolog 2
mTOR	Mechanistic target of rapamycin
NADP	Nicotinamide adenine dinucleotide phosphate
NCID	Notch intracellular cytoplasmic domain
NHEJ	Non-homologous end joining
NSCLC	Non-small cell lung cancer
nt	Nucleotide
NTD	N-Terminal domain
PALB2	Partner and localizer of BRCA2
PAM	Protospacer adjacent motif
PAnIN	Pancreatic intraepithelial neoplasia
PAP	Prostatic acid phosphatase
PARP	Poly (ADP-ribose) polymerase
PBS	Phosphate buffered saline
PCa	Prostate cancer
PCBP	Poly r(C) binding protein
PDAC	Pancreatic ductal adenocarcinoma
PDL-1	Programmed death-ligand 1
PEDF	Pigment epithelium-derived factor
PEG	Polyethylene glycol
Pen/Strep	Penicillin/Streptomycin
Pi	Inorganic phosphate
PI3K	Phosphoinositide 3-kinase
PKA	Protein kinase A
PKC	Protein kinase C
PM	Plasma membrane

5-FU	5-Fluorouracil
PMSF	Phenylmethanesulfonyl fluoride
PRR	Pro-renin receptor
PSA	Prostate specific antigen
PTEN	Phosphatase and tensin homologue
RAC1	Ras-related C3 botulinum toxin substrate 1
RAG	Recombination activating gene
RANKL	Receptor activator of nuclear factor kappa-B ligand
RAVE	Regulator of ATPase of vacuoles and endosomes
RIPA	Radioimmunoprecipitation assay
RNA	Ribonucleic acid
ROS	Reactive oxygen species
RP	Radical prostatectomy
RPM	Rotations per minute
RPMI	Roswell park memorial institute medium
RT-qPCR	Quantitative reverse transcription–polymerase chain reaction
SD	Standard deviation
SDS	Sodium dodecyl sulphate
SDS-PAGE	SDS-polyacrylamide gel electrophoresis
SD-URA	Synthetic defined - uracil
SEM	Standard error of the mean
sgRNA	Single guide RNA
SHBGR	Sex hormone binding globulin receptor
shRNA	Small hairpin RNA
siRNA	Small interfering RNA
SNP	Single nucleotide polymorphism
Src	Steroid receptor co-activator
STAT	Signal transducer and activator of transcription protein
SUMO	Small ubiquitin-like modifier
TCA	Trichloroacetic acid
TCGA	The cancer genome atlas
TE	Tris-EDTA
TEMED	Tetramethylethylenediamine

5-FU	5-Fluorouracil
Tm	Primer melting temperature
TMPRSS2	Transmembrane protease serine 2
TMSG1	Tumour metastasis suppressor gene 1
TR4	Testicular nuclear receptor 4
Tris	Trishydroxymethylaminomethane
Ura	Uracil
UTR	Untranslated region
UV	Ultraviolet
V	Voltz
Vmax	Maximal velocity
WB	Western blot
Wnt	Wingless-type MMTV integration site family member
WT	Wild-type
WW	Watchful waiting
YPD	Yeast extract peptone dextrose
β-ME	β-Mercaptoethanol

Chapter One

Chapter 1 Introduction

Introduction

1.1 Overview

Vacuolar-ATPase (V-ATPase) is a multi-protein complex that catalyses the ATP-dependent transport of protons across intracellular and plasma membranes. The resulting acidification of organelle lumens and the extracellular space influences a diverse range of cellular processes, many of which are dysregulated in cancers (1). One cancer type in which V-ATPase dysregulation has been shown to increase the potential of cancer cell invasion and metastasis is prostate cancer (2). Prostate cancer can progress to an aggressive form known as castrate resistant prostate cancer (CRPC) which currently has no treatments with curative intent. Due to the adaptive responses of the cancer cells such as alterations to the androgen receptor, splice variants and alternative signalling pathways, drug resistance is a significant problem. It is essential that either novel targets are found for next generation therapeutics, or new options are provided for existing treatments. V-ATPase may represent an ideal target for which to satisfy both of these criteria.

The overall goal of this thesis was to investigate the role of V-ATPase in cancer. This introduction will therefore provide background information regarding the two key elements of the project; (1) the effect of selected V-ATPase somatic missense mutations on V-ATPase activity and function, and (2) the potential interactions between androgen receptor signalling and V-ATPase in prostate cancer.

1.2 V-ATPase

V-ATPase are large multi-subunit protein complexes involved in a number of intracellular processes including vesicular trafficking, receptor recycling, protein processing and degradation (3, 4). They are also important for pH dependent entry of various viruses like influenza, and bacterial toxins, such as the anthrax toxin, into healthy human cells (4).

Whilst intracellular V-ATPases are ubiquitous, plasma membrane (PM)-localised V-ATPases play more cell specific roles and are overexpressed in specialized acidifying cells (5). Misregulation of PM V-ATPases can lead to numerous pathological conditions including osteoporosis, renal distal tubular acidosis, proteinuria and deafness (6-9). They are also localised to the membrane of clear epididymal cells and play a role in sperm storage and maturation (10). More recently, PM V-ATPases have been shown to play a

key role in many types of cancer and have been associated with increased invasive and metastatic potential (11).

1.2.1 Structure and mechanism

The mammalian V-ATPase is composed of two domains: the cytosolic V_1 domain and the integral membrane complex, V_O. These two domains are further divided into 13 different subunits, which are illustrated in Figure 1-1. The V_1 domain, which is responsible for ATP hydrolysis, is composed of 8 subunits (A-H), whereas the V_O domain, responsible for proton translocation, is composed of 5 subunits (a,c,c'',d,e) (3). Yeast V-ATPases have a similar structure but contain an extra V_O subunit (c') (12). Moreover, V-ATPases are also evolutionarily similar to the F_0 and F_1 ATP synthases (F-ATPases) found in bacteria (13).

V-ATPases use a rotary mechanism, involving both domains, to drive the transport of protons across membranes. ATP hydrolysis occurs in the catalytic $V_1A_3B_3$ hexamer composed of alternating V_1A and V_1B subunits. Energy generated during hydrolysis acts as the driving force of the rotary mechanism, rotating the central stalk made up of subunits V_1D, V_1F and V_Od. The proteolipid subunits in the V_O domain, V_Oc and V_Oc'', are organised into a highly hydrophobic ring formation. Protons enter a cytoplasmic hemi-channel in subunit V_Oa and bind to glutamic acid residues in the proteolipid ring (14, 15). The clockwise rotation of the central stalk sequentially rotates the proteolipid ring, allowing the protonated glutamic acid residues to come into contact with a hemi-channel in subunit V_Oa. Within subunit V_Oa, a critical arginine residue is thought to then stabilise the glutamic acid residues (16). This results in the deprotonation of the glutamic acid of the V_Oa subunit and the release of the proton, thereby acidifying the lumen (17). It is noteworthy that the majority of the V-ATPase specific inhibitors bind to the proteolipid ring, including bafilomycin-A1, concanamycin-A and archazolid (18-20).

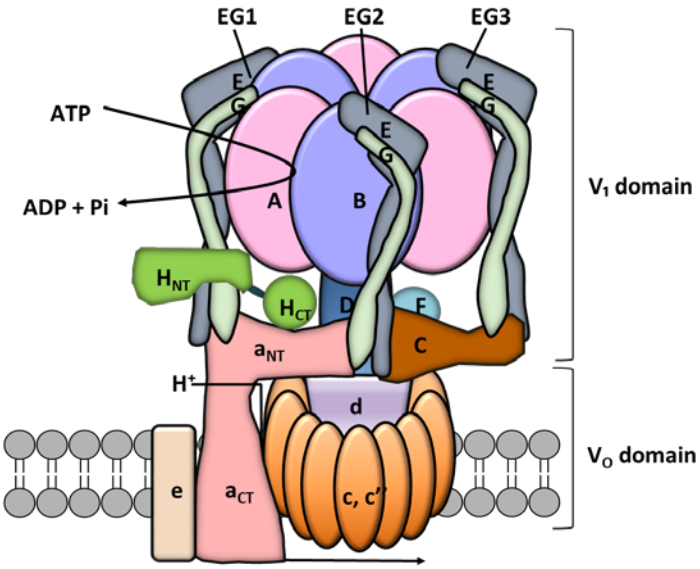

Subunits with tissue-enriched distribution

V_1 domain

B1 - renal cells, epididymal cells, hair cells of inner ear
C2 - kidney
E2 - testis
G2 - neuronal
G3 - kidney, epididymis

V_O domain

a1 - neuronal
a2 - endothelium, neuronal
a3 - osteoclasts, premature melanosomes, β-pancreatic cells
a4 - renal cells, epididymal cells, hair cells of inner ear
d2 - osteoclasts, kidney, epididymis, dendritic cells

Figure 1-1. The mammalian V-ATPase structure

The V_1 domain contains the $V_1A_3B_3$ catalytic hexamer, the peripheral stalk made up of subunits V_1E, V_1G, V_1C and V_1H, and subunits V_1D and V_1F of the central rotor. ATP hydrolysis occurs in the $V_1A_3B_3$ catalytic hexamer and the energy generated is used to drive the rotary mechanism. The V_O domain is integrated into the membrane and is responsible for proton translocation; it consists of subunits V_Oa, V_Od, V_Oe and the proteolipid ring made up of V_Oc and V_O c''. Taken from (1).

The peripheral stator/stalk is composed of subunits V_1E, V_1G, V_1C, V_1H and the N-terminus of V_Oa (21). This peripheral stator has an important role in tethering the $V_1A_3B_3$ hexamer to the N-terminus of subunit V_Oa, thus resisting the torque generated by the rotation of the central stalk (22). It is made up of a central V_1EG heterodimer, which acts to anchor the membrane to the peripheral complex (13). Eukaryotic V-ATPases have three V_1EG heterodimers (EG1, EG2, EG3) (23), whereas archaeal-ATPases have two (24) and F-ATPases have only one (25). Subunit V_1C contains two globular domains, one at the foot and one at the head, which contact two of the three V_1EG heterodimers (EG2 and EG3). The head domain can interact with EG3 with high affinity, whereas the foot domain can bind to the EG2 heterodimer and the N terminus of subunit V_Oa with lower affinity. Crystal structure analyses of the EGC complexes show that the V_1E and V_1G subunits have a coiled-coil structure giving the peripheral stalks flexibility (12). This flexibility allows the A_3B_3 hexamer catalytic sites to undergo conformational changes (12). Subunit V_1C, along with V_1H, also play a large role in a regulatory process known as reversible dissociation, which is explained in more detail in a later section.

1.2.2 V-ATPase subunit isoforms

1.2.2.1 Yeast V-ATPase subunit isoforms

Of the 13 mammalian V-ATPase subunits, at least seven have multiple isoforms in mammalian cells, with subunit V_Oa being the most extensively studied. In yeast, only subunit V_Oa is encoded by two genes (*Vph1* and *Stv1*), whereas all other subunits are encoded by a single gene. Table 1-1 summarises the differences between the mammalian and yeast V-ATPase subunit isoforms. The two genes play different roles as *Stv1* targets the V-ATPase to the Golgi whereas *Vph1* targets it to the vacuole (26). Key differences in the properties of V-ATPases containing either *Stv1* or *Vph1* have been identified (26), which may reflect the differences in pH between the Golgi and vacuole. Additionally, as there are no subunit isoforms in yeast and yeast null mutants have a conditional lethal phenotype (27), mammalian subunit isoforms can replace yeast subunits so that the function of individual mammalian subunits can be studied.

Table 1-1 Eukaryotic V-ATPase subunit isoforms

Mammalian V-ATPases have a variety of isoforms encoded by separate genes, which differ from that of yeast V-ATPases. The table below lists the different isoforms for both mammalian and yeast V-ATPases.

Eukaryotic V-ATPase subunits				
	Mammalian		Yeast	
Sector	Subunit isoform	Gene	Subunit isoform	Gene
V_1	A	*ATP6V1A*	A	*VMA1*
	B1	*ATP6V1B1*	B	*VMA2*
	B2	*ATP6V1B2*	-	-
	C1	*ATP6V1C1*	C	*VMA5*
	C2	*ATP6V1C2*	-	-
	D	*ATP6V1D*	D	*VMA8*
	E1	*ATP6V1E1*	E	*VMA4*
	E2	*ATP6V1E2*	-	-
	F	*ATP6V1F*	F	*VMA7*
	G1	*ATP6V1G1*	G	*VMA10*
	G2	*ATP6V1G2*	-	-
	G3	*ATP6V1G3*	-	-
	H	*ATP6V1H*	H	*VMA13*
V_O	a1	*ATP6V0A1*	a	*VPH1/STV1*
	a2	*ATP6V0A2*	-	-
	a3	*ATP6V0A3*	-	-
	a4	*ATP6V0A4*	-	-
	d1	*ATP6V0D1*	d	*VMA6*
	d2	*ATP6V0D2*	-	-
	c	*ATP6V0C*	c	*VMA3*
	-	-	c’	*VMA11*
	c’’	*ATP6V0B*	c’’	*VMA16*
	e	*ATP6V0E*	e	*VMA9*

1.2.2.2 Mammalian V-ATPase subunit isoforms

The most extensively studied V-ATPase subunit regarding isoform function is the V_Oa subunit. In mammalian cells, subunit V_Oa exists in four isoforms (a1-a4) and, similarly to yeast, are involved in the targeting of V-ATPases to specific organelles. The V_Oa1 subunit is expressed ubiquitously but has been shown to localize at nerve terminals, and therefore may play a role in the acidification of synaptic vesicles (28). It has also been suggested that V_Oa1 is involved in the endocytic pathway as it might be involved in phagocytosis in the brain (29). Expression of the V_Oa2 isoform has been identified in the spleen, lung and epididymis, but is thought to play its predominant role in the kidney. This is where it functions to decrease the pH in proximal tubule cells to release peptides involved in absorption (30). Subunit V_Oa3 is involved in bone resorption and targets the V-ATPase to the PM of osteoclasts (31). Mutations in this isoform are associated with osteoporosis, and therefore V_Oa3 could be a potential therapeutic target for new osteoporosis treatments (8). Finally, the V_Oa4 isoform is present in the epididymis, inner ear and the kidney (10, 32). Similarly to V_Oa2, V_Oa4 also plays a large role in targeting V-ATPases to the kidney, although V_Oa4 targets to membranes of intercalated cells in the collecting duct and distal tubule. As a result, germline mutations in V_Oa4 are commonly present in patients with renal tubular acidosis (32).

In addition to subunit V_Oa, many other mammalian subunits have different isoforms, of which at least one isoform is expressed in specific tissues, and another is ubiquitously expressed. Many of the subunit isoforms share amino acid sequence homology and the similarities are as follows: V_1B (83%) (33), V_1C (62%) (34), V_1E (77%) (35), V_1G (53-64%) (34) and V_Od (68%) (34).

Subunit V_1B has two isoforms, V_1B1 and V_1B2. V_1B2 is expressed ubiquitously but tends to localize in intracellular organelles and V_1B1 is expressed in renal cells, epididymal cells and cells of the inner ear. As a result, mutations in V_1B1 have been shown to cause renal tubular acidosis and deafness. (36). Although it appears as if the two isoforms may have different functions, one study showed that V_1B2 could compensate for a loss of V_1B1 in knockout mice models (37). V_1B2 is often referred to as the brain isoform due to its localised high levels of expression. Using an *ATP6V1B2* knockdown mouse model, *Yuan et al.* demonstrated that V_1B2 deficiency results in severe sensorineural hearing loss and that a single mutation (Arg506X) results in dominant deafness-onychodystrophy syndrome due to abnormal lysosomal acidification (38, 39). Recently, somatic mutations in the V_1B2 isoform have been associated with autophagic flux and mTOR activation in follicular lymphoma patients (40), which is discussed in more detail in the next section.

The V_1C subunit also has two isoforms, V_1C1 and V_1C2, and in mice two further mRNA splicing variants of V_1C2 have been identified, V_1C2-a and V_1C2-b. V_1C1 is ubiquitously expressed whereas V_1C2 is expressed specifically in lung and kidney tissues. Further diversity of the V_1C2 isoform in mice shows that V_1C2-a is expressed in type II alveolar cells, whereas V_1C2-b was found in the PM of renal intercalated cells. Moreover, the V_1C1 isoform is highly expressed in osteoclasts, where it interacts with the V_Oa3 isoform, and was found to co-localise with microtubules in the PM and F-actin in the cytoplasm (41). In agreement with this, *Sun-Wada et al*. demonstrated that expression of the ubiquitous subunit isoforms (V_1B2, V_1C1, V_1G1, and other V_Oa isoforms) were present in one complex, whereas the kidney-specific isoforms (V_1B1, V_1G3, V_Od2, V_Oa4, V_1C2-b) were found in another (42). These findings were significant because they showed an *in vivo* selective assembly of V-ATPase isoforms, indicating that V-ATPase complexes may have different functional characteristics depending on the expression of individual isoforms. Furthermore, a chimeric yeast V-ATPase with mouse V_1C1 had a higher *Km* and proton transport activity than that of the V_1C2-a or V_1C2-b isoforms. The chimeric V_1C2-b complex had a significantly lower energy coupling efficiency compared to complexes with V_1C1 or V_1C2-a, suggesting the V_1C subunit is important for V-ATPase energy coupling (42). This is supportive of the fact that the V_1C1 isoform is highly expressed in osteoclasts (41), suggesting the higher rate of activity is consistent with the increased functional requirement. In addition to this, *Wang et al.* showed that silencing the V_1C1 subunit in periapical tissues reduced bone resorption by 70%, inhibited T-cell mediated inflammation by 75% and reduced expression of pro-inflammatory cytokines, highlighting V_1C1 as a potential novel therapeutic target for endodontic disease (43).

The mammalian V_1E subunit has two isoforms, V_1E1 and V_1E2. V_1E2 is specific for the testes and the spermatozoa whereas V_1E1 is expressed ubiquitously, although both are well conserved across species (12). Interestingly, subunits V_1A and V_Oa2 were found to be localised in the same membranes in the testis as V_1E2, indicating a unique V-ATPase complex is expressed in the acrosomes of spermatids (44). Furthermore, chimeric yeast cells expressing the V_1E2 isoform were shown to be temperature sensitive and could not grow at 37°C, exhibiting a functional coupling defect between proton and transport and ATP hydrolysis. This was not observed for the ubiquitously expressed V_1E1 isoform, which may represent a V-ATPase specific function as the optimal temperature for spermatid cell culture is 33°C, and therefore cells expressing the V_1E2 isoform would have dysregulated V-ATPase activity above this temperature (44). The V_1E2 subunit is primarily believed to have a role in sensing the environment of the V-ATPase complex. *Okamoto et al*. showed that the V_1E subunit is important for V-ATPase disassembly in response to glucose deprivation. In addition, the group identified the Glu-44 residue as the key residue

that may prevent V-ATPase disassembly by inhibiting the formation of a strong-coiled coil in the enzyme complex (12).

Compared to the other mammalian subunits the V_1G and V_Od isoforms are less well characterised. The V_Od subunit exists in two isoforms; V_Od1 is ubiquitously expressed whereas V_Od2 is present in osteoclasts and renal epididymal cells (45-47). *Lee et al*. demonstrated that silencing the V_Od2 subunit is mice results in development of osteoporosis, suggesting V_Od2 may play a role in osteoclast fusion (48). In comparison, V_1G has three isoforms: V_1G1, V_1G2 and V_1G3. The V_1G1 isoform is ubiquitously expressed, V_1G2 is expressed in the brain and V_1G3 in the kidney and epididymis (34). Additionally, V_1G3 has been shown to be a potential novel immunohistochemical marker for chromophobe renal cell carcinoma (49).

1.2.3 Mechanisms of regulation

In addition to regulation of V-ATPase by differential expression of its composite subunits, other mechanisms can regulate V-ATPase function by direct modulation of assembly or function of the complex. Reversible dissociation of V_1 from the V_O complex is an essential mechanism for rapidly regulating V-ATPase activity without the synthesis of new proteins. This mechanism of reversible dissociation is illustrated in Figure 1-2. In yeast, disassembly occurs in response to glucose deprivation, and the enzyme re-assembles with the addition of glucose. During dissociation, the peripheral interactions that hold the enzyme complex together are broken, releasing subunit V_1C from both domains into the cytoplasm. For V-ATPase re-assembly to occur the interactions must be restored and it is essential that subunit V_1C is re-incorporated into the complex (50). This re-incorporation involves bending of the third peripheral stalk, which induces an enormous amount of physical stress leading to a phenomenon referred to as ‘spring loading’. A specific region within the V_1G-subunit, characterised by a random coil bulge, may play an important role in this spring loading process (50).

The purpose of the spring mechanism is thought to be so that the V-ATPase can quickly disassemble after glucose depletion, preserving vital ATP (51). It is crucial that both sectors can become inactivated so that the pump activity decreases; if free catalytic V_1 was to enter the cytoplasm then it could deplete cellular ATP stores and have catastrophic effects. Subunit V_1H has been shown to play a large role in this essential inhibition (52). Much like subunit V_1C, subunit V_1H is composed of two globular domains connected by a flexible linker (53). The proposed mechanism of V-ATPase inhibition is through the tethering of the peripheral stalk to the central stalk. This is achieved via the binding of subunit V_1H to a loop in subunit V_1F in the central rotor. As a result, a bridge forms

between the rotor and stator segments of the enzyme, blocking the rotation of the central stalk (53, 54).

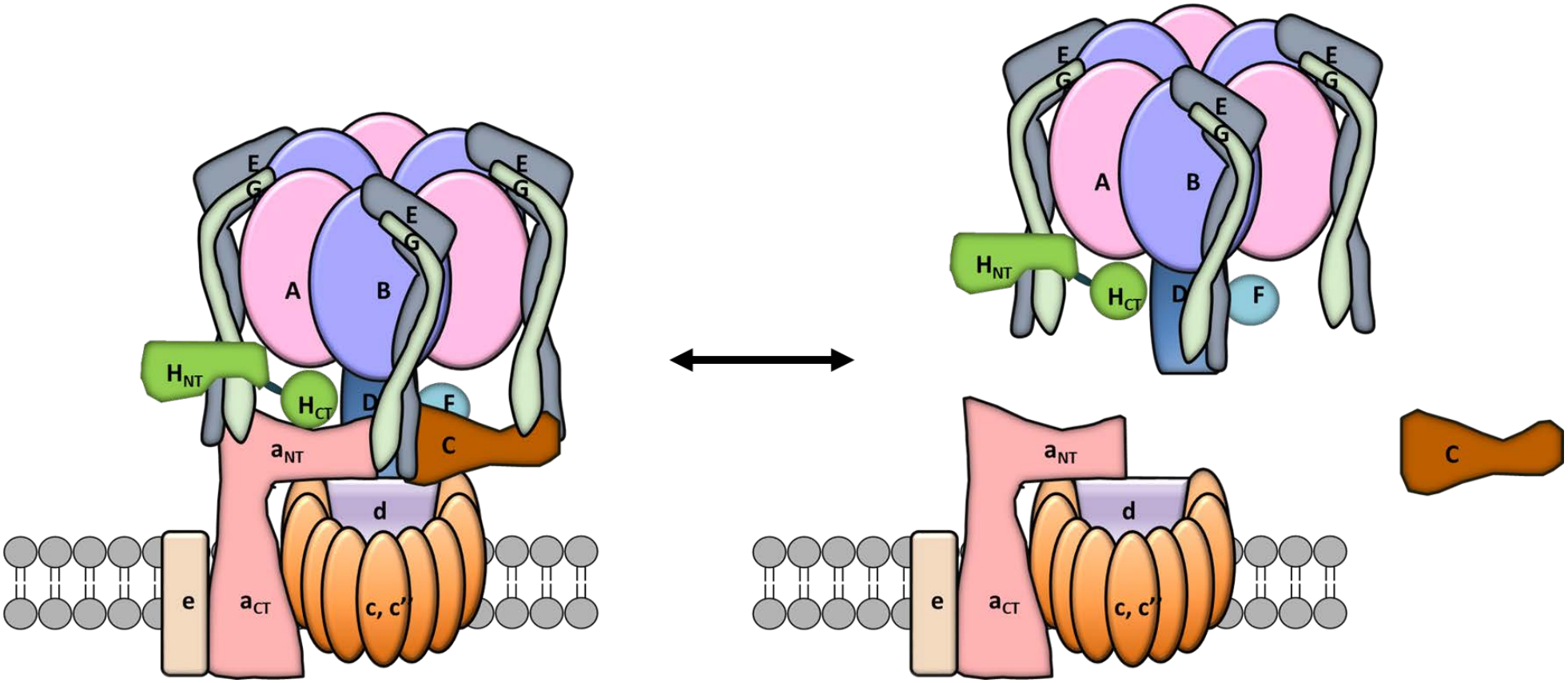

Figure 1-2. Reversible dissociation of V-ATPase

Reversible dissociation is an important V-ATPase regulatory mechanism. Dissociation of the V_1 from the V_0 complex releases subunit V_1C, which needs to be re-incorporated upon reassembly.

This reversible assembly requires another heterotrimeric protein complex known as RAVE (regulator of the ATPase of vacuolar and endosomal membranes), which is composed of three separate proteins (Rav1P, Rav2P and SkP1) (55). RAVE is thought to bind subunits V_1E, V_1G and V_1C to stabilize the dissociated V_1 domain and to help regulate the dissociation process (55, 56). Interestingly, in yeast reversible dissociation appears to depend on where the enzyme is localised. V-ATPases localised to the Golgi containing Stv1p do not dissociate upon glucose deprivation, whereas those localised to the vacuole that contain Vph1p do dissociate (57). RAVE also appears to preferentially bind to Vph1p (58). Furthermore, when V-ATPase complexes that contain Stv1p are overexpressed in the vacuole, the complex does dissociate in response to glucose deprivation (57). Why this phenomenon occurs is not exactly known but may be due to the differences in luminal pH. In mammalian cells, the protein rabconnectin 3 may play a similar role to RAVE (59). Moreover, PI3K and EGF are also involved in glucose-regulated assembly (60, 61).

In addition to reversible dissociation, other mechanisms are key to regulating V-ATPase activity. One such mechanism involves the insertion of active V-ATPase complexes into membranes and is particularly important in renal-intercalated cells and clear epididymal cells. In both cell types, cAMP levels are increased in response to low cytoplasmic pH. This is aided by a bicarbonate-sensitive adenylate cyclase (62). As a result, PKA activity increases, which in turn directly phosphorylates subunit V_1A, localizing the enzyme complex at the respective apical membrane (63). Furthermore, the enzyme AMPK also has the ability to phosphorylate the V_1A subunit directly and can inhibit PKA-dependent phosphorylation (64, 65). This represents a co-regulatory effect of both PKA and AMPK on proton transport across apical membranes. Additionally, the HRG-1 protein (66), pro-hormone processing (67), and transcription factor EB (TFEB) (68) have all been found to regulate V-ATPase activity in human cells, without altering the enzymes assembly.

1.2.4 V-ATPase functions

Our understanding of the functions of the V-ATPase complex is continuously developing and we are starting to unravel the complexity of the enzyme. Research is moving away from the idea that it serves only as a proton pump and it is now understood to have a central role in environmental sensing including as a pH sensor.

1.2.4.1 Vesicular and luminal acidification

The key function of V-ATPase is to acidify intracellular vesicles such as endosomes and lysosomes. V-ATPase is present on the surface of endosomes and functions to mediate processes like vesicular trafficking and receptor recycling through acidification. This

acidification is critical for the internalisation of essential receptor ligand complexes into the endosome, and the reduction in pH has been shown to result in the recycling of ligands, which are then transported to the PM (69). V-ATPases in the lysosome contribute to the maintenance of the acidic pH required for lysosomal function. They also assist in transporting newly synthesised acid hydrolases to lysosomes from the Golgi. Many proteins undergo glycosylation in the Golgi, which is an important post-translational modification (70). Interestingly, mutations in the V-ATPase V_Oa2 subunit have been associated with the development of a recessive autosomal wrinkly skin syndrome known as cutis laxa. However, despite the genetic link to a defect in glycosylation, the direct involvement of Golgi acidification in protein maturation is not fully understood (71). Furthermore, phagosomes and autophagosomes require a V-ATPase mediated acidic environment for the activity of degradative enzymes (72). Within specialised cells, V-ATPase expression is linked to specific cell-type functions. For example, V-ATPase has been shown to be important for: the formation of synaptic vesicles during neurotransmission (73), insulin exocytosis in pancreatic cells (66) and mediating fission-fusion of the vesicular system (74). In addition to these vesicular functions, there is a growing interest in V-ATPase activity in the PM, especially with regards to cancer (1, 75). Many of the luminal functions of the V-ATPase are attributed to the expression of specific subunit isoforms in specialised cells, which are outlined in 1.2.2.

1.2.4.2 Additional functions

It is well established that the primary function of the V-ATPase is to acidify intracellular compartments and the extracellular environment. However, novel V-ATPase functions are beginning to emerge and a summary of these key functions is shown in Figure 1-3. One of the more novel concepts to develop is that V-ATPase is required for amino acid mediated mTORC1 signalling. Amino acids can initiate a signalling cascade that leads to activation of mTORC1, which is a master regulator of many catabolic and biosynthetic processes associated with cell growth. Amino acids promote mTORC1 signalling by initiating binding to Rag-GTPases that recruit mTORC1 to the surface of lysosomes. The regulator complex anchors Rag GTPases to the lysosome forming an mTORC1 docking site. *Zoncu et al*. demonstrated that components of the V-ATPase complex formed functional and physical links with the Rag-Ragulator complex. Furthermore, they showed that it was the V-ATPase ATP-hydrolysis, and not the lysosomal pH gradient, that was required for the amino acid dependent activation of mTORC1. The group proposed a lysosome-centric inside-out model in which the V-ATPase functions between amino acids and loading of the Rag GTPases with nucleotides, forming a critical component of the sensing mechanism. This finding was particularly interesting because it demonstrated that it was the physical

rotation of the V-ATPase complex that was responsible for regulating mTORC1 activity and that the V-ATPase is more than just a proton pump (76).

In addition to acting as an amino acid sensor, V-ATPases may be able to operate as pH sensors and regulate the recruitment of cytosolic proteins. Cyothesin-2 and Arf6 interact with V-ATPase to mediate endosomal and lysosomal degradation pathways. The Arf-family GTP-binding proteins are small GTPases that act as regulatory molecular switches. Cytohesin-2 and Arf-6 are both specifically targeted to early endosomes and their recruitment is pH dependent (77). More importantly, the V_Oa2 subunit isoform has been shown to directly interact with cytohesin-2 and subunit V_Oc (78). These specific interactions depend on acidification of the endosomal lumen by V-ATPases. Thus, the V_Oa2 isoform in the V-ATPase complex has the ability to sense pH levels and can transmit information across membranes. Recently, *Meruklova et al.* used pull down experiments to show that in fact all four subunit V_Oa isoforms could interact with cytohesin-2 (79). This regulatory complex may therefore be able to mediate trafficking between early and late endosomes and regulate specific signalling proteins such as insulin (80).

Notch and Wnt pathways are two key signalling pathways involved in many physiological processes. They both require intact V-ATPases for the accurate trafficking and processing of cell surface receptors. The Notch receptor is key to cell-cell signalling and is important in cellular development. Upon ligand binding, the Notch receptor is activated by a series of cleavage events that release the Notch intracellular domain (NICD). This allows its translocation to the nucleus and activation of target genes (81). Inappropriate Notch activation is becoming an important feature of cancer development (82) and it is therefore crucial that we understand the full involvement of V-ATPase. In V-ATPase deficient cells, Notch and other components accumulate in lysosomal compartments and are not processed (83). This is because when V-ATPases are perturbed, γ-secretase cleavage in endosomes is greatly reduced, preventing the release of NICD. Furthermore, this suggests that V-ATPase inhibitors could be used to reduce endosomal acidification and prohibit the increased levels of Notch activation seen in many cancers (84).

V-ATPases are essential for endosomal acidification and this acidification consequently affects Wnt signalling (85). For example, V-ATPases are required for the phosphorylation of cell surface Wnt receptor LRP6 in the canonical pathway. The proposed mechanism is that the prorenin receptor (PRR) forms part of the Wnt/Fz/LRP6 receptor complex and acts as an adaptor between the V-ATPase and LRP6. This complex is then endocytosed upon Wnt stimulation and the V-ATPase generates a proton gradient that is crucial for LRP6 phosphorylation (86). Thus, this demonstrates that V-ATPases are involved in the regulation of early endosomes in the protein degradation pathway. Moreover, inhibition of V-ATPase using bafilomycin-A1 results in inhibition of Wnt activity (85) and can therefore

prevent Wnt-induced transcription. This reiterates the significance of V-ATPases as a therapeutic target due to their widespread effects throughout the human body.

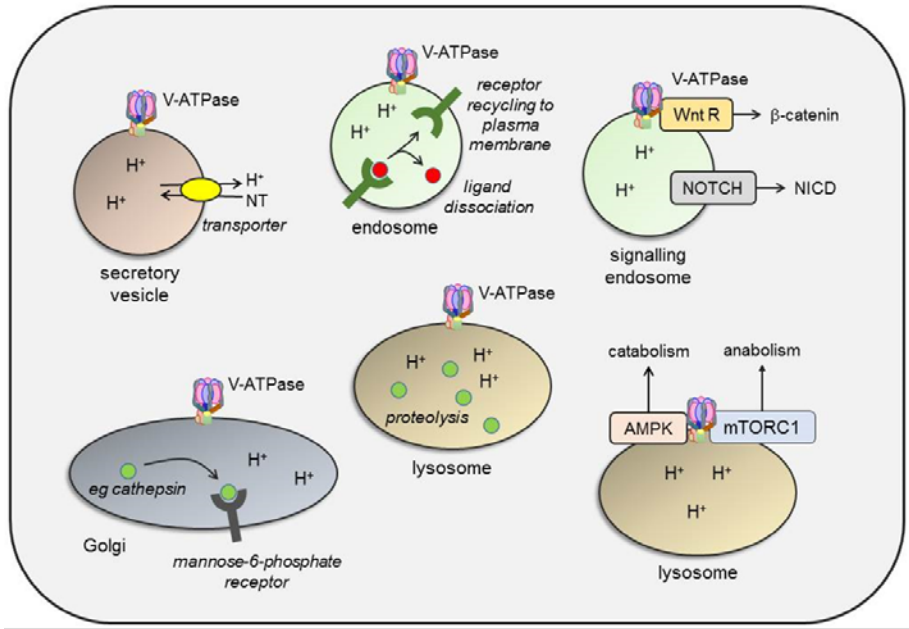

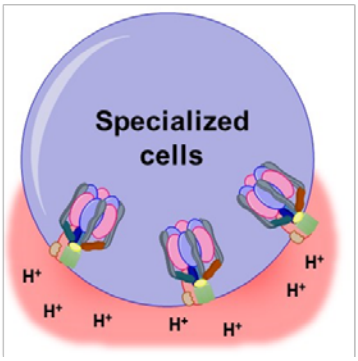

Renal intercalated cells - V-ATPase targeted to apical membrane facilitates urinary acidification.
Osteoclasts - V-ATPase targeted to ruffled border creates acidic environment required for bone resorption.
Epididymal clear cells - V-ATPase targeted to apical membrane creates acidic environment necessary for sperm development and storage.

Figure 1-3. V-ATPase function

Intracellular V-ATPase regulates multiple intracellular processes. In secretory vesicles, V-ATPase generates a proton gradient that is used to drive the H+-dependent uptake of neurotransmitters. In endosomes, low pH promotes the dissociation of ligands, such as low density lipoproteins, from their receptors, facilitating receptor recycling to the plasma membrane. In signalling endosomes, V-ATPase promotes signalling to β-catenin downstream of Wnt receptors, and can promote NOTCH signalling via enhanced cleavage to generate NICD. In the Golgi, V-ATPase promotes binding of hydrolases to the mannose-6-phosphate receptor which is important for their delivery to the lysosome. In lysosomes, low pH is required for optimal activity of acid-dependent proteases, such as cathepsins. Lysosomal V-ATPase also acts to coordinate activity of AMPK and mTORC1 to regulate cellular catabolism versus anabolism in responses to shifting microenvironmental cues. Note the figure is designed to illustrate some key functions of V-ATPase and is not intended to portray all of the diverse functions that have been ascribed to V-ATPase. Plasma membrane functions of V-ATPase in specialized cell types including renal intercalated cells, osteoclasts and clear epididymal cells. Taken from (1)

.

1.3 Role of V-ATPases in cancer

1.3.1 Overview

Due to the complexity of the V-ATPase, it is logical to propose that their dysregulated expression and activity may play a crucial role in cancer development. There is now a large body of research supporting this, and V-ATPase have been linked to a number of different cancers including breast, pancreatic, gastric, lung, prostate and many more (2, 87-90). V-ATPase subunits are overexpressed in many tumour samples and in various cancer cell lines (2, 91-93). The information in this section was adapted from my review paper (1).

1.3.2 Dysregulation of V-ATPase in cancer

The bulk of the evidence linking dysregulation of V-ATPase to cancer derives from studies showing altered expression or subcellular localisation of specific V-ATPase subunits in malignant cells versus normal counterparts and/or correlations between variable subunit expression and clinical features of disease.

For example, analysis of the TCGA database revealed that amplification/overexpression of *ATP6VC1* was observed in 34% of human breast cancers and was associated with a relatively poor outcome (94). In a separate study, expression of the V_1C1 subunit, which bridges between the V_1 and V_O domains, was detectable in all examined stages of Barrett's oesophagus (a precursor lesion for oesophageal squamous cell carcinoma associated with an ~0.3% annual risk of progression to adenocarcinoma) using immunohistochemistry (IHC), indicating that its increased expression may play a role early in the transformation in these tissues (95). Interestingly, immunofluorescence staining revealed that at least a proportion of V-ATPase was localised to the PM in oesophageal squamous cell carcinoma (ESCC) cells (96). Furthermore, a recent detailed study using IHC showed that the V_1E1 subunit was overexpressed in ESCC compared to normal oesophagus. Unusually high V_1E1 subunit protein levels in cancer cells was associated with tumour invasiveness and lymph node (LN) metastasis, and with reduced disease-free and overall survival, including in early stage disease. Importantly, V_1E1 expression was an independent predictor of outcome (97) and could potentially be used as a marker of disease. A similar study has investigated the significance of the V_1A subunit in gastric cancer using IHC. Again, increased V-ATPase subunit expression was observed in cancer, compared to normal tissue, and high tumour expression was associated with poor

differentiation, LN metastasis, advanced stage and was an independent predictor of poor outcome (87).

Other studies have described expression of V-ATPase/specific subunits in pancreatic cancer (88, 98), non-small cell lung cancer (90), oral squamous cell carcinoma (92, 99), ovarian cancer (100), cervical cancer (101), breast cancer (102, 103), gliomas (104) and hepatocellular carcinoma (91). A summary of studies investigating clinical significance of V-ATPase in cancer is provided in Table 1-2. It is important to note that most of these studies focussed on individual subunits and lack information on localisation, expression of other subunits, and/or analysis of the ATP hydrolysis and proton transport activities of V-ATPase. Further investigation into whether altered gene expression and/or protein accumulation of one of the subunits of V-ATPase lead to malfunction of V-ATPase function in the primary human tumours remains an important area for future investigation.

An important new advance that moves beyond differences in subunit expression in cancer is the recent identification of V-ATPase subunit mutations. Somatically acquired mutations of *ATP6V1B2* or the accessory subunit *ATP6AP1* are detected in ~20% of follicular lymphoma (FL) patients (105, 106). These V-ATPase mutations frequently co-occur with mutations in the *RRAGC* gene encoding the Rag-GTPase family member RagC, that with V-ATPase and the V-ATPase interaction partner Ragulator, form an amino acid “sensing” supercomplex which is required for mTORC1 activation (76). FL *RRAGC* mutations appear to be gain-of-function and promote inappropriate mTORC1 activity following amino-acid depletion (106). Functional data are lacking, but V-ATPase mutations may also promote inappropriate mTORC1 activation in FL. A relatively large number of V-ATPase subunit sequence variants have been reported in the COSMIC database in a wide spectrum of cancer types (107) suggesting that the occurrence and importance of V-ATPase mutations may extend beyond lymphoma. However, validating studies will be required to confirm which sequence variants are truly cancer-specific and have important functional consequences.

Table 1-2. Evidence for V-ATPase subunit dysregulation in patient tumour tissues

IHC, Immunohistochemistry; IF, Immunofluorescence; WB, Western-blot; IP, Immunoprecipitation. Taken from (1).

Cancer type	Subunits investigated	Techniques	Key evidence	Reference
Breast	V_Oa	RT-qPCR, IHC	V_Oa3 mRNA expression was upregulated in all breast cancer tissues tested compared to normal tissue and a3 mRNA expression correlated with tumour grade. Invasive breast cancer tissue had greater a3 staining than ductal carcinoma *in situ*, suggesting a3 expression increases with invasive potential.	(102)
Breast and melanoma	V_Oa2	IHC, IF	Highly positive staining of V_Oa2 in breast and skin tumours compared to their respective normal tissues.	(103)
Cervical	V_1C1	IHC	V-ATPase expression significantly increased in patients with cervical adenocarcinoma. In patients with bulky cervical tumour expression was correlated with poor disease-free survival	(101)
Gastric	V_1A	IHC	V_1A overexpressed in gastric cancer tissue compared to normal tissue. V_1A expression correlated with advanced tumour grade, vascular invasion, lymph node metastasis and was associated with worse survival than patients with negative V_1A staining.	(87)
Glioma	V_oa	RT-qPCR	V_Oa4 isoform increased compared to brain biopsies of epileptic patients.	(104)
Human hepatocellular carcinoma	V_Oc (ATP6L)	RT-qPCR, WB, IHC	Greater ATP6L mRNA and protein expression in HCC tissues compared to normal liver tissue. Baf-A1 inhibition retarded growth of HCC in liver of mice.	(91)
Lung	V-ATPase complex	IHC	V-ATPase complex overexpressed in NSCLC. Expression was significantly lower in grade II adenocarcinoma and squamous cell lung cancer than grade III. V-ATPase expression was found to be positively correlated to drug resistance in NSCLC samples and a significant positive correlation was obtained for V-ATPase expression and common cancer chemotherapeutic agents.	(90)
Oesophageal	V_Oa and V_1C1	Confocal microscopy, IHC	V-ATPase expressed in all stages of neoplastic progression in Barrett's oesophagus.	(95)
	V-ATPase complex	IHC/IF	Complex highly expressed in oesophageal squamous cancer cells.	(96)
	V_1E1	IHC	V_1E1 expression increased in oesophageal cancer tissues than normal oesophageal tissue and was directly correlated with tumour invasiveness and poor prognosis. Can act as independent prognostic factor.	(97)
Oral squamous cell carcinoma	V_1C1	RT-qPCR	V_1C1 overexpressed in OSCC tissues compared to healthy oral mucosa samples.	(99)
	V_1C1	IHC	V_1C1 overexpressed in OSCC tissues compared to healthy oral mucosa tissue.	(92)
Ovarian	V_Oa	IF, IHC	V_Oa2 expression increased and a3 subunits had greater staining in ovarian cancer tissues compared to normal ovarian tissues.	(100)
Pancreatic	V_Oc	RT-qPCR, IHC, IP	V_Oc overexpressed in pancreatic carcinoma tissues compared to normal pancreatic tissue. Expression was linked to invasive capabilities as the overexpression of V_Oc was characteristic of invasive ductal adenocarcinomas.	(98)
	V_1E	IHC	V-ATPase staining was significantly increased from low-grade pancreatic intraepithelial neoplasia (PanIN) to invasive PDAC.	(88)

1.3.3 V-ATPase function in cancer cells

Functional characterisation of V-ATPase in human cancer cells has focused on its role in potentiation of migration and invasion, consistent with the common association between elevated subunit expression and advanced stage/metastasis observed in several cancer types (Table 1-2). Increased cancer cell invasive activity is frequently associated with aberrant V-ATPase PM localisation suggesting that increased acidification of the extracellular space plays an important role (2, 11, 88, 90, 93, 96, 100, 108-110).

Various cell lines have been used to study the functional links between V-ATPase and invasive activity. For example, using two closely related human breast cancer cell lines, MCF10a and MCF10CA1a, *Capecci et al.* found that the levels of mRNA encoding V_Oa1 and V_Oa3 were highest in the invasive MCF10CA1a cells (93). Furthermore, the V_Oa3 isoform was also expressed in lung and bone metastasis of B16-F10 cells, suggesting this isoform might be relevant to the increased metastatic potential of melanoma cells (110). As previously discussed, V_Oa isoforms can be expressed in a tissue-enriched pattern and are associated with PM localisation. Therefore, overexpression of these isoforms might be an example of cancer cells hijacking a normal cellular process to increase H^+ extrusion.

V-ATPase in the invasive breast cancer MDA-MB-231 cell line was shown to be localised to the PM and V-ATPase activity was significantly higher than in less invasive cell lines. To investigate whether PM or intracellular V-ATPases were responsible for the invasive phenotype of breast cancer cells, *Cotter et al.* inhibited PM V-ATPase activity in MDA-MB-231 cells with a monoclonal antibody to the V5 epitope of a V5 tagged V_Oc subunit construct (which, in contrast to pharmacological inhibitors or RNAi-mediated subunit ablation, would be expected to specifically target PM localised V-ATPase) and found that specific inhibition significantly decreased *in vitro* invasion (109). Other studies of breast cancer cells have also linked V-ATPase subunit expression to invasion. For example, siRNA knockdown of V_Oa3 (but not a1, a2 or a4) significantly decreased invasion of MCF10CA1a cells. Interestingly, in this system, knockdown of V_Oa4 led to an increase in V_Oa3 expression and a combined knockdown of both V_Oa3 and V_Oa4 led to the greatest reduction in MCF10CA1a cell invasion (93).

The precise mechanisms by which V-ATPase promotes invasion/migration require further investigation, but appear multifactorial. V-ATPase can increase the activity of extracellular proteases, such as cathepsins and matrix metalloproteinases (MMP), via both increased protease secretion and decreased extracellular pH which enhances activity of these enzymes (111-113). Once activated, these proteases increase extracellular matrix degradation and facilitate migration of cancer cells. For example, in ovarian cancer cells,

V_Oa2 was found to be localised in endosomes and inhibition showed a decrease in MMP-9 and -2 activity (100). A study in hepatocellular carcinoma (HCC) found that inhibiting the V_Oc subunit led to decreased MMP-2 expression and extracellular MMP-2 activity (114).

Other potential mechanisms may involve modulation of intracellular organelles. Intracellular V-ATPase may play a role in tumour cell invasion by either assisting in the activation of lysosomal proteases or by activating cytosolic proteins which aid in trafficking these proteases to the surface of the cell (115, 116). V-ATPase localises with vesicles containing the small GTPase Rab27B, which promotes secretion of proinvasive growth factors and is associated with poor prognosis in breast cancer. V-ATPase inhibition alters distribution and size of Rab27B vesicles, and reduces collagen type I invasion, cell cycle and invasive growth in the chorioallantoic membrane assay. Importantly, V-ATPase inhibition reduces the Rab27B dependent extracellular secretion of Hsp90α, which is a molecular chaperone required for MMP-2 activation (115).

The role of V-ATPase in tumour migration has also been linked to tumour cell stiffness. Recent evidence suggests that a loss of cell stiffness is correlated with an increase in invasion and proliferation (117). For example, in HCC V-ATPase inhibition was shown to increase cell stiffness due to depletion of cholesterol in the PM and decreased Ras signalling (118). However, due to the complexity of the tumour microenvironment, the impact of V-ATPase on tumour membrane stiffness is not clear. In breast cancer, *in vivo* deletion of the *ATP6V0A2* gene encoding V_Oa2 subunit caused a reduction in breast tissue stiffness due to defective extracellular matrix glycosylation and altered Golgi morphology, resulting in an inflammatory and metastatic phenotype. Furthermore, normal breast tissue from patients who had reported lymph node metastasis (LNM) was analysed using IHC and was found to have significantly lower V_Oa2 expression than those without LNM, indicating that low V_Oa2 expression is associated with metastatic disease (119).

V-ATPases may also promote increased cancer cell migration via interaction with the cytoskeleton. In breast cancer 4T1 cells, following lentiviral depletion of V_1C1 subunit expression, the actin cytoskeletons lost their regular orientation resulting in decreased migratory and invasive activity, suggesting that V_1C1 is able to regulate actin cytoskeleton rearrangements (120). Moreover, V-ATPase inhibition is associated with F-actin reorganisation in PC-3 prostate cancer cells (121). Additionally, inhibition of V-ATPase using archazolid A or V_Oc subunit siRNA in SKBR3 breast cancer cells altered the distribution and localization of EGFR and Rac-1, which are associated with cellular migration (122).

In addition to effects on migration/invasion linked to extracellular acidification, it has been proposed that H^+-extrusion by V-ATPase can counter intracellular acidification associated

with altered metabolism (75). Thus, cancer cell growth is often associated with a reprogramming of metabolism towards aerobic glycolysis. This is termed the Warburg effect and is associated with tumour hypoxia as well as activation of oncogenes, such as MYC and RAS, and inactivation of tumour suppressors, such as p53 (123-125). This results in production of lactic acid and H^+, and PM V-ATPase may be key under these conditions for maintaining intracellular pH homeostasis (126). In addition, via its action as a coordinator of regulators of opposing anabolic versus catabolic pathways (eg, mediated via mTORC1 or AMPK, respectively) (127). V-ATPase may support "metabolic plasticity" allowing tumour cells to adapt to distinct and shifting tumour microenvironments (e.g. nutrient/O_2 deplete versus limited).

Finally, V-ATPase expression in cancer cells may influence immune cells to promote tumorigenesis indirectly. For example, a soluble cleavage fragment of V_Oa2 (a2NTD) has been shown to polarise macrophages towards a "tumour-associated" or M2 macrophage phenotype (103, 128).

1.3.4 V-ATPase as a potential cancer therapeutic target

V-ATPase function is intimately involved in the control of multiple normal cellular processes. However, genetic manipulation experiments suggest the potential to target V-ATPase function in cancer cells, with relatively little effect in normal cells, both *in vitro* and *in vivo*. This suggests that cancer cells may become particularly dependent on V-ATPase complex function, or on specific subunits, to support cancer-associated hallmarks, including growth and survival.

In the breast cancer cell lines MDA-MB-231, MCF-7 and MDA-MB-435, shRNA mediated knockdown of the V_1C1 subunit significantly inhibited cell proliferation, whereas in the untransformed C3H10T1/2 cell line, there was no effect on proliferation (94). In addition, 4T1 cells with 90% V_1C1 depletion had significantly less metastatic potential and reduced osteolytic lesions. (94). Alternatively, siRNA knock-down of the ATP6L (V_Oc) subunit in HCCLM3 hepatocellular carcinoma cells resulted in significantly reduced invasion, decreased MMP-2 expression, reduced average xenograft size and a dramatic reduction in intrahepatic metastases (114). In support of this, siRNA mediated knockdown of the V_Oc subunit led to a reduction of both SK-N-MC and A-673 Ewing sarcoma cell number (108).

In addition to these genetic experiments, chemical inhibitors of V-ATPase, plecomacrolide bafilomycin-A1 (baf-A1), concanamycin-A (con-A), benzolactone enamides, and archazolid, have been used to understand consequence of V-ATPase inhibition *in vitro* and *in vivo* (chemical structures shown in Figure 1-4). Both baf-A1 and con-A bind to the

V_Oc subunit responsible for proton translocation and are highly specific V-ATPase inhibitors with IC_{50} values in the nanomolar range (4-400 nM) (129). Benzolactone enamides have been extracted from marine organisms such as the sponge *Haliclona sp.* and the tunicate *Aplidium lobatum* as well as the gram negative bacterium *Pseudomonas sp.* and the myxobacterium *Chondromyces sp.* Archazolid is one of the novel V-ATPase inhibitors originally isolated from *Archangium gephyra*, which competes with con-A for binding to the V_Oc subunit and also has IC_{50} values in the low nanomolar range (130).

V-ATPase inhibition has been shown to reduce cancer cell growth and induce apoptosis in a number of cell lines across a range of cancer types. Importantly, chemical inhibition appears to show selectivity for cancer cells compared to normal cells. For example, baf-A1 inhibition resulted in significant reductions in hepatoblastoma cell growth compared to normal human hepatocytes (131). One of the benzolactone enamides and a derivative of salicylihalamide was shown to have a significantly synergistic effect on the viability of NCI-H1155 lung cancer cells when applied with paclitaxel increasing the sensitivity to the latter 1000-fold (132) (133). Additionally, archazolid had a significantly increased toxic effect in SKBR3 breast carcinoma cells compared to non-tumour MCF10A cells (134).

The biological mechanisms in which V-ATPase inhibition induces cancer cell death are diverse and complex. V-ATPase inhibition has been shown to result in increased reactive oxygen species (ROS) in cancer cells (135-137) and HIF-1α upregulation (134). Furthermore, V-ATPase inhibition induces caspase-dependent apoptosis in invasive tumour cells via the mitochondrial pathways (134, 138). Archazolid was also shown to induce cell cycle arrest in MDA-MB-231 cells and double-strand breaks in all cell lines investigated (139). This evidence indicates that V-ATPase inhibition can induce a cellular stress response, autophagy and eventually apoptosis in tumour cells. However, it should be noted that the relationship between V-ATPase and autophagy is complex particularly since the V-ATPase has a well-established role in activation of lysosomal acid hydrolases that mediate proteolysis during autophagy (140-142). Moreover, although V-ATPase inhibition can result in increased autophagic markers in some settings (134), V-ATPase is required for activation of non-canonical autophagy (143). In a very recent study, the autophagy-related protein ATG5 was demonstrated to displace *ATP6V1E1* from V-ATPase, causing it to accumulate in exosomes (144).The function of autophagy in cancer is also complex; both pro-survival and pro-death rolls have been described, dependent on cellular context (145).

In addition to activation of pro-apoptotic pathways, V-ATPase inhibition may promote cell survival pathways. For example, V-ATPase inhibition can result in activation of MAPKs including ERK in colon cancer cells (138). Thus, outcomes following V-ATPase inhibition are likely to reflect the balance of activation of pro-survival and pro-apoptotic pathways

and coordinate the inhibition of survival responses that may enhance apoptosis following V-ATPase inhibition. For example, inhibition of ERK using sorafenib augmented bafilomycin mediated cell death in tumour cells under hypoxic conditions (146).

Furthermore, iron chelators deferoxamine and 3-AP, showed a synergistic cytotoxic effect when used in combination with archazolid. It was therefore suggested that V-ATPase induced cytotoxicity might primarily be due to disturbed iron receptor recycling, impairing the iron metabolism of tumour cells (139). Consistent with this, the expression of genes responsive to a decrease in iron concentration were greatly increased in response to V-ATPase inhibition. Iron concentration was also inversely related to the cytotoxic hypersensitivity of cancer cells and therefore may act as a key determinant of cancer cell sensitivity to V-ATPase inhibition (147).

In addition to these *in vitro* cell line studies, chemical V-ATPase inhibition has recently been shown to be effective using *in vivo* mouse models. For example, in a 4T1-Luc mouse breast cancer xenograft model, archazolid treatment inhibited lung metastasis at a concentration (1 mg/kg i.v.) which did not cause signs of obvious toxicity (122). Similar results were obtained using baf-A1, in which treatment led to the reduction of tumour volume by 50% on average in MCF-7 and MDA-MB-231 xenograft mouse models. Again, no toxic side effects were observed using baf-A1 (1 mg/kg). Additionally, when combined with sorafenib, V-ATPase inhibition resulted in tumour regression in MDA-MD-231 xenograft mice (146). Another study demonstrated that growth of a HepG2 orthotopic HCC xenograft model in nude mice was retarded by baf-A1 (91).

Finally, the potential “repurposing” of protein pump inhibitors (PPI), which are widely used for the treatment of gastroesophageal reflux and gastric ulcers, has garnered considerable interest (148). Although deployed as H^+/K^+-ATPase inhibitors, PPI such as omeprazole and esomeprazole, also inhibit V-ATPase and can increase sensitivity to chemotherapeutics *in vitro* and *in vivo* (149, 150). However, it should be noted that the concentration of PPIs required to inhibit V-ATPase is considerably higher than for H^+/K^+-ATPase (151).

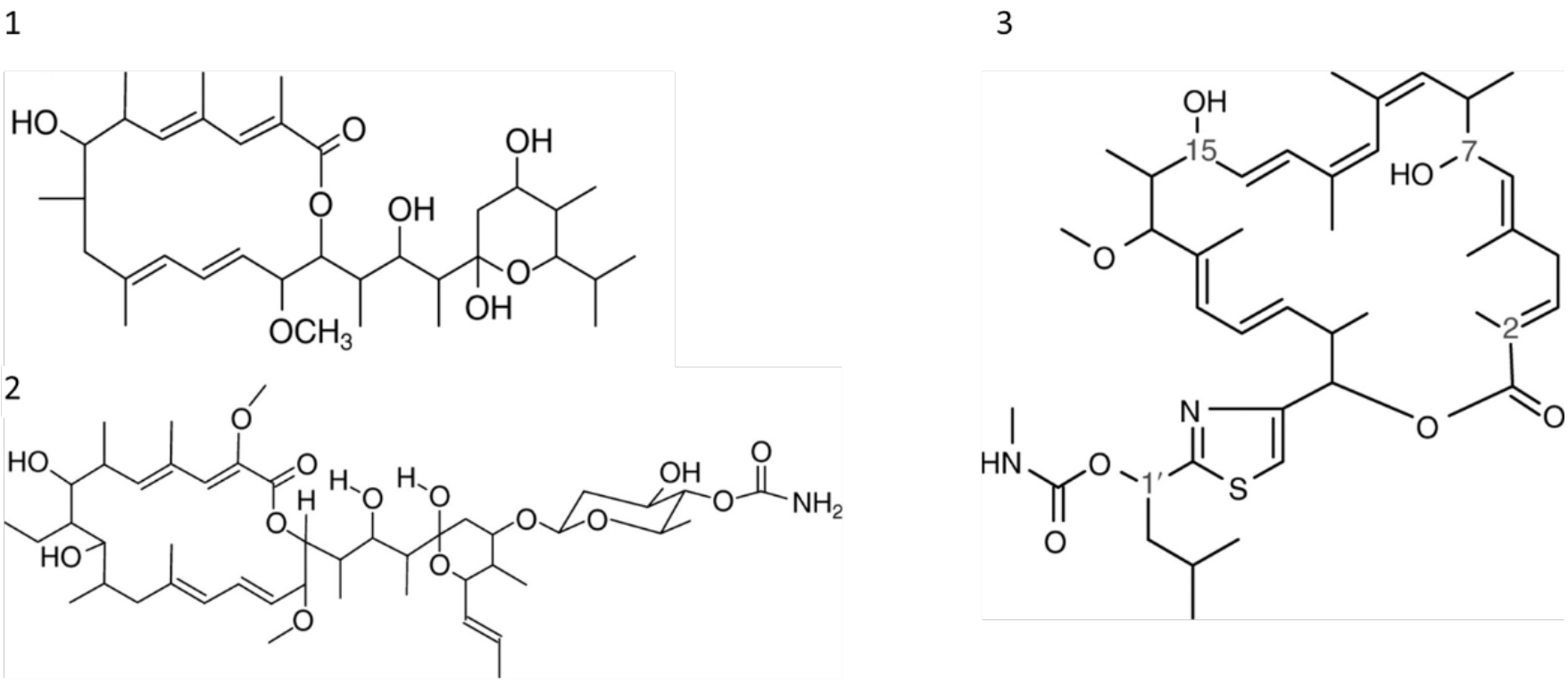

Figure 1-4. Chemical structures of bafilomycin-A1, concanamycin-A and archazolid

The chemical structures for (1) bafilomycin-A1, (2) concanamycin-A and (3) archazolid. Adapted from (130).

1.3.5 V-ATPase as a mediator of resistance for conventional cancer therapies

In addition to a role in cancer cell growth, survival, migration and invasion, V-ATPase dysregulation is also linked to therapy resistance. Indeed, it remains unclear whether correlations between V-ATPase (subunit) dysregulation and poor clinical outcome (Table 1-2) reflect an impact of V-ATPase on cancer cell behaviour per se versus a response to treatment. Effects of V-ATPase on drug responses may be explained, in part, by the reversal of the normal pH gradient between the cytoplasm and extracellular environment associated with overexpression of PM V-ATPases (75), and since, in some cases, lowering of extracellular pH protonates drugs leading to impaired cellular entry and/or vesicular trapping.

In breast cancer, V-ATPase inhibition was able to induce apoptosis in the trastuzumab resistant JIMT-1 cells, impair HER2 signalling and decrease HER2 surface expression. Moreover, treatment with archazolid significantly reduced the proportion of strongly HER2 positive cells and tumour growth in a JIMT-1 cell xenograft (152). Chemical V-ATPase inhibition was also shown to overcome Bcl-xL- and Bcl-2 mediated resistance in Ms-1 cells and induce apoptosis. Baf-A1 was able to supress the mitochondrial protective function of Bcl-xL and allow paclitaxel to decrease MMP levels (153). V-ATPase expression was found to be higher in cisplatin resistant cells than other drug resistant cell lines. It has been shown that baf-A1 and cisplatin had a synergistic effect on cell cytotoxicity, which was greater in cisplatin resistant cells than cisplatin sensitive (154).

Again, a potential role for V-ATPase in drug resistance has been demonstrated using siRNA ablation of specific subunits. *You et al* used siRNA targeting the ATP6L (V_oc) subunit in human drug resistant MCF-7/ADR breast cancer cells. The knockdown cells were more sensitive to chemotherapeutic agents such as doxorubicin and 5-FU than control MCF-7/ADR cells. ATP6L knock-down was associated with an increase of lysosomal pH (ie alkalinisation) and increased caspase-3/7 activity and PARP expression (155).

1.3.6 Role of V-ATPase modulatory proteins in cancer

In addition to the core V-ATPase subunits Figure 1-1, proteins which directly modulate V-ATPase activity have been shown to contribute to cancer progression. LASS2/TMSG1 is a negative V-ATPase regulatory protein which directly binds to the V_Oc subunit and was found to be inversely related to the metastatic potential of tumour cells (156). Furthermore, these modulatory proteins may also have a role in cancer therapy resistance. It has been demonstrated that the expression of LASS2/TMSG1 was

significantly lower in doxorubicin resistant MCF-7/ADR breast cancer cells than sensitive MCF-7 cells. LASS2/TMSG1 positive tumours had a positive correlation with disease-free and overall survival. Overexpression of LASS2/TMSG1 increased chemosensitivity to a number of chemotherapeutic agents in drug resistant MCF-7/ADR cells. Overexpression of LASS2/TMSG1 inhibited intracellular pH recovery and significantly decreased MCF-7/ADR cell migration due to the suppression of V-ATPase function via LASS2/TMSG1 binding to subunit V_Oc (157). Furthermore, the downregulation of a positive regulator of V-ATPase activity, TM9SF4, significantly inhibited tumour cell invasiveness and increased the cytotoxic effect of 5-FU in colon cancer cells. This group hypothesized that in malignant cancer cells TM9SF4 binds to the V_1H subunit, leading to stabilization of the V-ATPase complex and permanent activation of the enzyme (158).

1.3.7 Summary

There is emerging evidence to support a role for V-ATPase in cancer biology through impact on processes including cancer cell invasion, metastasis, and proliferation. Evidence also supports a potential link between V-ATPase and conventional cancer therapy and that V-ATPase may represent a direct anti-cancer target. Future work is still required to understand whether the expression of individual subunits represents a casual or causal relationship with cancer progression. It is also important to uncover whether there are other functional consequences of V-ATPase dysregulation in cancer and if more specific agents can be developed with more acceptable toxicity profiles.

1.4 Prostate cancer

Prostate cancer (PCa) is now the most common cancer in males in the UK with around 47,740 men diagnosed each year (159). It is an age related disease that is commonly diagnosed at the low risk localized stage and is often associated with a favourable survival rate (160). Initially, cancer cell growth is dependent on androgenic activation of the androgen receptor (AR). However, despite initial treatment success, recurrence occurs in a proportion of patients and some will progress to an advanced form of the disease. Most patients who develop the advanced disease will undergo hormone therapy in an attempt to limit the growth and spread of the cancer. Following castration, the disease will inevitably progress to a more aggressive prostate cancer phenotype known as castration-resistant prostate cancer (CRPC), which is currently incurable (161).

1.4.1 Classification of prostate cancer

The human prostate gland is located below the bladder and plays an important role in reproduction, producing several constituents of the seminal fluid. Early prostate development requires epithelial and mesenchymal interactions and is dependent on androgen production. Huggins Nobel prize winning work in the 1940s revealed that androgens are also central to prostate cancer development (162). The revolutionary work conducted by Huggins' and Hughes found that acid phosphatase activity (PAP) was higher in prostate cancer specimens and that PAP levels fell after castration. This indicated that PAP biomarker expression was dependent on androgen concentration (and thus AR function) and that castration led to an anti-cancer effect (162). Since then our understanding of the underlying mechanisms that drive PCa progression has greatly increased but treatment for advanced PCa remains critically dependent on androgen deprivation therapy.

1.4.1.1 Definition and classification of CRPC

CRPC by definition is the progression of prostate cancer following androgen deprivation therapy. In 2015, 41 prostate cancer experts concluded that a CRPC diagnosis should meet the following criteria: The circulating testosterone level is <1.7 nmol/l, and there should be an indication of biochemical progression. Biochemical progression is characterized by PSA expression levels that have 'increased twice in a row from an interval of 1 week or >3 consecutive measurements with the lowest value increased >50% and >2 g/l'. PSA is an AR transcriptional target, used clinically, as a measure of PCa activity, as it can be measured in blood. Further characterization of CRPC includes '≥2 increases in novel lesions based on bone scanning or soft tissue lesions with the corresponding evaluation criteria of the solid tumour' (163).

1.4.2 Androgen receptor physiology

The androgen receptor is a nuclear transcription factor that is important for both prostate cancer and normal prostate development. In all males, testosterone is the predominant androgen and it circulates in the blood. Once it enters prostate cells, around 90% is converted into the more potent ligand dihydrotestosterone (DHT) via the enzyme 5α-reductase. Although fundamentally studied with regards to the prostate, the AR plays a crucial role throughout the human body by regulating cell cycle processes such as cell division, differentiation and apoptosis (164). Therefore, dysregulation of AR signalling can lead to a number of different pathological conditions, which is why it is imperative that we fully understand every aspect of AR biology.

1.4.2.1 Androgen biosynthesis

Androgens belong to the steroid hormone family and are important for male phenotypic expression. Testosterone is the main circulating androgen and it is synthesized in Leydig cells in the testis from cholesterol. The synthesis of testosterone from cholesterol involves several steps, which first involves the transport of cholesterol to the inner mitochondrial membrane where it undergoes side chain cleavage by P450scc. This conversion results in the formation of pregnenolone and this is also the rate-limiting step in the biosynthesis pathway (165) shown in Figure 1-5. Testosterone is then metabolised to 5α-dihydrotestosterone by 5α-reductase type 2, which is an important step for the development and differentiation of the urogenital sinus into the prostate. This irreversible conversion of testosterone to DHT is also essential for the differentiation of male genitalia including the penis, scrotum and urethra (166). Both testosterone and DHT interact with the AR but have different binding affinities and characteristics. For example, testosterone has a two-fold lower affinity for the AR than DHT, and the rate of dissociation of testosterone from the AR is five-fold faster than DHT (167).

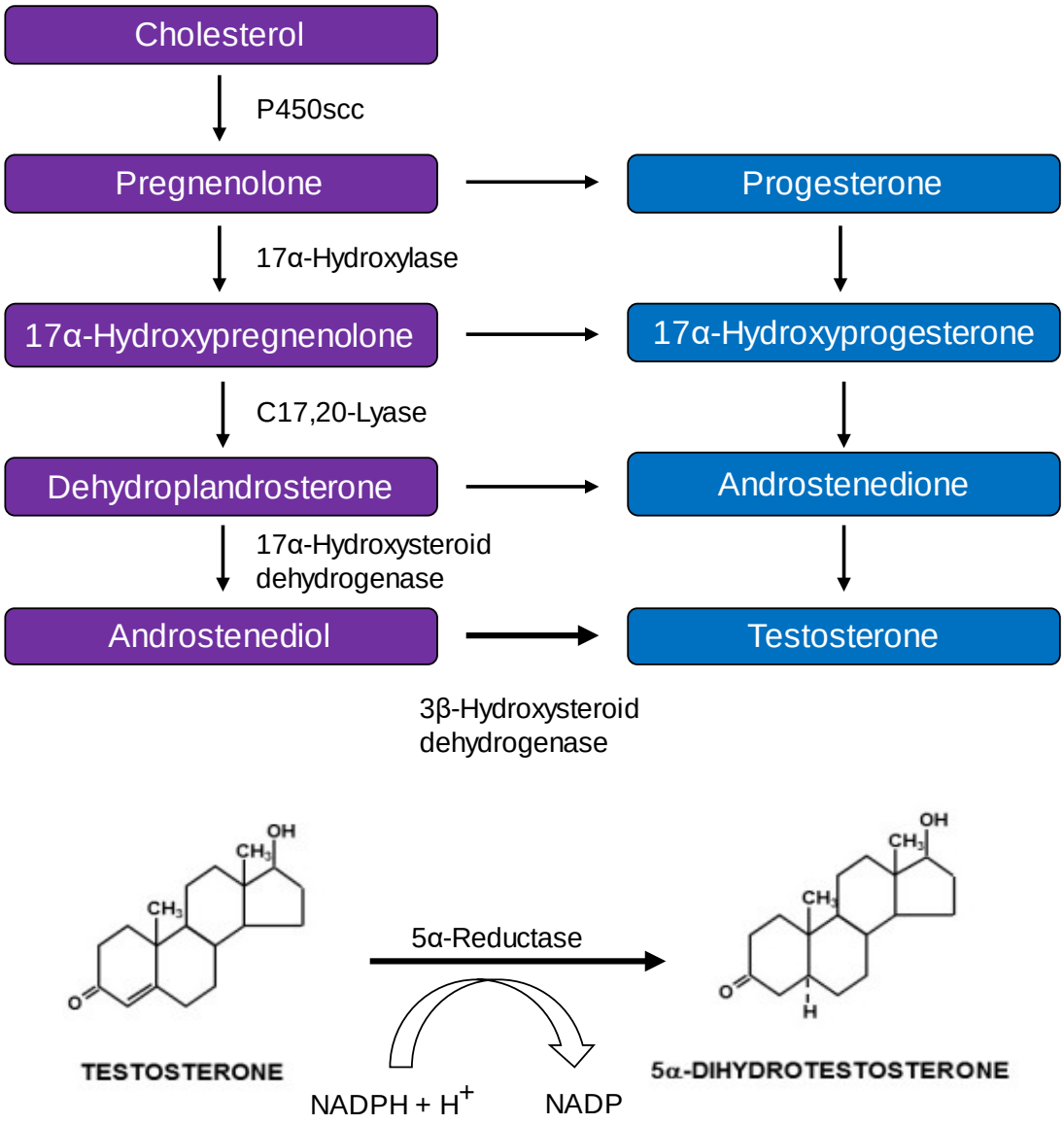

Figure 1-5. Testicular testosterone biosynthesis pathway

The testicular testosterone biosynthesis pathway results in the production of 5α-dihydrotestosterone (DHT) via the conversion of testosterone by 5α-reductase.

1.4.2.2 Nuclear receptor family

The activity of different androgens is mediated by the AR, which is a transcription factor belonging to a nuclear receptor superfamily. There are currently 48 known human nuclear receptors that respond to ligands including thyroid hormones, 1,25 dihydroxy-vitamin D, all-trans and 9-cis retinoic acid and steroid hormones. Some of the key steroid hormone receptors that share similar protein homology to the AR include the progesterone receptor, mineralocorticoid receptor, glucocorticoid receptor and the oestrogen receptors α and β (167). Additionally, there are a number of nuclear proteins that have been identified with an amino acid structure similar to that of nuclear receptors, but do not have a known ligand. These proteins have been termed 'orphan' receptors and they are a subfamily of transcription factors that act either without an endogenous ligand or in the absence of ligands (168).

1.4.2.3 The androgen receptor

1.4.2.3.1 Androgen receptor structure

The AR gene shown in Figure 1-6 is located on the X chromosome (Xq11-12) and spans 186,587 kilobases (kb), encoding a protein with a molecular weight of 110 kDa. It consists of 8 exons which encode four active domains: the DNA-binding domain (DBD), the ligand binding domain (LBD), the hinge region and N-terminal A/B activation domain (169). The AR also contains two activation functions (AF-1 and AF-2). AF-2 resides in the N-terminal A/B activation domain and responds to hormone-dependent activation, whereas AF-1 is located in the LBD and is hormone independent (170).

It should be noted that as of 17/05/19 the numbering of amino acids for the corresponding AR protein was recently updated based on a new NCBI reference sequence (NM_000044.6), which is different to the Gen-Bank sequence (M20132.1) used for the past 20 years (171). The polyglutamine tract is two amino acids longer, whereas the variable polyglycine tract is one shorter, resulting in an AR protein that is one amino acid longer (920 vs 919). This means that compared to the previous numbering system there is a +1 shift in all amino acids in the DNA binding domain and ligand-binding domain (Figure 1-6).

1.4.2.3.2 Androgen receptor regulation

Transcription of the AR is primarily driven by the Zn-finger transcription factor Sp1, which binds to GC-boxes within the 5'UTR and binds upstream of the transcription start site (172). Additionally, the promoter for the AR gene lacks CCAAT and TATA elements. Transcriptional control of the AR is under both negative and positive regulation (173).

Binding sites for ligand bound AR have been identified in the second intron and another negative androgen response element (ARE) has been found in the 5'UTR (174). In addition to hormonal regulation, there is an important balance between negative (Purα) and positive (Sp1) transcription factors binding to the 5'UTR of the AR, which determines AR mRNA expression (172). Uncovering the mechanisms of androgen-dependent down regulation is an on-going area of research.

1.4.2.3.3 Androgen receptor polymorphisms

Although the ligand-binding and DNA-binding domains of the AR have high homology with other members of the steroid receptor family, there is an intriguingly low homology observed for the N-terminal domain (175). There is a poly-glutamine stretch, which is encoded by a polymorphic (CAG)nCAA repeat that varies in length (9-38 glutamine residues) in the general population (176). This (CAG)nCAA repeat has been associated with modulation of androgen receptor activity and there is debate as to whether having shorter or longer repeat lengths can induce differential biological effects. Some studies have shown that shortening of this repeat can result in an earlier onset of prostate cancer, which is more aggressive and has a higher tumour grade (177). However, in other studies shorter repeat lengths have been found to have no overall biological effect (178). Furthermore, an association between longer repeat lengths and male infertility due to defective spermatogenesis was found, suggesting that the AR was less active. This (CAG)nCAA repeat is expanded in patients with spinal and bulbar muscular atrophy (SBMA) and is associated with an accumulation of AR protein in the nucleus, which results in patients frequently exhibiting endocrinological abnormalities (179).

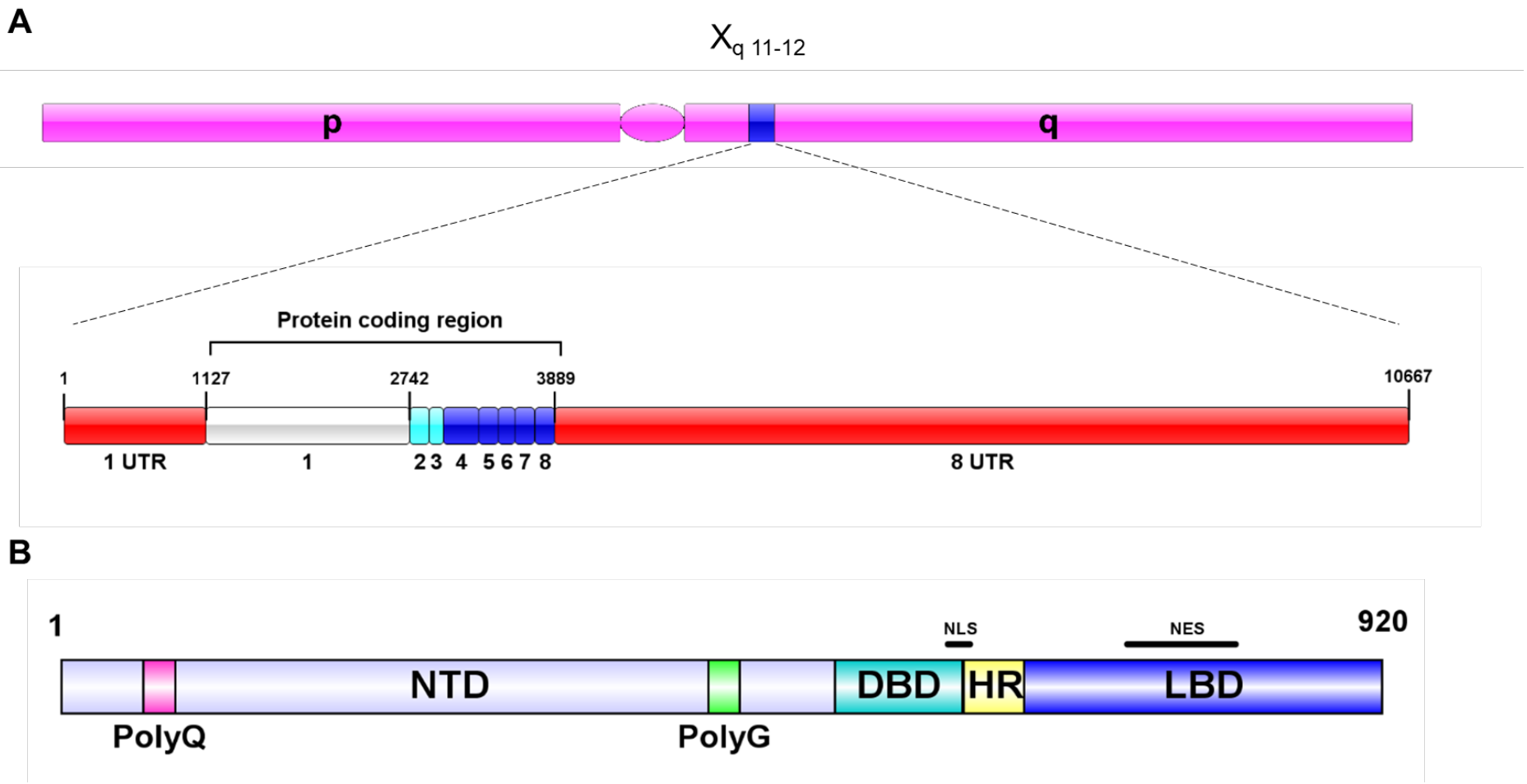

Figure 1-6. The androgen receptor

(A) The androgen receptor is located on chromosome $X_{q\ 11-12}$ and is encoded by exons 1-8; the exons 1 and 8 also both have long UTR's. (B) The N-terminal domain is encoded by exon 1, the DNA binding domain by exons 2-3 and the hinge region and ligand binding domain are encoded by exons 4-8. UTR, untranslated region; NTD, N-terminal domain; DBD, DNA binding domain; HR, hinge region; LBD, ligand binding domain; PolyQ, polyglutamine; PolyG, polyglycine; NLS, nuclear localisation signal; NES, nuclear export signal.

1.4.2.3.4 Androgen receptor post-translational modifications

The AR can undergo many post-translational modifications including acetylation, phosphorylation, methylation, ubiquitination or SUMOylation. These reactions are fully reversible and enzymes that mediate these modifications are consequently also potential modifiers of AR activity (180). The AR itself has 23 sites that have been identified as direct modulatory sites (Figure 1-7) and modifications at these key positions can influence AR structure, stability and activity (181). For example, the histone methyltransferase SET9 can methylate lysine residues 631 and 633 in the hinge region, resulting in an increase in AR transcriptional activity (182). Additionally, the same two residues and lysine 634 can be acetylated and mutants which are acetylation-deficient have been shown to have decreased transcriptional activity (183). Interestingly, disruption of acetylation led to receptor ubiquitination and degradation (184), highlighting the importance of post-translational modifications.

AR phosphorylation is the most studied post-translational modification and has been shown to have a number of functional effects. Phosphorylation of the AR can occur at threonine, tyrosine and serine residues (181). The AR becomes immediately phosphorylated after translation, leading to two isoforms that can be separated using SDS-polyacrylamide electrophoresis. The non-phosphorylated form is 110 kDa and once phosphorylated it is converted into a 112 kDa phospho-isoform. Two of the key residues that are likely responsible for AR phosphorylation are serine 83 and serine 96 (185). Furthermore, serine 83 phosphorylation was found to recruit histone acetyltransferase p300 and enhance receptor stability and transcriptional activity (186). Additionally, the presence of androgen induces another shift resulting in the formation of a 110-112-114 kDa AR triplet. This triplet is formed due to both an addition and re-distribution of phosphorylation sites (185). It has been shown that mutations that inactivate AR function inhibit the generation of the 114 kDa isoform, suggesting that part of the AR phosphorylation occurs during or after AR transcriptional regulation. Phosphorylation has also been demonstrated to occur at three tyrosine residues at positions 536, 365 and 269, which enhances cellular growth in an androgen-depleted environment (187, 188).

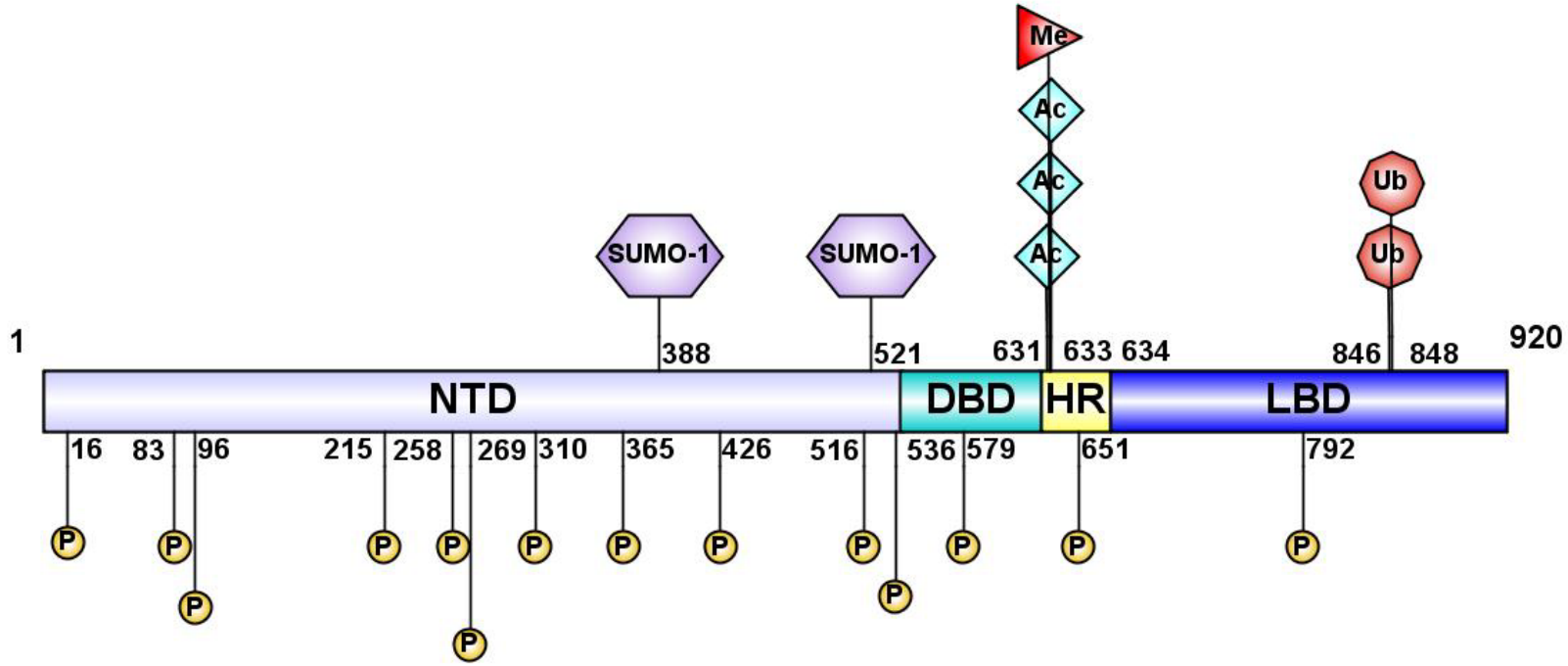

Figure 1-7. AR post-translational modification sites

Phosphorylation on serine residues (16, 83, 96, 215, 258, 310, 426, 516, 651, 792) and tyrosine residues (269, 365, 536); SUMOylation on lysine (388, 521); acetylation on lysine residues (631, 633, 634); methylation of lysine residue (633); and ubiquitination of lysine residues (846, 848). P, phosphorylation; SUMO-1, SUMOylation; Ac, acetylation; Me, methylation; Ub, ubiquitination; NTD, N-terminal domain; DBD, DNA-binding domain; HR, hinge region; LBD, ligand-binding domain.

1.4.2.4 Androgen receptor signalling

There are two main types of AR signalling known as genomic signalling and non-genomic signalling. Genomic signalling is often referred to as 'classical' signalling because it is the principal pathway of AR activation. When the AR is not bound to ligand, it is localized in the cytoplasm. This is where it associates with heat shock proteins (HSPs), which are thought to tether the AR to cytoskeletal proteins, securing it in the cytoplasm. When ligands such as DHT bind to the AR, it induces a conformational change forming the AF-2 binding surface, which results in dissociation from the HSPs and exposes a nuclear localization sequence (shown in Figure 1-6). This process then allows co-regulatory proteins to bind and induce dimerization and nuclear localisation (189). Although the AR primarily forms homodimers, it is also possible that it can form heterodimers with nuclear receptors such as TR4 (170). Once inside the nucleus the AR can bind to the major groove of androgen response elements and recruit additional co-regulatory proteins, resulting in the activation of target gene expression (190). There is an ever growing list of co-regulatory proteins being uncovered including ARA55, ARA70 and SRC-1 (169), some of which may prove to be ideal PCa therapeutic targets. Loss of ligand can result in the AR being re-tethered inside the cytoplasm or degraded by ubiquitination (191), demonstrating the high level of AR control and regulation. A summary of the genomic AR pathway is shown in Figure 1-8.

Many downstream transcriptional targets of the AR have been identified but none have been as well characterised as PSA. The PSA gene is a member of the family of genes which encode kallikrein-like serine proteases. Currently 15 kallikrein genes have been identified, which cluster at chromosome 19q13.3-13.4 and encode 5 exons (190). The PSA gene, *KLK3*, encodes a glycoprotein enzyme with a molecular weight of 33 kDa. In the prostate, the function of PSA is to inhibit semen coagulation by degrading high molecular weight proteins. PSA enters the serum only through leakage into the extracellular fluid. However, in prostate cancer the normal glandular structure is disrupted resulting in increased serum PSA levels (190). Another downstream AR transcriptional target is *TMPRSS2*. *TMPRSS2* is an androgen regulated gene, which encodes a type 2 transmembrane serine protease thought to be important in mammalian homeostasis (192). Furthermore, it is encoded by 5 domains and is highly expressed in normal prostate tissue (193). The *TMPRSS2* gene has been shown to be upregulated by androgens in prostate cancer cell lines and has reduced expression in androgen-independent prostate cancer cell lines (193). Additionally, *TMPRSS2* has also been shown to play a role in prostate cancer due to its ability to fuse with ETS family members, such as ERG, leading to the overexpression of ETS genes seen in many prostate cancer patients (194).

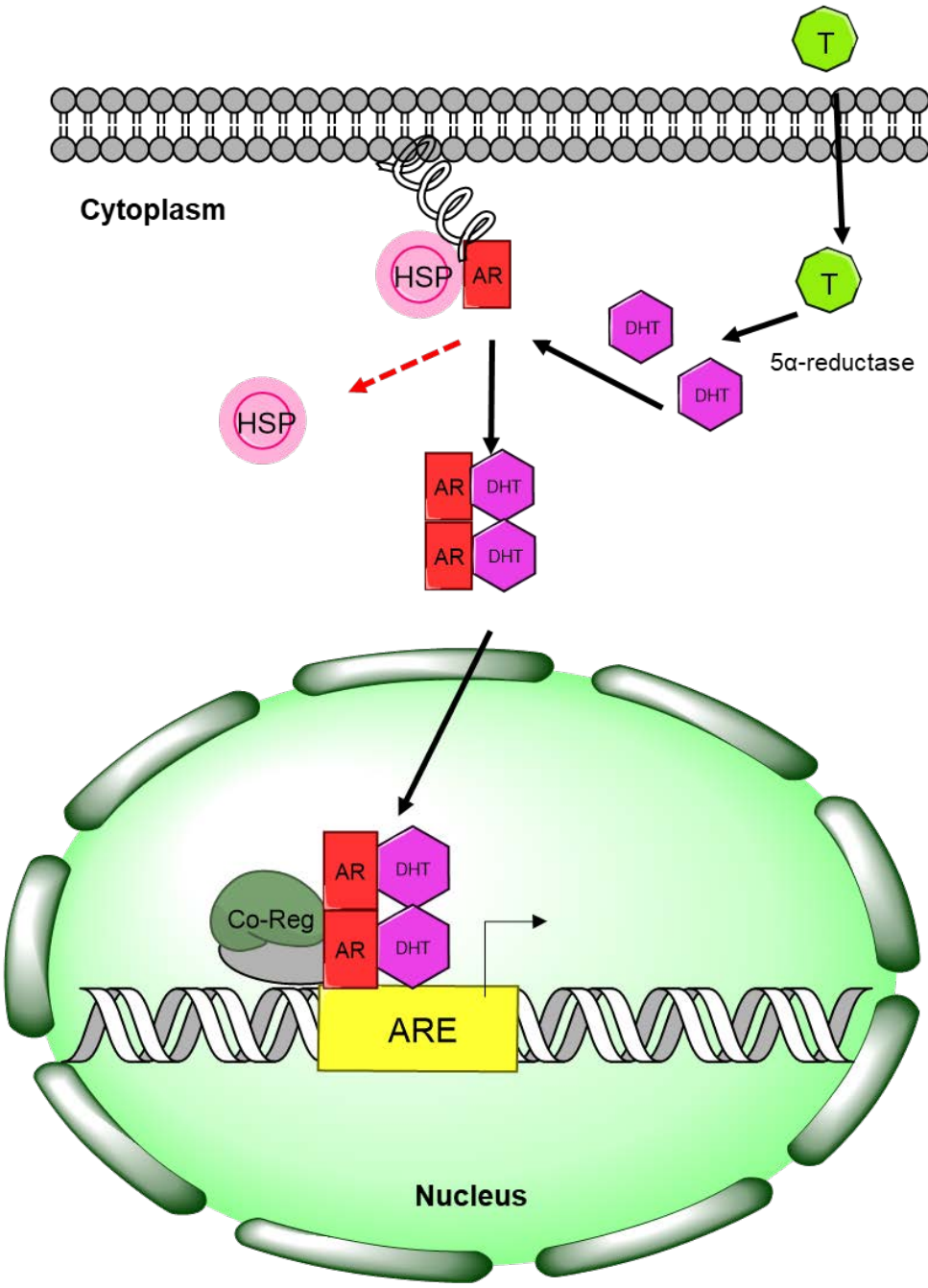

Figure 1-8. 'Classical' androgen receptor signalling

Testosterone (T) enters the cytoplasm and is converted to DHT by 5α-reductase. DHT then binds to the AR, releasing it from the HSP's tethering it to the cytoplasm. This dissociation exposes a nuclear localization signal, which induces dimerization and transport to the nucleus. The AR dimer binds to ARE's to upregulate AR specific genes such as PSA. Additional co-regulatory proteins bind to complete the transcriptional complex. Unbound AR can either be shuttled back to the cytoplasm via the nuclear export signal or it can be targeted for degradation in the proteasome. T, testosterone; DHT, dihydrotestosterone; AR, androgen receptor; HSP, heat-shock protein; Co-Reg, co-regulatory proteins; ARE, androgen response element.

Over the past few years mounting evidence suggests that the ‘classical’ AR signalling pathway has a non-genomic counterpart, which is summarised in Figure 1-9. This alternative signalling pathway becomes fundamentally important in cancer progression and has different characteristics than the ‘classical’ genomic pathway. Perhaps its most defining feature is the rapid speed in which the effects of non-genomic signalling occurs (secs/mins), compared to the slower speed (mins/hours) of genomic AR signalling (195). This is because it takes a long time for AR transcription and translation processes to occur, indicating that non-genomic signalling requires neither. It is also membrane mediated and does not require AR DNA binding for activation of target genes. Instead, AR can regulate gene transcription indirectly through the activation of different proteins and pathways including MAPK, PKA, PKC and PI3K, leading to the activation of various transcription factors (189). The most consistent effect of non-genomic activation is the rapid change in calcium levels, which is responsible for the quick response to androgen. Interestingly, it seems that the mechanisms that lead to an increase in calcium levels are different in different cell types. However, it is unclear whether the non-genomic effects are regulated by a distinct membrane-bound AR (195).

Additionally, the non-genomic signalling pathways regulated by the AR have also been shown to be able to independently regulate downstream AR transcriptional activity, indicating a possible feedback mechanism. The MAPK, PKA, AKT and PI3K pathways have all been implicated in the activation of the AR and ARE. Recent genomic profiling revealed that PI3K was altered in 42% of primary and 100% of metastatic prostate cancers (196). PI3K is an intracellular kinase which, when activated, can phosphorylate AKT and subsequently activate mTOR. Activation of this pathway leads to such downstream effects as cellular growth, survival, migration, proliferation and angiogenesis (197). The AR and PI3K pathway have in fact been found to operate a reciprocal negative feedback mechanism in which the suppression of AR signalling leads to an increase in PI3K activation, and vice versa (198). Loss of the tumour suppressor PTEN is the most common defect observed in this pathway, resulting in over-activation of AKT and enhanced progression to the CRPC phenotype (198).

Other signalling pathways such as the EGF, insulin-like growth factor, JAK/STAT and Wnt signalling pathways have also been associated with promoting persistent AR activity (199). Specifically, Wnt cross-talk with AR signalling pathways has been shown to be correlated with tumour aggressiveness (200). There are three main pathways that are activated as a result of Wnt receptor activation: the canonical pathway, the noncanonical planer cell polarity pathway and the Wnt/calcium pathway (201). However, the cross-talk with AR signalling appears to occur via β-catenin, which is a product of canonical pathway activation. β-catenin is responsible for the regulation of many target genes associated with

cell proliferation and apoptosis and can amplify AR transcription (202). Moreover, levels of β-catenin were found to be higher in invasive androgen independent cells compared to non-invasive androgen dependent cells, indicating Wnt signalling plays a role in CRPC (200). The complexity of the interacting AR signalling pathways is further increased by the fact that different pathways may interact differently in different cell lines. For example, in LNCaP cells, an androgen sensitive cell line, activation of the ERK pathway was androgen dependent, whereas in an androgen-independent LNCaP model, the ERK pathway was found to be constitutively active (203). Furthermore, in the androgen-independent PC-3 cell line, expression of the AR interfered with EGFR signalling and reduced invasion (204). This could imply that there is contrasting non-genomic activity when in fact cell lines may not be directly comparable. Dissecting the importance of the interactions between these pathways and the AR is extremely difficult as most of them also cross talk with each other. However, understanding the way in which the pathways interact has allowed the development of new-targeted therapies for PCa.

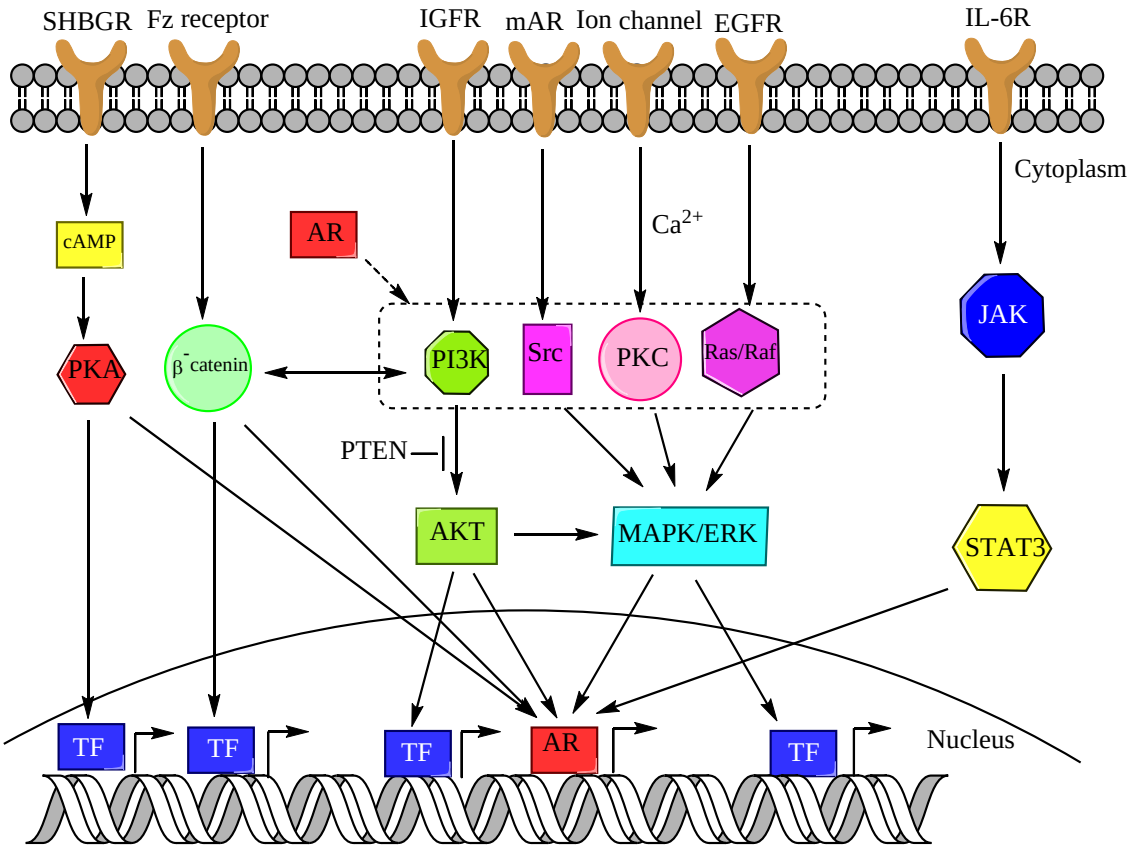

Figure 1-9. Non-genomic AR signalling pathways

The AR can indirectly regulate gene transcription via other signalling pathways. AR can activate the AKT pathway though direct interaction with PI3K, which can then activate the MAPK pathway. Akt activation may also lead to the phosphorylation of mTOR and FOXO1. Additionally, AR can interact with Src, PKC and Ras/Raf leading to the activation of MAPK pathway and phosphorylation of ERK. These signalling pathways regulated by the AR are also capable of independently regulating AR transcriptional activity. The SHBGR along with GPCRs may act to modulate intracellular calcium levels by increasing cAMP levels. Increased cAMP may then increase PKA and PKC activation, which can subsequently activate the AR and other transcription factors inside the nucleus. Furthermore, the JAK/STAT pathway and Wnt pathway have both been shown to regulate AR transcriptional activation. TF, transcription factor; AR, androgen receptor; AKT, protein kinase B; PI3K, phosphoinositide 3-kinase; MAPK, mitogen-activated protein kinase; mTOR, mechanistic target of rapamycin; PKC, protein kinase C; ERK, extracellular receptor kinase; SHBGR, sex hormone binding globulin receptor; GPCR, G-protein coupled receptor; cAMP, 3',5'-cyclic adenosine monophosphate; JAK/STAT, janus kinase/ signal transducer and activator of transcription protein; Src, steroid receptor co-activator; Fz, frizzled; IGFR, insulin-like growth factor receptor; EGFR, epidermal growth factor receptor; IL-6R, interleukin-6 receptor.

1.4.3 Prostate cancer diagnosis

Historically PCa has been difficult to diagnose but the discovery of the prostate specific antigen (PSA) revolutionized clinical diagnosis. Although measuring PSA levels is not a good screening test due to large variability between individuals, it is still a useful biomarker for prostate cancer detection and for monitoring treatment success. Moreover, digital rectal examinations (DRE) are also routinely used to detect the presence of PCa. Despite the fact that an abnormal DRE is a good diagnostic indicator of PCa and rising PSA levels are directly correlated with PCa risk, the diagnosis of PCa is dependent on histopathologic confirmation. This requires single or multiple transrectal ultrasound (TRUS)-guided biopsies which are then usually evaluated using the Gleason score. The Gleason score involves assigning a number between 1 and 5 based on how similar the cells in the cancerous tissue appear to resemble cells in normal prostate tissue. For example, a score of 1 means the cancerous tissue closely resembles normal prostate tissue and a score of 5 means that it does not, or only slightly, resembles normal prostate tissue. Two scores are usually taken, which reflect the 1st and 2nd commonest grade because the disease is commonly heterogeneous through the prostate, and they are combined to give the final Gleason grade between 2 and 10 (occasionally also a tertiary score is given but only the first 2 are combined). However, biopsies can be invasive and unnecessary, therefore the need for a biopsy is determined by several factors including: PSA level, result of DRE, biologic age and potential comorbidities of the patient (205). In addition to this, other factors are necessary for accurate PCa diagnosis including the primary tumour status, which ranges from organ restricted to the invasion of other organs (T1-4). The involvement of regional lymph nodes (N0 or N1) and the presence of metastasis (M0 or M1) are also important factors in diagnosis. It is interesting to note that there is currently no evidence to support nationwide early prostate cancer screening programmes in all men despite the high frequency of cases.

1.4.4 Risk factors

Prostate cancer is a highly heterogeneous disease and cannot be attributed to a single cause. Many factors have been linked to prostate cancer development with varying levels of risk associated with each. The first and probably most significant risk factor is an individual's age. The highest rates of prostate cancer are in older men and only 1% of patients in the UK are diagnosed under 50. Incidence rates rise sharply in the 50-54 group and peak in the 75-79 age group. However, prostate cancer is not just a consequence of ageing as the incidence varies across populations. It is believed that the interplay between genetics and the environment plays a significant role in cancer progression. The fact that

ethnicity is a major risk factors demonstrates this, with black males having a significantly higher risk than white males and Asians (159). Inflammation, oxidative stress (primarily imbalance of reactive oxygen species), telomere shortening and cellular senescence have also all been linked to PCa initiation (206).

There are many genetic and epigenetic alterations that are commonly associated with the incidence of aggressive prostate cancers. Genetic abnormalities within families can lead to a hereditary form of prostate cancer that begins on average 6-7 years before the more common sporadic form (207). Furthermore, germline mutations in the DNA repair genes *BRCA2* and *BRCA1* have been found to be associated with increased prostate cancer risk (208). Other germline mutations in genes associated with DNA repair pathways such as *ATM, CHEK2, PALB2, MSH2* and *MLH1* also appear to contribute to PCa risk (208). Interestingly, it was recently found that the incidence of germline mutations in DNA repair genes was significantly higher in individuals with metastatic disease than those with localized prostate cancer (209). Genome-wide association studies (GWAS) have identified many SNPs linked to cancer risk with one of the most significant considered to be the *C154T* polymorphism in the *NKX3.1* gene. The *NKX3.1* gene is androgen regulated and is critical for the regulation of prostate epithelial cell differentiation; it is frequently downregulated or lost in almost all PCa cases (210). Epigenetic alterations, such as chromatin modifications, have also been shown to be key in carcinogenesis and may be useful as biomarkers in the future. For example, one important alteration is the tri-methylation of lysine 27 in histone H3, which is associated with the repression of vital tumour suppressor genes (211).

Although these risk factors are considered largely unmodifiable, there have been studies that link dietary and lifestyle factors to PCa development. Smoking, UV exposure and BMI all appear to correlate with PCa progression (212). In fact, one study revealed that individuals who are underweight (BMI <22.5 kg/m^2) have a risk of prostate cancer specific mortality that is almost as high as those who are overweight (BMI ≥27.5 kg/m^2) (213). The degree to which environmental factors contribute to PCa progression is not fully understood and there may be many other factors that increase the overall lifetime risk of PCa.

1.4.5 Treatment of localised PCa

The treatment of prostate cancer, even at the localized stage, is widely debated and is becoming increasingly complex. To help overcome this complexity, the European Association of Urology (EAU) have published guidelines to help standardize classification, diagnosis and treatment of PCa. Moreover, the treatment of localized PCa is generally

based on the risk of patient mortality, which can be divided into low, intermediate and high risk (214).

It is recommended by the EAU that patients with very low risk PCa are not initially treated, and instead a management approach referred to as active surveillance (AS) should be used to monitor potential PCa progression. This solution was designed with the consideration that early PCa patients have a high survival rate and there is a risk of overtreatment in these patients. AS is used to identify the minority (in those it is suitable) who develop clinical stage or histological grade progression so that they can be selected for radical (curative) treatment whilst sparing the majority (who undergo AS) that will never need treatment. For example, AS might be an appropriate option for patients under 70 years of age or those with a life expectancy greater than 10 years (214). The eligibility criteria for patients suitable for AS can generally include the following: patients with a clinically organ confined PCa, a Gleason score of 6 or below, three or fewer biopsies with cancer (where 12 biopsies are normally taken), less than 50% of each biopsy with cancer and a PSA level below 10 ng/mL (214). An alternative to AS is watchful waiting (WW), which is used for patients who are not suitable for radical treatments (207). Watchful waiting is primarily used to control the disease and manage symptoms without curative intent, thereby deferring treatment until intervention is actually required because (as with AS) a proportion will never need treatment. These treatments are required because cancers are discovered that may not need treatment as a result of wide use and availability of the PSA test, which has poor qualities as a screening investigation.

Despite the EAU guidelines there is still confusion concerning how to define cancer progression. Most of this confusion derives from different words and phrases being used to describe the same thing. In general, the criteria used for progression during AS includes a Gleason score ≥ 7 at re-biopsy and PSA progression above 10 ng/mL. In patients that meet this criteria, radical prostectomy (RP) can be used to treat PCa progression. Radical prostectomy is the only surgical treatment available for localized disease and has shown a survival benefit compared to WW. In fact, nerve sparing RP is usually the treatment of choice for men with intact erectile function (214). Alternatively, radiation therapy can also be used, with external-beam radiotherapy (EBRT) being the most commonly used (207). The ProtecT trial evaluated AS, RP and EBRT as viable treatment options and found that the disease progression for patients treated with either RP or radiotherapy was significantly lower than those assigned to AS. This shows that there is a clear benefit to using immediate radical treatment over AS. However, the study revealed that prostate cancer specific mortality was low at 1% after 10 years follow up and that there were no significant differences in mortality between treatments. Therefore,

despite reduced disease progression as a result of radical therapy, the results did not translate into an overall reduction in patient mortality (215).

Advances have led to improved prostate specific radiation treatment options and the EAU now suggest that image-guided intensity-modulated radiation therapy (IMRT) should be the standard treatment for localized PCa. Furthermore, transperineal brachytherapy is another option that is considered safe and effective with high recurrence-free survival rates after 5 years (214). Intermediate and high risk PCa cases are even more complex and at the moment there is no clear consensus on which treatment approach is the most effective. A multi-disciplinary approach is recommended for tackling high-risk disease due to the likelihood that a large number of patients will have lymph node metastasis. Much like with low risk disease, RP can be used and is considered a logical first choice therapy. However, in patients with T3 stage cancer, experienced surgeons are required to keep the morbidity low and to perform lymph node dissections.

1.4.6 Initial treatment of metastatic and advanced PCa

PCa is largely a hormone driven cancer and therefore castration is a common treatment for recurring locally advanced and metastatic cancer. Castration can either be surgical or chemical and aims to deplete the patient's androgen levels. Surgical castration is known as orchiectomy, which involves the removal of both of the testicles and can result in side effects such as decreased libido and impotence (207). Obviously this is aesthetically challenging for many men, which is why chemical castration is almost exclusively used instead. Luteinising hormone-releasing hormone (LHRH) analogues and antagonists are hormonal treatments that are commonly used to slow cancer progression and reduce the size of the tumours (216). Analogues over-stimulate the LHRH receptors causing the pituitary gland to stop producing LHRH via a negative feedback mechanism. On the other hand, LHRH antagonists rapidly decrease LHRH and testosterone levels, completely depleting the androgen without a testosterone 'surge'. The LHRH analogues are more commonly used in standard care because the process is reversible so androgen depletion therapy (ADT) can potentially be used intermittently (216).

AR antagonists such as flutamide and bicalutamide can be used as an alternative hormonal therapy. They can also slow the progression of PCa and are often initially given in combination with LHRH analogues to reduce the negative effects of surging testosterone levels (often referred to as testosterone flare) (216). The combination of both is quite controversial and leads to a more complete androgen blockade. Several studies have reported a 3-9% survival advantage compared to LHRH monotherapy, whereas others have reported no significant increase in 5 year survival rate (217). Both sides of the argument rely heavily on patient cohorts as different treatments have varying levels of

effectiveness depending on the stage and aggressiveness of the cancer. It does appear that combination with antiandrogens may be more effective than LHRH alone but the additional negative side effects reduce patient benefit (216, 218). ADT is therefore initially successful and can result in remission of the tumour for several years.

Chemotherapeutic agents such as docetaxel are also used as an initial treatment for advanced disease. It was recently found that when docetaxel treatment was given at the same time as ADT in hormone sensitive PCa it resulted in reduced PCa deaths, longer progression time to CRPC and longer overall survival, compared to ADT alone (219). Furthermore, the STAMPEDE trial comparing standard of care (ADT for at least 2 years), zoledronic acid with standard of care, docetaxel with standard of care, or all three combined also showed a clear survival benefit of using docetaxel with ADT. In fact, the authors of the study advised that docetaxel should be an addition to the standard of care for patients undergoing long-term ADT (220).

Although ADT is a good palliative treatment for advanced PCa, patients will inevitably progress to the castration-resistant phenotype. Figure 1-10 illustrates the treatment options available for various stages of PCa progression. Due to the fact that the AR is the main driver of PCa progression, many treatments for CRPC are aimed at targeting the AR and its associated signalling pathways.

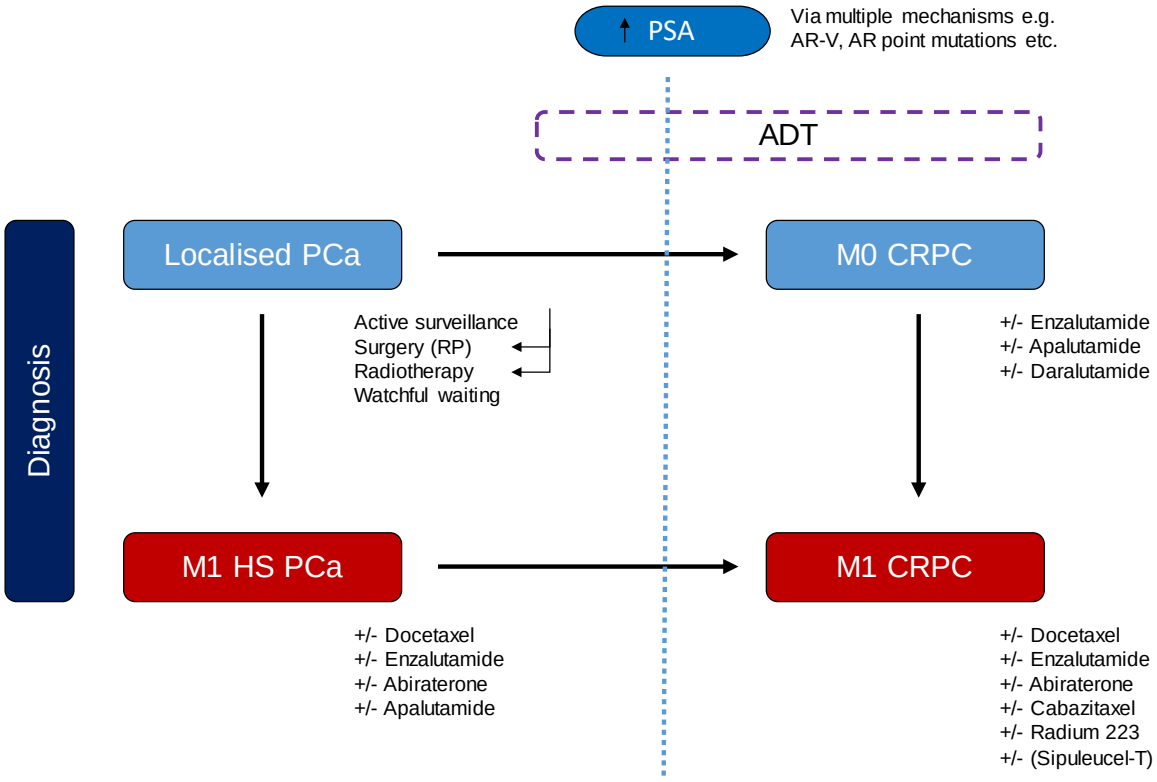

Figure 1-10. Simplified schematic of treatment options available for PCa

PCa can be initially diagnosed at either the localised or metastatic stage. At this point the disease is hormone sensitive and potentially curative. Options available include active surveillance, radiotherapy (with or without hormone therapy), surgery and watchful waiting. Some patients may progress to the advanced stage, which is still hormone sensitive and hormone therapy is administered as standard practise (with or without chemotherapy). On the other hand, a subset of patients may develop metastatic disease but the cancer may remain hormone sensitive, in which case treatments such as docetaxel, enzalutamide, abiraterone or apalutamide may be given. Inevitably, some patients will progress to the castrate resistant phenotype, which is incurable and not hormone sensitive by definition. This is usually due to an increase in a variety of different adaptive molecular mechanisms, in which tumours continue to grow despite castrate levels of androgen. Some of the molecular mechanisms responsible for this include the emergence of AR splice variants and point mutations, usually accompanied by an increase in circulating PSA levels. Hormone therapy is still given to CRPC patients but is combined with other treatments such as chemotherapy (docetaxel, cabazitaxel), AR antagonists (enzalutamide), antiandrogens (abiraterone), radium-223, and others. PCa, prostate cancer; CRPC, castration resistant prostate cancer; ADT, androgen deprivation therapy; PSA, prostate specific antigen; HS, hormone sensitive; M1, metastatic; M0, non-metastatic; RP, radical prostectomy.

1.4.7 Treatments for castration resistant prostate cancer

Once an individual progresses to CRPC or metastatic CRPC (mCRPC), treatment options are limited and none of which are curative. However, many new treatments are being evaluated in phase III trials and are becoming available to patients. Established treatments for mCRPC include docetaxel, cabazitaxel, radium-223, sipuleucel-T and hormonal therapies (Figure 1-11) (216).

1.4.7.1 Chemotherapeutic agents

Docetaxel was the first therapy to show an improvement in overall survival rates in mCRPC patients in two significant phase III trials (221, 222). It is a taxane based chemotherapeutic agent that works by binding to the β-tubulin subunit of microtubules, which stabilizes the mitotic spindle during mitosis and interphase, resulting in an arrest of mitosis and consequently cell death (223). It is commonly administered intravenously every three weeks at a dose of 75 mg/m^2 for 10 cycles (224). Side effects are comparable to other chemotherapeutic agents and include vomiting, nausea and cytopenias.

Cabazitaxel is another taxane based chemotherapeutic agent approved for use in mCRPC patients, which causes cell death due to microtubule disruption (225). Therefore, side effects are similar to docetaxel and include nausea, diarrhoea, fatigue and neutropenia. This therapy was originally selected to counteract the emergence of taxane resistance and, after the results of the phase III TROPIC trial, it became approved by the FDA as a second-line treatment post-docetaxel. TROPIC showed that cabazitaxel treatment conferred a survival advantage when combined with prednisolone compared to prednisolone and mitoxantrone (226). A further two phase III trials have investigated the efficacy of cabazitaxel, which are called FIRSTANA and PROSELICA. FIRSTANA examined whether two doses of cabazitaxel (20 and 25 mg/m^2) was more effective in improving the overall survival rate of chemotherapy-naïve mCRPC patients than docetaxel (75 mg/m^2). Results from FIRSTANA showed that cabazitaxel did not show a significant improvement in overall or progression free survival rates compared to docetaxel, but did show that tumour responses were higher for cabazitaxel and that is was tolerated better than docetaxel (227). PROSELICA was designed to compare the efficacy of two concentrations of cabazitaxel (20 vs 25 mg/m^2) in mCRPC patients who had been previously treated with docetaxel. Results showed that the lower dose of 20 mg/m^2 retained approximately 50% of the overall survival benefit of 25 mg/m^2 (228).

1.4.7.2 Hormonal therapies

Abiraterone acetate is an irreversible cytochrome p450 17A1 (CYP17) inhibitor that blocks steroid biosynthesis and extra-gonadal androgen synthesis, including intra-tumoural androgen synthesis (229). It can be administered orally and taken at 1000 mg/day, usually with prednisolone. Common side effects include hypokalaemia, fluid retention and hypertension, which are due to increased mineralocorticoid levels resulting from blocking CYP17 (230). Phase III trials have shown that abiraterone significantly improves survival rates and increases time to PSA progression in metastatic CRPC, either pre-(231) or post-(232) docetaxel treatment. This is a successful hormonal therapy and shows that despite the fact the cancer is no longer sensitive to systemic androgens (i.e. castrate resistant), it still expresses the AR, making the AR a viable therapeutic target. Furthermore, pre-clinical data indicates that abiraterone is metabolised to generate an AR antagonist that is as effective at blocking the AR as enzalutamide, suggesting it may affect the AR both directly and indirectly (233).

Enzalutamide acts as an effective irreversible AR antagonist and has an AR binding affinity that is ten times higher than that of its first generation counterpart bicalutamide (234). As an efficient AR antagonist, enzalutamide has the ability to reduce the nuclear translocation of AR, disrupt the activity of AR coactivators and can prevent the AR from binding to ARE's. The AFFIRM trial compared enzalutamide to a placebo arm and found that enzalutamide reduced the risk of death by 37% (235). In addition to this, results from the PREVAIL trial showed that after 12 months progression-free survival was 65% in patients treated with enzalutamide compared to 14% of patients receiving placebo. Enzalutamide treatment also had a significant benefit for all secondary end-points including time until PSA progression (236).

There is no clear benefit to selecting abiraterone over enzalutamide or vice versa as both are well tolerated. Therefore, selection usually depends on patient preference and comorbidities. For example, abiraterone is generally not used in patients with cardiovascular disease due to the side effects resulting from increased mineralocorticoid levels, but may be preferred in patients who have jobs that require a high level of intellectual ability (237). A few studies have shown that some patients respond to abiraterone post-enzalutamide and enzalutamide post-abiraterone (10-15%) (238), however in general response rates are lower than predicted due to cross-resistance mechanisms that include the emergence of AR splice variants (232, 239).

1.4.7.2.1 Novel antiandrogens

Apalutamide (ARN-509) is an AR antagonist that has a binding affinity five-times higher than bicalutamide and has greater efficacy in xenograft models (240). Results from a phase II trial in high-risk CRPC patients showed 89% of patients had ≥50% PSA decline at 12 weeks (241). It has been evaluated in phase III studies for non-metastatic CRPC (SPARTAN) and hormone sensitive metastatic PCa (TITAN). Results from the SPARTAN trial found that time to progression and metastasis-free survival was significantly longer compared to a placebo (242). The first results from the TITAN trial were recently published and show that in patients with high- and low-volume disease, with or without prior docetaxel treatment, the addition of apalutamide to ADT significantly improved progression free survival and overall survival. It also had an acceptable safety profile and supports the use of apalutamide with ADT for patients with hormone sensitive metastatic PCa (243).

Darolutamide is another AR antagonist that has a greater binding affinity than both enzalutamide and apalutamide. It is has been shown to be effective in phase I and II clinical trials (ARADES) in patients with mCRPC (244). Recently the results from a phase III clinical trial have been published, which examined darolutamide in non-metastatic CRPC (ARAMIS). The results from ARAMIS were that darolutamide treated patients had a median metastasis-free survival of 40.4 months compared to 18.4 months with a placebo. There were also benefits associated with all secondary endpoints (245). Currently there is another phase III underway that is investigating the impact of darolutamide in patients with mCRPC (ARASENS) (246).

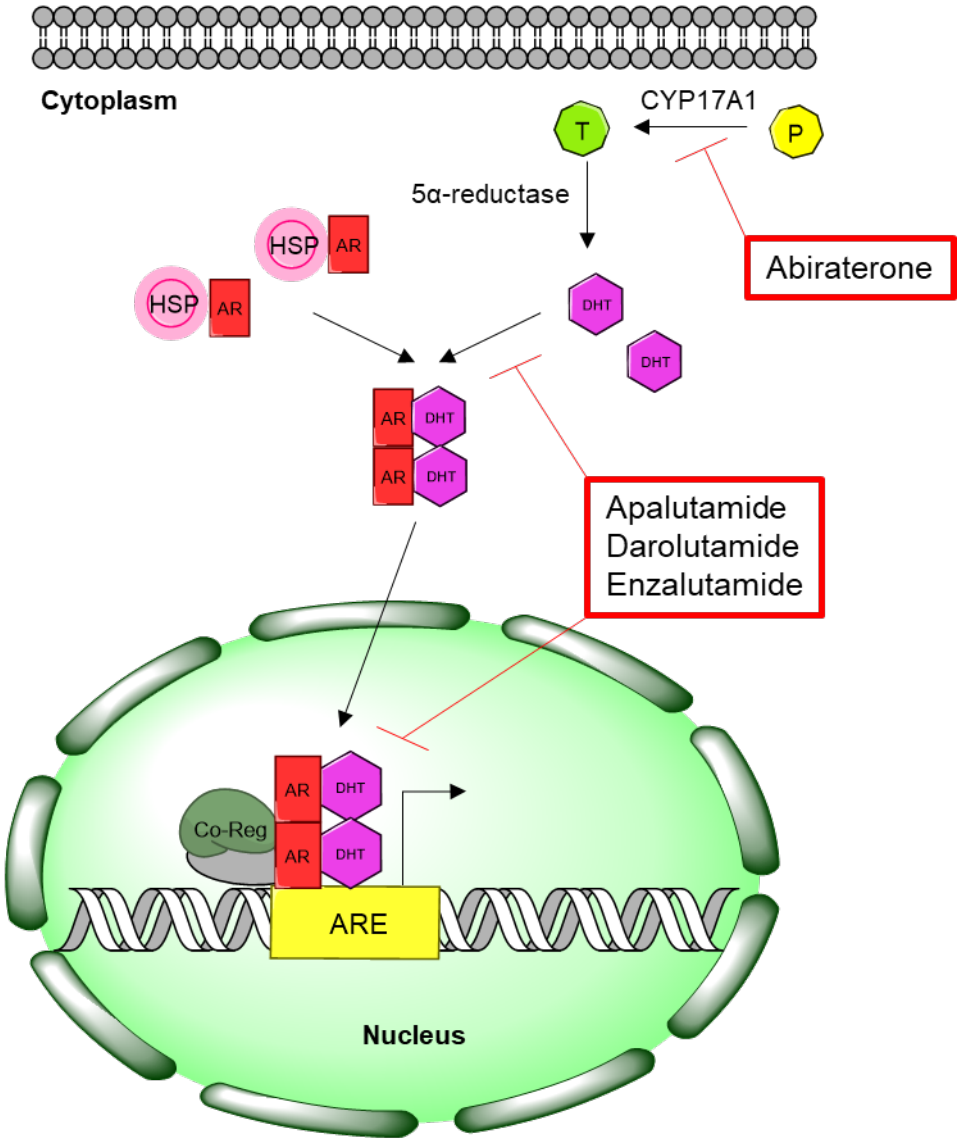

Figure 1-11. Hormonal therapies for prostate cancer

A summary of the hormonal therapies established for the treatment of prostate cancer. Abiraterone is an inhibitor of CYP17A1 and prevents the biosynthesis of testosterone. Apalutamide, darolutamide and enzalutamide are all AR antagonists, which can reduce the nuclear translocation of AR, disrupt the activity of AR coactivators and can prevent the AR from binding to ARE's. P, steroid precursor; T, testosterone; DHT, dihydrotestosterone; AR, androgen receptor; HSP, heat-shock protein; Co-Reg, co-regulatory proteins; ARE, androgen response element.

1.4.7.3 Other therapies

Radium-223 is a bone seeking radioisotope that emits high-energy radiation in a localised area, resulting in double strand DNA breaks in tumour cells. ALSYMPCA was a phase III trial that demonstrated a significant improvement in overall survival in patients who received radium-223 compared to a placebo. Additionally, as it is a localised treatment, side effects are minimal and it was well tolerated. Common side effects include gastrointestinal upset, fatigue and bone pain. It is important to note that ALSYMPCA included symptomatic mCRPC patients with bone metastasis, as it is a calcium mimetic so localises to bone, and therefore it is not a recommended treatment for patients who have disease outside of their skeleton (247).

Another therapy approved by the FDA for the treatment of mCRPC is sipuleucel-T, which is the first therapeutic cancer vaccine, and currently the only immunotherapy, approved for use in prostate cancer. It is a dendritic cell vaccine that involves first extracting mononuclear cells from a patient's peripheral blood using leukapheresis. The antigen presenting cells are then activated ex-vivo using a protein called PA202, and the activated cells are transfused back into the patient, triggering the activation of the patients own immune system (248). Results have been encouraging and a small phase III trial showed an improvement in overall survival of more than four months compared to a placebo (249). However, the drug is very expensive and costs approximately $35,000 per cycle (250), meaning that it is not widely used. It also has a large number of side effects associated with the treatment including bleeding, bruising, rigors, pyrexia, fatigue, nausea and headaches.

There are additional treatments that are available for reducing skeletal related events such as denosumab (a monoclonal antibody against RANKL) and zoledronic acid. In terms of clinical use, zoledronic acid is the standard treatment, although a recent study showed that denosumab is more effective at delaying skeletal-related events in some patients (20.7 vs 17.1 mo) (251).

1.4.8 Adaptive responses and drug resistance

Despite the success of targeted drugs, resistance can develop quickly and AR activation continues to persist. It is believed that malignant PCa cells will ensure AR signalling persists by undergoing numerous adaptive changes to maintain the AR axis. The exact mechanisms of how PCa cells can escape and evade the tight regulatory controls are not known, nor fully understood. However, a number of mechanisms have been suggested including alterations to the AR, persistent levels of androgen, growth factors, AR

coregulators, alternative signalling pathways and AR splice variants (252). Alterations to the AR itself can be further separated into AR gene amplification, AR overexpression, AR mutations and splice variants.

1.4.8.1 AR gene amplification and overexpression

An increase in AR protein levels is a hallmark of progression to CRPC, which is presumed to accelerate AR signalling. The increase in AR protein levels is partly due to an increase in AR gene amplification and overexpression (253). Firstly, *Visakorpi et al.* found that AR amplification occurred in 30% of recurrent prostate cancer patients, but was not seen in untreated primary carcinoma samples. Their findings suggest that AR amplification can occur as a result of selection during ADT and that the tumour adapts to the low level of androgen through an elevated AR copy number (254). Although this is a very important finding, as you would expect AR gene amplification to result in increased AR levels, this is not always the case. One study found that there was no increase in AR copy number in the transition from the hormone sensitive to the castration resistant stage. Furthermore, additional studies have proposed that the AR is self-regulating and can bind to the AR gene, increasing AR mRNA levels (255).

1.4.8.2 AR adaption though translational regulation

Another mechanism that may lead to an increase in AR signalling is regulation through post-transcriptional modulation of AR expression. As shown in Figure 1-6, the AR has a long 3'UTR, which is bound by RNA binding proteins. PolyC-binding proteins (PCBPs) and Hu antigen R are key RNA binding proteins that have been found to regulate translation of AR mRNA by binding the AR 3'UTR (256). Additionally, PCBP1 was shown to block AR translation in endometrial cells, which was confirmed in LNCaP cells (257). ErbB3 binding protein (EBP1) is another posttranscriptional inhibitor of the AR that binds to the UC-rich 3'UTR and an RNA stem-loop, which encodes the polyglutamine stretch in the AR N-terminal (258). Interestingly, binding of EBP1 to the UC-rich 5'UTR results in mRNA decay, whereas binding to the RNA-stem loop initiates translation. It was also found to be downregulated in advanced prostate cancer and inhibited prostate cancer growth when overexpressed (259, 260). Furthermore, the ribonucleoprotein transcriptional enhancer complex assembled by midline 1 (MID1) has recently been shown to enhance translation of the AR, and MID1 knockdown resulted in a reduction of AR protein expression. Although MID1 modulates the AR via translation control, the AR is also a negative regulator of MID1, and therefore forms a regulatory feedback loop. This represents a mechanism responsible for AR protein homeostasis and MID1 is overexpressed in prostate cancer in a stage-dependent manner (261).

1.4.8.3 AR mutations

Mutations in the AR are rare during the early stages of PCa progression, particularly in un-treated localised PCa, but become more prevalent after hormonal therapy and in CRPC (262). There are over 100 established AR point mutations, which are mainly found to occur in the N-terminal domain (~37%) and the ligand-binding domain (~49%) (263). Gain-of-function mutations, particularly in the ligand-binding domain, may provide a growth advantage despite castrate levels of AR ligands and the presence of anti-androgens. Some of the most well characterised AR mutations include L702H, W742C, H875Y/T, F877L and T878A, which are summarised in Figure 1-12.

The T878A mutation (formerly T877A) is the most frequently observed and most well characterised AR point mutation (264, 265). It is able to convert antagonists like flutamide into strong agonists (266), and the mutation results in broadening of the AR ligand binding-specificity, making it sensitive to a wider range of hormones including progesterone (266-268). One study identified the mutation in 6/24 patients with advanced metastatic prostate cancer (269), and in another the mutation was observed in 3/3 metastatic patients (270). Recently, this mutation was frequently found in abiraterone treated CRPC patients and it produced a progesterone-activated mutant, resulting in abiraterone resistance (271).

The H875Y mutation has similar functional effects to that of T878A as it also increases AR ligand promiscuity, and increases binding affinity for progesterone and estradiol (268, 272). Similarly to T878A and H875Y, the L702H mutation results in broadening of AR ligand specificity. It is also the only single mutant activated by hydrocortisone and it was reported in patients undergoing glucocorticoid treatment who were abiraterone and enzalutamide resistant (273). Additionally, *Romanel et al.* found that pre-abiraterone patients with T878A or L702H mutations, or *AR* gain, had a significantly worse progression-free and overall survival (273). The H875Y, L702H and T878A mutations have been detected in CRPC patients during abiraterone treatment, which has been associated with an increase in progesterone levels (271, 274, 275).

Another clinically relevant mutation is the F877L mutation. This mutation is capable of converting some of the second-generation antiandrogens, such as enzalutamide and apalutamide, from antagonists to agonists (276). Additionally, in an LNCaP xenograft model with the F877L mutation, tumours showed increased growth in mice treated with enzalutamide in castrate conditions (277). Furthermore, the F877L mutation was identified in the endogenous T878A allele of LNCaP cells after repeated enzalutamide treatment (277), which shows that drug treatment is selective for specific mutations. Importantly, F877L was detected in the plasma DNA of CRPC patients previously treated with

apalutamide (276), highlighting the clinical significance of this mutation. *Balbas et al.* demonstrated that these mutations could potentially be overcome with the synthesis of new compounds that could inhibit AR signalling in cells expressing these specific AR mutations (278).

Much like F877L, the W742 mutation is capable of activating antiandrogens (279). Whereas the F877L confers an antagonist to agonist switch for enzalutamide, W742C converts bicalutamide into an agonist. This mutation has been detected in CRPC patients who have been previously treated with apalutamide (280).

A

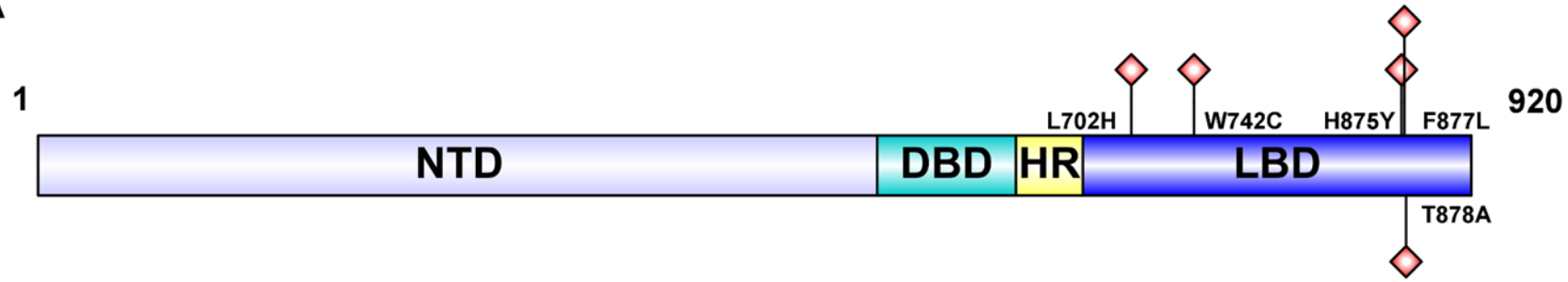

B

Mutation	Effect
None (WT)	Testosterone and Dihydrotestosterone
T878A	Activated by progesterone, estrogen, flutamide, bicalutamide, enzalutamide and apalutamide
W742C	Activated by bicalutamide, flutamide
H875Y	Activated by estrogen, progesterone, glucocorticoids, adrenal androgens, bicalutamide, flutamide, enzalutamide and apalutamide
F877L	Activated by flutamide, apalutamide and enzalutamide
L702H	Activated by glucocorticoids

Figure 1-12. Androgen receptor activating mutations in the ligand-binding domain

(A) Five of the most well characterised AR functional mutations are present in the ligand-binding domain; L702H, W742C, H875Y, F877L and T878A. (B) Table summarizing the effects of the point mutations, adapted from (262).

1.4.8.4 AR splice variants

In addition to AR alterations, AR variants (AR-V) represent another clinically important mechanism of drug resistance. AR splice variants are truncated forms of the AR resulting in constitutive activation that is ligand independent. The CWR22 xenograft model is very useful for the study of the progression of PCa to CRPC and it was discovered that CWR22Rv1 cells express two different AR proteins (one has a length of 112 kDa whereas the other is 75-80 kDa) in almost equal proportions (281). The smaller sized AR was androgen resistant, lacked the LBD and was constitutively active in the nucleus, whereas the full-length AR remained androgen dependent, giving rise to the idea that AR variants may play a role in drug resistance (281). Recently many AR-Vs have been identified with varying structures but they all lack the LBD, or at least portions of it (282), which is highlighted in Figure 1-13.

Perhaps the best-studied and most commonly observed splice variant is AR-V7. It is thought to derive from mRNA splicing of exons 1–3 and a loss of exons 4–8. The addition of the cryptic exon 3 (CE3) in the AR gene is also thought to contribute to AR-V7 expression (283). It is associated with enzalutamide and abiraterone resistance and patients with positive AR-V7 expression had reduced survival rates compared to AR-V7 negative patients. AR-V7 expression is heterogeneous and can form heterodimers with full-length AR as well as homodimers with itself. Furthermore, in the absence of androgens AR-V7 can bind to ARE's, which facilitates a protumorigenic transcriptome (284). In addition to this there is a decreased or completely abolished PSA response to both enzalutamide and abiraterone (285) due to the fact that both treatments target the ligand binding domain. Interestingly, AR-V7 mRNA expression has been found to be 20 times higher in CRPC patients than in hormone sensitive PCa patients (286), and protein levels of AR-V7 have been shown to increase as patients develop CRPC (287). Recently, *Sharp et al.* investigated AR-V7 expression in patient tumour samples. It was found that AR-V7 was detected in less than 1% of primary PCa samples but was expressed in 75% of samples following ADT, which further significantly increased after abiraterone or enzalutamide treatment. AR-V7 expression was found to be heterogeneous and there were varying levels of expression in different metastases from a single patient. Additionally, chemotherapy naïve patients without detectable levels of AR-V7 had an improved overall survival (74.3 vs. 25.2 months) and a better PSA response (100% vs. 54%) compared to AR-V7 positive patients (288).

Additional relevant splice variants include AR-V12 (AR^{v567es}) and AR-Q641X. AR-V12 has exons 1-4 and 8 intact but skips exons 5,6 and 7 (282). This variant is constitutively active and can interact with full length AR increasing its sensitivity to ligand. Furthermore, in

castrate conditions, it can enhance the growth of the cancer by generating larger malignant cells and can produce tumour populations that favour the selection of cells expressing AR-V12 (282). AR-Q641X contains a nonsense mutation in the hinge region of the AR, which results in a truncated C-terminal protein that is constitutively active (289). This nonsense mediated splice variant was originally isolated by *Ceraline et al.* but is yet to be fully characterised and the prevalence in PCa remains unknown (289).

Identification of novel variants represents a challenge for directed treatment, due to the fact that AR variant biology is not fully understood and treatments are not yet specific enough to target individual AR variants. This is because all AR directed treatments currently approved for clinical use mediate AR activity through the ligand-binding domain; therefore, there is no treatment that would be effective in cancers driven by splice variant activity. As the majority of AR variants retain the N-terminus, new classes of drugs targeting this region of the protein have been developed. EPI-001 and its later derivatives were designed to covalently bind to the N-terminus of the AR and inhibit the transcriptional activity. In *in vitro*, *in vivo* and xenograft models, EPI showed promising results but a phase I/II clinical trial was terminated early due to high pill burden (290). Research is ongoing to improve the potency and metabolic stability of the EPI compounds and recently EPI-7170 was shown to be active in AR-V7 expressing LNCaP95 cells (291). Despite this, splice variants may be suitable for detection in the blood and therefore may be useful as predictive biomarkers and offer a tractable option for personalised medicine (285). There is an urgent need for treatments that are effective in patients who express spice variants and have functional AR mutations.

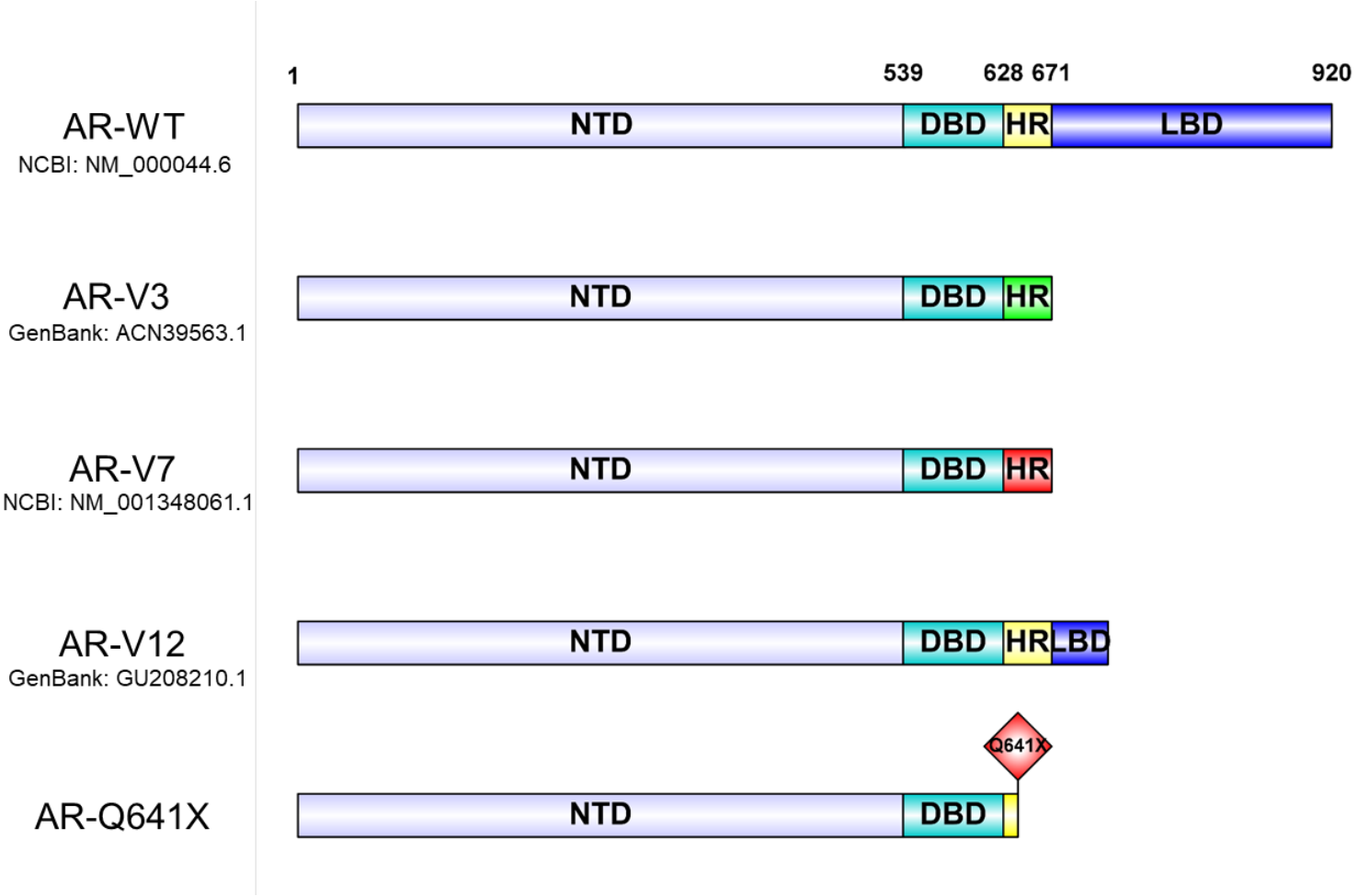

Figure 1-13. Selected androgen receptor splice variants

The AR wild-type represents the full length AR with all four functional domains intact. AR-V7 lacks the LBD, whereas AR-Q641X also lacks part of the HR. NCBI or GenBank references are shown for each variant except for AR-Q641X (unavailable reference). Different colours represent sequence differences in the hinge region. AR, androgen receptor; WT, wild-type; NTD, N-terminal domain; DBD, DNA binding domain; HR, hinge region; LBD, ligand binding domain.

1.4.9 Future therapies

Although there are a plethora of treatments aimed at improving the prognosis of patients with CRPC or mCRPC, these agents only realistically provide small survival benefits. However, advances in next-generation sequencing techniques has improved our understanding of the molecular mechanisms that drive prostate cancer progression, allowing for the development of therapies aimed at novel targets such as the PTEN/AKT pathway, DNA repair pathway, mismatch repair pathway, PARP and platinum-based chemotherapy.

1.4.9.1 PTEN/AKT pathway

Approximately 50% of mCRPC patients have activation of the PI3K/AKT pathway, which increases tumour cell growth and proliferation, and has been linked to an increase in treatment resistance (292). This pathway is negatively regulated by PTEN, a protein that is downregulated in ~40% of mCRPC patients. Loss of PTEN has also been linked to poor outcome and disease progression (293). One study found that as a monotherapy the AKT inhibitor perifosine had limited benefit in recurrent hormone sensitive PCa, but suggested that combinational therapy may still prove effective (294). In fact, AKT inhibitors provided an increased benefit when combined with MEK inhibition in an enzalutamide resistant CRPC model. However, it was also found that the effects appeared to be cell line dependent and that the effectiveness of the treatment was correlated to the activation of the pathways in the tumour (295). Although the results from preclinical data using single-agent AKT inhibitors have been modest, there are several phase I/II trials underway that are investigating combinatorial therapy with AR antagonists such as enzalutamide (RE-AKT) (296) or docetaxel and prednisolone (ProCAID) (297).

1.4.9.2 DNA repair pathway

Mutations in genes associated with DNA repair have been identified in mCRPC patients including *BRCA1*, *BRCA2*, *PALB2* and *ATM*, which are commonly deleted and are associated with an increased risk of disease. Germline *BRCA1* and *BRCA2* mutations have also been linked to a higher tumour grade at diagnosis and worse patient outcomes (298). Targeting these important repair defects may be a future avenue for the development of immunotherapeutics (299).

1.4.9.3 Mismatch repair pathway

Defects in the mismatch repair (MMR) pathway have been estimated at between 3-12% in mCRPC. MMR loss of function has been linked to high mutational load and microsatellite

instability, which has been associated with a higher burden of neo-antigens (299). These neo-antigens are tumour specific, allowing for an increase in immune recognition. Therefore targeting immune checkpoints such as CTLA-4 and PD-L1 might increase the immune response. The CTLA-4 pathway can be blocked using a monoclonal antibody (ipilimumab) but two phase III trials in mCRPC patients (pre- and post-docetaxel) failed to meet their primary endpoints (300, 301). Targeting PD-L1 using immunotherapy has been FDA approved for a number of tumour types including melanoma (nivolumab) and small cell lung cancer (pembrolizumab). Although initial phase I trials using nivolumab in prostate cancer were underwhelming, two phase II clinical trials using pembrolizumab (KEYNOTE-028 and -199) suggested that a small proportion of mCRPC patients would benefit from single use pembrolizumab treatment and two patients had a complete response in a PD-L1 positive cohort (302, 303). This highlights the importance of the development of reliable molecular and genomic biomarkers (304) to identify patients who would benefit from single use therapies.

1.4.9.4 PARP

A recent trial investigated the use of the PARP inhibitor olaparib in patients who had metastatic CRPC and no longer responded to standard treatments. PARP is a key enzyme in DNA repair and PARP inhibitors have already been successfully used in the treatment of ovarian cancer (305). The results of the mCRPC trial revealed that there was a substantial response to olaparib, with large reductions in PSA levels and circulating tumour cells. Out of the 49 evaluable patients in the study, 16 patients responded to olaparib monotherapy. These impressive responses were associated with DNA-repair defects in tumour cells including *BRCA2, BRCA1, ATM, CHEK2* (306). Therefore, due to the success of the treatment, the FDA granted accelerated approval for the use of olaparib in mCRPC patients with mutated *BRCA2*, *BRCA1* and *ATM* genes (307).

1.4.9.5 Platinum-based chemotherapy

Platinum-based chemotherapy agents have shown promise in phase II trials and work by initiating double strand breaks by cross-linking DNA. Results showed an increase in progression free survival but failed to identify a target group (308). If trials were to be conducted in patients with confirmed mutations in DNA repair genes, the outcome may prove to be successful. Additionally, a number of ovarian cancer patients who had defects in the nucleotide excision repair pathway and were resistant to PARP inhibitors responded to a platinum based treatment (309). Therefore, the use of platinum based chemotherapy warrants further investigation in mCRPC patients with defects in the DNA repair pathway.

1.4.10 Summary

To summarize, CRPC is an aggressive and incurable PCa phenotype. Current treatments are primarily aimed at targeting the androgen receptor but due to cancer cell adaptive responses, drug resistance is an ever-present challenge. It is therefore necessary to develop novel targeted therapies and provide new options for existing treatments. Considering the need for novel therapies and the pre-clinical evidence demonstrating V-ATPase subunit overexpression in cancer, there was a rationale for investigating the role of V-ATPase in prostate cancer.

1.5 V-ATPase in prostate cancer

This section will summarize what is known about V-ATPase in PCa and the current evidence supporting a link to the AR.

Using a V-ATPase inhibitor known as Iejimalide B, *Wang et al.* were one of the first groups to publish on the effect of V-ATPase inhibition in PCa (310). Lejimalide B is a marine macrolide lysosomal V-ATPase inhibitor. The group selected the AR WT hormone sensitive LNCaP and AR null hormone insensitive PC-3 cell lines to model early stage PCa and CRPC respectively. The group were primarily interested in investigating the effects of Iejimalide B on the cell cycle rather than the direct effects of V-ATPase inhibition in PCa, or in fact a link with AR signalling. Treatment with Iejimalide B induced cell cycle arrest and cell death in the LNCaP cells, but no cell death, and only S phase arrest, was observed in the PC-3 cells. There were distinct changes in gene expression suggesting Iejimalide B had an effect on transcriptional regulation, and Iejimalide B treatment induced both p53 dependent and independent responses (310). This study demonstrated that there were differences in how prostate cancer cells responded to V-ATPase inhibition and that inhibition consequently resulted in cell cycle arrest.

1.5.1 Specific V-ATPase subunit isoforms contribute to the invasive and metastatic potential of prostate cancer cells

To investigate the role of V-ATPase in PCa further, *Licon-Munoz et al.* studied the downstream physiological consequences of V-ATPase inhibition in the hormone insensitive PC-3 cells (121). PC-3 cells were found to express *ATP6V0A2* and *ATP6V0A3* but not *ATP6V0A1* or *ATP6V0A4* mRNA suggesting these were the two dominant V_Oa subunit isoforms expressed. Immunofluorescent staining revealed that V-ATPases were primarily localised to the Golgi and clathrin-coated vesicles in PC-3 cells, and there were less V-ATPase complexes detected in the lysosomes and endosomes. After treatment with 5 nM con-A, V-ATPase mediated proton transport was blocked as evidenced by an

increase in the pH of lysosomes and endosomes from pH 6.7 to 7.1. Additionally, V-ATPase inhibition increased the size and number of intracellular vesicles, indicating V-ATPase function was vital for the exit of V-ATPase from the Golgi and for its redistribution to different cellular membranes. Interestingly, V-ATPase was not found to be expressed at the PM of PC-3 cells, but cell motility assays demonstrated that the redistribution of V-ATPase-containing vesicles to the front of migrating cells was inducible. Furthermore, the V-ATPase co-localised with F-actin in migratory cells but not in non-migratory cells, and V-ATPase inhibition resulted in F-actin reorganisation. It was suggested that the purpose of the F-actin ring assembly was to overcome a toxic blockage of intracellular vesicles caused by V-ATPase inhibition (121). This study provided evidence for the role of V-ATPase in the invasive and migratory capabilities of prostate cancer cells.

An additional study by *Smith et al.* investigating the role of V-ATPase in extracellular and luminal pH regulation found that the V_Oa1 and V_Oa3 subunit isoforms were the dominant V_Oa isoforms expressed in PC-3 cells, and that *ATP6V0A4* gene expression was not detectable at the PM (311). This disagrees with the data published by *Licon-Munoz et al.* who did not find V-ATPase expression at the PM of PC-3 cells, and instead suggested a mechanism of inducible trafficking to the PM (121). These differences are likely due to the detection methods used (gene array chip analysis vs RT-qPCR). However, western blot analysis revealed V_Oa4 protein expression in the total membrane fraction, but not the PM fraction (311), agreeing with the observation by *Licon-Munoz et al*. that *ATP6V0A4* is not expressed at the PM. Regardless, *Smith et al.* went on to study the effect of siRNA mediated knockdown of V_Oa1, V_Oa3 and the accessory protein Ac45 (*ATP6AP1*) on V-ATPase function and localisation (311).

Firstly, levels of V_Oa1 and V_Oa3 were not affected by V_1A knockdown, indicating V_O stability is not dependent on V_1A expression, but there was a loss of V_1F, implying a disruption in the assembly of the V_1 domain. In addition to this, loss of V_Oa1 and V_Oa3 did not result in a compensatory upregulation of the other V_Oa subunit isoforms, which has been previously described for other subunit isoforms (7). However, there was a loss in V_1A signal in the PM fractions, supporting the idea that there is a reduction in V-ATPase assembly due to the reduced availability of V_Oa subunits. Confocal microscopy showed that V_Oa1 co-localised with transferrin receptor enriched early endosomes, whereas V_Oa3 co-localised with the late endosomal/lysosomal marker LAMP-1. Additionally, V_Oa1 and V_Oa3 were both found to have 95% co-localisation with V_1A, suggesting little of the V_O domain was detached from V_1 (311). Together, this shows that V_Oa1 and V_Oa3 exist in different endocytic compartments.

The siRNA mediated knockdown of V_Oa1, V_Oa3 and Ac45 in PC-3 cells resulted in a cessation of cell growth but not cell death after 48 hours compared to non-targeting

controls. This finding highlights the importance of V-ATPase in cell motility and cell physiology. In support of this, results from a Matrigel invasion assay showed that V_Oa1 and V_Oa3 knockdown suppressed migration and reduced metastatic potential. Furthermore, knockdown of V_Oa1 removed 78±6% of the concanamycin-sensitive component of the PM proton pumping rate, whereas V_Oa3 knockdown only removed 34±17% of the proton pumping rate, suggesting V_Oa1 expressing V-ATPase contribute to a greater degree than V_Oa3 V-ATPase complexes to the rate of PM proton flux. It appears as if knockdown of V_Oa3 affects the invasive potential of PC-3 cells more than the PM proton pumping activity, and therefore resulting effects are more likely to be mediated by changes to trafficking processes than decreased extracellular acidification. Knockdown of V_Oa1 and Ac45 (and to a less extent V_Oa3) resulted in an arrest of transferrin receptor recycling, which was likely due to altered vesicular acidification. The depletion of Ac45 resulted in an increase in extracellular pH and a reduction in the trafficking of MMP-14 to the cell surface, leading to an overall reduction in the invasive potential of the PC-3 cells. Finally, Ac45 knockdown inhibited both internalisation of the transferrin from the PM and its transportation back to the cell surface (311). This study showed that the V_Oa1 and V_Oa3 isoforms were predominant in different compartments and that they directly contribute to the invasive and metastatic characteristics of PC-3 cells. Importantly, it showed that Ac45 plays a crucial role in navigating the V-ATPase to the plasma membrane, highlighting the relevance of V-ATPase accessory proteins in prostate cancer progression.

1.5.2 The role of V-ATPase modulatory proteins in prostate cancer progression

In addition to the direct link between the V-ATPase complex and prostate cancer, V-ATPase modulatory proteins also contribute to the metastatic potential of PCa cells. LASS2/TMSG1 was expressed at low levels in the highly metastatic prostate cancer cell line PC-3M-1E8 and highly expressed in the low metastatic PC-3M-2B4. Furthermore, MMP-9 and -2 activity was found to be significantly increased in LASS2/TMSG1 shRNA PC-3M-2B4 cells. Moreover, mouse xenografts of PC-3M-2B4 cells transfected with LASS/TMSG1 shRNA exhibited significantly increased average tumour size and weight compared to controls. Those with LASS/TMSG1 shRNA also had more LNM, suggesting loss of LASS2/TMSG1 induced tumour cell growth, proliferation, invasion and metastasis likely as a result of a loss of control in V-ATPase activity (156).

In addition to this, *Sennoune et al.* demonstrated that pigment epithelium-derived factor (PEDF), which is a potent endogenous angiogenic inhibitor, is another regulator of V-ATPase in prostate cancer (312). PEDF is downregulated in prostate cancer cells and it was hypothesised that PEDF transduction would reduce V-ATPase function. The prostate

cancer cell lines LNCaP and its castration-refractory derivative CL1 were manipulated to stably co-express DsRed fluorescent protein with or without PEDF. PEDF expression was found to decrease proton flux in the metastatic CL1 cells, but not in the non-metastatic LNCaP cells. Furthermore, PEDF expression significantly decreased the levels of V_Oa4 and *ATP6AP2* in the CL1 cells, without altering levels in the LNCaP cells. This suggests that PEDF regulates V-ATPase function via a reduction in the subunit isoforms responsible for targeting the V-ATPase to the PM, which correlates with metastatic potential (312).

1.5.3 Evidence for interactions between V-ATPase and AR signalling in prostate cancer

Michel et al. went on to characterise the effect of V-ATPase inhibition in PCa (2). By inhibiting V-ATPase with baf-A1 and con-A in the hormone sensitive (LNCaP) and hormone insensitive (C4-2B) PCa cell lines, they showed a reduction of *in vitro* invasion of both cell lines by 80%. Expression of V-ATPase was found at the PM of the highly invasive C4-2B cell line but not the poorly invasive LNCaP cell line, supporting data from other cancer types that expression of V-ATPase at the PM directly correlates with an increase in invasive potential. Additionally, V-ATPase co-localised with PSA and V-ATPase inhibition resulted in a relocalisation of PSA to lysosome-like intracellular vesicles (2). V-ATPase inhibition significantly reduced PSA secretion and removal of baf-A1 from the media restored PSA compartmentalization with V-ATPase. The expression of V_1A was absent in the lysosomal vesicles containing PSA suggesting that organelle acidification had not occurred and that endosomal and lysosomal acidification was defective. This was supported by the fact that V-ATPase inhibition prevented acridine-orange vesicular staining. Furthermore, intracellular PSA levels were greater when the cells were stimulated with androgen in the presence of baf-A1, indicating that PSA was not degraded upon V-ATPase inhibition. Interestingly, in androgen-sensitive LNCaP prostate cancer cells, V-ATPase inhibition also reduced *PSA* mRNA expression, suggesting upstream inhibition of AR's transcription activating activity (2). Taken together, the group were able to demonstrate that V-ATPase expression at the PM was correlated with invasive potential, V-ATPase inhibition reduced prostate cancer cell invasion and results in defective PSA vesicle degradation with a reduction in *PSA* mRNA expression.

As *PSA* gene expression is a regulated by the AR, the group later went on to investigate AR expression in response to V-ATPase inhibition (313). Inhibition of V-ATPase with con-A in LNCaP and LAPC4 cells, which are both AR positive hormone sensitive PCa cell lines, resulted in a reduction of AR protein levels by ~90% and ~49% respectively. This reduction in AR protein levels was complemented by a ~50% reduction in *AR* mRNA.

These results suggest a link between the AR-PSA axis and V-ATPase function in prostate cancer. Furthermore, con-A inhibition resulted in endo-lysosomal alkalinisation in both cell lines. However, chloroquine treatment, which is a lysosomotropic amine that accumulates in acidic vesicles, also caused a reduction in AR mRNA and protein expression, suggesting that the reduction in AR expression observed after con-A inhibition is likely due to aberrant pH homeostasis rather than a direct effect of the V-ATPase itself. To explain the decrease in AR expression, mRNA stability and turnover was measured by RT-qPCR and it was concluded that con-A treatment did not stimulate *AR* mRNA degradation, and therefore V-ATPase inhibition probably impairs *AR* transcription. At this stage, it appeared as if there was a link between the AR and V-ATPase but it remained unclear exactly how V-ATPase inhibition reduced AR expression.

In an attempt to provide a mechanism for the link between the AR and V-ATPase, *Licon-Munoz et al*. suggested the potential involvement of Hypoxia Inducible Factor-1 (HIF-1α). HIF-1α regulates AR gene expression and has been reported to reduce transcription of the estrogen receptor, ERα, in breast cancer cell lines. Treatment with con-A increased HIF-1α protein expression, but not mRNA expression, in LNCaP and LAPC4 cells, suggesting an increase in protein translation or protein stability but not HIF-1α transcription. Interestingly, confocal microscopy analysis revealed that HIF-1α translocated to the nucleus upon con-A treatment, which indicates activation of HIF-1α. HIF-1α is rapidly turned over under normoxic conditions and is targeted to the proteasome for degradation via HIF-1α hydroxylation. Con-A treatment resulted in an increase in HIF-1α and a reduction in hydroxylated HIF-1α, which was rescued with the addition of iron. An increase in iron concentration also partially rescued *AR* mRNA expression in cells treated with con-A, indicating that HIF-1α acts as a transcriptional repressor of the AR. Additionally, this increase in iron concentration did not rescue the defective con-A induced endo-lysosomal pH, which again provides evidence that the link between the V-ATPase and AR is downstream of V-ATPase mediated pH alterations. Moreover, treatment with Dimethyloxalylglycine (DMOG) prevents HIF-1α hydroxylation and consequently prevents HIF-1α degradation. The addition of DMOG resulted in a decrease in AR protein and mRNA levels, and an increase in HIF-1α levels, which were comparable to those induced with con-A treatment. This indicates that the V-ATPase mediated downregulation of AR occurs via a reduction of HIF-1α hydroxylation and an increase in HIF-1α stability. Together this study provides evidence that AR expression is V-ATPase dependent and that V-ATPase inhibition indirectly reduces downstream AR expression via HIF-1α. The biological mechanism suggested by *Licon-Munoz et al.* is that V-ATPase inhibition results in defective transferrin receptor recycling due to alkalization of endo-lysosomal compartments. This in turn blocks iron uptake and reduces HIF-1α hydroxylation, resulting

in an increase in HIF-1α stability, which then translocates to the nucleus and downregulates AR expression (313).

Although this is an interesting study, which provides evidence for the role of HIF-1α as the link between V-ATPase and AR signalling in prostate cancer, there are still many questions left unanswered. For example, it is not known if HIF-1α binds directly to the AR or whether there is another molecule regulated by HIF-1α that represses AR expression. It is also not known whether this mechanism the same in CRPC or what V-ATPase subunits are important for maintaining the AR-PSA axis.

1.5.4 Summary

Overall, relatively few studies have investigated the role of V-ATPase in PCa and, in particular, on modulation of the AR. The main findings from these published studies are that V-ATPase expression is directly correlated to the invasive and metastatic potential of PCa cells as evidenced by; (1) its expression in the PM, (2) the V-ATPase dependent activation of proteases such as MMP-2, -9 and -14, and (3) an increase in cell motility. Evidence suggests that the V_Oa3 isoform (and potentially V_Oa1, V_Oa2 and V_Oa4) plus the V-ATPase accessary subunit Ac45, are the key subunits responsible for targeting the V-ATPase to the PM in PCa cells. Additionally, individual subunit isoform knockdown results in a reduction in proton flux and V-ATPase function, leading to alkalization of endo-lysosomal compartments. V-ATPase modulatory proteins such as LASS2/TMSG1 and PEDF can affect tumour cell growth and invasion via regulation of V-ATPase activity. Chemical inhibition of V-ATPase significantly reduces PCa cell invasion and induces cell death.

In terms of the critical interaction between V-ATPase and the AR, there is a link between V-ATPase and AR signalling that may involve HIF-1α regulation, but the mechanism is yet to be fully elucidated. Taken together, there is compelling evidence that V-ATPase plays an important role in PCa, which might affect progression to the CRPC phenotype. Furthermore, the emergence of clinically relevant AR mutations and AR splice variants adds greater complexity to the AR/V-ATPase axis. However, there are still questions as to whether V-ATPase subunit expression directly relates to V-ATPase function and what impact the expression of specific subunit isoforms, other than V_Oa, has on PCa progression. There is a lack of genetic evidence for the specific roles of these subunit isoforms, and genetic tools such as siRNA and CRISPR are required to improve our understanding of V-ATPase subunit expression in PCa. Additionally, the recent discovery of V-ATPase somatic mutations also raises its own questions about their importance in PCa and whether these mutations alter V-ATPase functionality. Finally, it is crucial to fully understand the role of V-ATPase in CRPC and how it is linked to AR signalling.

1.6 Hypothesis and aims

1.6.1 Hypothesis

The primary hypothesis is that V-ATPase dysregulation is directly linked to cancer via alterations in activity. The secondary hypothesis is that V-ATPase inhibition influences androgen receptor signalling in prostate cancer, potentially including mechanisms relevant to a CRPC phenotype, and therefore makes an attractive therapeutic target.

1.6.2 Aims

To investigate these hypotheses, the focus of the experiments described in this thesis was to first determine how selected somatic mutations alter V-ATPase activity and function in a chimeric yeast model system, before inhibiting V-ATPase activity and silencing subunit expression in prostate cancer cell lines with clinically relevant AR aberrations.

The main aims were to:

- Measure the effect of selected somatic missense mutations on V-ATPase catalytic activity and function.
- Investigate the effect of V-ATPase inhibition on AR signalling in prostate cancer cell lines with AR splice variants and point mutations.
- Investigate the effect of genetically silencing V-ATPase subunits on AR signalling in prostate cancer cell lines.

Chapter Two

Chapter 2 Materials and Methods

Materials and Methods

Cell Culture Techniques

2.1 Cell culture materials and methods

Table 2-1. Cell culture materials

List of materials used for cell culture techniques. All materials were purchased from Sigma-Aldrich or Thermo Fisher unless otherwise stated. All drugs were dissolved in DMSO unless otherwise stated.

Reagent	Components
Complete Growth Media	RPMI-1640 or DMEM (without L-glutamine) supplemented with: 10% Fetal Bovine Serum (v/v), 1% Penicillin/Streptomycin (v/v), 1% L-Glutamine (v/v) and 1% Pyruvate (v/v).
Charcoal Stripped Growth Media	RPMI-1640 without phenol red and with L-glutamine supplemented with: 10% Fetal Bovine Serum- Charcoal Stripped (v/v), 1% Penicillin/Streptomycin (v/v).
Freeze Media	50% FBS (v/v), 10% DMSO (v/v), 40% RPMI-1640 (v/v).
1x Phosphate Buffered Saline (PBS)	137 mM NaCl, 2.7 mM KCl, 10 mM Na_2HPO_4, 1.8 mM KH_2PO_4.
1x Phosphate Buffered Saline with Tween-20 (PBS-T)	1x PBS, 0.1% Tween 20 (v/v).
5x Sample buffer	60 mM Tris-Cl pH 6.8, 2% SDS, 10% glycerol, 5% β-mercaptoethanol, 0.01% bromophenol blue.
5x RIPA buffer	0.75M NaCl, 5% NP40 (v/v), 2.5% DOC (v/v), 0.5% SDS (w/v), 0.25M Tris pH8.0, diluted in 100 mL ddH_2O.

2.1.1 Cell lines

Cells were maintained in an incubator (Galaxy 170S, New Brunswick) at 37°C and 5% CO_2 on 10 cm plates unless otherwise stated.

Table 2-2. Cell lines used for investigations

List of cell lines used for investigations. WT, wild-type; AR, androgen receptor; PSA, prostate specific antigen.

Cell line	Tissue	Suitable growth media	Hormone sensitive	AR abnormality	AR expression	PSA expression
HeK-293	Embryonic kidney	DMEM	No	No expression	No	No
LNCaP	Prostate	RPMI-1640	Yes	Point mutation at T877A	Yes	Yes
DuCaP	Prostate	RPMI-1640	Yes	WT	Yes	Yes
22Rv1	Prostate	RPMI-1640	Yes	V7 splice variant	Yes	Yes
LNCaP F877L/T878A	Prostate	RPMI-1640	Yes	Double point mutation at F877L and T878A	Yes	Yes

2.1.2 Preparation of cells from frozen stocks

Cells stored in cryo vials in liquid nitrogen were defrosted in a water bath at 37° C. 1 mL of cells and 9 mL of either complete DMEM or RPMI-1640 was added to a 10 mL falcon tube. The falcon was centrifuged at 1,500 g for 3 minutes at 21°C, and the supernatant was aspirated and discarded. The pellet was re-suspended in 10 mL fresh media, pipetted onto a 10 cm plate and placed in the incubator at 37°C.

2.1.3 Maintenance of cell lines

Cells that were approximately 80% confluent were passaged. The appropriate complete growth media, 1x PBS and 0.25% trypsin-EDTA were all pre-warmed to 37°C. In a 10 cm plate, the existing media was aspirated and 5 mL 1x PBS was used to wash the cells. The PBS was then aspirated and 1.5 mL trypsin was added. After trypsinization, the trypsin was aspirated and the cells were incubated at 37°C for 1-2 minutes. The plates were gently tapped to detach clumps of cells and 10 mL of fresh complete media was added to inhibit the action of trypsin. The cells were then split and fresh complete media was added to make the final volume 10 mL. Plates were then placed back in the incubator at 37°C.

2.1.3.1 CSS media

Complete growth media with phenol red contains an array of different hormones whereas CSS media is hormone free. As prostate cancer is largely a hormone driven cancer, it was essential for the majority of experiments that cells were cultured in a hormone free environment. This was particularly important so that the direct effect of androgens could be studied. To address this, cells were cultured in CSS media and were split (as in 2.1.3), but fresh CSS media was added instead of complete media after trypsinization. Cells were cultured in CSS media for at least 24 hours prior to experimental use. This was to remove the effect of any hormones present in the complete growth media.

2.1.4 Freezing cell lines

Once the cells were approximately 80% confluent they could be frozen for future experiments. The same process was followed as in 2.1.3, however freeze media was used instead of complete growth media. Instead of adding 10 mL of fresh media after trypsinization, 3 mL of freeze media was added to each plate and re-suspended. The media was then transferred to 3 separate cryo vials and stored at -80°C.

2.1.5 MTS cell viability assay

The MTS cell viability assay (Promega) is a colorimetric method for quantification of cell viability in proliferation and cytotoxicity assays. The MTS tetrazolium compound is reduced by viable cells to generate a coloured formazan product. This conversion occurs in metabolically active cells by NAD(P)H-dependent dehydrogenase enzymes. The resulting formazan product produced is then quantified by measuring the absorbance at 490 nm.

Cells were seeded in 96-well plates in their appropriate growth medium (Table 2-2). After 24 hours, the experimental compounds were added to the cells for 24-72 hours depending on the experimental design. MTS reagent (7 µL) was then added to each well of the cells for 4 hours. After 4 hours, the absorbance of the plate was recorded at 490 nM.

2.2 Luciferase reporter assay

HeK-293 cells were seeded (12,500 cells) into 96-well white microtitre plates in 100 µL CSS media and were grown for 18 hours. The cells were transfected with the androgen response element reporter vector p(ARE)$_3$Luc, the AR expression vector pE-AR and the pRL-CMV *Renilla* luciferase control reporter vector (Figure S 8-1) using Fugene HD transfection reagent (Promega). The AR firefly reporter plasmid was transfected at a ratio

of 9:1 to the ARE expression plasmid. CSS media (200 µL) was used to dilute 2 µg of total DNA plasmid (1.8 µg AR, 0.2 µg ARE) and 6 µL Fugene HD was added. The reaction mixture was incubated for 5 minutes at room temperature. From the transfection mixture, 5 µL was added to each of the wells on the microtitre plate. The cells were gently mixed and then incubated at 37°C for 18 hours. Following this, DHT was diluted in 1 mL CSS media and was split into 10 (100 µL) aliquots. Drugs were then diluted in the DHT aliquots to ensure that each drug dilution contained the same 1 nM DHT concentration. From the dilution series, 20 µL was added to the wells of the microtitre plate in triplicate (3 x 20 µL per dilution). The plate was then incubated for either 18 or 24 hours at 37°C. Following incubation, the media was aspirated from each of the wells and passive lysis buffer (Promega) was added (20 µL). The cells were incubated at room temperature for 10 minutes with gentle shaking.

The dual luciferase reporter assay was performed using the Varioskan Flash plate reader (Thermo Scientific, Essex, UK). Firstly, 100 µL of LARII reagent (Promega) was added to each of the wells of the microtitre plate and the luminescence detected in 5 seconds was recorded. Luminescence is the result of the oxidation of luciferin, which requires ATP, Mg2+ and oxygen for the reaction. Stop and Glo reagent (100 µL) (Promega) was then added to each well and the *Renilla* luminescence signal was recorded. The Stop and Glo reagent prevents autoluminescence of the *Renilla* substrate, coelenterazine. In the presence of *Renilla*, coelenterazine is converted into coelenteramide, which can produce a detectable luminescent signal, and a summary of this biological mechanism is shown in Figure 2-1.

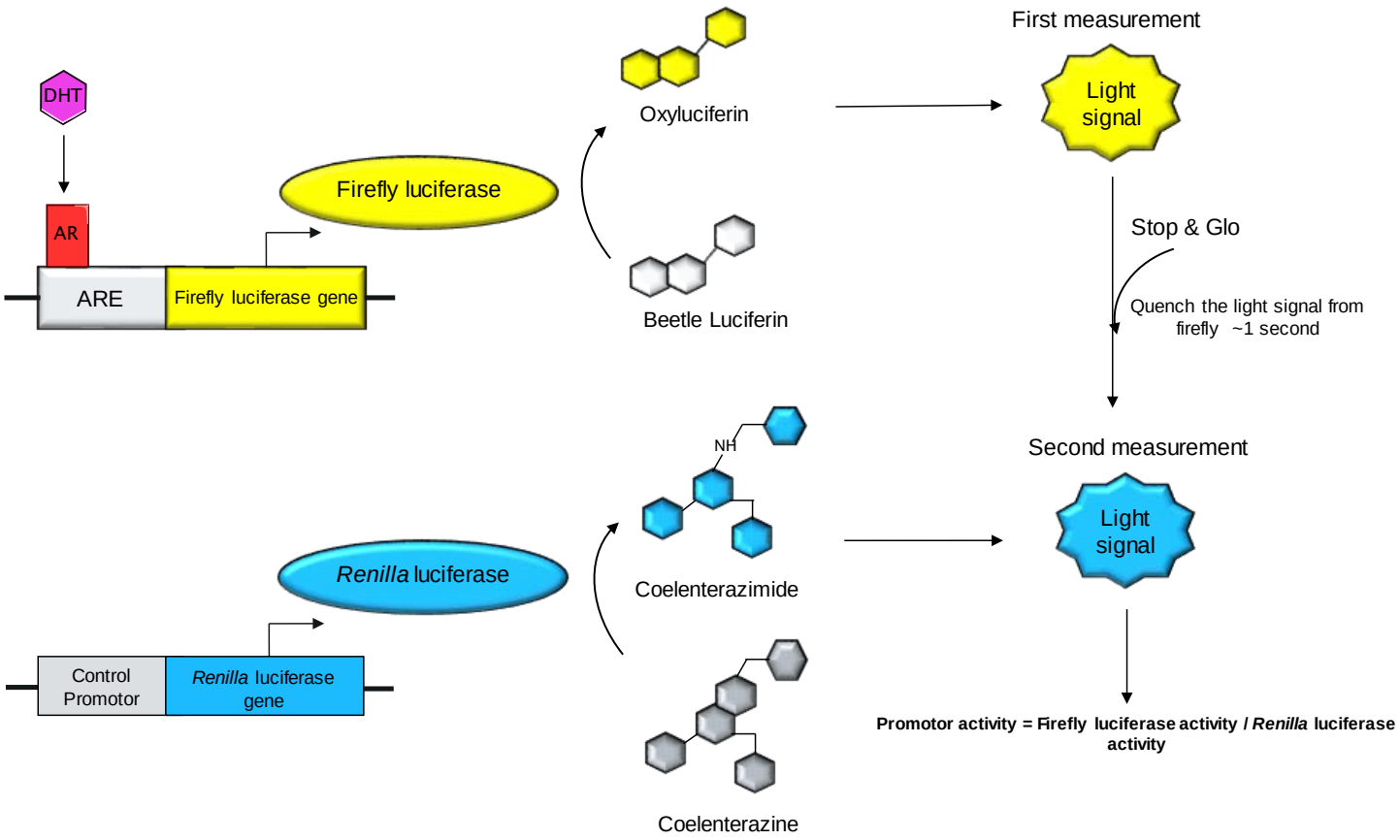

Figure 2-1. Dual luciferase reporter assay biological mechanism

DHT stimulation promotes the binding of the AR to the ARE, resulting in downstream transcription of the firefly luciferase gene. The upregulation of firefly luciferase induces the conversation of beetle luciferin to oxyluciferin, which produces a quantifiable luminescent signal. As a control for transfection efficiency, cells were also transfected with plasmids expressing the *Renilla* luciferase gene, which upregulates the *Renllia* luciferase protein and consequently converts coelenterazine to coelenterazimide. This conversion produces a second quantifiable luminescent signal and the promoter activity can be calculated by normalising the firefly luciferase signal to the *Renilla* luciferase signal. DHT, dihydrotestosterone; AR, androgen receptor; ARE, androgen response element.

Protein Techniques

2.3 Materials for protein techniques

2.3.1 List of materials for protein techniques

Table 2-3. Materials list for protein techniques

List of materials used for protein techniques.

Reagents	Components
10x Running buffer	250 mM Tris (w/v), 1.92 M glycine (w/v), 1% SDS (w/v) made up to 1 L with ddH_2O
Transfer buffer	100 mL 10x Running buffer (v/v), 200 mL 100% methanol (v/v) made up to 1 L with ddH_2O
Milk blocking solution	2.5 g Marvel milk powder (w/v) dissolved in 50 mL PBS-T
BSA solution	2.5 g BSA powder (w/v) dissolved in 50 mL PBS-T
Polyacrylamide gels	
Resolving gel (12%)	ddH_2O, 30% acrylamide mix, 1.5 M Tris (pH 8.8), 10% SDS, 10% APS, TEMED
Stacking gel (6%)	ddH_2O, 30% acrylamide mix, 1.0 M Tris (pH 6.8), 10% SDS, 10% APS, TEMED

2.3.2 Antibodies

Table 2-4. Antibodies and their dilution factors

Primary and secondary antibodies used for western blotting with recommended dilutions.

Antibody	Catalogue number	Species	Dilution	Company
Androgen Receptor (D6F11) XP Rabbit mAb	5153	Rabbit	1:1000	Cell Signalling Technology
PSA/KLK3 (D11E1) XP Rabbit mAb	2475	Rabbit	1:1000	Cell Signalling Technology
β-Actin (8H10D10) Mouse mAb	3700	Mouse	1:2000	Cell Signalling Technology
V-ATPase C1 Antibody (G-5)	sc-271077	Mouse	1:1000	Santa-Cruz Biotechnology
ATP6V1E1 Unconjugated Polyclonal Antibody	HPA029196	Rabbit	1:1000	Sigma
ATP6V1E2 Unconjugated Polyclonal Antibody	HPA052784	Rabbit	1:250	Sigma
HRP-conjugated Anti-Mouse IgG Concentrate (RABHRP2)	RABHRP2	Mouse	1:20,000	Sigma
HRP-conjugated Anti-Rabbit IgG Concentrate (RABHRP1)	RABHRP1	Rabbit	1:20,000	Sigma
ATP6V1C2 Monoclonal Antibody (OTI3E9)	MA5-26964	Mouse	1:500	Thermo Fisher - Invitrogen
c-Myc Monoclonal Antibody	MA1-980	Mouse	1:500	Thermo Fisher - Invitrogen
V-ATPase A Polyclonal Antibody (PA5-26779)	PA5-29191	Rabbit	1:2000	Thermo Fisher - Invitrogen

2.3.3 Enhanced chemiluminescence (ECL) substrates

Table 2-5. ECL substrates

List of ECL substrates used in western blotting and their recommended suitable primary antibodies. All ECL substrates were purchased from ThermoFisher.

Substrate	Suitable primary antibodies
Pierce ECL substrate	β-Actin
SuperSignal West Pico Chemiluminescent Substrate	AR
SuperSignal West Dura Extended Duration Substrate	PSA, ATP6V1A
SuperSignal West Femto Maximum Sensitivity Substrate	ATP6V1E1, ATP6V1E2, ATP6V1C1, ATP6V1C2

2.4 Western blotting

2.4.1 Cell harvest

When cells were approximately 80% confluent, the media was aspirated from the plates, cells were washed with PBS and then trypsinized. RIPA buffer supplemented with cOmplete Mini Protease Inhibitor Cocktail (Roche) and phosphatase inhibitor PhosSTOP (Roche) was added to lyse the cells. The cells were then were incubated in RIPA buffer on ice for 30 minutes. Next, the cells were scraped using a cell scraper and transferred to 1.5 mL microcentrifuge tubes. Samples were then sonicated on ice at a power output level of 2.0 for a total of 15 seconds processing time (3x5 secs with 2 sec pulse-off). Following this, they were centrifuged at 13,000 rpm (16,060 g) for 8 minutes at 4°C and the supernatant was transferred to fresh microcentrifuge tubes. Cell pellets were discarded and the lysates were kept on ice. The Bradford assay was used to determine the protein quantification before sample preparation.

2.4.2 Protein quantification

The amount of protein in sample lysate was quantified using the Bradford assay, which was used to ensure equal loading in the western blot. Firstly, the BioRad dye reagent was diluted using 4 parts ddH_2O and 1 part dye reagent, and 250 µL was added to empty wells of a 96-well plate. A standard curve was then constructed using concentrations of BSA (1mg/mL) ranging from 0-5 µg/mL. Next, 1 µL of the experimental samples was added to individual wells in triplicate and the absorbance was measured at 595 nm. Based on the protein quantification, volumes of the samples were pipetted into new microcentrifuge tubes and diluted with appropriate volumes of ddH_2O. Sample buffer (5x) was added to

each sample and the samples were boiled at 95°C for 5 minutes. The excess lysates were aliquoted and stored at -20°C for future experiments.

2.4.3 Electrophoresis using SDS-PAGE

With the completion of the sample preparation, 12% resolving gels and 6% stacking gels (Table 2-3) were cast and placed in a mini-PROTEAN tetra cell (Biorad). The tank was filled with 1x running buffer (~800 mL) and the samples were loaded into the wells. To assess the size of the proteins in the samples, 4 µL of Spectra Multicolor Broad Range Protein Ladder (Thermo Fisher) was run alongside the samples. The gels were run at 120 V for between 90 and 120 minutes. Proteins were transferred from the gels to a nitrocellulose membrane (Amersham Protran 0.45 NC, GE healthcare) using 1x transfer buffer in the Mini-Trans Blot Module (BioRad). The transfer was performed at 100 v for 60 minutes with the addition of an ice pack to assist in maintaining the voltage.

2.4.4 Protein detection

Once the proteins had transferred from the resolving gel to the membrane, the nitrocellulose membranes were placed in an empty pipette box and 5% milk solution was added to block non-specific protein binding. The membranes were blocked for 60 minutes with gentle shaking. During blocking, the primary antibodies were diluted in 5 mL of 5% BSA solution. The membranes were then incubated with the primary antibody/BSA solution for 16 hours at 4°C. After the blots had been washed with PBS-T 3 times for 5 minutes, anti-mouse or anti-rabbit secondary HRP antibodies were diluted to 1:20,000 in 5 mL 5% BSA. The blots were then incubated with the HRP antibodies for 60 minutes at room temperature. They were then washed again in 1x PBS-T 3 times for 5 minutes. After the final wash, the appropriate ECL substrates (Table 2-5) were mixed at a ratio of 1:1 and added to the corresponding membranes. The membranes were incubated with ECL substrate for 1 minute, as per the manufacturer's instructions, and sandwiched between two layers of cling film. The substrate's signal was then detected and processed by the imager, with an exposure time of between 30 seconds to 3 minutes, giving the final image of the blot. A complete summary of the western blot procedure is illustrated in Figure 2-2.

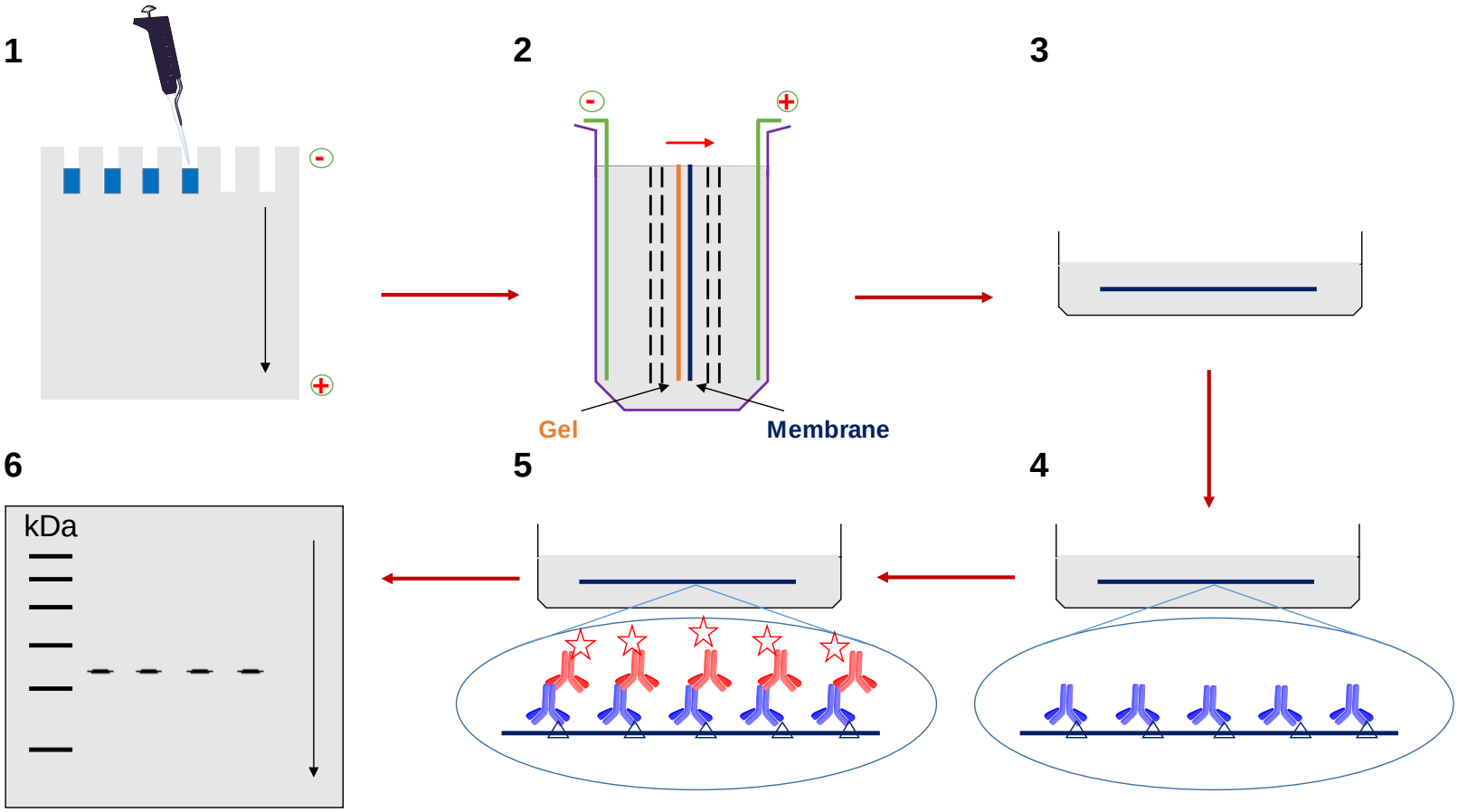

Figure 2-2. Western blotting procedure

Following the figure: (1) Samples are loaded into the wells of the SDS-polyacrylamide gel and the proteins migrate towards the positive charge. (2) The proteins are transferred from the gel to a nitrocellulose membrane. (3) Membrane is blocked using BSA or milk blocking solution to prevent the binding of non-specific proteins. (4) The membrane is incubated with primary antibodies to enable specific binding to the target of interest. (5) Membrane is washed and incubated with HRP-labelled secondary antibody, which is specific to the primary antibody. (6) The blot is then washed again, incubated with enhanced chemiluminescence substrates and visualised on an imager.

Molecular Biology Techniques

All RNA techniques were conducted in an RNase free environment. RNase Zap (Invitrogen) was used to remove RNAses from all pipettes and surfaces. Filter tips and RNase free microcentrifuge tubes were also used to prevent RNA degradation.

2.5 Materials for Molecular Biology techniques

Table 2-6. Materials for Molecular Biology techniques

List of materials used for Molecular Biology techniques. All reagents were purchased from Sigma or Fisher Scientific unless otherwise stated.

Reagents	Components
1x TE	1 ml of 1 M Tris-HCl (pH 8.0), 0.2 mL EDTA (0.5 M), made up to 100 mL with ddH_2O
25x TAE buffer	5 g Fisher BioReagents 25X TAE Powder, made up to 1 L with ddH_2O
Solution AL1	1 mL 10% SDS (w/v) , 1 mL 2M NaOH, 8 mL ddH_2O
Solution AL2	60 mL 5 M Potassium acetate, 11.5 mL Glacial acetic acid, 28.5 mL ddH_2O
Ampicillin resistant plates (10 plates)	300 mL LB agar, 100 mg/mL ampicillin

2.6 RNA extraction

Cells were harvested in 1X PBS on ice and scraped into microcentrifuge tubes using a cell scraper. The samples were centrifuged at 300 g for 5 minutes and the supernatant was discarded. The Promega ReliaPrep RNA Cell Miniprep System was used to extract the RNA from the samples according to the manufacturer's protocol. After the RNA was extracted it was eluted in 40 µL of RNAse free water and quantified using the NanoDrop (ThermoScientific).

2.7 Complementary DNA (cDNA) synthesis

For cDNA synthesis, 1 µg of RNA was diluted in RNase free water to make a total volume of 14 µL per sample. Oligo(dT) primers (Promega) were added (1 µL) to the samples and heated to 70°C in the PCR machine for 5 minutes, and then cooled to 4°C. The master mix (5 µL 5X M-MLV RT buffer (Promega), 1.25 µL 10 mM dNTPs (Promega), 0.625 µL RNAsin (Promega), 1 µL MLV RT enzyme (Promega) and 2.125 µL RNase free water) was added to each sample (10 µL). This mixture was heated to 42°C in the PCR thermal

cycler for 60 minutes, then 95°C for 5 minutes and finally cooled to 4°C. The cDNA was stored at -20°C for future use.

2.8 Quantitative Polymerase Chain Reaction (qPCR)

Table 2-7. TaqMan primers used in RT-qPCR

List of commercial TaqMan qPCR primers and the company they were purchased from.

TaqMan qPCR primer	Catalogue number	Company
AR (Hs00171172_m1)	#4331182	Thermo Fisher Scientific
ATP6V1C1 (Hs00940702_m1)	#4331182	Thermo Fisher Scientific
ATP6V1C2 (Hs00375969_m1)	#4331182	Thermo Fisher Scientific
ATP6V1A (Hs01097169_m1)	#4331182	Thermo Fisher Scientific
GAPDH (Hs02786624_g1)	#4331182	Thermo Fisher Scientific
KLK3/PSA (Hs02576345_m1)	#4331182	Thermo Fisher Scientific
TMPRSS2 (Hs01122322_m1)	#4331182	Thermo Fisher Scientific

TaqMan primers and probes were used for the quantitative polymerase chain reaction. For the qPCR reaction, 15 µL of master mix (10 µL Universal Master Mix (without Amperase), 1 µL of Assay on demand probe and primer set (Table 2-7) and 4 µL of RNase free H_2O) was added to each well of a 96-well PCR plate. The cDNA samples were diluted with 75 µL of RNAse free H_2O and 5 µL was added to each of the wells. Once all of the reagents had been added, a clear plastic film was pressed over the top of the plate and was sealed so that all wells were covered. The plate was then briefly centrifuged so that all liquid was collected at the bottom of the wells. Each sample was completed in triplicate and a control GAPDH probe was included on every PCR plate. This was so that the results from the probes of interest could be normalised against the GAPDH results. The 7500 Real-Time PCR thermal cycler machine (Applied BioSystems) was used to conduct the qPCR reaction via thermo-cycling and detection of the subsequent fluorescence. The Real-Time qPCR software v2.0.6 (Applied BioSystems) then calculated Ct values for each of the samples. From these Ct values, the comparative ΔΔCt method was used to calculate fold changes in gene expression against untreated control samples. The overall formula for the ΔΔCt method is $2^{-\Delta\Delta Ct}$ in which ΔCt represents the difference between the Ct value for a gene of interest and the Ct value for a housekeeping gene for a given sample. The ΔΔCt value is then calculated by making the ΔCt values for a given sample relative to the ΔCt values for a control sample using the following formula: ΔΔCt = ΔCt (Sample) – ΔCt (Control average). Finally, the fold gene expression is calculated using 2 to the power of negative ΔΔCt.

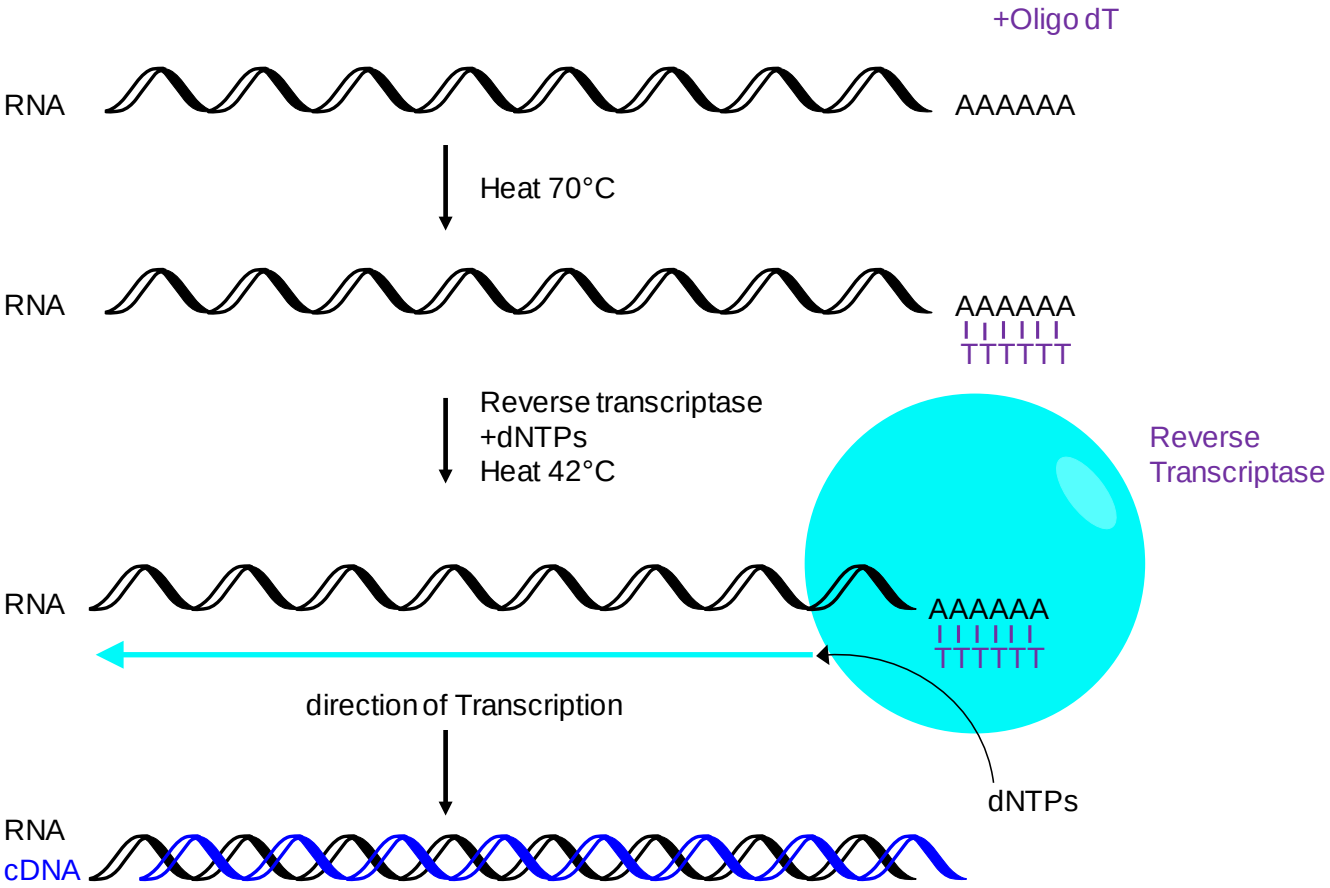

Figure 2-3. cDNA synthesis

Complementary DNA was produced by binding the oligo dTprimer to the polyA tail, and the reaction was then heated to 70°C to prevent non-specific binding. Reverse transcriptase and dNTP's were added and the reaction was heated to 42°C to enable DNA synthesis, which was complementary to the target mRNA sequence. A final heating step of 95°C was incorporated to inactivate the transcriptase enzyme. Illustration prepared in ChemDraw Professional 16.0.

2.9 Molecular cloning

2.9.1 Primer design

The human V_1E2, V_1E1 and yeast Vma4 subunit sequences were identified using BLAST (Basic Local Alignment Searching Tool). Using Clustal Omega, the V_1E2 sequence was aligned with the V_1E1 subunit sequence and Vma4. Somatic mutations in the N-terminal alpha helix of the V_1E2 subunit were selected using the COSMIC database (314). Three missense mutations were chosen relating to a glutamic acid residue at position 61 of the V_1E2 and V_1E1 subunits (E61K, E61V and E61Q). These mutations were aligned to the Vma4 yeast sequence and the corresponding residue was a leucine at position 66 (L66K, L66E, L66Q). Specific primers for these three mutations were designed for the human V_1E2, V_1E1 and yeast Vma4 sequences. The primer sequences are shown in Table 2-8. Primers arrived in powder form as they had been desalt purified and so they were diluted to a final concentration of 100 µM in 1x Tris-EDTA. They were then diluted to 10 µM in ddH_2O before the PCR reaction mixture was assembled.

Table 2-8. Primer sequences

Primers were designed using OligoEvaluator: Oligonucleotide Sequence Calculator (Sigma). The mutated bases are shown in red and the restriction enzyme cut sites are shown in green.

Target	Name	Sequence (5' to 3')	Length (bp)	Tm (°C)	GC (%)
Yeast Vma4	ForVMA4_EcoRIatg	ATGGGAATTCCATGTCCTCCGCTATTACTGCT	32	76.0	46.8
	RevVMA4_XhoIstop	TAACCGCTCGAGCGGTCAATCAAAGAACTTT CTTGTCTTG	40	81.0	45
	ForVMA4 L66K	AACTTCAAGAGCAAGAAGAAGAAG	24	28.4	37.5
	RevVMA4 L66K	CTTCTTCTTCTTGCTCTTGAAGTT	24	35.6	37.5
	ForVMA4 L66E	AACTTCAAGAGCAAGGAGAAGAAG	24	28.6	41.6
	RevVMA4 L66E	CTTCTTCTCCTTGCTCTTGAAGTT	24	35.7	41.6
	ForVMA4 L66Q	AACTTCAAGAGCAAGCAGAAGAAG	24	28.9	41.6
	RevVMA4 L66Q	CTTCTTCTGCTTGCTCTTGAAGTT	24	35.6	41.6
Human V_1E2	ForV1E2_EcoRIatg	ATGGGAATTCCATGGCCCTGAGTGATGT	28	76.9	50
	RevV1E2_XhoIstop	TAACCGCTCGAGCGGTTATATAAAGAACTTT CTGTTGGTGTT	42	77.7	40.4
	ForV1E2 E61K	AAGAAGAAGCAGATAGAGCAGCA	23	63.4	43.4
	RevV1E2 E61K	TGCTGCTCTATCTGCTTCTTCTT	23	63.4	43.4
	ForV1E2 E61V	AAGGTGAAGCAGATAGAGCAGCA	23	66.3	47.8
	RevV1E2 E61V	TGCTGCTCTATCTGCTTCACCTT	23	66.3	47.8
	ForV1E2 E61Q	AAGCAGAAGCAGATAGAGCAGCA	23	66.5	47.8
	RevV1E2 E61Q	TGCTGCTCTATCTGCTTCTGCTT	23	66.5	47.8
Human V_1E1	ForV1E1_EcoRIatg	ATGGGAATTCCATGGCTCTCAGCGATGCT	29	79.0	51.7
	RevV1E1_XhoIstop	TAACCGCTCGAGCGGTTAGTCCAAAAACTT CCTTGTT	37	79.3	45.9
	ForV1E1 E61K	TATGAGAAGAAAAAGAAACAGATT	24	56.9	25
	RevV1E1 E61K	AATCTGTTTCTTTTTCTTCTCATA	24	56.9	25
	ForV1E1 E61V	TATGAGAAGAAAGTGAAACAGATT	24	57.7	29.1
	RevV1E1 E61V	AATCTGTTTCACTTTCTTCTCATA	24	57.7	29.1
	ForV1E1 E61Q	TATGAGAAGAAACAGAAACAGATT	24	57.7	29.1
	RevV1E1 E61Q	AATCTGTTTCTGTTTCTTCTCATA	24	57.7	29.1

2.9.2 Two-step PCR

A two-step PCR process was used to produce the full-length PCR fragment. The reaction setup from the New England Biolabs PCR Protocol for Phusion High-Fidelity DNA Polymerase protocol was used. Firstly, the PCR reagents were combined in a PCR microfuge tube on ice (31 µL nuclease-free water, 10 µL 5x Phusion HF Buffer (NEB), 1 µL 10 nM dNTPs (Promega)). This was followed by the addition of 2.5 µL of 10 µM forward EcoRI primer and 2.5 µL of one of the 10 µM reverse mutational clone primers. Approximately 200 ng of template DNA vector was then added to the reaction mixture. The template DNA vectors were pCMV-SPORT6 (V_1E2) and pOTB7 (V_1E1) (Source BioScience, Nottingham). These vectors had also been verified by sequencing and the plasmid maps are shown in Figure S 8-2. To complete the reaction mixture, 1.5 µL of DMSO (3%) and 0.5 µL of Phusion DNA polymerase (NEB) was added. The first PCR step was then carried out as follows:

1. Initial denaturation at 98°C for 30 seconds
2. 30 cycles of heating (98°C for 5 seconds, 55-72°C * for 30 seconds and 72°C for 15 seconds)
3. Final extension at 72°C for 5 minutes
4. Hold at 4°C

*The temperature of the second heating step at step 2 varied depending on the Tm of the primer (Table 2-9, Table 2-10 and Table 2-11).

This first step PCR was then repeated for a separate reaction except with 2.5 µL of 10 µM reverse XhoI primer and 2.5 µL of one of the 10 µM forward mutational clone primers. The purpose of this step was to form two individual PCR fragments, one which contained the EcoRI restriction enzyme site and one which contained XhoI. Following this, the two PCR fragments had to be joined to form one complete DNA product. To do this, the PCR fragments were diluted to a 1:1 ratio by combining 1 µL of each fragment and 998 µL of ddH_2O in a microcentrifuge tube. The same PCR protocol was followed as in step 1, however instead of the template vector DNA, 1 µL of the diluted PCR product solution was used, which was to act as the new DNA template. After this second step of the PCR, the final PCR products were confirmed using agarose gel electrophoresis.

Table 2-9. V_1E2 PCR programme

List of steps used for the V_1E2 two-step PCR, with specific temperatures and times.

V_1E2 PCR	STEP	TEMP	TIME
Denaturation	Initial Denaturation	98°C	30 seconds
	All	98°C	5 seconds
30 Cycles	E61K	61°C	30 seconds
	E61V	64°C	30 seconds
	E61Q	64°C	30 seconds
	Second cycle (Both fragments combined)	72°C	30 seconds
Extension	All	72°C	15 seconds
	Second cycle	72°C	25 seconds
	Final Extension	72°C	5 minutes
	Hold	4°C	

Table 2-10. V_1E1 PCR programme

List of steps used for the V_1E1 two-step PCR, with specific temperatures and times.

V_1E1 PCR	STEP	TEMP	TIME
Denaturation	Initial Denaturation	98°C	30 seconds
	All	98°C	5 seconds
30 Cycles	E61K	55°C	30 seconds
	E61V	56°C	30 seconds
	E61Q	56°C	30 seconds
	Second cycle (Both fragments combined)	72°C	30 seconds
Extension	All	72°C	15 seconds
	Second cycle	72°C	25 seconds
	Final Extension	72°C	5 minutes
	Hold	4°C	

Table 2-11. Vma4 PCR programme

List of steps used for the Vma4 two-step PCR, with specific temperatures and times.

Vma4 PCR	STEP	TEMP	TIME
Denaturation	Initial Denaturation	98°C	30 seconds
	All	98°C	5 seconds
30 Cycles	L66K	59°C	30 seconds
	L66E	61°C	30 seconds
	L66Q	62°C	30 seconds
	Second cycle (Both fragments combined)	72°C	30 seconds
Extension	All	72°C	15 seconds
	Second cycle	72°C	25 seconds
	Final Extension	72°C	5 minutes
	Hold	4°C	

2.9.3 Agarose gel electrophoresis

To visualise the PCR product DNA, 10 µL of each product was combined with 2 µL of 5x loading dye in a microcentrifuge tube. Following this, 10 µL of the product was loaded onto a 1% agarose gel (1 g agarose, 100 mL 1x TAE, 4 µL Gel Red nucleic acid stain (Bio-Rad)). The gel was then placed in a tank containing 1x TAE buffer and an electrical current was passed through the buffer. The negatively charged DNA then moves towards the positively charged electrode, separating the DNA based on its molecular size. Agarose gels were run at 100 V for approximately 1 hour. After it had finished running, the DNA was visualised using UV light, which was possible due to the Gel Red stain intercalating with the DNA and then producing a detectable luminescent signal under UV light.

2.9.4 Agarose gel DNA extraction

To select for the correct clone sequences the DNA was extracted and purified using agarose gel electrophoresis. However, this process normally causes a large loss of product. To counteract this, I duplicated step two of the two step PCR procedure to double the amount of final PCR product. The PCR products were run next to each other and once the gel had finished running the PCR fragments were extracted from the gel. To do this the gel had to be transported to a UV imager so that the DNA bands could be visualised. Using a scalpel, the PCR product DNA was cut out of the gel and transferred to a microcentrifuge tube. To digest the agarose and release the PCR product, the Qiagen Gel Extraction Kit was used as per the manufacturer's instructions.

2.9.5 Bacterial transformation

The recipient vector of interest (pKT10-N-myc) needed to be isolated and purified. This was achieved by first quantifying the concentration of pKT10-N-myc vector DNA using a NanoDrop. Based on the concentration, around 5 ng of the expression vector was combined with 20 µL of Sub-cloning Efficiency DH5α cells (Invitrogen) in a microcentrifuge tube. This was then gently mixed and incubated on ice for 30 minutes. Following incubation, the cells underwent heat shock at 42°C for 45 seconds on a heat block. The cells were then placed immediately on ice for exactly 3 minutes. Using a flame to sterilise the bottle neck of LB media, 200 µL of LB was added to the microcentrifuge tube. This transformation mixture was then incubated for 30 minutes at 37°C. To select for the vector of interest, 100 µL of transformed cells were spread on ampicillin plates (50 µg/mL), which were then placed in an incubator overnight at 37°C. Once bacterial colonies were present on the plates, one colony was extracted and inoculated in 5 mL of liquid LB media

containing ampicillin. The LB culture was then incubated overnight at 37°C with gentle shaking (120 rpm). The following day, 1.5 mL of LB culture was used for DNA extraction. The Qiagen Spin MiniPrep Kit was used as per the manufacturer's instructions. Purified vector DNA was stored at -20°C for future use.

2.9.6 DNA restriction digest

The pKT10-N-Myc vector and the PCR products were digested using two restriction enzymes (EcoRI and XhoI). EcoRI recognises the sequence GAATTC and digests double stranded DNA creating 'sticky ends' with a 5'-AATT overhang. On the other hand XhoI recognises CTCGAG creating a 5'-TCGA overhang. To digest the DNA the following reaction mixture was assembled in a microcentrifuge tube: approximately 1 µg/µL DNA (either vector or PCR product), 2 µL XhoI (NEB), 2 µL EcoRI (NEB), 3 µL CutSmartBuffer (NEB) and 0.2 µL BSA (NEB). The reaction mixture was made up to 50 µL with ddH_2O. The double digest mixture was incubated overnight at 37°C to ensure complete digestion.

The following day, agarose gel electrophoresis was used to verify that the digestion had been successful. The digested products were run alongside their undigested counterparts at 100 V for 1 hour. Once the double digest had been confirmed, the PCR product digests were heated to 65°C for 15 minutes to inactivate the restriction enzymes. To prevent recircularization and re-ligation of the vector DNA, 3 µL of Thermosensitive Alkaline Phosphatase (Promega), 6 µL of Multicore 10x buffer (Promega) and 1 µL of ddH_2O was added to the vector only digest mixture. To activate the phosphatase, the mixture was heated at 37°C for 15 minutes. Following this, the vector digest mixture was then heated at 72°C for 15 minutes to deactivate the phosphatase. As an additional DNA purification step, agarose gel DNA extraction was repeated for both the digested vector and PCR products.

2.9.7 DNA ligation

The DNA concentration of the vector and PCR products was quantified using the NanoDrop. Based on their respective concentrations, a ratio of 3:1 (Insert:vector) of the PCR product and vector were combined in a microcentrifuge tube. To concentrate the PCR products and vector DNA, 2x volume of 100% ethanol and 0.1x volume sodium acetate was added to the reaction mixture. This was then stored at -80°C for at least 2 hours. The reaction mixture was centrifuged at 13,000 rpm (16,060 g) for 15 minutes and the supernatant was discarded. To wash the pellet, 250 µL of 70% ethanol was added to the mixture and centrifuged at 16,060 g for 5 minutes. The supernatant was again removed and the pellet was air dried for approximately 1 hour. Once completely dry, 17 µL

of 1x TE was used to re-suspend the pellet, which was then transferred to a PCR microfuge tube. For the ligation reaction to occur 10% (2 µL) of T4 DNA Ligase Buffer (NEB) and 0.5 µL of T4 DNA ligase (NEB) was added to the microfuge tube and gently mixed. The reaction mixture was then incubated in a PCR thermal cycler at 16°C overnight.

2.9.8 Alkaline lysis DNA extraction

To verify the DNA ligations had been successful, Library Efficiency DH5α cells (Invitrogen) were transformed with the ligated DNA. After incubation in liquid LB media, the alkaline lysis method was used for DNA extraction. In a microcentrifuge tube, 1.5 mL of overnight inoculant was centrifuged at 8000 rpm (6800 g) for 2 minutes. The supernatant was then discarded and 100 µL of Tris-EDTA solution was added to the pellet, which was then vortexed until the pellet had completely dissolved. To this, 200 µL of solution AL1 was added and mixed gently until the solution became transparent. This was followed by the addition of 150 µL of solution AL2, which was again mixed gently for several minutes. After 5 minutes of incubation at room temperature the solution was centrifuged at 13,000 rpm (16,060 g) for 15 minutes. To a new microcentrifuge tube, 450 µL of the supernatant was combined with 450 µL of isopropanol and was thoroughly mixed. This was again centrifuged at 13,000 rpm (16,060 g) for 15 minutes and the supernatant was discarded. The resulting pellet was washed with 250 µL of 70% ethanol and centrifuged at 13000 rpm (16,060 g) for 5 minutes. Following this, the supernatant was discarded and the pellet was air dried. Finally 1x TE with RNase A was added and the pellet was dissolved by incubating on ice for at least 30 minutes. The extracted DNA was then run on an agarose gel to verify that the ligated product was at approximately the right band size. Once this was confirmed, the DNA was extracted from the bacterial cultures using the Qiagen Mini Prep Kit as per the manufacturer's instructions.

The purpose of using two different DNA extraction methods was because the alkaline lysis method was quick and relatively inexpensive when using a large volume of samples. However, the resulting DNA was not as 'clean' as the DNA extracted using the Qiagen Mini Prep Kit. Therefore, the Qiagen Mini Prep Kit DNA was sent for Sanger sequencing.

2.9.9 DNA sequencing

Plasmid DNA (~100 ng/µL) with the appropriate forward and reverse primers (10 pmol/uL) were sequenced. Sanger DNA sequencing was completed by Eurofins Genomics EU using the TubeSeq service. The chromatogram sequencing traces are shown for V_1E1 mutants (Figure S 8-3), V_1E2 mutants (Figure S 8-4), and Vma4 mutants (Figure S 8-5).

2.10 Gene editing

2.10.1 SiRNA mediated gene knockdown

Short interfering RNA (siRNA) are short double-stranded RNAs, which are able to degrade mRNA encoding a protein of interest. They are an example of RNA interference (RNAi) technology designed to target specific mammalian mRNA and induce a knockdown of a protein of interest. The siRNA becomes part of a RNA-induced silencing complex (RISC), which then identifies the complementary mRNA of the target and cleaves it. Once cleaved, the target is degraded and protein expression is therefore reduced. A summary of the biological mechanism in which siRNA silences gene expression is shown in Figure 2-4. To ensure that the transcript was efficiently cleaved, multiple siRNAs were pooled together, each targeting different regions of the desired transcript.

Experimental siRNA and non-specific siRNA were purchased from Dharmacon and were diluted with 1x siRNA buffer to give a final concentration of 25 nmol (Table 2-12). To achieve better gene knockdown efficiency, the cell lines were reverse transfected with the appropriate siRNA. Firstly, both the siRNA and Dharmafect 1 reagent were diluted in serum free CSS and in separate microcentrifuge tubes. After a 5 minute incubation at room temperature, the siRNA and Dharmafect solutions were mixed at a 1:1 ratio and were incubated for a further 20 minutes. Whilst incubating, cells were washed in CSS media, trpysinized, counted and diluted in CSS media. After 20 minutes, the siRNA/Dharmafect solution was added to the wells of a 96- or 6-well plate and the cells were added on top. Depending on the downstream application, the cells were incubated in the siRNA containing media for 24, 48 or 72 hours prior to harvesting.

Table 2-12. siRNA used in genetic knockdown experiments

List of commercial siRNA and the final concentrations that were used.

siRNA	Catalogue number	Final concentration
ON-TARGETplus Non-targeting Pool	D-001810-10-05	25 nmol
ON-TARGETplus Human ATP6V1C1 (528) siRNA - SMARTpool	L-013139-01-0005	25 nmol
ON-TARGETplus Human ATP6V1C2 (245973) siRNA - SMARTpool	L-016263-01-0005	25 nmol
ON-TARGETplus Human ATP6V1A (523) siRNA - SMARTpool	L-017590-01-0005	25 nmol

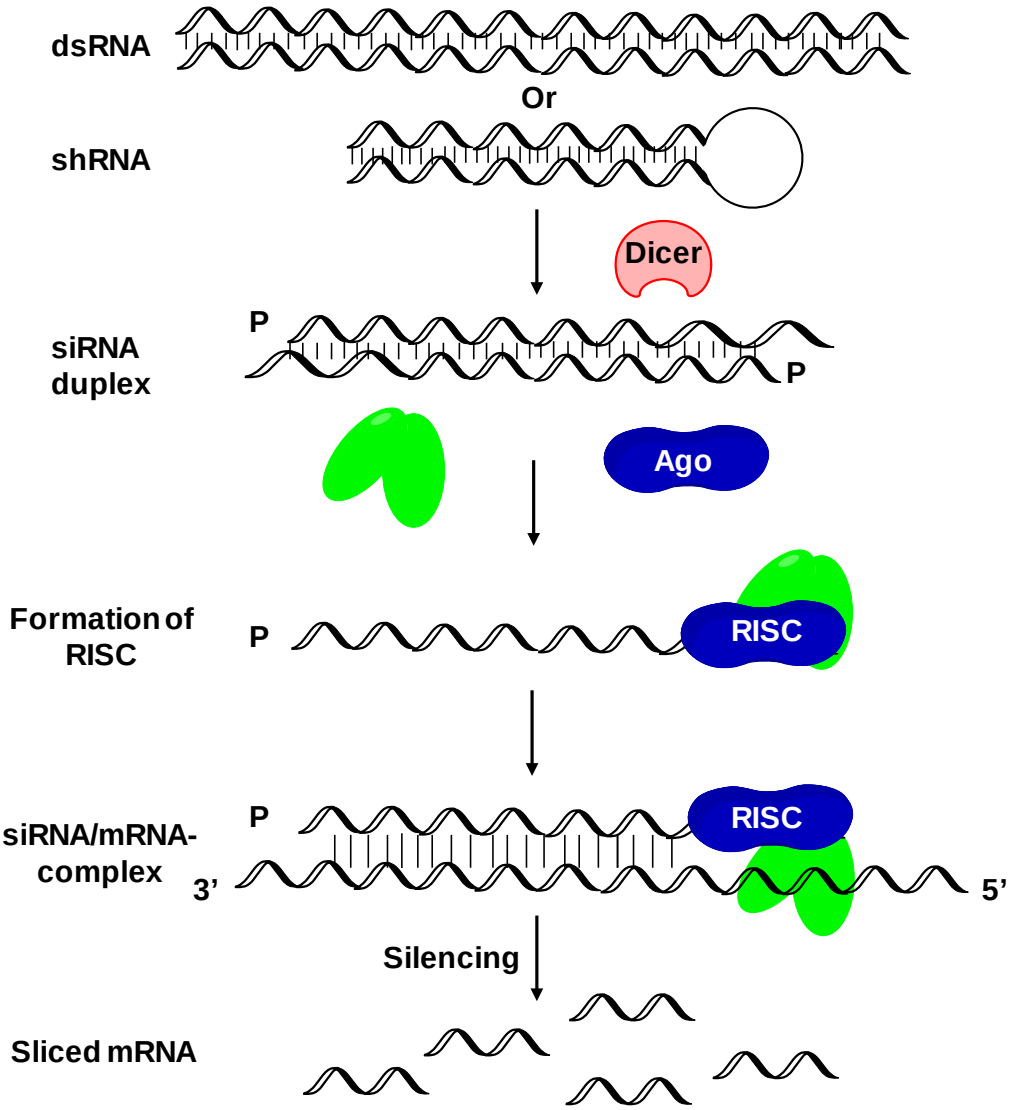

Figure 2-4. siRNA mechanism of action

Double-stranded or small-hairpin RNA is cleaved by an endonuclease called Dicer, forming the siRNA. The siRNA enters the cell and forms the RISC complex, which results in unwinding of the siRNA to form single-stranded RNA. Single-stranded RNA finds complementary mRNA, binds to it, and induces mRNA cleavage. The cleaved mRNA is now recognised as abnormal and is degraded by the cell, resulting in gene silencing. Illustration prepared in ChemDraw Professional 16.0. RISC, RNA-induced silencing complex; dsRNA, double-strand RNA.

2.10.2 CRISPR-Cas9

2.10.2.1 Introduction

Clustered Regularly Interspaced Short Palindromic Repeat (CRISPR) systems are well characterised immune systems found in bacteria and archaea. The systems were first observed by *Moijica et al.* in *Haloferax mediterranei* in 1993 (315), and over the past 30 years have been developed into efficient gene editing tools. The Zhang group were the first to successfully utilize CRISPR-Cas9 for genome editing in eukaryotic cells. They produced two Cas9 orthologs and demonstrated specific cleavage of genomic targets in mammalian cells (316).

Modern CRISPR-Cas9 systems are comprised of two key components: a CRISPR-associated endonuclease (Cas protein) and a guide RNA (sgRNA). The sgRNA is a short RNA sequence, which incorporates a scaffold sequence required for Cas9-binding and nucleotide spacer (~20 nt) that defines the genomic target. Genomic knockout cells can be produced in mammalian cells by co-expressing this sgRNA and an endonuclease such as Cas9. Theoretically, any ~20 nucleotide sequence can be targeted providing that, compared to the rest of the genome, the nucleotide sequence is unique and the desired target is adjacent to a Protospacer Adjacent Motif (PAM) (317).

The PAM sequence is a binding signal for the Cas9 endonuclease, but the sequence is dependent on which Cas protein is used. Expression of SpCas9 and the introduction of a sgRNA results in the formation of a ribonucleoprotein complex via interactions with the scaffold portion of the guide and the positively-charged grooves on Cas9. The binding of the sgRNA leads to a Cas9 conformational change, consequently shifting Cas9 to an active DNA-binding conformation, and the sgRNA spacer region is free to interact with target DNA. Cleavage will only occur at a specific locus if the sgRNA spacer region is homologous with the DNA of the target. The seed sequence (8-10 bases at the 3′ end of the sgRNA) will then begin to anneal the DNA once the Cas9-sgRNA complex is bound to the target. If the DNA target matches the seed sequence, the sgRNA will continue to anneal in a 3′ to 5′ direction. Therefore, mismatches between the 3’ seed sequence and the target will result in a termination of cleavage, whereas mismatches in the 5’ end are often tolerated and the target is still cleaved. Upon target binding, Cas9 undergoes another conformational change and positions the nuclease domains, RuvC and HNH, to cleave opposite strands of DNA. This DNA cleavage results in a double-strand break within the target sequence, which is illustrated in Figure 2-5, and usually occurs ~3-4 nucleotides upstream of the PAM sequence (317).

The resulting DSB is then repaired by the non-homologous end joining (NHEJ) or homology directed repair (HDR) pathways. NHEJ tends to be more efficient but more prone to error and the HDR is less error prone but high-fidelity. Both repair pathways have their advantages and disadvantages but I opted to utilize the NHEJ repair mechanism.

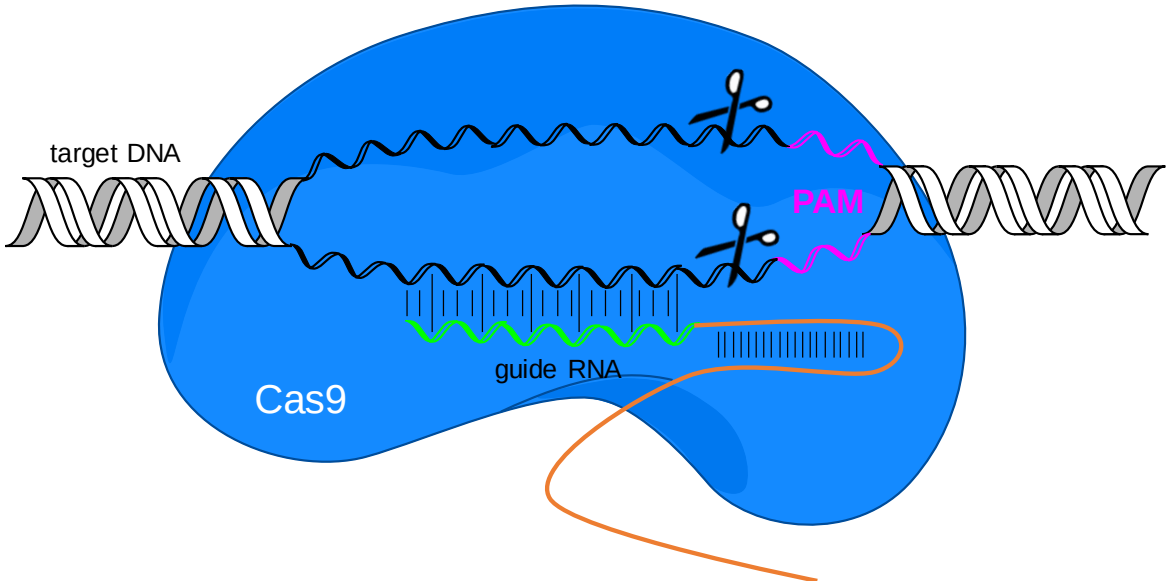

Figure 2-5. CRISPR-Cas9 mediated DNA cleavage

Cas9 is an endonuclease that is directed to its target by a guide RNA sequence (sgRNA), where it cuts both strands of DNA. This cut occurs adjacent to a PAM site, which is a specific sequence of DNA at the 3' end of the sgRNA. The PAM sequence acts as a binding signal for the Cas9 endonuclease, but each Cas endonuclease protein recognises a specific PAM sequence. After cleavage of the target, either the DNA is repaired by the non-homologous end-joining pathway (NHEJ) or homology directed repair pathway (HDR).

2.10.2.2 Non-homologous end joining (NHEJ)

NHEJ does not require a repair template and is active throughout the cell cycle, and therefore has a higher capacity for repair than HDR. The key proteins involved in the NHEJ process are Ku protein, DNA-dependent protein kinase (DNA-PKc), XRCC4 and DNA ligase IV (318). If any of these important proteins are defective or reduced, there is an increase in the sensitivity to DSB-inducing agents, such as radiation. The three main steps that are involved in the NHEJ process are DNA binding, terminal end processing and ligation. It begins with the recognition and binding of the Ku heterodimer (Ku70 and Ku80) to the broken ends of the DNA, forming a bridge between the ends, which protects them from degradation and aligns the DNA to promote end joining (318). The Ku heterodimer than recruits DNA-PKCs, which phosphorylate nuclear proteins such as DNA ligase IV and XRCC4. Terminal end processing is required in some cases to generate the two blunt ends required for the NHEJ process. For example, single stranded overhangs can be trimmed by nuclease activity or new elements can be synthesised by a DNA polymerase. Once the Ku complex has the blunt ends in place, the two subunit DNA ligase complex, formed of XRCC4 and DNA ligase IV, is recruited to ligate the ends together. Although the DNA ligase IV conducts the ligation, the XRCC4 is required to stabilise and direct the complex to the appropriate DNA site. After ligation the resulting DNA strands are thus repaired and the process is complete (317, 318).

The repair process is also much quicker than HDR and takes approximately 10 minutes for most DNA breaks (319). NHEJ is particularly useful if the aim is to make a gene knockout as the process is prone to producing heterogeneous indel errors, consequently creating the chance of a frameshift mutation in around two-thirds of NHEJ-mediated Cas9-generateed breaks (320). Given that the Cas9 double strand breaks are usually blunt ended, indel events are actually quite rare, predicted to be less than 5% of all potential repair events (320). However, products that are repaired accurately are more easily re-cleaved than the indel products, and therefore later cell cycles will result in the accumulation of indel events. A summary of the Cas-9 mediated NHEJ outcomes are shown in Figure 2-6.

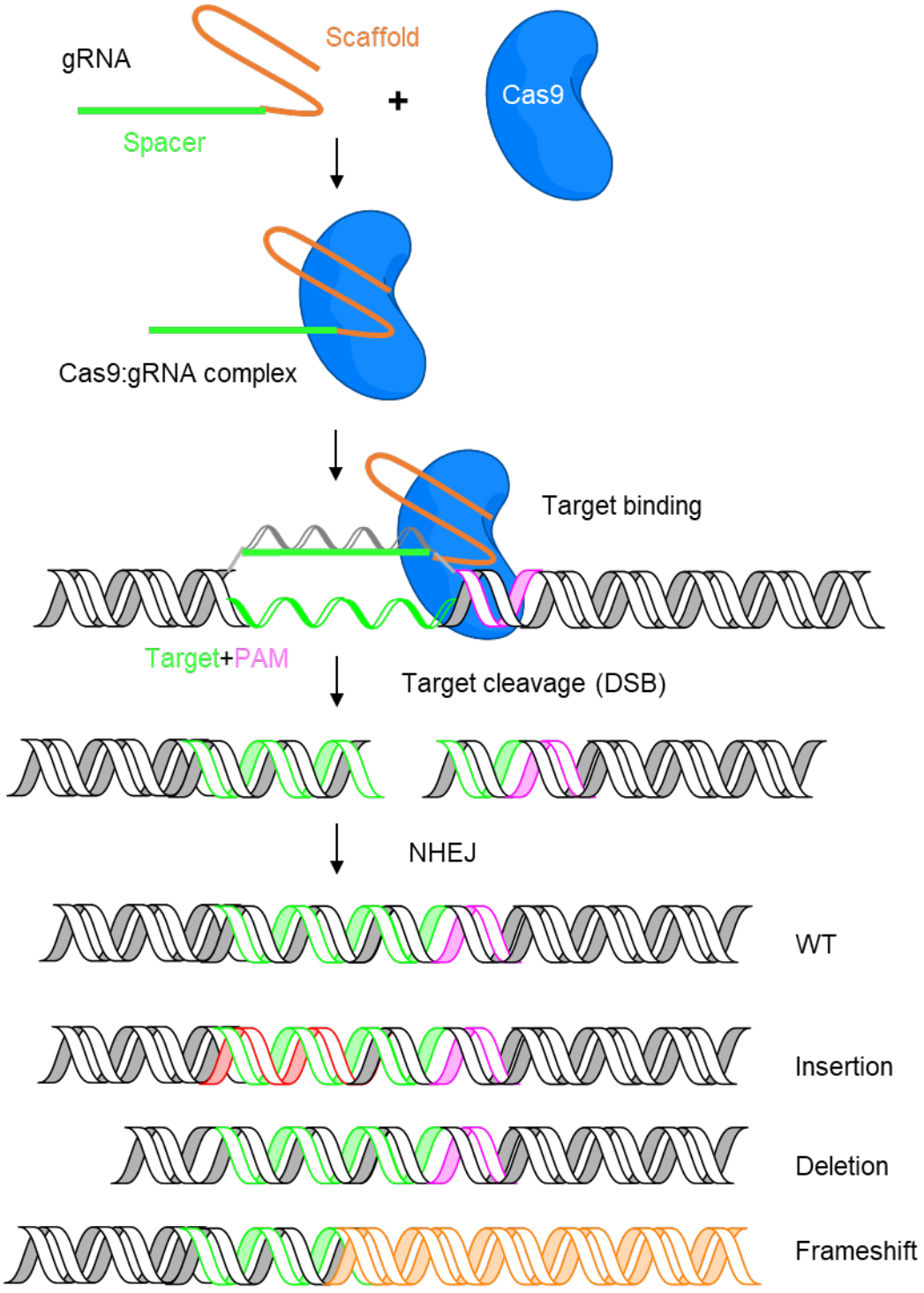

Figure 2-6. Cas-9 mediated non-homologous end joining

The guide RNA (gRNA) is composed of a RNA scaffold and 20 nucleotide spacer sequence. When expressed with the Cas9 protein, the Cas9:gRNA complex is directed to a specific target adjacent to a PAM site. The Cas9 endonuclease then cleaves the target resulting in a DNA double strand break. This break is then repaired by either the non-homologous end-joining (NHEJ) or homology directed repair (HDR) pathway. The NHEJ pathway can have several outcomes including; repairing the wild-type sequence, an insertion of nucleotides, a deletion of nucleotides or a base-pair induced frameshift.

2.10.2.3 Methodology

2.10.2.3.1 Design

To produce stable gene knockouts, a CRISPR plasmid with puromycin resistance was selected as the sgRNA vector. The plasmid pSpCas9(BB)-2A-Puro (PX459) V2.0 was a gift from Feng Zhang (Addgene plasmid # 62988 ; http://n2t.net/addgene:62988 ; RRID:Addgene_62988) (317) and is depicted in Figure S 8-6. This plasmid contained the Cas9 gene for Cas9 protein expression as well as the sgRNA scaffold sequence under the control of a U6 promoter. Therefore, the single plasmid contained everything that was required for expression of a complete sgRNA:Cas9 complex, except the 20 nt spacer that was specific for the target DNA.

The sgRNA was designed by first selecting the human protein coding transcript for the full length target gene of interest, *ATP6V1C1* (ATP6V1C1-202; ENST00000518738.2). All of the known transcripts (coding and non-coding) and their chromosomal locations were then viewed in the NCBI nucleotide database (GRCh3, Ensembl release 97). Using this tool, the earliest exon that was present in all *ATP6V1C1* transcripts was selected as the CRISPR target (exon 5). By selecting an exon present in all available transcripts it meant that there was the highest possible chance of successfully targeting the *ATP6V1C1* gene. After selecting exon 5 as the target, the exon sequence was downloaded from Ensembl (ENSE00001019174) and pasted into two different online CRISPR algorithms for predicting sgRNA specificity; CRISPOR and Wellcome Sanger Institute Genome Editing (WGE). The online tools then ranked potential 20 nt guide sequences based on how specific they are for the target and the number of potential mismatches. Both of the two algorithms selected the following sequence as the optimal sgRNA sequence for targeting exon 5 of *ATP6V1C1*, which was adjacent to a TGG PAM site: GGACTGCTTGATTGGATATT. The guide RNA summary produced by WGE is shown in Table 2-13.

Table 2-13. WGE sgRNA summary

The sgRNA sequence used for cas9-mediated *ATP6V1C1* knockout was designed using the Wellcome Sanger Institute Genome Editing (WGE) online tool.

	WGE sgRNA summary
WGE ID	1045537945
Sequence	GGACTGCTTGATTGGATATT TGG
Location	8:103051092-103051114
Mismatches	0
Strand	Negative
Type	Exonic

Following sgRNA sequence selection, forward and reverse primers were designed with BbsI 5'CACC and 5'AAAC overhangs to generate sticky-ends upon restriction digest, allowing effective ligation into the CRISPR-Cas9 plasmid. The respective forward and reverse primer sequences purchased (Sigma) were as follows: ATP6V1C1-F CACCGGGACTGCTTGATTGGATATT, and ATP6V1C1-R AAACAATATCCAATCAAGCAGTCCC. Upon arrival, the primers were diluted to 10 µM in ddH_2O as in 2.9.1.

2.10.2.3.2 Plasmid preparation

The next stage was to clone the sgRNA sequence into the CRISPR vector. To do this, 1 µg of plasmid, 2 µl 10x buffer G (Thermo Fisher), 1 µL BbsI (Thermo Fisher) and ddH_2O were combined in a microcentrifuge tube to make a 20 µL restriction digest mixture, which was incubated at 37°C for an hour before cooling on ice. Whilst plasmid digestion was occurring, the forward and reverse sgRNA primer sequences were annealed. In a PCR tube, 1 µL of forward and 1 µL of reverse sgRNA primers were combined with 8 µL of ddH_2O. The reaction mixture was heated in a PCR machine at 37°C for 30 minutes, 95°C for 5 minutes before a slow ramp to 25°C at 0.1°C per second. Once both primer PCR fragment and plasmid digest were complete the resulting products were ligated by adding 18 µL of digested plasmid, 20 µL of 2x Quick ligase buffer (NEB), 1 µL of annealed sgRNA oligos and 1 µL of Quick ligase (NEB) to a microcentrifuge tube and incubating for 10 minutes at room temperature. Following ligation, 20 µL of DH5α cells were transformed with 2 µL of ligation mixture as described in 2.9.5. The transformed cells were plated onto ampicillin LB plates and incubated at 37°C overnight. Five bacterial colonies were then picked, inoculated in 5 mL of LB broth each and incubated overnight at 37°C with shaking (200 rpm). The following day, 1.5 mL of LB culture was used for DNA extraction using the Qiagen Spin MiniPrep Kit. The five bacterial colonies were then screened to assess which colony had the sgRNA insert. This was completed by combining 2 µL Buffer G, 1 µg DNA, 0.5 µg BbsI, 1 µL AgeI and ddH_2O in a microcentrifuge tube to make a 30 µL double digest reaction mixture. The reaction mixture was then incubated at 37°C for 90 minutes before the digested DNA products were run on an agarose gel as described in 2.9.3. If the sgRNA had been successfully inserted then only 1 band would be present on the gel as successful insertion destroys the BbsI site. The DNA with the sgRNA inserts were then sent for confirmation using Sanger sequencing as described in 2.9.9.

2.10.2.3.3 Clonal selection

Following confirmation that the Cas9 plasmid contained the sgRNA insert, the next step was to transfect the desired cell lines with the sgRNA:Cas9 plasmid and select for the positive cells. The cell lines used were the LNCaP and 22Rv1 cell lines, which were

selected to model hormone sensitive and insensitive prostate cancer respectively. The LNCaP and 22Rv1 cells were seeded in RPMI complete media at a density of $5x10^5$ cells per well in a 6-well plate. They were then transfected with the sgRNA:Cas9 plasmid containing the *ATP6V1C1* INDEL guide and an empty control Cas9 plasmid using FugeneHD (Promega). The FugeneHD transfection reagent (6 µL) was added to 100 µL of phenol-red free CSS RPMI in one microcentrifuge tube, and 2 µg of sgRNA:Cas9 plasmid DNA was added to 100 µL of the same media in another tube. After 5 minutes of individual incubation at room temperature, both microcentrifuge tubes were combined and were incubated for a further 30 minutes at room temperature. This was repeated for the empty Cas9 plasmid controls and another well in which just FugeneHD reagent was added to act as a non-transfected control in both cell lines. Following 24 hours post-transfection, cells were treated with 1.5 µg/mL puromycin for a further 48 hours.

Once cell death was observed in the non-transfected control wells, the surviving transfected cells were washed with fresh RPMI media to remove any remaining toxic transfection reagent. To isolate a single cell to develop a clonal population, the cells underwent a selection process that is summarised in Figure 2-7. The sgRNA:cas9 and Cas9 plasmid control cells were grown at 37°C until they reached 80% confluence and then they were split into four 10 cm plates per cell line. One 10 cm plate per cell line was seeded at a density of $5x10^5$ cells for freezing the mixed population at -80°C, the other three plates were seeded a density of 50 cells only. The plates were incubated for 5-8 days to allow individual colony formation. Once colonies were large enough they were picked and re-plated into numbered 24 well plates. To do this, the plates were first washed with 5 mL 1x PBS, trypsinized and incubated for 5 minutes to allow detachment. As both LNCaP and 22Rv1 cell lines are adherent, the best way to select individual colonies was to use a pipette tip with 5 µL of trypsin on the end and to scrape the colony off the plate and transfer it to a well with 500 µL of RPMI media. This was repeated for each well of the 24-well plate for the sgRNA:Cas9 cells and Cas9 control cells for both cell lines. The colonies were then incubated until they reached 80% confluency, where sgRNA:Cas9 cells were then split and re-seeded into 2x 12-well plates, whereas the Cas9 control cells were split into a single 12-well plate. After they again reached 80% confluence, they were split and re-seeded into 4x 6-well plates (or 1x 6-well plate for Cas9 controls). Once confluent, the 4x 6-well plates were split and seeded into 8x 6-well plates, and the Cas9 control cells into 2x 6-well plates. At 80% confluency, 4x 6-well plates (or 1x Cas9 control) were split and seeded for maintenance whereas the other 4x 6-well plates (1x Cas9 control) were harvested for western blot validation (2.4.1). At this point I had 24 samples from sgRNA:Cas9 LNCaP cells, 6 from Cas9 control LNCaP cells, 24 from sgRNA:Cas9 22Rv1 cells and 6x Cas9 control 22Rv1 cells.

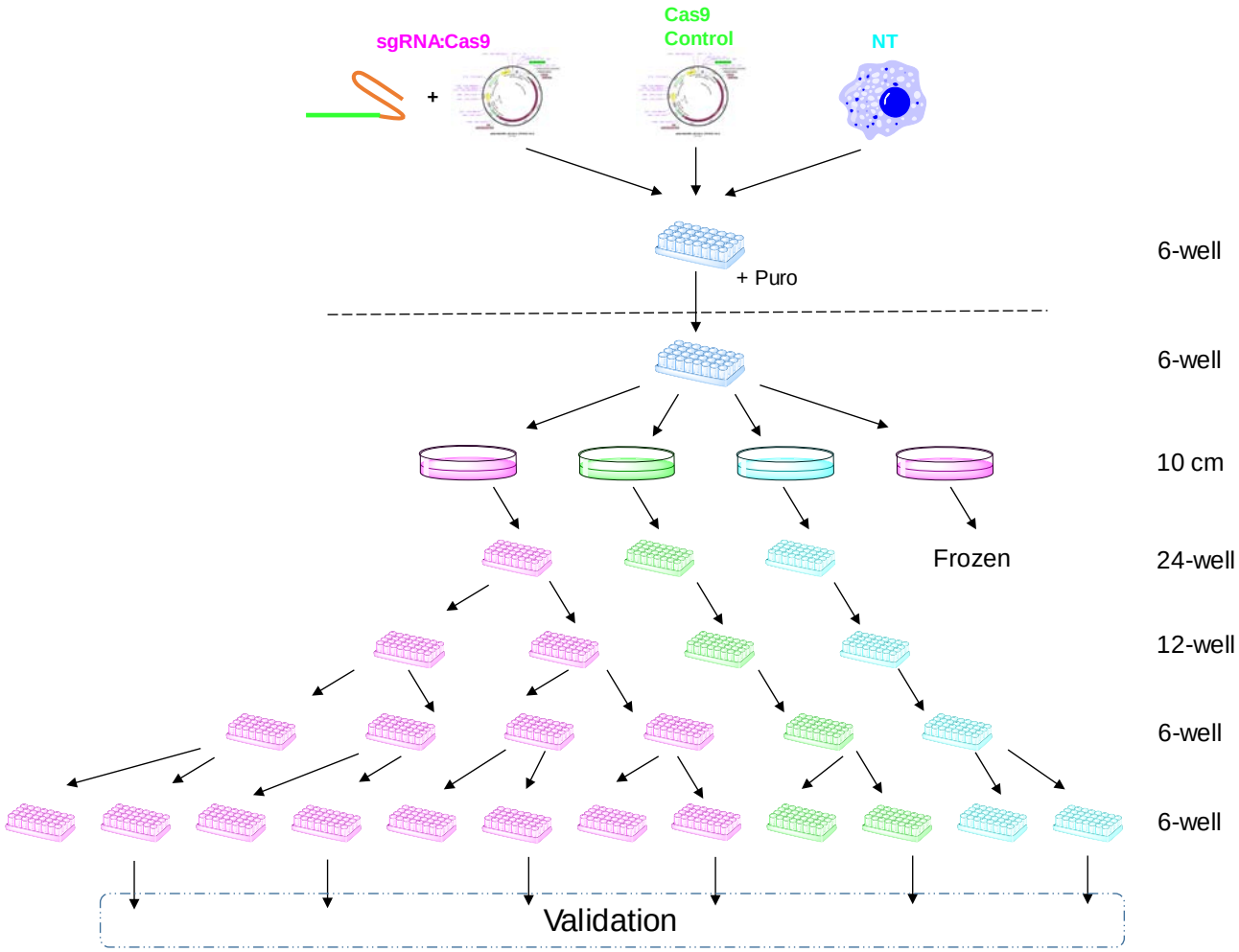

Figure 2-7. CRISPR-Cas9 clonal selection process

Cells were transfected with either a Cas9 plasmid with sgRNA or an empty Cas9 control plasmid, and a non-transfected control was also included. Puromycin was added and the surviving cells were grown to confluency in a 6-well plate. From each well, cells were seeded at a density of 50 cells per 10 cm plates, except for one sgRNA:CRISPR mixed population plate that was seeded at $5x10^5$, ready to be frozen and stored at -80°C. After colony formation, 24 colonies were picked and re-plated into numbered wells of a 24-well plate. Once the cells were confluent, they were split and seeded into 12-well plates before re-seeding into 6-well plates. At the final 6-well stage, one plate was used for maintenance, whilst cells in the other plates were harvested for validation by either western blotting or Sanger sequencing. NT, non-transfected; Puro; puromycin.

2.10.2.3.4 Validation

To validate that the CRISPR-Cas9 system had successfully deleted the *ATP6V1C1* gene in both LNCaP and 22Rv1 cells, the samples were run on a western blot, which was probed for V_1C1 protein expression. The Cas9 control samples were run first next to a non-transfected control sample to ensure the Cas9 empty plasmid had not affected V_1C1 protein expression. Following this the experimental sgRNA:Cas9 cells were run with a control sample to compare V_1C1 expression. The samples which had no V_1C1 expression visible on the western blot were identified as potential knockouts. Going back to the sgRNA:Cas9 cells that were still in culture, only the positive knockout cells were kept and the remaining cells were discarded. At this stage, there was one LNCaP sample with a potential knockout and two 22Rv1 samples. Once the cells were confluent enough, they were split into 3x 10 cm plates; one for maintenance, one for further validation and one for storage at -80°C. It is important to note that it was particularly difficult to achieve complete clonality in LNCaP cells as they grow poorly as individual cells, which is why it is likely that only one colony appeared to have a V_1C1 knockout.

The cells destined for further validation were harvested in PBS and the DNA was extracted using the Qiagen DNA MiniPrep kit. Following extraction, the DNA products were amplified using PCR as described in the first step of 2.9.2 at an annealing temperature of 55°C, with the following forward and reverse primers: V1C1-Seq-F ATGTGGACTCCTGGAAACAATCA, and V1C1-Seq-R TAGTCCGAAGGGGTCAGAGA. The resulting PCR products were run on an agarose gel (2.9.3) next to a control sample, and an example gel image is shown in Figure S 8-7. A small proportion of the remaining DNA, including the Cas9 control DNA, was sent for Sanger sequencing validation (2.9.9) using the above primers.

The sequencing revealed interesting information about each of the CRISPR-Cas9 engineered cells, which I will describe in more detail. Firstly, the sequencing data showed at least three traces on the chromatogram for the LNCaP mutant, indicating heterozygosity and the presence of three separate alleles (Figure S 8-8). At least on the agarose gel a large bp deletion was visible (Figure S 8-7), but the chromatogram traces were too difficult to separate. Therefore, I cannot be certain that all of the alleles have been mutated, and that a wild-type allele is not present, which is why the LNCaP CRSIPR cells are referred to as knockdown (k/d) rather than knockout (k/o). Additionally, the two 22Rv1 cell lines (named V1C1-14 and -18) had different chromatogram sequencing traces. V1C1-14 had two traces visible on the chromatogram, indicating heterozygosity and that the population was not clonal. However, on the agarose gel three DNA products were visible (Figure S 8-7) indicating that there were two insertions and one other

alteration. The alterations could not be identified from the sequencing data but it looked as if all the CRISPR induced mutations occurred at the same point and the sequences were mutated enough to prevent protein expression (Figure S 8-9). Furthermore, V1C1-18 had two chromatogram traces, suggesting two different alleles were present. Both of the alleles were edited at the same position but one had a two base deletion leading to a premature stop-codon and the other allele had a large base pair insertion (Figure S 8-10).

Yeast Manipulation Techniques

2.11 Materials for yeast manipulation techniques

Table 2-14. Materials for yeast manipulation techniques

List of materials used for all yeast manipulation techniques. All materials were purchased from Sigma or Fisher Scientific unless otherwise stated.

Reagents	Components
Solution 1	45 mL 1 M Tris/Cl pH9.4, 405 mL ddH_2O, 78 µL β-Me
Solution 2	8 g Yeast Extract, 16 g Bacto Peptone, 16 g Glucose, 360 mL ddH_2O, 280 mL 2 M Sorbitol,160 mL 0.5 M MES/Tris pH7.5, 156 µL β-Me
Solution 3	4.5 g Yeast Extract, 9 g Bacto Peptone, 9 g Glucose, 250 mL ddH_2O, 180 mL 2 M Sorbitol
Buffer A (12%)	1 mL 0.5 M MES/Tris pH6.9, 25 mL 24 % Ficoll 400, 24 mL ddH_2O, 5 µL 1M MgCl2
Buffer B (8%)	1 mL 0.5 M MES/Tris pH6.9, 16.6 mL 24 % Ficoll 400, 33 mL ddH_2O, 25 µL 1 M $MgCl_2$
Buffer B (4%)	1 mL 0.5 M MES/Tris pH6.9, 8.3 mL 24 % Ficoll 400, 41 mL ddH_2O, 25 µL 1 M $MgCl_2$
Buffer B (0%)	1 mL 0.5 M MES/Tris pH6.9, 49 mL ddH_2O, 25 µL 1 M $MgCl_2$
Buffer C (0%)	1 mL 0.5 M MES/Tris pH6.9, 47.5 mL ddH_2O, 1.25 mL 1 M KCl, 250 µL 1 M $MgCl_2$
Buffer Cg	20 µL 0.5 M MES/Tris pH6.9, 620 µL ddH_2O, 25 µL 1 M KCl, 5 µL 1 M $MgCl_2$, 330 µL 60 % Glycerol
Pi colouring solution	2.3 g $FeSO_4$, 20.16 mL ddH_2O, 2.5 mL 10 % Ammonium Molybdate
2x ATPase Buffer	4 mL 200 mM Mes/Tris pH 7.0, 6 mL 1 M KCl, 10 mL ddH_2O
50 mM ATP	100 µL 100 mM ATP, 100 µL 100 mM $MgCl_2$
1 mM ATP	20 µL 50 mM ATP/$MgCl_2$, 980 µL ddH_2O
YPD media (1.5 L)	15 g Yeast Extract, 30 g Bacto Peptone, 1.425 L ddH_2O, 75 mL 40 % Glucose
YPD agar pH 5.0	5 g Yeast Extract, 10 g Bacto Peptone, 10 g Bacto agar, 425 mL ddH_2O, 25 mL 40 % Glucose, buffered with 50 mL 0.5M KH_2PO_4
YPD agar pH 7.5	5 g Yeast Extract, 10 g Bacto Peptone, 10 g Bacto agar, 425 mL ddH_2O, 25 mL 40 % Glucose, buffered with 50 mL 0.5M K_2HPO_4
SD-ura media (1 L)	6.7 g Yeast Nitrogen Base, 0.7 g Complete Supplement Mixture (CSM) –ura, 950 mL ddH_2O, 24 g Agar (if making solid plates), 50 mL 40 % glucose (filtrated)

2.12 Yeast transformation

A single Vma4 positive yeast colony was inoculated in 5 mL of liquid YPD media and incubated for 24 hours so that the colony could grow and multiply. After incubation, 1 mL of yeast overnight culture was transferred to a microcentrifuge tube and centrifuged at 1,000 rpm (95 g) for 2 minutes at room temperature. The supernatant was discarded and 1 mL of ddH_2O was added to dissolve the pellet. To make sure the pellet was completely dissolved it was vortexed for 30 seconds. The microcentrifuge tube was centrifuged again at 1,000 rpm (95 g) for 2 minutes and the supernatant was discarded. This process was repeated twice more to wash the pellet. After the last centrifugation step, 100 µL of PEG mixture (100 µL of 10x TE, 100 µL of 1 M LiAc and 800 µL of 50% PEG) was added to the microcentrifuge tube and was thoroughly mixed using the vortex. Salmon sperm DNA (Thermo Fisher) was denatured at 95°C and 2 µL was added to the microcentrifuge tube prior to being vortexed. Following this, 2 µL of the desired plasmid DNA was added and mixed using the vortex for 30 seconds. The mixture was then heated at 45°C for 10 minutes and mixed for 30 seconds. This process was repeated twice more to ensure the plasmid would be incorporated into the yeast cell DNA. The cells were spread on SD-ura plates, which were then incubated at 30°C for 2-3 days.

2.13 Yeast vacuolar membrane purification

2.13.1 Inoculation

Up to 10 of the transformed yeast colonies were inoculated in 15 mL of liquid SD-ura media. The inoculant was incubated for 24 hours at 30°C with shaking at 220 rpm. After the incubation period, 1 mL of the inoculated solution was added to 25 mL of YPD media so that the OD-600 could be measured using a spectrophotometer. Based on the OD-600 result, between 2-10 mL of the overnight culture was used to inoculate 1.5 L of fresh YPD media. The culture was incubated for approximately 18 hours at 30°C with shaking at 125 rpm.

2.13.2 Cell collection

The overnight inoculant was centrifuged in large polycarbonate centrifuge vessels at 5,000 rpm (6220 g) for 10 minutes (Beckman Coulter J-Lite JLA-8.1000) and the supernatant was discarded. Solution 1 was added to the pellet and was mixed until the pellet had completely dissolved. This solution was then incubated at room temperature for 30 minutes, followed by centrifugation at 5,000 rpm (6220 g) for 10 minutes. Once again,

the supernatant was discarded before half of Solution 2 (400 mL) was added to the pellet, which was mixed until it had completely dissolved. The solution was centrifuged for a third time at 5,000 rpm (6220 g) for 10 minutes, the supernatant was discarded and the remainder of Solution 2 (400 mL) was used to dissolve the pellet. After the pellet had completely dissolved, the solution was transferred to a fresh 1.5 L flask and 18 mg zymolyase was added to aid in the destruction of the yeast cell wall. The zymolyase culture was incubated at 30°C for at least 4 hours to ensure complete yeast cell wall lysis. Following this incubation, the culture was centrifuged at 5,000 rpm (6220 g) for 10 minutes, the supernatant was discarded and all of Solution 3 was used to completely dissolve the pellet. The final centrifugation step was carried out as described above and the pellet was weighed and stored on ice at 4°C overnight.

2.13.3 Vacuolar membrane isolation

A series of buffers and centrifugation steps were necessary to isolate the vacuolar membrane. Firstly, based on the weight of the pellet collected in 2.13.2, 10x volume of Buffer A was added to the pellet and was mixed until the pellet had completely dissolved. This solution was then divided into several 33 mL centrifuge tubes so that the tubes were half filled. Buffer B (8%) was carefully layered on top of the solution so that there was a clear separation between the two layers. The tubes were centrifuged at 20,000 rpm (50,000 g) in the ultracentrifuge (Beckman Coulter Optima XE) for 30 minutes at 4°C (JA 25.50 Fixed Angle Rotor). After centrifugation, a white coloured layer was visible at the top of the centrifuge tubes. This white layer was collected and transferred to 12 mL centrifuge tubes until a third of each individual tube was filled. Buffer B (4%) was very carefully layered on top until two thirds of the tube was full. Finally Buffer B (0%) was layered on top until it reached the top of the centrifuge tube. At this point, 3 different layers were clearly visible. The tubes were centrifuged at 16,500 rpm (48,000 g) for 30 minutes at 4°C (SW 40 Ti Swinging-Bucket Rotor). After this centrifugation step, a thick white layer was visible between the top 2 layers (between B (0%) and B (4%)). This layer was collected, transferred to fresh 12 mL centrifuge tubes and was completely dissolved in Buffer C (0%). Once dissolved, the tubes were centrifuged at 22,800 rpm (90,000 g) for 30 minutes at 4°C. The supernatant was then removed, leaving vacuolar membrane pellets. All of the membrane pellets were completely dissolved in Buffer Cg using the vortex. After they had dissolved, the Cg vacuolar solutions were combined in 1 12 mL centrifuge tube, which was vortexed again before being aliquoted. The purified vacuolar membrane aliquots (130 µL) were snap frozen and stored at -80°C.

2.14 Yeast cell complementation

Yeast cells lacking the V_1E subunit (ΔE null) were generated by Dr Okamoto. They were then transformed as in section 2.12 with V_1E1/E2 mutant DNA. The colonies were picked and inoculated in SD-ura liquid media. After 15-18 hours of growth the culture was diluted and plated in series on either pH 5.0 or pH 7.5 buffered SD-ura agar plates. The agar plates were then incubated at 37°C for 4 days and images of the plates were taken using the GelDoc imager.

2.15 Measuring V-ATPase activity and function

2.15.1 Measuring vacuolar membrane ATPase activity using inorganic phosphate detection

To measure the activity of the V-ATPase enzyme in the vacuolar membrane, increasing concentrations of ATP (µM) were added to the purified vacuolar membrane. Furthermore bafilomycin-A1, a specific V-ATPase inhibitor, was used to specifically measure the activity of V-ATPases. This was achieved by creating 2 sets of ATP reactions, one with bafilomycin-A1 and one with DMSO/ddH_2O. The absorbance values for the bafilomycin-A1 reaction could then be subtracted from that of the DMSO/ddH_2O reaction, resulting in a non-linear curve of V-ATPase activity.

A Pi standard curve was first created by adding 300 µL of 2x ATPase buffer, 300 µL of 1 M TCA and increasing volumes of 10 mM KH_2PO_4 to a plastic test tube. Double distilled water was also included to make the total volume up to 900 µL per tube, making a Pi standard curve ranging from 0 – 100 µM. Once the standard curve had been made, 300 µL of 2x ATPase buffer and 5 µL of purified vacuolar membrane were combined in separate test tubes. Different volumes of ddH_2O were then added so that upon ATP addition there would be a final volume of 600 µL. Finally, 6 µL of 10 µM bafilomycin-A1 was added to the tubes to give a final bafilomycin-A1 concentration of 100 nM. The tubes were then incubated on ice for 60 minutes. After incubation, increasing volumes of either 50 mM or 1 mM ATP were pipetted into the tubes creating final ATP concentrations of 0, 2, 4, 10, 20, 40, 100, 200, 400, 1000, 2000 and 4000 µM. The reaction mixtures were heated at 30°C for 10 minutes before 300 µL of 1 M TCA was added to quench the reaction. This process was then repeated with 6 µL of 1% DMSO diluted in ddH_2O instead of bafilomycin-A1 to establish a control set of reactions. To measure the absorbance of reactions, 500 µL of Pi colouring solution was added to each tube in both control and bafilomycin-A1 samples. All tubes were then incubated at 30°C for 5 minutes with gentle shaking. The absorbance was calculated by adding 200 µL of each reaction mixture to a

96-well plate and measuring the absorbance at 690 nm. This assay was repeated at a 37°C.

After the assay had been completed the Pi standard curve was plotted on GraphPad Prism 7 creating a non-linear curve with an acceptable R^2 value ≥ 0.9985. Each ATP concentration used in the assay represented a different data point, giving a total of 12 data points per assay. The Pi standard curve was used to determine the relative Pi concentration (µmol) for each of the 12 data points in both the bafilomycin-A1 and DMSO datasets. The bafilomycin-A1 dataset was then subtracted from the corresponding data point in the DMSO control dataset. For example, in one assay at 30°C, the V_1 E2 wild-type membrane in the bafilomycin-A1 dataset produced a relative Pi concentration of 24.53 µmol at 200 µM ATP, whereas in the DMSO dataset the value was 68.67 µmol. Therefore, subtracting the bafilomycin-A1 value from the DMSO gave a positive result of 44.14 µmol. This was repeated for each concentration of ATP per dataset and the values were normalised to 1 minute by dividing each subtracted value by 10 (number of minutes in assay). These values were then normalised to the protein concentration of the membrane used for the individual assay (determined using the Bradford assay as in section 2.4.2), giving the µmol/min/mg. Finally, the µmol/min/mg values were plotted in GraphPad 7 to produce a non-linear curve of V-ATPase activity. Only assays that produced a non-linear curve with an R^2 value ≥ 0.985 were deemed acceptable to be used for further analysis and comparisons.

2.15.2 Measuring proton transport using acridine orange

Acridine orange is a pH dependent dye, which accumulates in acidic compartments. The H^+ gradient of cells is relative to the efficiency of proton pumping and can therefore be determined by measuring the quenching of acridine orange (321).

Vacuolar membranes were isolated from yeast cells as described in section 2.13 and the proton transport rate (ΔF/min/mg protein) was measured using acridine orange as described previously (322). Membranes (5 uL) were mixed with 2x ATPase buffer, 1 uL of 1 mM acridine orange (AO) solution and 10 nM baf-A1 in a cuvette containing a magnetic stirrer. A time scan recording was started on the spectrofluorimeter and the stirrer was initiated to enable efficient mixing of the membrane with AO. During the time of recording, a water bath was used to maintain the temperature of the samples at 20°C. Once the recording had stabilized, 30 uL of 50 mM ATP/Mg solution was added to the cuvette for 5 minutes. After 5 minutes, 15 uL of ammonium chloride was added to reverse the proton gradient and quench the reaction, and the fluorescence was recorded for a further 2 minutes. The rate of proton transport was determined by the quenching of acridine orange

fluorescence when excited at 495 nm and recorded at 530 nm. The fluorescence produced at the ATP max was subtracted from the maximum value post ammonium chloride addition. Data was then normalized to time (min) and protein concentration (mg).

Chapter Three

Chapter 3 Functional impact of V-ATPase subunit mutations on V-ATPase activity

Functional impact of V-ATPase subunit mutations on V-ATPase activity

3.1 Introduction

V-ATPase has many important physiological functions including endosomal trafficking and receptor recycling. However, the V-ATPase is more complex and versatile than a simple proton pump and novel functions, such as lysosomal amino acid sensing (76), are still being discovered. There is now emerging data showing that V-ATPase subunits are overexpressed in a number of different cancer types including breast, lung and prostate cancer (1). This overexpression has been directly linked to an increase in the invasive and metastatic capabilities of these cancers (1). More recently, mutations in V-ATPase subunits are being identified in patient tumour samples and are being linked with specific tumour types (323).

To date, most of the research into V-ATPase subunit mutations in cancer has been focussed on follicular lymphoma. For example, mutations in the *ATP6V1B2* and *ATP6AP1* genes have been detected in approximately 20% of follicular lymphoma patients. These mutations were found to commonly occur with *RRAGC* mutations, which promote inappropriate mTORC1 activation, and therefore may contribute to increased tumorigenesis in follicular lymphoma (323). Additionally, in a separate study nine patients were found to have *ATP6V1B2* mutations, with six of them harbouring the previously reported R400Q mutation. Two of the mutations identified were aligned to the yeast *Vma2p* homolog and were predicted to result in a complete loss of enzyme activity. Furthermore, the study also reported novel mutations in *ATP6V0A1*, *ATP6V1F* and *ATP6AP2* genes in follicular lymphoma patients (324). Recently, *ATP6V1B2* mutations were shown to activate autophagic flux and enable lymphoma cells to survive in low leucine conditions (325). Taken together, these findings indicate that V-ATPase mutations have a role in cancer development, at least with regards to follicular lymphoma.

Despite the emergence of V-ATPase subunit mutations in other cancer types, the role of such mutations has not been extensively studied and functional data is lacking. Therefore, the aim was to use publicly available data to identify V-ATPase subunit mutations in a variety of different tumour types. Once identified, these mutations would be re-created in a chimeric yeast model system and the effect of the mutations on V-ATPase function would be assessed. Firstly, yeast cells would be transformed with the human V-ATPase subunit isoforms containing the specific mutations to create the human/yeast chimeric V-ATPase system. Confocal microscopy would then be used to observe whether the mutations effect

V-ATPase complex localisation. V-ATPase catalytic activity would be measured using an ADP+Pi detection system, whilst V-ATPase function would assessed using the fluorescent dye, acridine orange. This would give an insight into whether V-ATPase mutations identified in tumour samples actually have a direct functional impact on V-ATPase activity.

3.2 Hypothesis and Aims

3.2.1 Hypothesis

Somatic point mutations in the V_1E2 subunit alter the biochemical properties of the V-ATPase complex, which consequently affects V-ATPase activity and function.

3.2.2 Aims

The aim of this chapter was to evaluate the effect of V-ATPase V_1E subunit somatic mutations on V-ATPase activity using a chimeric yeast model system. This aim was investigated by:

- Identifying mutations in the V_1E2 subunit using the COSMIC database
- Cloning the mutations into the mammalian V_1E1/E2 and yeast Vma4 subunits
- Transforming ΔE null yeast cells with the mammalian subunits containing the mutations
- Observing the effect of V_1E1/E2 subunit mutations on V-ATPase complex localisation using confocal microscopy
- Measuring the effect of the mutations on the kinetics of the V-ATPase complex using an ATP-based detection assay
- Measuring the effect of the mutations on the V-ATPase proton coupling efficiency

3.3 Results

3.3.1 Identifying V-ATPase subunit alterations across multiple cancer types

To determine the mutational landscape of the V-ATPase subunits across different cancer types, mutation and copy number data from multiple cancer cohorts was analysed. The purpose of this was to gain an understanding of how mutations within individual subunits contributed to the V-ATPase complex as a whole. The cancer genome atlas (TCGA) is one of the largest publicly available collections of cancer cohorts with data from over 11,000 patients across 33 studies. Each provisional data set includes information from a different cancer type ranging from adrenalcortical carcinoma to uterine carcinosarcoma. Therefore, the TCGA database was an ideal source of data to gain an insight into V-ATPase subunit expression and mutations across multiple cancer types. To analyse the large amount of TCGA data, the cBioPortal for Cancer Genomics was used, which is an open access tool developed by Memorial Sloan-Kettering Cancer Centre (MSKCC). All of the 23 V-ATPase subunit encoding genes, and the two accessory V-ATPase subunit genes *ATP6AP1* and *ATP6AP2*, were queried across the TCGA provisional studies. Out of the 11,317 samples that were analysed, the V-ATPase genes were found to be altered in 3509 samples (31%).

Figure 3-1 shows that the *ATP6V1C1* gene encoding the V_1C1 subunit was altered (by copy number change or mutation) the most out of any of the V-ATPase subunits (7% of samples). Despite this high number of alterations, it is important to note that most of the recorded alterations were an increase in copy number rather than somatic mutations, which were generated using the GISTIC 2.0 algorithm. In addition, *ATP6V1C1* is on chromosome 8 and copy number segment analysis revealed that the long arm of chromosome 8 was amplified across the dataset, indicating the increase in copy number was not specific to *ATP6V1C1*. Further research also indicated that this chromosomal arm was commonly amplified in a number of different cancer types (326, 327). Thus it is not clear whether *ATP6V1C1* is the driver for amplification of this region, or whether it is a passenger event.

The next subunit gene that was altered in the highest number of patients was *ATP6V0D2*. *ATP6V0D2* is a regulatory subunit which forms part of the membrane bound V_O complex. It is a tissue enriched subunit isoform found to be expressed in kidney cells and therefore may have a specialised role in the function of these cells. The fact that it was the second most altered subunit gene was surprising due to its tissue specific localisation.

Overall, it appeared as if most of the subunits had copy number amplifications and a relatively low somatic mutation rate. The *ATP6V1B2* gene encoding the V_1B2 subunit was the exception to this with a high number of copy number deletions. It is interesting to note that some of the known regulatory subunits (V_1C1, V_1H and V_1d2) were more highly altered than the key catalytic subunits (V_1A, V_1B1 and V_1B2).

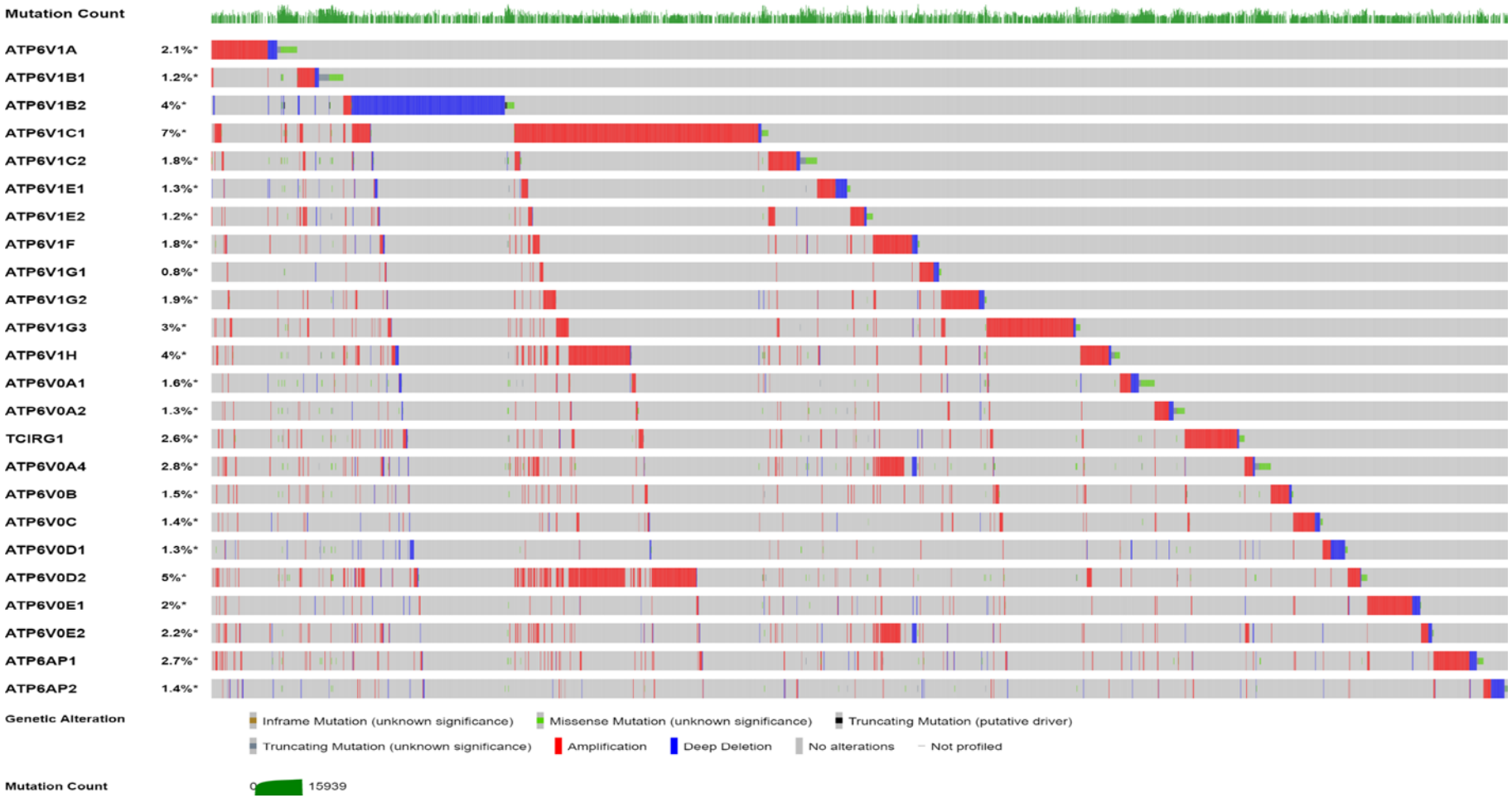

Figure 3-1. Oncoplot of V-ATPase subunit alterations across all provisional TCGA cohorts

V-ATPase genes were plotted as on Oncoplot displaying genetic alterations per patient sample using data from all provisional TCGA cohorts. Percentage altered (%) represents the number of samples that had a genetic alteration in the indicated gene as a percentage of all of the samples queried (11,317). The mutational burden (Mutation count) was also plotted along the top of the Oncoplot.

3.3.2 V_1E2 subunit mutations in cancer

3.3.2.1 Evolutionary conservation of the V_1E subunits

The TCGA data was useful to gain an insight into the mutational landscape of V-ATPase subunit genes across multiple cancers, but to investigate individual somatic subunit mutations it was more suitable to use the Catalogue Of Somatic Mutations In Cancer (COSMIC) database (version 89) (328). The reason for this is that the COSMIC database is the world's largest and most comprehensive collection of somatic mutations in human cancer. The COSMIC database is manually curated and combines data from multiple sources including genome wide screens, gene focussed screens, cell line data and information from other databases such as TCGA. As the percentage of V-ATPase genes altered varied drastically across different cancer types, the most appropriate way to select mutations for further investigation was to consider subunit functionality.

One of the most researched and well-characterised regulatory V-ATPase subunits is the V_1E subunit. The V_1E subunit forms the peripheral stalk with the V_1G subunit (Figure 1-1), which functions to tether the V_1 catalytic hexamer to the V_O domain (14). In yeast, single genes *Vma4* and *Vma10* encode the V_1E and V_1G subunits respectively. Alternatively, in mammals the V_1E subunit had two isoforms (V_1E1 and V_1E2) and the V_1G subunit has three isoforms (V_1G1, V_1G2 and V_1G3). The V_1E1 isoform is ubiquitously expressed whereas the V_1E2 isoform is enriched in the testis and acrosome of the spermatozoa (44). The mammalian V_1E subunits are well conserved and share ~30% similarity to the yeast Vma4 subunit (12). Figure 3-2 shows the similarity of the mammalian V_1E1 and V_1E2 isoforms across species indicating that the isoforms have been evolutionarily conserved. As the V_1E2 isoform shows tissue enriched expression, it was interesting to consider how mutations in this isoform would affect V-ATPase activity, and whether alterations in activity could be related to a specialised function.

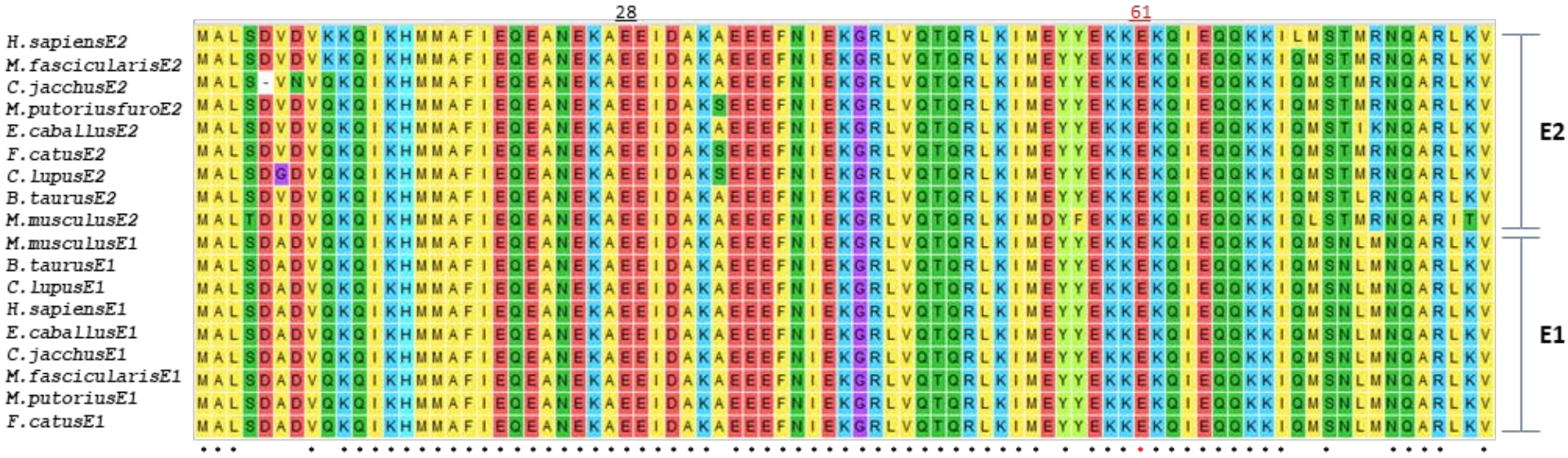

Figure 3-2. The mammalian V_1E subunit N-Terminal alpha helix is conserved across species

The first 83 amino acids of the N-terminal alpha helix of the mammalian V_1E1 and V_1E2 isoforms were aligned using ClustalW. Sequences show similarity across species and the glutamic acid residue at position 61 of the V_1E1 and V_1E2 isoforms is highly conserved. aa, amino acid.

3.3.2.2 V_1E2 somatic mutations identified in the COSMIC database

Using the COSMIC database, several mutations were identified in the N-terminal alpha helix of the V_1E2 isoform (Table S 8-1), with multiple mutations at the glutamic acid residue at position 61 (Figure 3-3 A). The N-terminal alpha helix was of particular interest because it was previously shown to be important for regulating V-ATPase assembly (12). Therefore, it was hypothesised that mutations in the N-terminal alpha helix might affect V-ATPase activity through changes in catalysis. Furthermore, as shown in Figure 3-3 (A) there seems to be an enrichment for mutations in the N-terminal alpha helix of the V_1E2 isoform relative to the remainder of the protein. The potential hotspot at position 61 corresponds to a glutamic acid residue (E), which was found to be substituted in different patient tumour samples to four amino acids. These amino acids were glycine (G), lysine (K), valine (V) and glutamine (Q). Since the COSMIC database was originally queried (version 81) several updated versions have been released, and the data presented is relative to the most recent release (version 89). In the version originally used to identify the mutations (version 81) only three substitutions had been found (K, V and Q) at position 61, so these three substitutions were the focus of the investigation.

E61 is conserved across both V_1E1 and V_1E2 subunit isoforms (Figure 3-3 B). Additionally, the mammalian V_1E1 and V_1E2 amino acid sequences were aligned with the yeast V_1E subunit sequence, and at position 61 the mammalian glutamic acid residue corresponds to a leucine residue at position 66. To understand the potential functional relevance of these substitutions, it was important to consider the key features of the amino acids (Figure 3-3 C). For example, in yeast the leucine residue is hydrophilic and is uncharged whereas in mammals the glutamic acid residue has a negative charge. Therefore, changes in the functional characteristics of the individual amino acids may alter the overall structure and function of the subunit.

Another point to consider is the clinical characteristics of the samples in which the mutations were identified. Further research into the three substitutions showed that the V_1E2 E61K mutation was identified in a melanoma sample whereas both V_1E2 E61V and V_1E2 E61Q were identified in lung adenocarcinoma samples (Table 3-1). Another interesting sample feature is that the mutation count of the sample with the V_1E2 E61V mutation was very low (71) compared to the V_1E2 E61K and V_1E2 E61Q mutations (1323 and 1765 respectively).

A

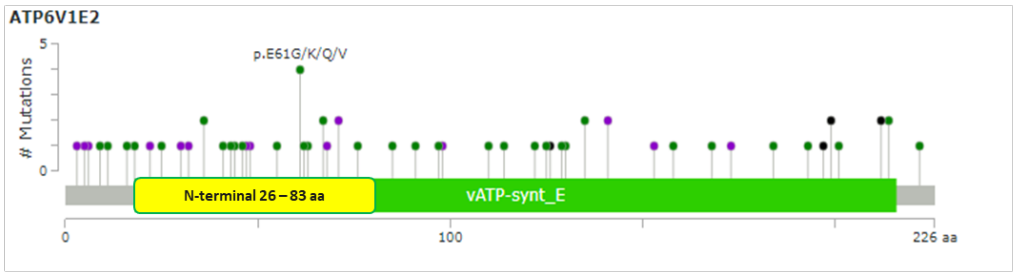

B

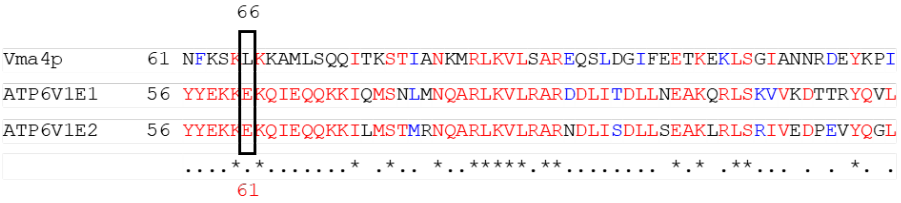

C

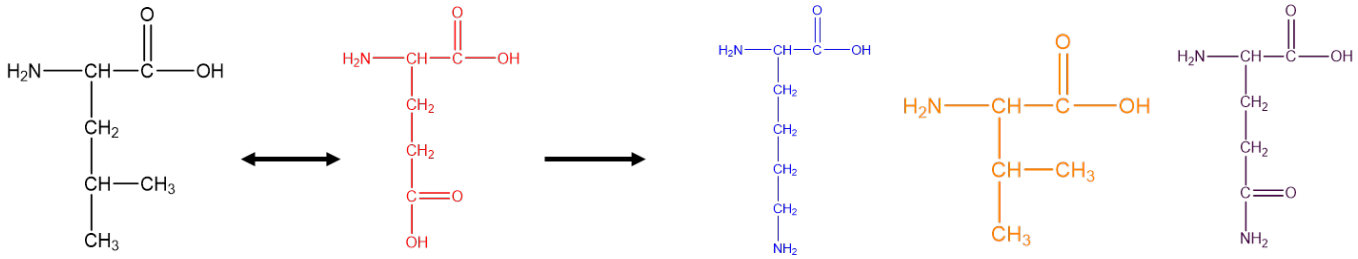

Name	3-Letter Symbol	1-Letter Symbol	Molecular Weight	Molecular Formula	Charge	Hydropathy	pKa, COOH	pKa, NH2
Glutamic acid	Glu	E	147.13	C5H9NO4	-	Hydrophillic	2.19	9.67
Glutamine	Gln	Q	146.15	C5H10N2O3	N	Hydrophillic	2.17	9.13
Leucine*	Leu	L	131.18	C6H13NO2	N	Hydophobic	2.36	9.6
Lysine*	Lys	K	146.19	C6H14N2O2	+	Hydrophillic	2.18	8.95
Valine*	Val	V	117.15	C5H11NO2	N	Hydophobic	2.32	9.62

Figure 3-3. Characteristics of the potential mutational hotspot at position 61 of the V_1E2 subunit isoform

(A) The mutational hotspot at position 61 of the N-terminal alpha helix of the V_1E2 subunit isoform was plotted on a Lollipop plot using the cBioPortal Lollipop plot tool. (B) V_1E1 and V_1E2 amino acid sequences were aligned to the yeast Vma4 sequences using ClustalW and the potential mutational hotspot at position 61 is highlighted. (C) The structure and key characteristics of the amino acids that were found to be substituted at position 61 in the V_1E2 subunit. An asterisk represents essential amino acids*. E, glutamic acid; K, lysine; V, valine; Q, glutamine; L, leucine; N, no-charge; aa, amino acid.

Table 3-1. Sample information for V_1E2 E61 mutations

Clinical data relating to the tumour samples from patients with V_1E2 E61 mutations was acquired from COSMIC and cBioPortal. NS, not specified; N/A, not applicable; LOH, loss of heterozygosity.

Mutation	E61K	E61V	E61Q
Sample Name	TCGA-EE-A2GR-06	LUAD-D02326	LUAD-S01315
Transcript	ENST00000306448	ENST00000306448	ENST00000306448
Primary Tissue	Skin	Lung	Lung
Tissue Subtype 1	NS	NS	NS
Primary Histology	Malignant melanoma	Carcinoma	Carcinoma
Histology Subtype 1	NS	Adenocarcinoma	Adenocarcinoma
Zygosity	Unknown	Unknown	Unknown
Somatic Status	Confirmed Somatic	Unknown	Unknown
Sample Type	NS	Tumour Sample	Tumour Sample
LOH	Unknown	Unknown	Unknown
Gender	Male	Female	Male
Age	78	49	77
Overall Survival (Months)	42	NS	NS
Tumour stage on diagnosis	4	2A	1B
Total Mutation count in Sample	1323	71	1765
Environmental variables	N/A	Non-smoker	Current smoker
Ethnicity	NS	European	European
Clinical remark	N/A	Chemotherapy-naïve	Chemotherapy-naïve

3.3.3 Complementation of mammalian V_1E subunits with *saccharomyces cerevisiae*

To study the effect of the E61 V_1E2 subunit mutations on V-ATPase activity, a hybrid mammalian/yeast system was used. Firstly, it was important to investigate whether the mammalian $V_1E1/2$ isoforms would complement the yeast model system. As previously discussed, a single gene encodes the yeast V_1E subunit (*Vma4*), which is genetically highly similar to the mammalian V_1E subunit isoforms. Structural studies have also shown that the yeast V-ATPase complex is structurally very similar to that of the mammalian complex (Figure 3-4) (329). Therefore, removing the yeast V_1E subunit and replacing it with the mammalian V_1E1 or V_1E2 isoform enables us to study how individual mutations affect the overall activity of the V-ATPase complex.

The three mutations of interest (E61K, V, Q) were first cloned into plasmids and were validated using Sanger sequencing (Figure S 8-3 and Figure S 8-4). Additionally, to account for species specific differences, the three mutations were also cloned into plasmids containing the yeast V_1E subunit (L66 WT, K, E, Q), and were again validated using Sanger sequencing (Figure S 8-5). Valine was changed for glutamic acid because in mammals glutamic acid is the conserved residue so I wanted to investigate whether substituting the conserved yeast leucine residue for glutamic acid would alter V-ATPase activity.

Yeast cells lacking the V_1E subunit (ΔE null mutant) were transformed with the mammalian wild-type V_1E2 subunit DNA and V_1E2 DNA containing the three mutations (E61 WT, K, V, Q). Furthermore, ΔE null mutant yeast cells were also transformed with the same three mutations and wild-type subunit DNA in the mammalian V_1E1 isoform (E61 WT, K, V, Q). This was because the mutations were identified in the V_1E2 isoform, it was therefore interesting to investigate whether the same mutations exhibited a subunit or cancer-specific effect on V-ATPase activity. Similarly, ΔE null mutant yeast cells were transformed with the yeast V_1E subunit expressing the WT or the three mutations (L66 K, E, Q).

Once transformed, the same amount of yeast cells ($5x10^4$) were diluted 10-fold 5 times and a single droplet (4 µL) was spotted onto yeast extract/peptone/dextrose (YPD) plates, which were buffered to a pH of either 5.0 or 7.5, as described in 2.14. Yeast cells lacking the V_1E subunit are able to grow at pH 5.0 but not at 7.5, whereas cells that possess the V_1E subunit are able to grow at both (44). This is due to the V-ATPase proton pumping capacity, and if the cells cannot grow at the higher pH then this suggests that the V-ATPase is not actively transporting protons, resulting in an inhibition of cell growth. At pH

5.0 the yeast cell colonies were able to form for all of the mutant V_1E1 (Figure 3-5 A), V_1E2 (Figure 3-5 B), Vma4 (Figure 3-5 C) and the ΔE null mutant control cells. All of the transformed V_1E1 yeast cells were able to form colonies on the pH 7.5 YPD plates after a $1x10^3$ dilution (Figure 3-5 A). In addition to this, there appeared to be no observable difference between the sizes of the colonies of the V_1E1 WT cells compared to the mutant V_1E1 cells. Similarly, the V_1E2 mutants were also able to grow after $1x10^3$ dilution at pH 7.5 (Figure 3-5 B) but the rate of colony formation was slower than that of the V_1E1 mutants. Again, the WT V_1E2 cells did not show a different growth phenotype compared to the mutant cells. Finally, the Vma4 mutant cells were able to form colonies after a $1x10^4$ dilution on pH 7.5 plates, with the mutant colonies forming quicker than the WT cells (Figure 3-5 C).

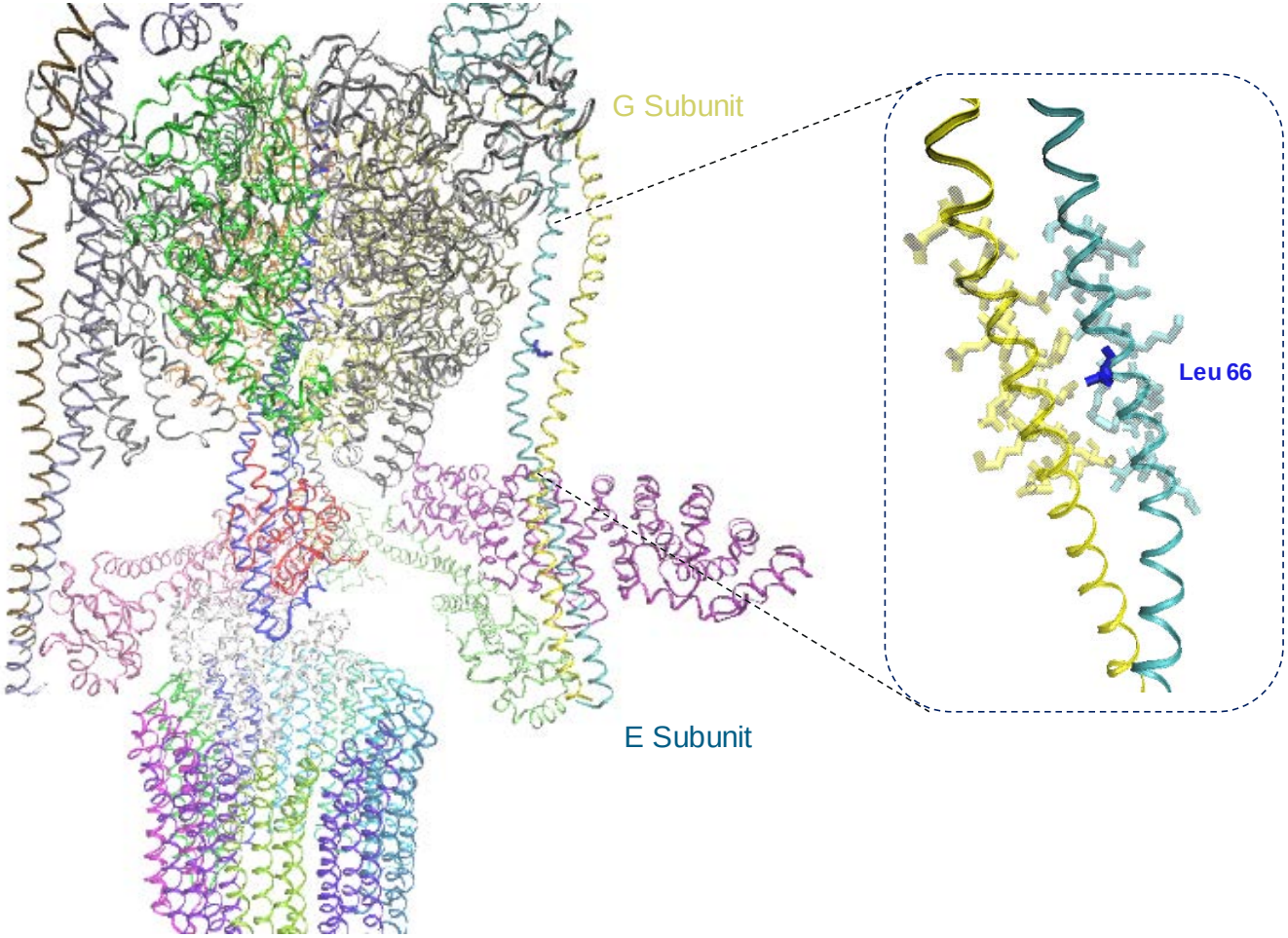

Figure 3-4. Cryo-EM structure of the yeast V-ATPase

Yeast Cryo-EM crystal structure was modified using the 3J9T structure (329) deposited in the Protein Data Bank online database. The leucine 66 residue and surrounding amino acids were highlighted on the V_1E and V_1G subunit ribbon structures. Leu, leucine; Cryo-EM, cryogenic electron microscopy.

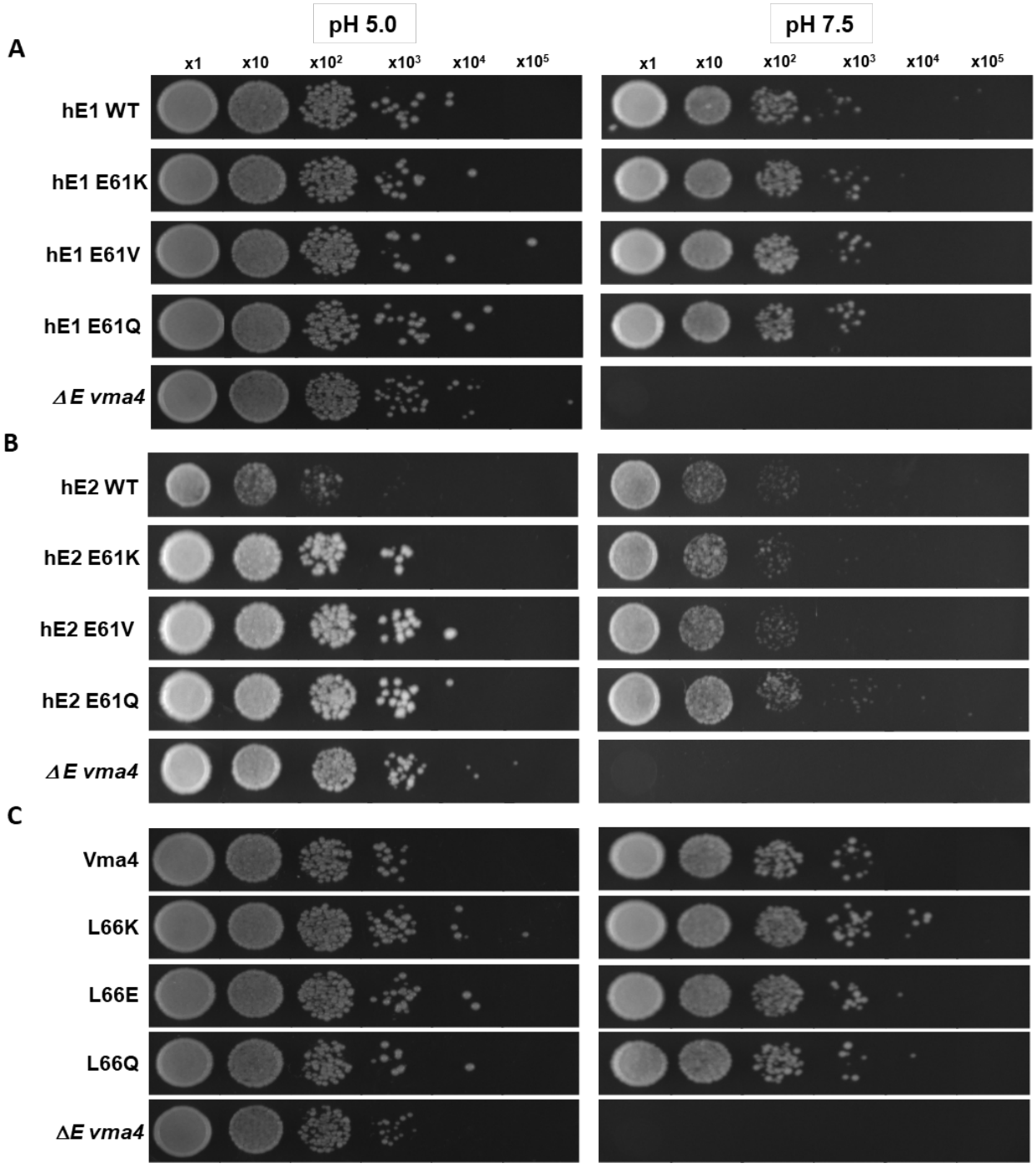

Figure 3-5. The human V_1E1 and V_1E2 E61 mutations complement the yeast model system

ΔE null mutant yeast cells were transformed with expression plasmids encoding WT or mutant human (A) V_1E1 or (B) V_1E2, or (C) WT or mutant yeast V_1E. The cells were diluted and plated on to YPD agar plates with a pH of either 5.0 or 7.5. Images were acquired after 3-4 days incubation at 37 °C. YPD, yeast extract/peptone/dextrose; WT, wild-type; E, glutamic acid; K, lysine; V, valine; Q, glutamine; L, leucine.

3.3.4 Investigating the effect of mammalian V_1E subunit mutations on V-ATPase localisation

Yeast V-ATPase activity is regulated by glucose availability, as the V_1C subunit is released from the enzyme complex within 5 minutes of glucose depletion. This removal of the V_1C subunit results in dissociation of V_1 from the V_O complex, which consequently leads to V-ATPase disassembly and termination of V-ATPase mediated proton-pumping activity (330, 331). Upon the addition of glucose, the V_1C subunit reincorporates into the V-ATPase complex and the V_1 and V_O domains assemble in a reversible manner.

To study the effect of the human V_1E1 and V_1E2 mutations on V-ATPase localisation, we generated a genetic yeast V-ATPase cross with a GFP-tagged V_1C subunit (C-GFP), which enabled me to observe the disassembly of V-ATPase. The yeast Δvma4::C-GFP cells, lacking the V_1E subunit (*VMA4*) gene, were then transformed with either the V_1E1 or V_1E2 WT, E61K, E61V or E61Q DNA plasmids. Once transformed the yeast cells were grown in SD-ura medium and then examined using a confocal microscope.

As can be seen in Figure 3-6, compared to the respective wild-types, all of the V_1E1 and V_1E2 mutant yeast cells have V-ATPase localised in the vacuole, as indicated by the white arrow. This suggests that the E61K, V and Q mutations do not alter the rate of V-ATPase disassembly in the presence of glucose, and therefore V-ATPase localisation is unaffected.

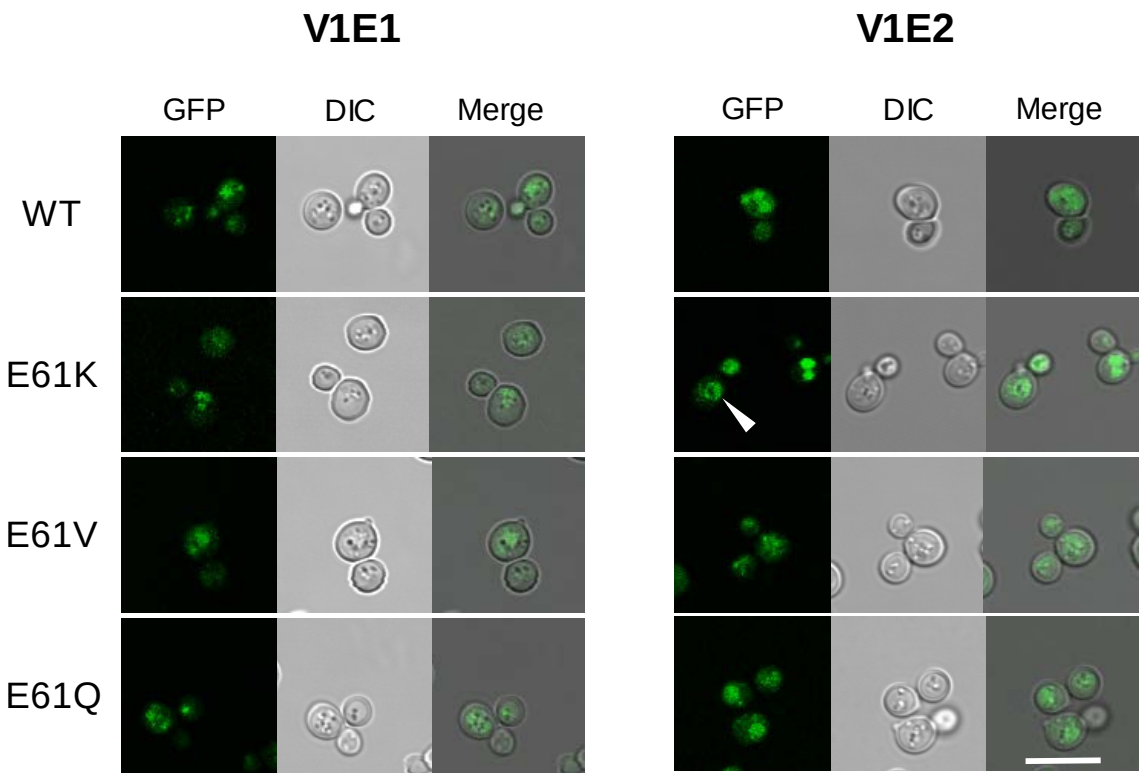

Figure 3-6. Localization of C-GFP in yeast cells expressing human V_1E1 or V_1E2 mutant yeast hybrid V-ATPase

Δvma4::C-GFP cells were transformed with recombinant plasmids expressing human V_1E1 or V_1E2 WT, E61K, E61V or E61Q, and were grown in SD-ura medium for 36 hours. WT, wild-type; E, glutamic acid; K, lysine; V, valine; Q, glutamine.

3.3.5 Effect of mammalian V_1E1 subunit mutations on V-ATPase hydrolytic activity and proton coupling efficiency

3.3.5.1 Effect of mammalian V_1E1 subunit mutations on V-ATPase mediated hydrolysis of ATP

To measure V-ATPase hydrolytic activity, the vacuolar membranes of the mammalian/yeast hybrid transformants were isolated and purified (Section 2.13). V-ATPase activity was then measured using an ADP+Pi based colorimetric assay in which generation of Pi was used as a measure of V-ATPase catalytic activity. The assay was completed at a range of ATP concentrations at both 30 and 37°C. This was because the optimal rate of yeast cell growth is 30°C whereas the homeostatic temperature of the human body is 37°C. Bafilomycin-A1 was used at a concentration of 100 nM, which is above the average IC_{50} reported in the low nanomolar range (20, 332, 333). This ensured that V-ATPase activity was fully inhibited in baf-A1 treated cells, so that V-ATPase independent Pi generation could be measured. The absorbance values at 690 nm were referenced to a Pi standard curve and then normalised to the protein concentration of the sample. It is important to note that this assay was also completed for the yeast Vma4 mutant complexes but the experiments failed to generate a Michaelis-Menten curve, suggesting low or non-existent V-ATPase activity.

Firstly, at 30°C the activity of the hybrid V-ATPase complex expressing the mammalian wild-type (WT) V_1E1 isoform had a direct non-linear relationship with ATP, as the rate of catalysis increased with ATP concentration (Figure 3-7 A). The V_1E1 E61K substitution had an increased V-ATPase catalytic activity compared to the WT, which peaked after the addition of 200 µM ATP and started to fall at 400 µM ATP. The complex expressing the V_1E1 E61V substitution had a higher rate of V-ATPase catalysis than the WT, but it was slightly lower than that of the complex with the E61K substitution. The E61Q substitution resulted in the greatest increase in V-ATPase catalysis compared to the WT V_1E1 isoform and activity started to plateau at 500 µM ATP.

At 37°C, the rate of V-ATPase catalysis of the V_1E1 WT complex (Figure 3-7 B) was similar to that of the WT complex at 30°C. However, after the addition of 500 µM ATP the rate of catalysis had substantially dropped. The V_1E1 E61K substitution again showed a large increase in catalytic activity compared to the WT, which peaked after 200 µM ATP and was higher at 37°C than at 30°C. Interestingly, at 37°C the E61V substitution resulted in a higher V-ATPase catalytic activity than both the WT and E61K expressing complexes. Furthermore, the E61Q substitution resulted in a significant increase in catalytic activity compared to the WT at 37°C, which again started to plateau after 500 µM ATP.

The differences in catalytic activity of the V-ATPase V_1E1 mutant complexes (Figure 3-7 A and B) was very interesting and the kinetic V_{max} (µmol/min/mg protein) and *Km* (µM) values for the enzyme were calculated (Figure 3-7 C). At 30°C, the V_1E1 E61K complex had a higher V_{max} (3.88) than the WT (1.88), which was increased ~2 fold. The V_{max} of the V_1E1 E61V complex (3.14) was slightly lower than E61K (3.88), but higher than the WT (1.88). Interestingly, the *Km* of the E61V complex (45.55) was increased almost ~1.6 fold compared to E61K (28.56) and ~1.8 fold higher than the WT complex (24.63). The V_1E1 E61Q complex had a V_{max} (5.54) and *Km* (60.96), which was ~3 fold higher than the WT.

The V_{max} of the V_1E1 WT complex at 37°C (1.97) was similar to the WT complex at 30°C (1.88) but the *Km* was decreased ~2 fold (Figure 3-7 C). Again, the V_{max} of the V_1E1 E61K complex at 37°C (4.76) was ~2 fold higher than that of the WT complex (1.97). However, the *Km* of the E61K complex (43.93) was similar to that of the WT at 37°C (42.61). The V_{max} of the V_1E1 E61V complex (5.18) was higher than both the WT (1.97) and E61K complexes (4.76); although the *Km* of E61V was similar at 37°C (49.29) to 30°C (46.55). Furthermore, the V_1E1 E61Q complex had a V_{max} (8.78) 37°C, which was ~5 fold higher than that of the WT (1.97). The *Km* of the E61Q complex (66.86) was higher than the V_1E1 WT and mutant complexes at 37°C.

3.3.5.2 Effect of mammalian V_1E1 subunit mutations on V-ATPase proton coupling efficiency

The V_{max} and *Km* values gave an insight into the rate of catalysis of the mutant V-ATPase complexes but not into the rate of proton transport. ATP hydrolysis occurs in the V_1 domain of the V-ATPase and is an enzyme reaction that may be independent of V-ATPase mediated acidification and proton pumping function. Therefore, the rate of hydrogen ion transport (∆Fluorescence/min/mg protein) was measured using the acridine orange-based proton transport assay in order to assess whether there was a correlation between the V-ATPase catalytic rate and proton coupling efficiency.

Quenching of acridine orange was to measure the proton coupling efficiency, which involved the addition of ATP/Mg^{2+} in the presence of potassium chloride (KCl) leading to a decline in fluorescence at 525 nm over a period of 5 minutes. This indicated that the pH was acidified in the purified vacuolar membranes, and the reaction was then quenched with ammonium chloride (NH_4Cl). The V-ATPase specific inhibitor bafilomycin-A1 (baf-A1) was included in the reaction mixture to ensure the proton transport rate measured was the product of V-ATPase only. The resulting proton flux is proportional to the initial rate of fluorescent quenching and the proton coupling efficiency was calculated.

The efficiency of proton transport was highest in the V_1E1 WT complex (869.9) compared to the E61K (403.50), E61V (399.26) or E61Q (525.11) complexes (Figure 3-7 C). Proton transport was similar in both the E61K (403.50) and E61V (399.26), but was increased in E61Q complexes (525.11).

Taken together, these results suggest the rate of catalysis was highest in the V_1E1 E61Q mutant complex compared to the WT, but the rate of proton transport was highest in the V_1E1 WT V-ATPase compared to all of the mutant complexes.

A

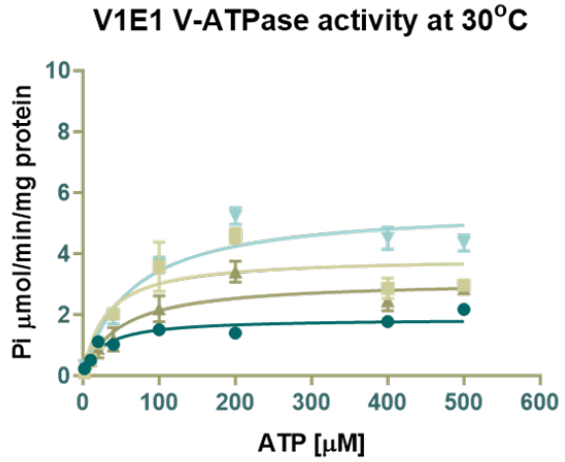

B

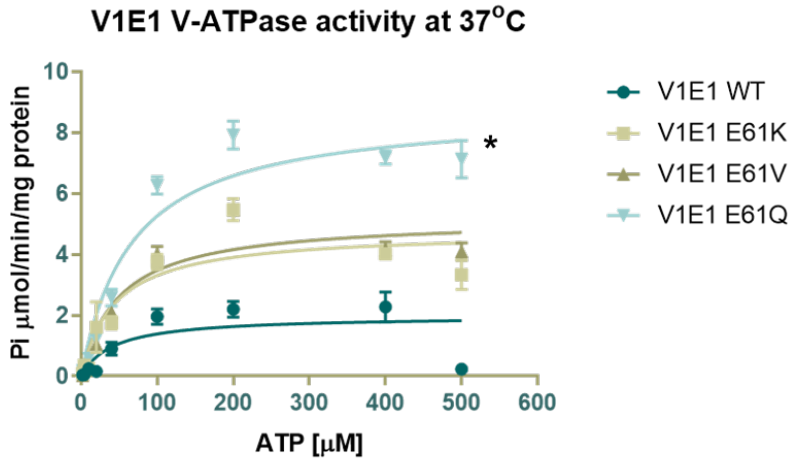

C

		30°C		37°C		
		V_{max}	*Km*	V_{max}	*Km*	
		µmol/min/mg protein	µM	µmol/min/mg protein	µM	**ΔF/min/mg protein**
E1	WT	1.88 (0.14)	24.63 (9.63)	1.97 (0.42)	42.61 (34.63)	869.9 (190.86)
	E61K	3.88 (0.54)	28.56 (19.04)	4.76 (0.43)	43.93 (15.56)	403.5 (69.59)
	E61V	3.14 (0.27)	46.55 (17.10)	5.18 (0.35)	49.29 (12.83)	399.26 (131.11)
	E61Q	5.54 (0.34)	60.96 (13.88)	8.78 (0.54)	66.86 (15.45)	525.11 (104.12)

Figure 3-7. V_1E1 V-ATPase activity at 30°C and 37°C

V-ATPase activity was assessed by incubating isolated vacuolar membranes from either the (A) V_1E1 or (B) V_1E2 clones with increasing concentrations of ATP in the presence and absence of the specific V-ATPase inhibitor bafilomycin-A1. Inorganic phosphate production was then measured at 30°C or 37°C. The values were normalised to µmol/min/mg protein. Data points represent three biological replicates with SEM and were plotted using GraphPad Prism 7 software. Statistically significant differences are indicated: * = p≤ 0.05, one-way ANOVA. WT, wild-type; E, glutamic acid; K, lysine; V, valine; Q, glutamine; ΔF, ΔFluorescence.

3.3.6 Effect of mammalian V_1E2 subunit mutations on V-ATPase hydrolytic activity and proton coupling efficiency

3.3.6.1 Effect of mammalian V_1E2 subunit mutations on V-ATPase mediated hydrolysis of ATP

The V_1E1 results indicated that the amino acid substitutions altered both V-ATPase catalytic activity and proton transport rate (3.3.4). Considering the mutations were originally identified in the COSMIC database in the V_1E2 subunit, it was necessary to investigate the effect of the substitutions in complexes containing the V_1E2 isoform. Similarly to 3.3.4, the catalytic activity of V_1E2 expressing WT and mutant V-ATPase complexes was measured using ADP+Pi detection.

V-ATPase catalysis was increased with an increase in ATP concentration in complexes expressing the V_1E2 WT isoform at 30°C, which plateaued with 500 µM ATP (Figure 3-8 A). Complexes expressing the V_1E2 E61K mutant subunit had an increased rate of catalysis compared to the V_1E2 WT complex. The complex expressing the E61V substitution had a significantly increased rate of catalysis compared to both the WT and E61K complexes. This rate of catalysis peaked after the addition of 200 µM ATP and began to plateau after 500 µM ATP. Furthermore, the E61Q expressing complexes had the highest rate of catalysis out of all of the investigated mutants, which was significantly higher than both the WT and E61K complexes. Similarly to the E61V mutant, the rate of catalysis peaked after the addition of 200 µM ATP but then dropped after 500 µM ATP.

At 37°C, the catalytic rate of WT V_1E2 expressing complexes (Figure 3-8 B) was ~2 fold higher than at 30°C. V-ATPase activity was higher in the V_1E2 E61K, E61V and E61Q mutants than the WT at both 30 and 37°C. Interestingly, the rate of catalysis for E61V mutant dropped slightly after 400 µM ATP and decreased sharply at 500 µM ATP, suggesting the increase in temperature resulted in an increase in catalytic sensitivity to ATP. The E61Q mutant again had the highest catalytic activity compared to the other V_1E2 mutants at 37°C. Similarly to the E61V mutant, the addition of 500 µM ATP resulted in a sharp drop in catalytic activity.

As with the V_1E1 isoform expressing complexes, the V_{max} (µmol/min/mg protein) and *Km* (µM) values for the V_1E2 complexes were calculated (Figure 3-8 C). At 30°C, The V_{max} of the V_1E2 E61K mutant (5.01) was ~1.6 fold higher than that of the WT (3.13), and the *Km* was also decreased. Furthermore, the E61V mutant complex had a substantially higher V_{max} (25.51) and *Km* (71.94), than both the V_1E2 WT and E61K complexes. The V_1E2

E61Q mutant complex had the highest V_{max} (26.38) compared to any of the other V_1E2 complexes, and had the lowest *Km* value (27.23).

The V_{max} of the V_1E2 WT V-ATPase complex was ~1.5 fold more at 37°C (4.97) than at 30°C (3.13) and the *Km* was increased (36.97) (Figure 3-8 C). The V_1E2 E61K mutant complex had a V_{max} (7.68) and *Km* (50.23) that was almost double that of the WT complex at 37°C. Furthermore, V_1E2 E61V had a substantially higher V_{max} (40.16) and *Km* (77.01) than the V_1E2 WT or E61K mutant complexes. Again, the E61Q mutant complex had the highest V_{max} (40.63) and the lowest *Km* (22.10) compared to any of the other V_1E2 expressing complexes

3.3.6.2 Effect of mammalian V_1E2 subunit mutations on V-ATPase proton coupling efficiency

The rate of hydrogen ion transport (ΔF/min/mg protein) was measured using the proton transport assay (Figure 3-8 C) to investigate whether the V_1E2 mutations altered V-ATPase proton transport. Interestingly, the efficiency of proton transport was highest in the E61Q mutant complex (3816.88) compared to the WT (1319.35), E61K (589.91) or E61V (640.35) complexes. This suggests that not only did the V_1E2 E61Q substitution result in a higher rate of enzyme catalysis but also that it almost tripled the rate of proton transport compared to the WT. Furthermore, despite the E61V mutant complex having a significantly higher rate of catalysis, the proton pumping capacity was approximately half of that of the V_1E2 WT complex.

Taken together, this data suggests that the V_1E2 E61V and E61Q mutations increase the rotational catalysis of V-ATPase compared to WT complexes. Additionally, the V_1E2 E61Q substitution greatly enhances the rate of proton transport.

A

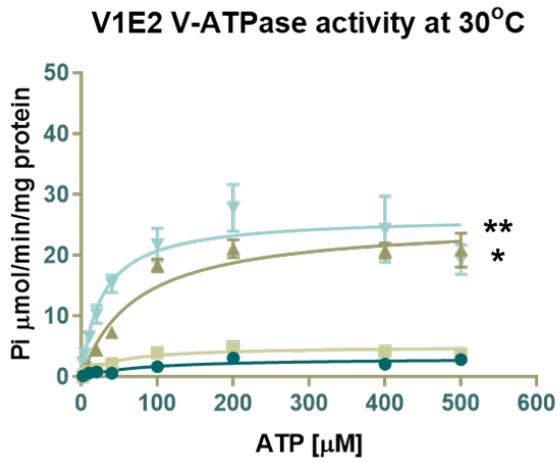

B

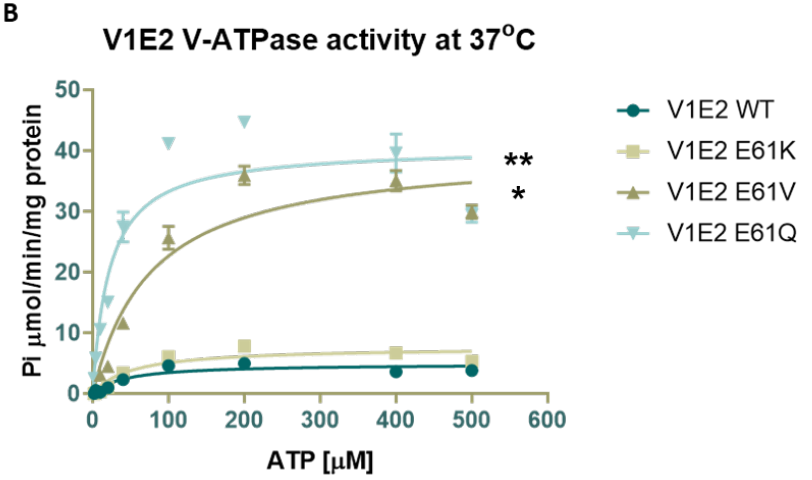

C

		30°C V_{max}	30°C *Km*	37°C V_{max}	37°C *Km*	
		µmol/min/mg protein	µM	µmol/min/mg protein	µM	**ΔF/min/mg protein**
E2	WT	3.13 (0.50)	82.01 (39.43)	4.97 (0.55)	42.41 (16.44)	1507.20 (67.78)
	E61K	5.01 (0.36)	42.42 (10.90)	7.68 (0.68)	50.23 (16.44)	589.81 (382.95)
	E61V	25.51 (1.57)	71.94 (14.93)	40.16 (2.91)	77.01 (17.96)	640.35 (300.38)
	E61Q	26.38 (1.91)	27.23 (7.40)	40.63 (2.35)	22.10 (5.525)	3816.88 (831.76)

Figure 3-8. V_1E2 V-ATPase activity at 30°C and 37°C

V-ATPase activity was assessed by incubating isolated vacuolar membranes from either the (A) V_1E1 or (B) V_1E2 clones with increasing concentrations of ATP in the presence and absence of the specific V-ATPase inhibitor bafilomycin-A1. Inorganic phosphate production was then measured at 30°C or 37°C. The values were normalised to µmol/min/mg protein. Data points represent three biological replicates with SEM and were plotted using GraphPad Prism 7 software. Statistically significant differences are indicated: * = p≤ 0.05, ** = p≤ 0.01, one-way ANOVA. WT, wild-type; E, glutamic acid; K, lysine; V, valine; Q, glutamine; ΔF, ΔFluorescence.

3.4 Summary of findings

The primary aim of this section of the project was to investigate whether selected somatic missense mutations in the V_1E2 subunit isoform altered V-ATPase catalytic activity and function. The key findings were as follows:

- There is a potential mutational hotspot at position 61 corresponding to a glutamic acid residue in the N-Terminal alpha helix of the mammalian V_1E2 subunit isoform, which is mutated to a lysine, valine or glutamine residue.
- The mammalian WT and mutant V_1E1 and V_1E2 subunit isoforms complement ΔE null mutant yeast cells and form an active V-ATPase complex, and the selected mutations do not affect V-ATPase localisation.
- In the V_1E1 isoform, the E61Q mutant complex had a significantly higher catalytic rate compared to the WT, but the rate of proton transport was highest in the V_1E1 WT complex compared to all of the mutant V_1E1 complexes.
- In the V_1E2 isoform, both the E61V and E61Q mutant complexes had significantly higher catalytic rates compared to the WT, and E61Q also had the highest rate of proton transport compared to all of the mutant and WT V_1E2 complexes.

Overall, these results support the hypothesis that somatic point mutations in the V_1E2 subunit alter the biochemical properties of the V-ATPase complex, which consequently affects V-ATPase activity and function.

3.5 Discussion

3.5.1 Identification of V_1E2 somatic mutations in cancer

The TCGA database provided initial insight into the mutational landscape of V-ATPase subunits in cancer (Figure 3-1). V-ATPase subunits were collectively altered in ~30% of all patient samples and so, despite a low mutation rate for individual subunits, the overall complex was found to be altered in almost a third of all patients across a spread of cancer types, which suggests that perhaps these mutations have a functional effect specific to cancer cells. Furthermore, although the TCGA cohorts are useful for understanding mutations across a large number of patients, one of the key limitations is that the cohorts are mainly representative of early stage cancer development. The percentage of V-ATPase alteration may in fact be higher in metastatic cohorts or even in specific cancer-types. For that reason, we must combine functional knowledge and alteration data to interpret the potential effects of any individual subunit mutation. Therefore, although the

ATP6V1E2 gene was only altered in 1.2% of patient samples in the TCGA cohorts (Figure 3-1), the decision to investigate mutations in the N-terminal alpha helix of the V_1E2 subunit was based on functional information.

The V_1E subunits form the peripheral stalk with the V_1G subunits and function to tether the V_1 complex to the V_O complex, providing stability during rotational catalysis. As the V_1E1 subunit is ubiquitously expressed it was interesting to investigate the tissue specific V_1E2 subunit. Considering that the N-terminal alpha helix is well conserved in both the V_1E1 and V_1E2 subunits (Figure 3-3), it was essential to measure V-ATPase activity in both isoforms. Previous research has shown that the V_1E N-terminal alpha helix is a key regulator of V-ATPase assembly, and the fact that this domain has been evolutionarily conserved across species indicates that it must be important for subunit function (Figure 3-2). Additionally, I established that somatic mutations were clustered in this region (Figure 3-3 A), providing more evidence to further investigate mutations in this domain.

3.5.2 V_1E somatic mutations alter V-ATPase activity and function

3.5.2.1 Mammalian V_1E subunits can complement yeast cells to form a functional V-ATPase complex

After identifying a recurrently mutated site at position 61 in the N-terminal alpha helix, the three mutations were selected (E61K, V, Q) and were cloned into the mammalian V_1E1 and V_1E2 subunit isoforms, plus the yeast V_1E (Vma4) subunit equivalent (L66K, E, Q). Given that the yeast V-ATPase structure (Figure 3-4) is similar to that of mammals, I could use yeast as a model system to investigate the effect of these mutations. Yeast cells lacking the V_1E subunit (Δ E null) were transformed with the mutant and wild-type (WT) V_1E1, V_1E2 and Vma4 DNA. All of the mutant and WT V_1E1, V_1E2 and Vma4 expressing yeast cells were able to form colonies at pH 7.5 suggesting that the V-ATPase was functional (Figure 3-5).

3.5.2.2 V-ATPase catalytic activity could not be detected in the yeast V_1E subunit mutant cells

The activity of the mammalian V_1E1/E2 hybrid V-ATPase complexes was assessed by measuring the rate of rotational catalysis and the rate of proton transport. Again, it is interesting to note that the activity of the yeast cells expressing the Vma4 mutants (L66K, E, Q) could not be measured accurately using our inorganic phosphate (Pi) detection system. The fact that the yeast cells containing the Vma4 mutations were able to grow at pH 7.5 suggests that the enzyme is still able to function (Figure 3-5 C). However, as Pi production could not be accurately detected for any of the three mutations, the rate of

catalysis must be severely reduced to very low levels. Conversely, the mutations in the V_1E1/E2 subunits had an increased catalytic rate compared to their respective WT subunits.

3.5.2.3 V-ATPase activity was increased in the V_1E1 mutants

V_1E1 E61K cells had an increased V_{max} and *Km* compared to the WT cells at 30°C. At 37°C, the V_{max} and the *Km* of E61K cells was further increased. In comparison, the V_{max} of the WT cells at 37°C was very similar to that at 30°C. The E61K mutant had a similar *Km* to the WT at both 30 and 37°C but the V_{max} was ~2 fold higher. This suggests that despite an increase in the maximal velocity of the enzyme, the energy required remained very similar. Adding to this, the V_1E1 E61V mutant had a similar V_{max} to E61K at 30°C but the *Km* was almost 2x as high. Furthermore, at 37°C the V_{max} of E61V was higher than E61K but the *Km* was still similar, indicating the E61V substitution results in a higher maximal velocity than the E61K but requires more energy to function. The V_1E1 E61Q mutant had the highest V_{max} out of all V_1E1 complexes investigated, which was significantly higher than the WT at 37°C. However, at 37°C, the *Km* of E61Q was higher than the WT and mutant cells, suggesting the enzyme has a higher catalytic rate but requires more energy than the other two mutations.

Taken together, there appears to be a temperature specific increase in the catalytic activity of mutant V-ATPase complexes expressing V_1E1 mutations at position 61 of the N-terminal alpha helix, but not in the WT V_1E1 complexes. This increase in catalytic activity was not always accompanied with an increase in the efficiency of the enzyme and more energy was often required for enzyme function, with E61K being the exception. Moreover, despite the mutations not being identified in the V_1E1 subunit, all three mutants had higher V_{max} than the V_1E1 WT cells at 37°C, indicating an increase in V-ATPase catalysis. Interestingly, this increase in catalytic rate was not consistent with the rate of proton pumping. It was expected that an increase in V-ATPase activity would result in an increase in the rate of proton transport, but this was not the case. The WT V_1E1 cells had the highest rate of proton transport, followed by the E61Q mutant and then E61K and E61V. The proton transport rate for the E61K and E61V mutants was half of that of the WT V_1E1 complex, suggesting catalytic rate was not necessarily indicative of the ability of V-ATPase to acidify vacuolar compartments.

3.5.2.4 V-ATPase activity was higher in the V_1E2 subunit complexes than V_1E1

The mutational hotspot at position 61 was originally identified in the N-terminal alpha helix of the V_1E2 subunit, but the mutations were expected to have a similar effect on V-

ATPase activity as in the V_1E1 subunit due to their structural similarity. Firstly, the V_{max} of the WT V_1E2 complex was higher than that of the V_1E1 at 30°C, and was almost twice as high at 37°C compared to 30°C. This was an interesting finding as it shows that the V_1E2 subunit had a higher catalytic rate than V_1E1 and there was a temperature dependent increase in activity, which was not observed in the V_1E1 isoform. This is supportive of previous data that showed that mouse V_1E1 chimeric yeast complexes did not exhibit temperature sensitivity but mouse V_1E2 chimeric yeast complexes did (44). Additionally, the *Km* was lower in the V_1E2 complex at 37°C than at 30°C, but at 30°C the Km was ~3 fold lower than that of the V_1E1 WT complex. This indicates that although the V_1E2 isoform had a higher catalytic rate, it also required more energy to function than the V_1E1 isoform at 30°C. Furthermore, the rate of proton transport was almost twice as high in the V_1E2 WT complex than the V_1E1. This agrees with the hypothesis that the V_1E2 isoform is expressed in specific tissues to support their specialised functions. For example, the acrosome of the spermatozoa expresses the V_1E2 subunit and requires a more acidic environment to function (44).

Compared to the V_1E1 E61K mutant, V_1E2 E61K had a higher V_{max} and *Km* at both 30°C and 37°C, indicating a higher rate of catalysis. The V_1E2 E61K mutants also had a higher rate of proton transport than the V_1E1 E61K mutants, which shows that the increase in catalytic activity was coupled with an increase in the proton transport function of the V-ATPase complex. Although, the V_1E2 E61K proton transport rate was still approximately half of that of the V_1E2 WT complex. The V_1E2 E61V results were the most surprising, as the V_{max} was significantly higher than the V_1E2 WT at both 30 and 37°C, but the *Km* was lower at 30°C, and higher at 37°C. This was surprising because in the V_1E1 complexes, the E61V mutant had only a slightly higher catalytic rate than that of the V_1E1 WT. In addition to this, the V_1E2 E61V mutant had a V_{max} that was ~5 fold higher than the V_1E2 E61K mutant at 30°C, which increased further at 37°C, and a *Km* that was only ~1.5 fold higher at both temperatures. This indicates that the large increase in the V_{max} observed between the E61V and E61K mutants was not relative to smaller increase in the *Km*, suggesting V_1E2 E61V complexes were more energy efficient than the V_1E2 E61K complexes. The rate of proton transport was higher in the V_1E2 E61V mutant compared to V_1E2 E61K, which was again surprising as the V_1E1 E61K mutant had a higher proton transport rate than V_1E1 E61V. It is also interesting that the proton transport rate was still approximately half of that of the V_1E2 WT, displaying a similar pattern to its V_1E1 E61V mutant counterpart.

Finally, the V_1E2 E61Q mutant proved to have the greatest effect on V-ATPase activity out of the three mutants investigated. It had a significantly higher V_{max} than the V_1E2 WT complex at both 30 and 37°C, and a lower *Km* at both temperatures. In fact, the V_1E2

E61Q had a higher V_{max} and lower *Km* than both V_1E2 E61K and E61V mutants. The E61Q mutant also had a proton transport rate that was ~3 fold higher than the V_1E2 WT, and was substantially higher than in the E61K and E61V mutants. This was interesting because the V_1E1 E61Q mutant had the highest V_{max} values compared to the other V_1E1 mutants but not the lowest *Km*, and the proton transport rate was lower than that of the WT. The proton transport rate in the V_1E2 E61Q mutant was also still over six fold higher than in the V_1E1 E61Q mutant. This data showed that the V_1E2 E61Q mutant had the highest V_{max}, lowest *Km* and highest proton transport rate, which may indicate that it is a gain of function mutation. Furthermore, the V_1E1 E61Q mutant had the highest catalytic rate compared to the V_1E1 WT and mutants, supporting the idea that this mutation can alter V-ATPase activity. However, the E61Q activity observed in the V_1E1 isoform was significantly less than in the V_1E2 isoform, and as the mutation was identified in the V_1E2 subunit but not the V_1E1 subunit, this suggests that this mutation may have a cancer specific functional effect on V-ATPase activity. The E61V may also exhibit a subunit or cancer specific effect as the catalytic rate was only slightly increased in the V_1E1 isoform compared to the WT, but substantially increased in the V_1E2 isoform.

3.5.2.5 Thoughts on why the amino acid substitutions affect V-ATPase activity

Firstly, as the mammalian V-ATPase crystal structure has not yet been solved it is difficult to draw direct conclusions about how changes in the amino acid structures may alter the V-ATPase complex. Therefore, by analysing the characteristics of the amino acid substitutions I can produce only hypothetical explanations as to why these mutations are changing V-ATPase activity and function.

The glutamic acid residue conserved in mammals has a negative charge and is hydrophilic (Figure 3-3 C). As both glutamic acid and lysine are similar in size and are hydrophilic, the key change in characteristics would be the negative charge changing to a positive charge. Furthermore, glutamine and valine are both uncharged amino acids but glutamine is hydrophilic whereas valine is smaller and hydrophobic. Considering that the significant increases in V-ATPase catalytic activity were a result of the valine and glutamine substitutions, and not the lysine substitution, we can speculate that the increase in activity might be due to the loss of the negative charge. This replacement of the negatively charged residue with an uncharged amino acid may result in a shift in the electrostatic forces. The potential loss of ionic or covalent bonds with surrounding amino acids could result in a weakening of the subunit structure. Alternatively, the change in amino acid structure may alter protein folding, consequently affecting interactions within the V-ATPase complex. As the V_1E subunit forms the peripheral subunit with the V_1G subunit, this potential loss of bonding or change in protein structure may provide

increased flexibility for the rotation of the catalytic subunit, which would then in turn increase the V-ATPase catalytic rate.

It is also interesting to speculate as to why these mutations have arisen in this particular subunit. There are some similarities between the samples in which the V_1E2 E61V and E61Q mutations were identified (Table 3-1). For example, they were both identified in lung adenocarcinoma patients as opposed to E61K, which was identified in a melanoma sample. The patients from which the lung adenocarcinoma samples were collected both had early stage cancer (1 and 2a) and had not been exposed to chemotherapy. The mutation count in the E61V patient was also very low (71 mutations), and therefore perhaps this substitution was not simply the result of a random mutation but that it had a functional purpose. Again, these mutations were only identified in three patients so I stress the clinical relevance is just speculative.

To summarize, I have shown for the first time that cancer associated V-ATPase subunit mutations directly affect the enzymatic activity of the complex, in terms of both V-ATPase catalytic activity and its function as a proton pump. Additionally, the precise biochemical effects on the complex depend on several key variables including: the amino acid that is replaced, the environmental temperature, and the subunit isoform in which the mutation occurs. Overall, the selected V-ATPase mutations contribute to an increase in V-ATPase activity. An increase in V-ATPase activity as a result of these mutations may have biological effects that are consistent with the effects of PM V-ATPase overexpression reported in different cancer types i.e. an increase in V-ATPase expression results in a decrease of extracellular pH and a subsequent increase in the metastatic and invasive potential of the cancer cells. It is also possible that these mutations might affect auxiliary functions of the V-ATPase such as inappropriate mTORC1 activation (323).

Chapter Four

Chapter 4 Investigating the effect of chemical V-ATPase inhibition on wild-type and mutant AR activity

Investigating the effect of chemical V-ATPase inhibition on wild-type and mutant AR activity

4.1 Introduction

To further explore the role of V-ATPase in cancer at a greater depth, it was appropriate to focus on a single cancer type. There is already a lot of evidence in different tumour types that V-ATPase plays a role in tumour growth, invasion and metastasis (75) and has been linked to many signalling pathways including Notch and Wnt (84, 86). However, very little is known about the impact of V-ATPase dysregulation in prostate cancer.

The androgen receptor (AR) signalling pathway is the key signalling pathway associated with prostate cancer development and progression. Therefore, it was logical to focus on investigating interactions between AR signalling and V-ATPase in prostate cancer. Previous research has shown that V-ATPase inhibition reduces invasion of PCa cells by up to 80% and has been directly linked to an increase in metastatic capability (2). In cell lines with low metastatic potential, V-ATPase inhibition decreased AR protein and reduced expression of PSA at the mRNA level. Surprisingly, reduced *PSA* mRNA was associated with increased PSA protein expression in V-ATPase inhibitor treated cells (2). Furthermore, V-ATPase has been linked with AR signalling via a mechanism involving HIF-1α and defective iron endocytosis (313). Taken together this early research suggests that V-ATPase may have a direct or indirect role in prostate cancer, but there is still a lack of understanding concerning key aspects of the interaction of AR and V-ATPase in PCa cells. In particular, the critical question of whether V-ATPase inhibition also alters the function of AR mutants or splice variants has not been addressed.

A fundamental aim of the project was to investigate whether V-ATPase inhibition would disrupt AR signalling in cells which expressed mutant forms of the AR. To do this I modelled different AR mutants, which reflect various stages of disease progression. The first of these models represented hormone sensitive prostate cancer in which the AR was sensitive to androgenic stimulation. Secondly, I studied the effect of AR splice variants on AR activity by focussing on the AR-V7 and AR-Q641X variants, which are constitutively active and have been found in CRPC patients (289, 334-336). Finally, I went on to investigate the AR point mutations AR-F877L and AR-T878A which confer an antagonist to agonist switch of the antiandrogens enzalutamide and hydroxyflutamide respectively (337, 338).

To study the effect of V-ATPase inhibition on AR activity in these models I used a number of different systems and techniques. One of the keys systems used was the dual-luciferase reporter assay, which enabled me to study the direct effect of V-ATPase inhibition on AR transactivation. Using this system, I transfected AR-negative HeK-293 cells with wild-type (WT) AR, AR splice variants or mutant AR expression plasmids alongside androgen response element (ARE)-containing and *Renilla* control luciferase reporter plasmids. The AR activity was measured by quantifying the luminescent signal produced due to the binding of the AR to the ARE. Other well established techniques that were utilized include RT-qPCR and western blotting, which were used to measure RNA or protein levels of endogenous AR or AR specific downstream targets. These experiments were conducted in cell lines that were either androgen sensitive (LNCaP and DuCaP), contained the AR-V7 splice variant (22Rv1), or expressed AR point mutations (LNCaP F877L/T878A). Figure 4-1 illustrates the approximate stage of disease progression the cell line models represent.

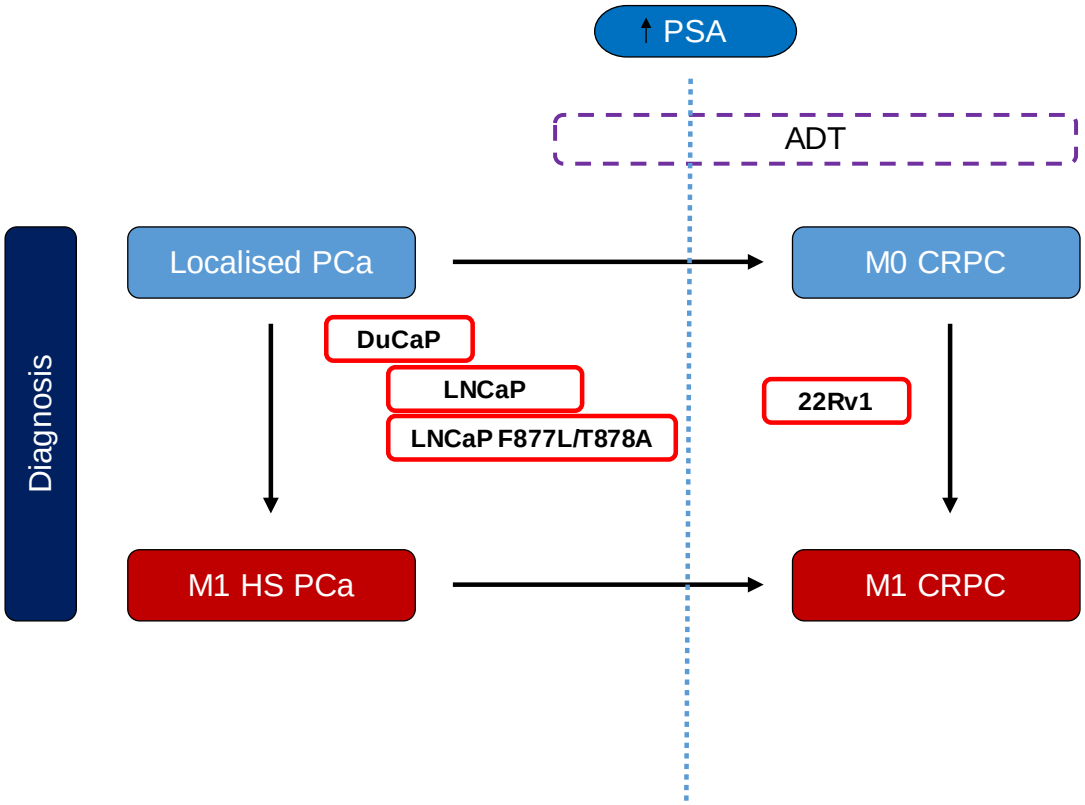

Figure 4-1. Simplified prostate cancer cell line models that are partly representative of disease progression

DuCaP, LNCaP and LNCaP F877L/T878A are all hormone sensitive prostate cancer cell lines. Mutations such as AR-F877L and AR-T878A are thought to emerge as a result of directed treatment. The 22Rv1 cell line expresses the AR-V7 splice variant, which is insensitive to hormone and is accepted to be representative of later stage disease. However, prostate cancer is a highly heterogeneous disease and progression is not necessarily linear, which is why none of the available cell lines perfectly model each individual stage. PCa, prostate cancer; CRPC, castration-resistant prostate cancer; HS, hormone-sensitive; PSA, prostate specific antigen; ADT, androgen deprivation therapy; M1, metastatic; M0, non-metastatic.

.

4.2 Hypothesis and Aims

4.2.1 Hypothesis

Chemical V-ATPase inhibition dysregulates AR activity regardless of AR mutational status.

4.2.2 Aims

The aim of this chapter was to investigate the impact of chemical inhibition of V-ATPase on AR activity in prostate cancer cell lines. This aim was investigated by:

- Using the MTS assay to assess cell line toxicity after treatment with V-ATPase inhibitors, bafiloymycin-A1 and concanamycin-A
- Using the luciferase reporter assay system to assess the impact of V-ATPase inhibition on AR transactivation in wild-type AR expressing cells
- Measuring AR and PSA protein levels after treatment with bafiloymycin-A1 or concanamycin-A in hormone sensitive prostate cancer cell lines (LNCaP and DuCaP)
- Measuring the RNA levels of downstream AR targets after V-ATPase inhibition in LNCaP and DuCaP cells
- Measuring AR and PSA protein levels in LNCaP cells after treatment with both bafiloymcin-A1 and the AR antagonist enzalutamide
- Using the luciferase reporter assay system to assess the impact of V-ATPase inhibition on AR transactivation in cells with AR splice variants and point mutations
- To support reporter data by measuring the RNA levels of downstream AR targets after V-ATPase inhibition in in prostate cancer cell lines containing clinically relevant AR aberrations
- Measuring AR and PSA protein levels after treatment with bafiloymycin-A1 or concanamycin-A in prostate cancer cell lines containing clinically relevant AR aberrations

4.3 Results

4.3.1 Effect of V-ATPase inhibition on AR signalling in hormone sensitive prostate cancer cell lines

4.3.1.1 Measuring cell line viability in response to baf-A1 and con-A inhibitor treatment

Firstly, the MTS assay (Promega) was used to asses potential toxicity of the V-ATPase chemical inhibitors bafilomycin-A1 (baf-A1) or concanamycin-A (con-A1) in the cell lines of interest (LNCaP, DuCaP, HeK-293 and 22Rv1). Both inhibitors are established, highly specific and have little known off-target effects (19). Furthermore, concentrations as low as 1 nM have been shown to be sufficient to inhibit lysosomal acidification, indicating effective V-ATPase inhibition (332). However, it was important to first determine potential cytotoxic effects in the cell lines of interest after 24 hours of treatment. The 24 hour time point was selected to test cell toxicity as previously published data shows inhibition for 24 hours substantially reduced AR signalling in prostate cancer cell lines (2).

The MTS assay is based on the reduction of the MTS compound to create a coloured formazan dye, which was directly proportional to cellular metabolic activity. The formazan product is directly quantified by measuring absorbance at 490 nm. The assay was used to assess cell toxicity in response to 100, 10 or 1 nM baf-A1 or con-A. As can be seen in Table 4-1, compared to the DMSO control, both 10 and 1 nM concentrations had no statistically significant effect on the MTS signal in any of the four cell lines investigated. This confirms that the inhibitors were safe to use at these concentrations without inducing substantial cell death. At 100 nM, baf-A1 caused a significant reduction in the MTS signal produced in the LNCaP cell line, indicating cell toxicity. In addition to this, 100 nM con-A treatment caused a significant reduction in the MTS signal in LNCaP, HeK-293 and 22Rv1 cells. Overall, con-A treatment led to a greater reduction in MTS signal compared to baf-A1 in all four cell lines, suggesting it is more toxic. Based on these results, a maximum concentration of 10 nM was selected for either drug in the majority of experiments.

Table 4-1. Using the MTS assay to determine cell line toxicity in response to bafilomycin-A1 and concanamycin-A

The indicated cell lines were treated with either 100 nM, 10 nM or 1 nM bafilomycin-A1 or concanamycin-A for 24 hours, and MTS assay data is presented relative to the DMSO treated cells set to 100% viability. Values were then plotted using GraphPad Prism 7 and are displayed as mean values ± standard deviation. Two-way ANOVA with Tukey's multiple comparison post-hoc test was used to generate P values and detect the statistical significance of the indicated differences: * = p≤ 0.05, ** = p≤ 0.01, *** = p≤ 0.001. Data shown represents three independent replicates completed in triplicate. SD, standard deviation; baf-A1, bafilomycin-A1; con-A, concanamycin-A.

Cell line	Baf-A1						Con-A					
	100 nM		10 nM		1 nM		100 nM		10 nM		1 nM	
	Mean(%) ± SD	P value (Adjusted)	Mean(%) ± SD	P value (Adjusted)	Mean(%) ± SD	P value (Adjusted)	Mean(%) ± SD	P value (Adjusted)	Mean(%) ± SD	P value (Adjusted)	Mean(%) ± SD	P value (Adjusted)
LNCaP	88.71 (±7.36)	0.001 **	101.36 (±6.78)	0.681	116.98 (±15.23)	0.338	86.85 (±5.34)	0.0002 ***	96.39 (±2.91)	0.585	102.20 (±5.82)	0.847
DuCaP	91.44 (±4.63)	0.205	99.34 (±9.03)	0.997	108.45 (±16.54)	0.167	89.85 (±5.91)	0.0609	94.65 (±4.03)	0.683	95.64 (±8.57)	0.843
HeK-293	97.34 (±7.34)	0.999	94.83 (±8.50)	0.896	102.36 (±8.67)	0.810	84.49 (±7.61)	0.0073 **	90.23 (±10.02)	0.209	97.89 (±12.77)	0.851
22Rv1	98.54 (±4.92)	0.490	108.69 (±5.38)	0.151	110.02 (±6.72)	0.064	94.89 (±1.97)	0.011 *	99.62 (±2.03)	0.572	99.20 (±11.80)	0.478

4.3.1.2 Determining the effect of V-ATPase inhibition on wild-type AR activity using the reporter assay system

To first determine the effect of V-ATPase inhibition on wild-type AR transactivation, the Dual-Glo Luciferase reporter assay (Promega) was used. The HeK-293 cell line does not express the AR and therefore acts as a good model for which to study the direct effect of V-ATPase inhibition on AR gene activity.

HeK-293 cells were washed 3x in CSS media before being cultured in CSS media for 24 hours prior to transfection. The purpose of this was to minimize the effect of endogenous androgens or androgenic compounds present in the complete RPMI media. Additionally, incubation for 24 hours in CSS media was selected as it was sufficient to substantially reduce endogenous androgen levels.

The cells were then transfected with the androgen response element (ARE_3) reporter vector, an AR expression vector and the *Renilla* control vector. After the cells had been transfected, they were cultured for 24 hours to allow vector uptake and AR expression. They were then treated with 1 nM DHT and concentrations of baf-A1 or con-A at a range of concentrations for 24 hours.

The purpose of transfecting all 3 vectors was so that stimulation of the AR by androgen would allow the AR to bind to the ARE, resulting in the downstream expression of the firefly luciferase. Levels of AR gene activation could therefore be detected via quantification of the luminescent signal produced by firefly luciferase. The *Renilla* reporter vector was co-transfected as an internal control, which served as a baseline transfection response to minimize experimental variability. Once normalised to the *Renilla* signal, the values were presented relative to the DMSO treated control cells set to 1.

It was found that treatment with either 20, 10 or 5 nM baf-A1 was sufficient to significantly reduce AR-WT transactivation (Figure 4-2 A). Additionally, con-A treatment resulted in a significant reduction in AR activity at the lower concentrations of 5, 2.5 and 1.25 nM (Figure 4-2 B). Con-A is a more potent V-ATPase inhibitor than baf-A1 (19) and therefore it was not unexpected that lower concentrations would be more effective at reducing AR activity than baf-A1.

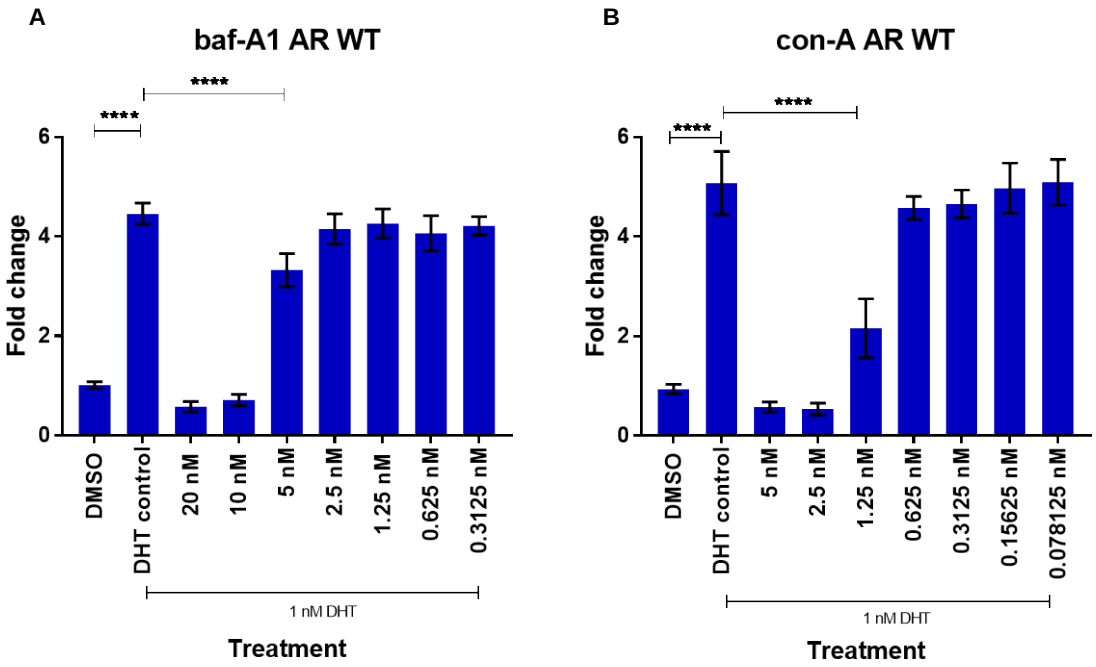

Figure 4-2. Effect of bafilomycin-A1 and concanamycin-A on ARE activity using firefly luciferase

HeK-293 cells were transfected with the androgen response element (ARE) reporter plasmid and wild-type AR expression vector along with a *Renilla* luciferase vector. The cells were cultured in CSS media and treated with 1 nM DHT and indicated concentrations of (A) baf-A1 or (B) con-A for 24 hours. Luciferase activity was determined and firefly luciferase values were normalised to negative DMSO control cells set to 1. Values were then plotted using GraphPad Prism 7 and are displayed as mean values ± standard deviation. Two-way ANOVA with Tukey's multiple comparison post-hoc test was used to generate P values and detect the statistical significance of the indicated differences: **** = p≤ 0.0001. Data shown represents three independent replicates completed in triplicate. DHT, dihydrotestosterone; baf-A1, bafilomycin-A1; con-A, concanamycin-A; AR, androgen receptor.

.

4.3.1.3 Investigating the expression of AR downstream target genes after chemical V-ATPase inhibition in LNCaP cells

The reporter data indicated that V-ATPase inhibition would sufficiently reduce AR activity in the nanomolar range. However, the dual-luciferase assay is a heterologous system and therefore further investigation was required to show V-ATPase inhibition could reduce endogenous AR signalling. Therefore, the next step was to assess direct AR downstream signalling targets *PSA* and *TMPRSS2* at transcript level in LNCaP cells, which are hormone sensitive and express the AR-T878A mutant. PSA and TMPRSS2 Taqman probes (Applied Biosystems - ThermoFisher) were used to measure mRNA levels as they are two of the most accepted and commonly published targets for measuring downstream AR signalling (2, 339, 340).

LNCaP cells were cultured in CSS media and treated with either 10 nM baf-A1 or 10 nM con-A, with or without 1 nM DHT for 24 hours. A subset of experimental cells were cultured only in phenol-red RPMI to act as a positive control for the CSS cultured cells. These concentrations were chosen for future investigations based on the results of the reporter assay (Figure 4-2) and to coincide with previously published data (2). The lower concentration of 1 nM DHT, compared to the commonly used 10 nM, was selected as it has been shown to significantly activate AR signalling (341) and therefore 10 nM was deemed unnecessarily high.

As can be seen in Figure 4-3, 1 nM DHT significantly increased *PSA* (A) and *TMPRSS2* (B) mRNA levels compared to DMSO only treated cells. This induction of *PSA* and *TMPRSS2* by DHT was then significantly reduced with baf-A1 treatment, indicating a reduction of downstream AR signalling at the transcript level. Interestingly there was no statistically significant reduction in either *PSA* or *TMPRSS2* expression when baf-A1 was used without DHT. This may suggest an androgenic dependence of V-ATPase mediated AR reduction.

Furthermore, *GAPDH* RNA levels did not significantly change between treatments and therefore fold changes in mRNA expression resulted from the treatments and were not masked by changes in *GAPDH* RNA expression (Figure S 8-11). This allows for the conclusion that baf-A1 was decreasing the expression of downstream AR targets and therefore V-ATPase is directly or indirectly linked to AR signalling in hormone sensitive PCa cells.

To validate that the results were not baf-A1 specific but rather due to V-ATPase inhibition, con-A was also used to inhibit the V-ATPase. The results obtained with con-A inhibition were similar to that with baf-A1 treatment as *PSA* transcript expression was increased

with DHT stimulation and was significantly reduced with con-A in the presence of DHT (Figure 4-4 A). Similarly, there was no significant effect on *PSA* expression when con-A was used without DHT. *TMPRSS2* showed a similar pattern to *PSA* as con-A treatment reduced expression in the presence of DHT, although it was not statistically significant (Figure 4-4 B).

These results support the reporter system data and suggest the AR signalling is reduced with chemical V-ATPase inhibition.

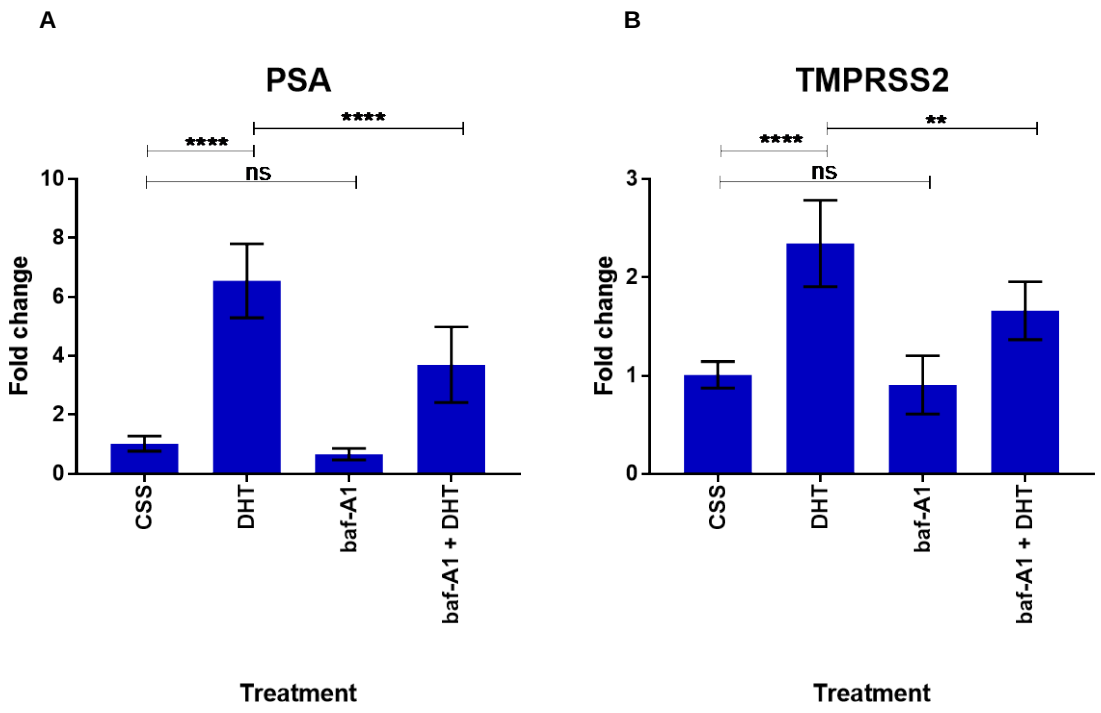

Figure 4-3. Expression of downstream AR target genes in LNCaP cells following treatment with 1 nM DHT and/or 10 nM bafilomycin-A1

LNCaP cells were treated for 24 hours with either 1 nM DHT, 10 nM con-A or both. RT-qPCR analysis was undertaken to assess mRNA levels of (A) *PSA* and (B) *TMPRSS2* and were normalised to *GAPDH*, relative to DMSO treated control CSS cells set to 1. Values were then plotted using GraphPad Prism 7 and are displayed as mean values ± standard deviation. Two-way ANOVA with Tukey's multiple comparison post-hoc test was used to generate P values and detect the statistical significance of the indicated differences: ns = non-significant, **= p≤ 0.01, **** = p≤ 0.0001. Data shown represents three independent biological replicates completed in triplicate. CSS, charcoal stripped serum; DHT, dihydrotestosterone; con-A, concanamycin-A; PSA, prostate specific antigen.

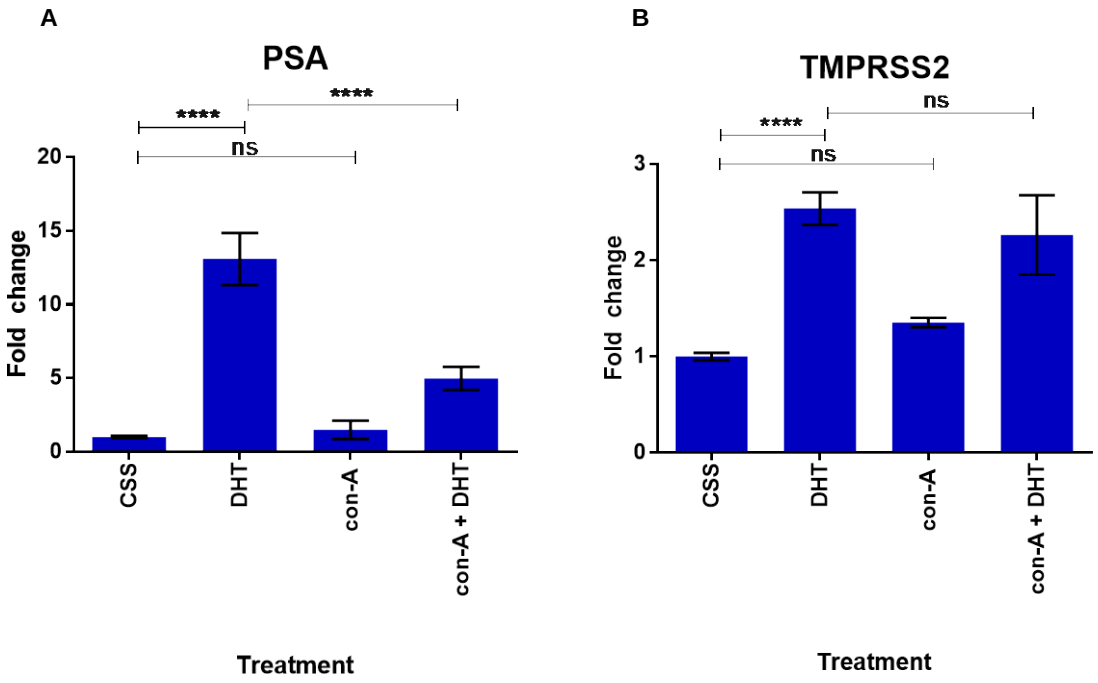

Figure 4-4. Expression of downstream AR target genes in LNCaP cells following treatment with 1 nM DHT and/or 10 nM concanamycin-A

LNCaP cells were treated for 24 hours with either 1 nM DHT, 10 nM con-A or both. RT-qPCR analysis was undertaken to assess mRNA levels of (A) *PSA* and (B) *TMPRSS2* and were normalised to *GAPDH*, relative to DMSO treated control CSS cells set to 1. Values were then plotted using GraphPad Prism 7 and are displayed as mean values ± standard deviation. Two-way ANOVA with Tukey's multiple comparison post-hoc test was used to generate P values and detect the statistical significance of the indicated differences: ns = non-significant, **** = p≤ 0.0001. Data shown represents three independent biological replicates completed in triplicate. CSS, charcoal stripped serum; DHT, dihydrotestosterone; con-A, concanamycin-A; PSA, prostate specific antigen.

4.3.1.4 Investigating the expression of AR signalling associated proteins after chemical V-ATPase inhibition in LNCaP cells

After investigating the response of downstream AR targets at the transcript level, the next stage was to measure the effect of V-ATPase inhibition on AR and PSA protein levels. LNCaP cells were cultured in CSS media for 24 hours and cells were then treated with either 10 nM baf-A1 or 10 nM con-A with or without 1 nM DHT. Cells were harvested after 24 hours of treatment and protein levels were measured using western blotting with antibodies specific for AR, PSA and β-Actin. TMPRSS2 protein levels were not assessed due to a lack of suitable antibodies.

The AR was stimulated with 1 nM DHT, which led to an increase in AR and PSA expression compared to the hormone depleted cells (Figure 4-5 A). When the cells were treated with 10 nM baf-A1 without DHT, there was a small decrease in AR protein expression but a large increase in PSA expression (lane 4 vs lane 2). Furthermore, when baf-A1 treatment was combined with hormonal stimulation there was a greater decrease in AR expression. Interestingly, despite the relative reduction in *PSA* mRNA, expression of PSA protein was not clearly downregulated in baf-A1+DHT treated cells compared to DHT only treated cells. Moreover, the PSA band on the western blot was slightly blurred after baf-A1+DHT treatment.

To validate the results observed with baf-A1 treatment, LNCaP cells were treated with 10 nM con-A (Figure 4-5 B). Con-A is a more potent inhibitor than baf-A1 (19) but results were expected to be similar. Again, cells treated with con-A without DHT had a decrease in AR expression (lane 4 vs lane 2), which was greater upon stimulation with the hormone (lane 5 vs 3). This reduction in AR expression was larger than seen with baf-A1 treatment, supporting the increase in expected compound potency with con-A. Similarly to Figure 4-5 A, the reduction in AR expression was not clearly associated with a reduction in PSA protein levels.

Despite the differences in potency between the inhibitors on PSA expression, both clearly had an impact on AR expression, which agrees with what has been previously published (2). This meant that LNCaP cells could be the primary model for studying V-ATPase inhibition in hormone sensitive PCa cells.

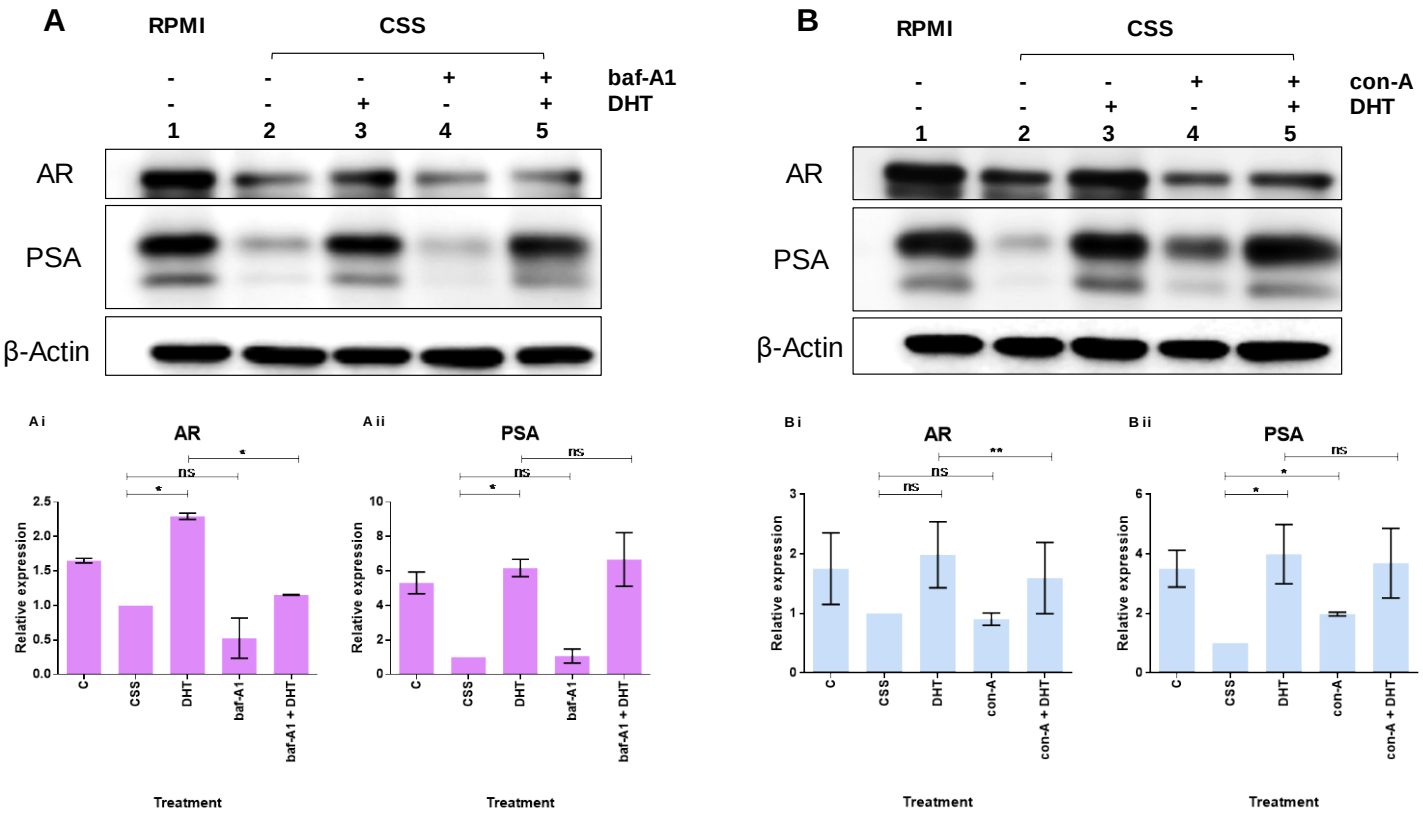

Figure 4-5. PSA and AR expression in LNCaP cells following treatment with 10 nM bafilomycin-A1 or concanamycin-A

LNCaP cells were treated for 24 hours with either (A) 1 nM DHT, 10 nM baf-A1, both or (B) 1 nM DHT, 10 nM con-A, both. A control LNCaP sample was included and was maintained in RPMI. Protein expression was measured using western blotting and cells were probed against AR, PSA and β-Actin. Blot is representative of three individual experiments. Densitometry data of AR (Ai and Bi) and PSA (Aii and Bii) normalised to β-Actin, relative to DMSO treated control CSS cells set to 1. Values were plotted using GraphPad Prism 7 and are displayed as mean values ± standard deviation. Student's T-Tests were used to generate P values and detect the statistical significance of the indicated differences: ns = non-significant, * = p≤ 0.05, ** = p≤ 0.01. C, control; CSS, charcoal stripped serum; DHT, dihydrotestosterone; baf-A1, bafilomycin-A1; con-A, concanamycin-A; PSA, prostate specific antigen; AR, androgen receptor.

4.3.1.5 Investigating the expression of AR downstream target genes after chemical V-ATPase inhibition in DuCaP cells

As the LNCaP cell line contains the AR-T878A mutation, which increases AR ligand promiscuity (337), it was necessary to extend results in a cell line expressing the wild-type AR. DuCaP cells were treated with 10 nM baf-A1 (Figure 4-6) or 10 nM con-A (Figure 4-7) with or without 1 nM DHT for 24 hours. The RNA levels of AR downstream targets, *PSA* and *TMPRSS2*, were measured using RT-qPCR and were normalised to the housekeeping gene *GAPDH*. Values were then presented relative to the DMSO treated CSS cells and fold changes were calculated using the ΔΔCt method.

Similarly to the LNCaP results, 1 nM DHT treatment significantly increased both *PSA* and *TMPRSS2* transcript expression (Figure 4-6). In the presence of DHT, baf-A1 treatment significantly reduced *PSA* mRNA expression levels compared to the DHT alone treated cells (Figure 4-6 A). Furthermore, *TMPRSS2* was also significantly reduced with baf-A1 treatment in the presence of DHT (Figure 4-6 B). Again, treatment with baf-A1 only did not significantly reduce *PSA* or *TMPRSS2* expression without DHT, supporting the requirement of androgenic stimulation for a V-ATPase mediated reduction in AR signalling.

As with baf-A1, con-A treatment significantly reduced *PSA* expression in the presence of DHT, but not in the absence of DHT (Figure 4-7 A). Con-A and DHT treatment also led to a statistically significant reduction in *TMPRSS2* levels compared to DHT alone treated cell (Figure 4-7 B). This result shows that AR signalling in DuCaP cells may be more sensitive to con-A mediated inhibition than LNCaP cells, in which *TMPRSS2* expression was not significantly reduced with con-A treatment (Figure 4-4 B).

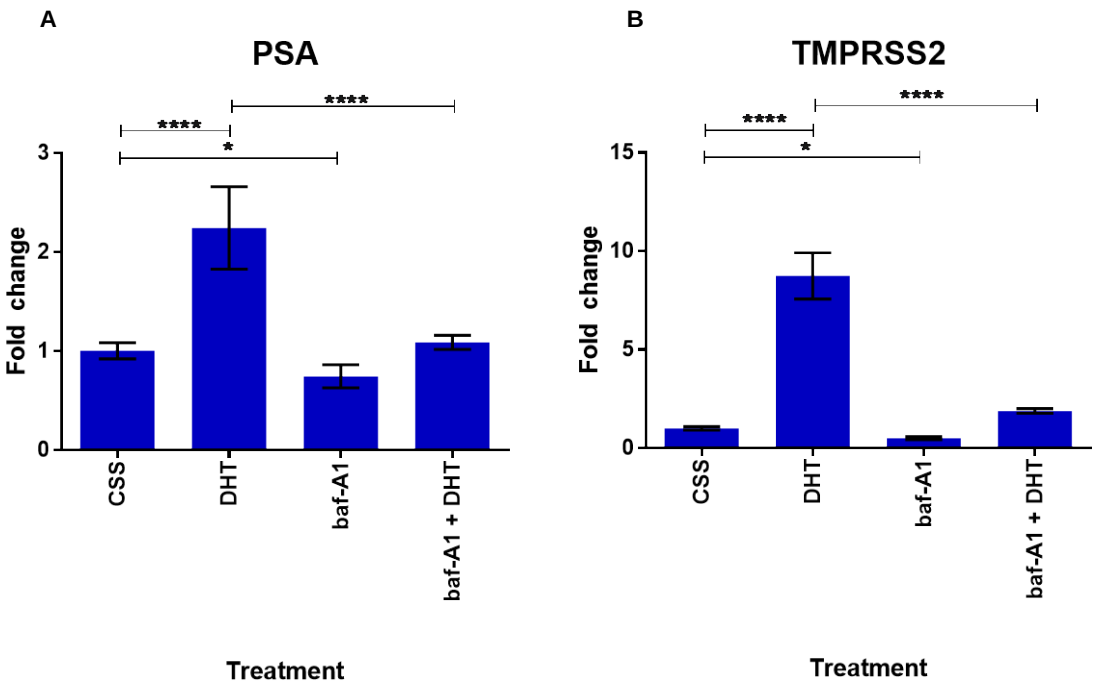

Figure 4-6. Expression of downstream AR target genes in DuCaP cells following treatment with 1 nM DHT and/or 10 nM bafilomycin-A1

DuCaP cells were treated for 24 hours with either 1 nM DHT, 10 nM baf-A1 or both. RT-qPCR analysis was undertaken to assess mRNA levels of (A) *PSA* and (B) *TMPRSS2* and were normalised to *GAPDH*, relative to DMSO treated control CSS cells set to 1. Values were then plotted using GraphPad Prism 7 and are displayed as mean values ± standard deviation. Two-way ANOVA with Tukey's multiple comparison post-hoc test was used to generate P values and detect the statistical significance of the indicated differences: * = p≤ 0.05, **** = p≤ 0.0001. Data shown represents three independent biological replicates completed in triplicate. CSS, charcoal stripped serum; DHT, dihydrotestosterone; baf-A1, bafilomycin-A1; PSA, prostate specific antigen.

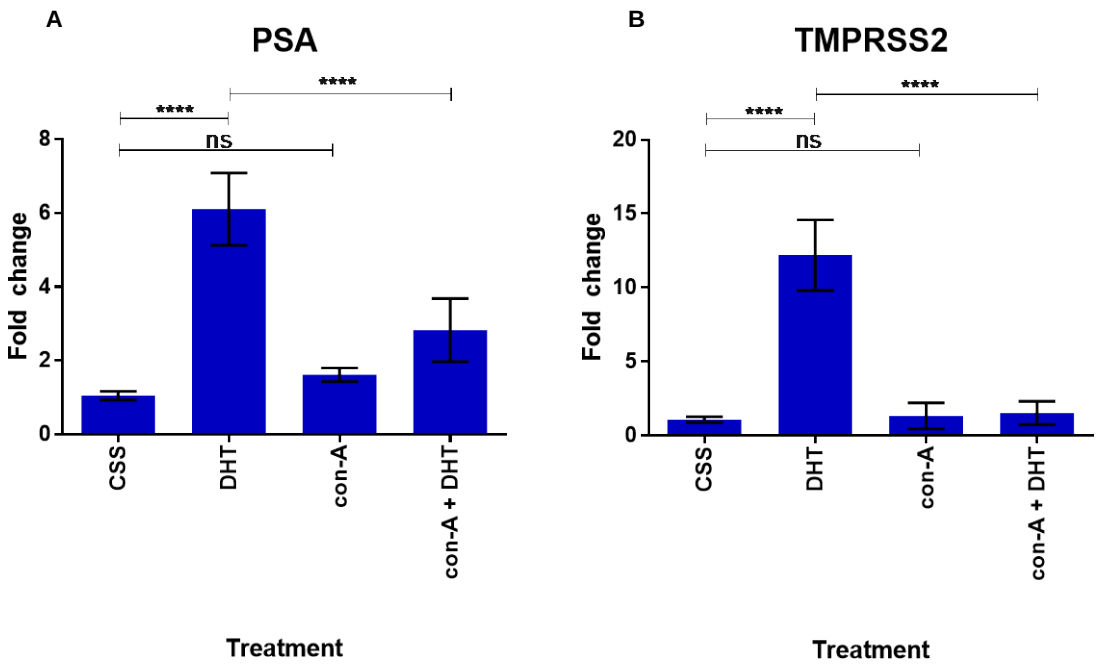

Figure 4-7. Expression of downstream AR target genes in DuCaP cells following treatment with 1 nM DHT and/or 10 nM concanamycin-A

DuCaP cells were treated for 24 hours with either 1 nM DHT, 10 nM con-A or both. RT-qPCR analysis was undertaken to assess mRNA levels of (A) *PSA* and (B) *TMPRSS2* and were normalised to *GAPDH*, relative to DMSO treated control CSS cells set to 1. Values were then plotted using GraphPad Prism 7 and are displayed as mean values ± standard deviation. Two-way ANOVA with Tukey's multiple comparison post-hoc test was used to generate P values and detect the statistical significance of the indicated differences: ns = non-significant, **** = p≤ 0.0001. Data shown represents three independent biological replicates completed in triplicate. CSS, charcoal stripped serum; DHT, dihydrotestosterone; con-A, concanamycin-A; PSA, prostate specific antigen.

4.3.1.6 Investigating the expression of AR signalling associated proteins after chemical V-ATPase inhibition in DuCaP cells

The results from 4.3.1.5 showed that chemical V-ATPase inhibition reduced the expression of downstream AR signalling targets in the AR-WT DuCaP cells. As with the LNCaP cells (4.3.1.4), it was important to investigate the protein levels of the AR and downstream targets in response to baf-A1 and con-A treatment. Therefore, DuCaP cells were cultured in CSS media for 24 hours, prior to treatment with either 10 nM baf-A1 or 10 nM con-A with or without 1 nM DHT.

Figure 4-8 (A) shows that there was an increase in AR and PSA expression in DHT treated cells compared to CSS DMSO treated cells, indicating that the AR was sensitive to androgenic stimulation. Again, despite the relative reduction in *PSA* mRNA, expression of PSA protein was not downregulated in baf-A1+DHT treated cells compared to DHT only treated cells. Conversely, Con-A treatment showed a reduction of AR protein levels, compared to baf-A1, without 1 nM DHT stimulation (Figure 4-8 B). In the presence of DHT, con-A treatment resulted in a reduction of AR expression (lane 5 vs lane 3).Similarly to what was seen with baf-A1 treatment, PSA expression was increased upon con-A treatment compared to the CSS control (lane 4 vs lane 2).

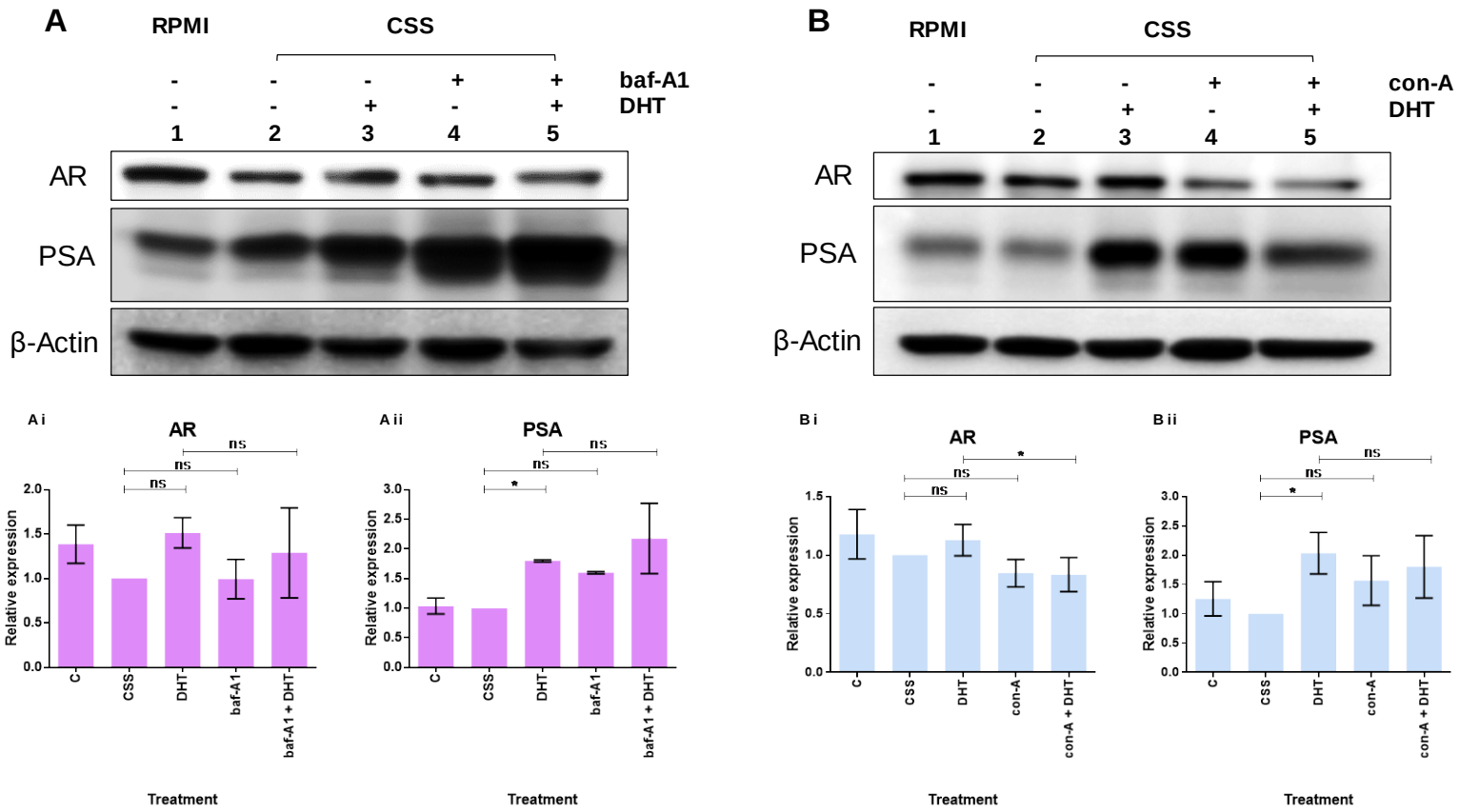

Figure 4-8. PSA and AR expression in DuCaP cells following treatment with 10 nM bafilomycin-A1 or concanamycin-A

DuCaP cells were treated for 24 hours with either (A) 1 nM DHT, 10 nM baf-A1, both or (B) 1 nM DHT, 10 nM con-A, both. A control DuCaP sample was included and was maintained in RPMI. Protein expression was measured using western blotting and cells were probed against AR, PSA and β-Actin. Blot is representative of three individual experiments. Densitometry data of AR (Ai and Bi) and PSA (Aii and Bii) normalised to β-Actin, relative to DMSO treated control CSS cells set to 1. Values were plotted using GraphPad Prism 7 and are displayed as mean values ± standard deviation. Student's T-Tests were used to generate P values and detect the statistical significance of the indicated differences: ns = non-significant, * = p≤ 0.05. C, control; CSS, charcoal stripped serum; DHT, dihydrotestosterone; baf-A1, bafilomycin-A1; con-A, concanamycin-A; PSA, prostate specific antigen; AR, androgen receptor.

4.3.1.7 Measuring the transcript expression of AR downstream targets after combining V-ATPase inhibition with AR antagonism in LNCaP cells

Having confirmed V-ATPase inhibition led to a reduction in AR signalling in hormone sensitive prostate cancer cell lines LNCaP and DuCaP, the next step was to investigate what effect combining V-ATPase inhibition with an existing antiandrogen treatment would have on AR signalling. Enzalutamide is an AR antagonist which blocks the binding of androgens such as DHT to the ligand binding domain and therefore prevents androgen-dependent stimulation of the AR (342).

LNCaP cells were treated with 1 nM DHT, 10 µM enzalutamide, 10 nM baf-A1 or a combination of each for 24 hours. The mRNA levels of AR downstream targets, *PSA* and *TMPRSS2*, were then measured using RT-qPCR and were normalised to the housekeeping gene, *GAPDH*.

Firstly, CSS only DMSO treated cells were used as a negative control whilst DHT treated cells were used as a positive control for activation of the AR pathway. Figure 4-9 (A) shows that 1 nM DHT significantly increased *PSA* mRNA expression, indicating induction of the AR signalling pathway. In the presence of DHT, enzalutamide significantly reduced *PSA* expression compared to DHT only treated cells, which shows that enzalutamide was successfully antagonising AR activity. Furthermore, in agreement with previous results (Figure 4-3), baf-A1 with DHT significantly reduced *PSA* expression levels compared to the DHT alone treated cells. Most importantly, the combination of enz and baf-A1 with DHT had the greatest reduction in *PSA* expression, resulting in a fold change lower than cells cultured in CSS media. Without androgenic stimulation, enzalutamide, baf-A1 and the combination of both did not reduce *PSA* expression compared to the CSS only cells.

As with *PSA*, DHT significantly increased *TMPRSS2* mRNA levels, which was reduced with enzalutamide treatment (Figure 4-9 B). Treatment with baf-A1 and DHT led to a reduction in *TMPRSS2* expression compared to DHT only treated cells, supporting what was observed with *PSA*. Finally, the combination of enzalutamide with baf-A1 and DHT significantly reduced *TMPRSS2* expression compared to the DHT only treated cells.

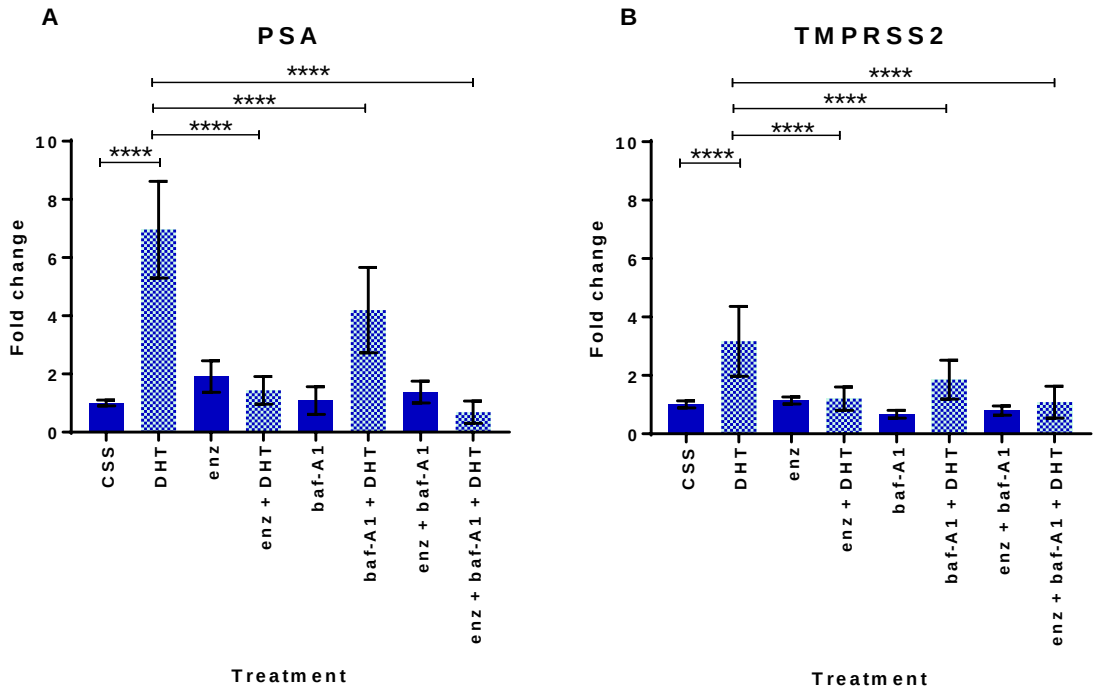

Figure 4-9. Expression of downstream AR target genes in LNCaP cells following treatment with 1 nM DHT, 10 nM bafilomycin-A1, 10 μM enzalutamide or a combination of each

LNCaP cells were treated for 24 hours with either 1 nM DHT, 10 nM baf-A1, 10 μM enz or a combination of each. RT-qPCR analysis was undertaken to assess mRNA levels of (A) *PSA* and (B) *TMPRSS2* and were normalised to *GAPDH*, relative to DMSO treated control CSS cells set to 1. Values were then plotted using GraphPad Prism 7 and are displayed as mean values ± standard deviation. Two-way ANOVA with Tukey's multiple comparison post-hoc test was used to generate P values and detect the statistical significance of the indicated differences: **** = p≤ 0.0001. Data shown represents three independent biological replicates completed in triplicate. CSS, charcoal stripped serum; DHT, dihydrotestosterone; enz, enzalutamide; baf-A1, bafilomycin-A1; PSA, prostate specific antigen.

4.3.1.8 Combining V-ATPase inhibition with AR antagonism in LNCaP cells

After measuring AR downstream target transcript expression in response to the combination of enzalutamide and V-ATPase inhibition, the next step was to investigate AR protein expression.

LNCaP cells were treated with either 1 nM DHT, 10 µM enzalutamide, 10 nM bafilomycin-A1 or a combination of each for 24 hours. Figure 4-10 shows cells treated with enzalutamide and DHT had a large reduction in AR protein expression compared to DHT only treated cells (lane 6 vs lane 3). This reduction in AR expression was also mirrored in the reduction of PSA expression, confirming that enzalutamide was effectively antagonising AR activity at the protein level. In addition, baf-A1 with DHT treatment (Lane 7) substantially reduced AR expression compared to DHT only treated cells (lane 3). Again, PSA expression was increased and the western blot band appeared to be blurred, which is supportive of previous results (Figure 4-5 and Figure 4-8). The combination of baf-A1 and enzalutamide with DHT (Lane 9) showed the greatest reduction in AR expression compared to the DHT only treated cells (Lane 3). PSA expression was also reduced with combinatorial treatment compared to DHT only cells, suggesting that enzalutamide could overcome the V-ATPase inhibition induced increase in PSA expression.

Without DHT stimulation, both enzalutamide (lane 4) and baf-A1 (lane 5) did not reduce AR expression compared to CSS only cells (lane 2). Furthermore, enzalutamide alone did not reduce PSA expression and baf-A1 led to a small increase. Interestingly, without the addition of DHT, the combination of enzalutamide and baf-A1 (lane 8) had an additive effect on AR expression, resulting in a greater reduction than CSS only cells (lane 2). This suggests that in hormone depleted patients, combining V-ATPase inhibitors with antiandrogens may reduce AR signalling, and therefore potentially reduce AR driven cancer growth.

These results are supportive of the reductions in AR activity observed with combination treatment at the transcript level (Figure 4-9). Taken together, they suggest that V-ATPase inhibition may be more effective at reducing AR activity when combined with existing antiandrogens, providing further evidence for an androgenic link between the AR and V-ATPase.

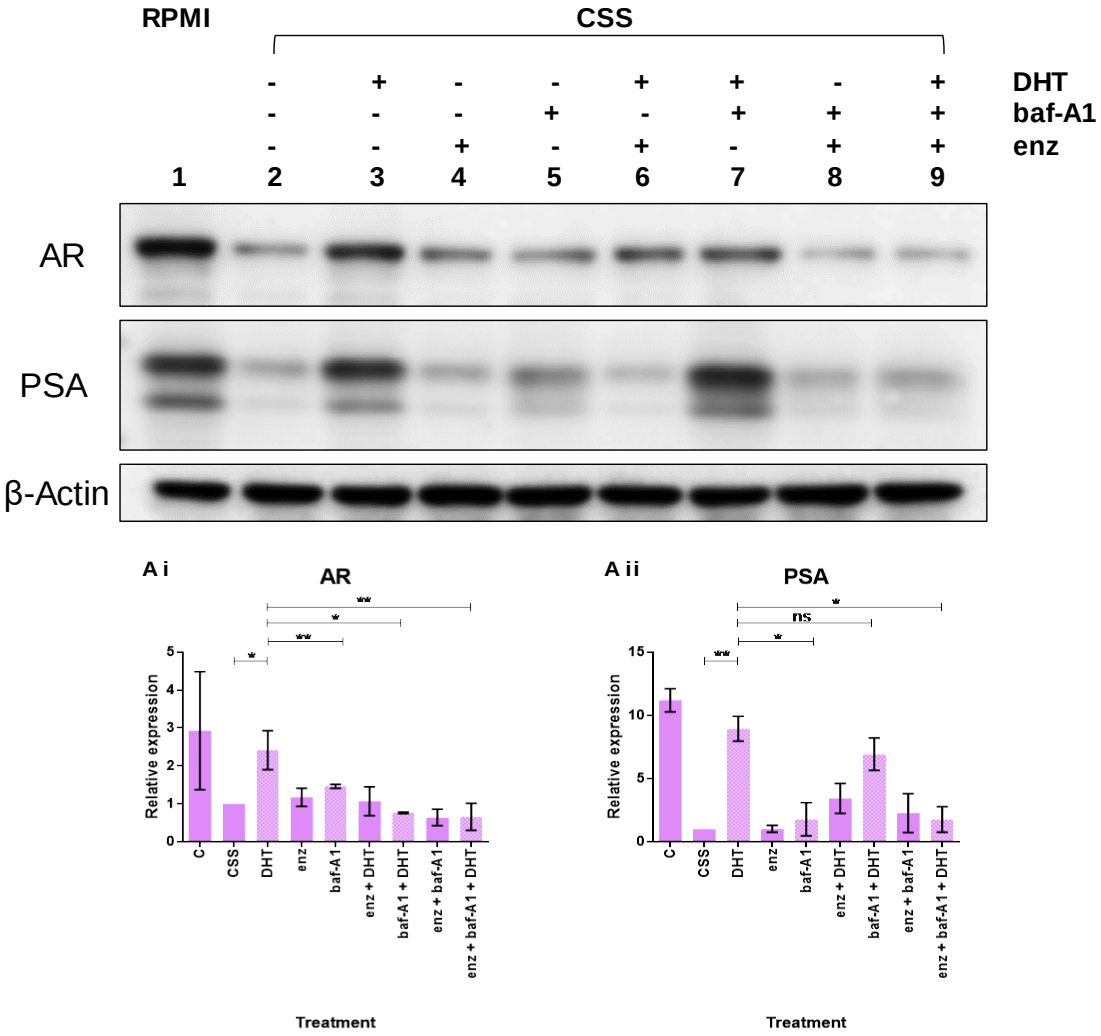

Figure 4-10. AR and PSA expression in LNCaP cells following treatment with 1 nM DHT, 10 nM bafilomycin-A1, 10 μM enzalutamide or a combination of each

LNCaP cells were treated for 24 hours with either 1 nM DHT, 10 nM baf-A1, 10 μM enz or a combination of each. A control LNCaP sample was included and was maintained in RPMI. Protein expression was measured using western blotting and cells were probed against AR, PSA and β-Actin. Blot is representative of three individual experiments. Densitometry data of AR (Ai) and PSA (Aii) normalised to β-Actin, relative to DMSO treated control CSS cells set to 1. Values were plotted using GraphPad Prism 7 and are displayed as mean values ± standard deviation. Student's T-Tests were used to generate P values and detect the statistical significance of the indicated differences: ns = non-significant, * = p≤ 0.05, ** = p≤ 0.01. C, control; CSS, charcoal stripped serum; DHT, dihydrotestosterone; enz, enzalutamide; baf-A1, bafilomycin-A1; PSA, prostate specific antigen; AR, androgen receptor.

4.3.2 Role of V-ATPase dysregulation in AR splice variants

4.3.2.1 Effect of V-ATPase inhibition on AR splice variant activity

Having demonstrated a link between AR signalling and V-ATPase in hormone sensitive prostate cancer cells (i.e. AR wild-type or AR-T878A in LNCaP cells), the next stage was to investigate whether V-ATPase inhibition would disrupt AR signalling in cells with AR alterations such as splice variants and point mutations. AR-V7 (Figure 1-13) is the most clinically relevant known splice variant that has constitutive activation of AR signalling, despite the loss of the ligand binding site (288, 336). The AR-Q641X variant (Figure 1-13) has similar ligand independent AR transactivational activity to that of AR-V7 and also acts to bypass the requirement of endogenous hormonal stimulation (335). Splice variants are found in CRPC patients and can be used as models to study advanced staged cancer (288). The AR-V7 and AR-Q641X expression plasmids were a kind gift from Jocelyn Ceraline, University of Strasbourg.

The reporter assay system (as described in 4.3.1.2) was used to measure AR-V7 and AR-Q641X activity in response to baf-A1 and con-A treatment. Firstly, the AR-V7 splice variant independently induced AR activity, without the requirement of DHT, to a much larger extent than the AR-WT (Figure 4-11). There was a 20-fold induction of ARE activity compared to the AR-WT using only DMSO, and there was no statistically significant effect of DHT on the AR-V7 activity. Similar to the AR-WT, 5 nM baf-A1 treatment significantly reduced AR transactivation (Figure 4-11 A). Furthermore, 10 nM baf-A1 was sufficient to reduce the AR-V7 activity to below DHT stimulated AR-WT levels. In agreement with this, con-A treatment also significantly reduced AR-V7 activity with 1.25 nM treatment (Figure 4-11 B). Therefore, both inhibitors were effective at reducing AR-V7 splice variant transactivation.

To extend the AR-V7 splice variant results the AR-Q641X variant was also investigated. Again, ARE activity was over 20-fold higher compared to the AR-WT, without the requirement of DHT stimulation (Figure 4-12). As with AR-V7, baf-A1 (Figure 4-12 A) and con-A (Figure 4-12 B) both significantly reduced ARE activation at nanomolar concentrations.

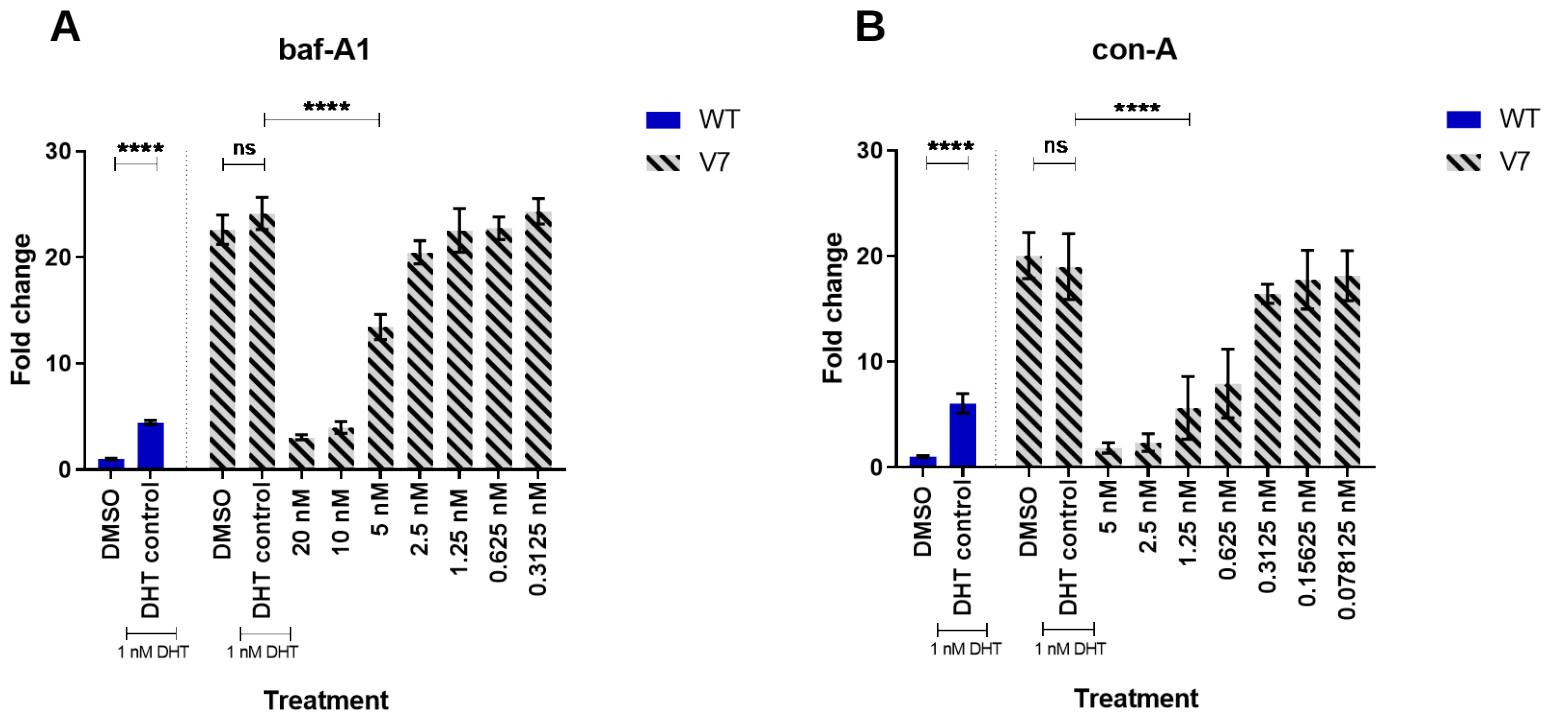

Figure 4-11. Measuring the effect of bafilomycin-A1 and concanamycin-A on AR-V7 activity using firefly luciferase

HeK-293 cells were transfected with the androgen response element (ARE) reporter plasmid and wild-type AR or AR-V7 expression vectors along with a *Renilla* luciferase vector. The cells were cultured in CSS media and treated with 1 nM DHT and indicated concentrations of (A) baf-A1 or (B) con-A for 24 hours. Luciferase activity was determined and firefly luciferase values were normalised to negative DMSO control cells set to 1. Values were then plotted using GraphPad Prism 7 and are displayed as mean values ± standard deviation. Two-way ANOVA with Tukey's multiple comparison post-hoc test was used to generate P values and detect the statistical significance of the indicated differences: ns = non-significant, **** = p≤ 0.0001. Data shown represents three independent replicates completed in triplicate. AR, androgen receptor; WT, wild-type; V7, variant 7; DMSO, solvent control; DHT, dihydrotestosterone; baf-A1, bafilomycin-A1; con-A, concanamycin-A.

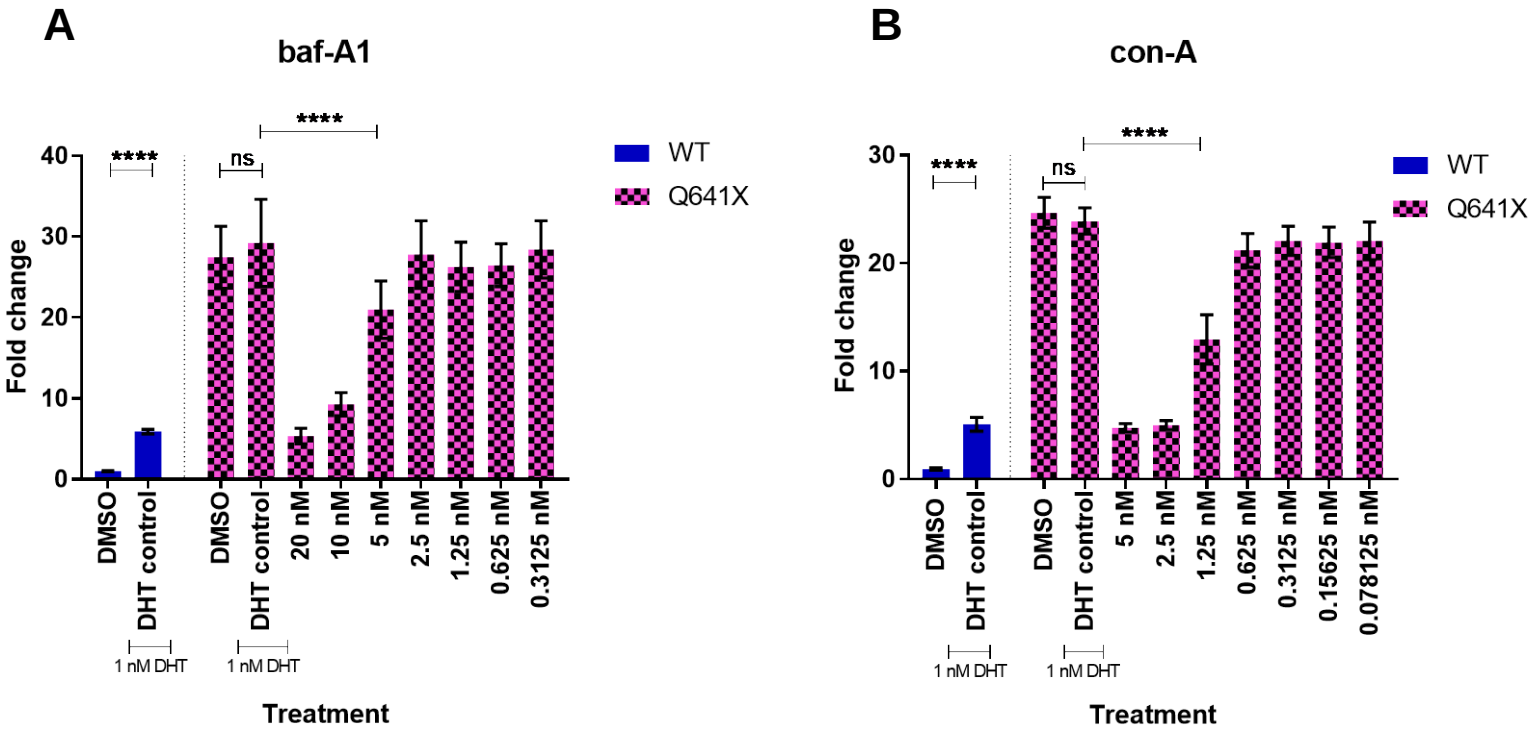

Figure 4-12. Measuring the effect of bafilomycin-A1 and concanamycin-A on AR-Q641X activity using firefly luciferase

HeK-293 cells were transfected with the androgen response element (ARE) reporter plasmid and wild-type AR or AR-Q641X expression vectors along with a *Renilla* luciferase vector. The cells were cultured in CSS media and treated with 1 nM DHT and indicated concentrations of (A) baf-A1 or (B) con-A for 24 hours. Luciferase activity was determined and firefly luciferase values were normalised to negative DMSO control cells set to 1. Values were then plotted using GraphPad Prism 7 and are displayed as mean values ± standard deviation. Two-way ANOVA with Tukey's multiple comparison post-hoc test was used to generate P values and detect the statistical significance of the indicated differences: ns = non-significant, **** = p≤ 0.0001. Data shown represents three independent replicates completed in triplicate. AR, androgen receptor; WT, wild-type; DMSO, solvent control; DHT, dihydrotestosterone; baf-A1, bafilomycin-A1; con-A, concanamycin-A.

4.3.2.2 Role of V-ATPase and AR splice variant signalling in PCa cell lines

The results from the reporter assays revealed that V-ATPase inhibition could reduce AR transactivation in cells with AR splice variants. However, the results were generated using a heterologous expression system so further investigation was required.

The 22Rv1 cell line expresses both AR-WT and the AR-V7 splice variant making it an excellent model to study endogenous mutant AR expression (343). 22Rv1 cells were cultured in RPMI for 24 hours before a further 24 hours in CSS media (Figure 4-13). As 22Rv1 cells contain the splice variant they are only weakly stimulated by DHT but they were cultured in hormone depleted media (CSS) to reduce any interference of endogenous androgens. The cells were treated for 24 hours with 10 nM baf-A1 and/or 1 nM DHT (Figure 4-13).

RNA expression was measured using RT-qPCR and it was found that there was no statistically significant *PSA* induction with DHT stimulation compared to CSS control cells (Figure 4-13 A). Baf-A1 treatment led to significant reduction in *PSA* expression both with and without the addition of DHT. This same pattern was observed with *TMPRSS2* expression (Figure 4-13 B), showing that downstream AR signalling was altered at the RNA level in 22Rv1 cells.

Figure 4-14 shows that the protein expression of AR-WT (full length) and AR-V7 was largely unchanged with different hormonal environments (lanes 1-3), which is supportive of the reporter and RT-qPCR data. There was a slight reduction in both AR-WT and AR-V7 expression with baf-A1 treatment (lane 4 vs lane 2), which was mirrored with DHT co-treatment (lane 5 vs lane 3).

.

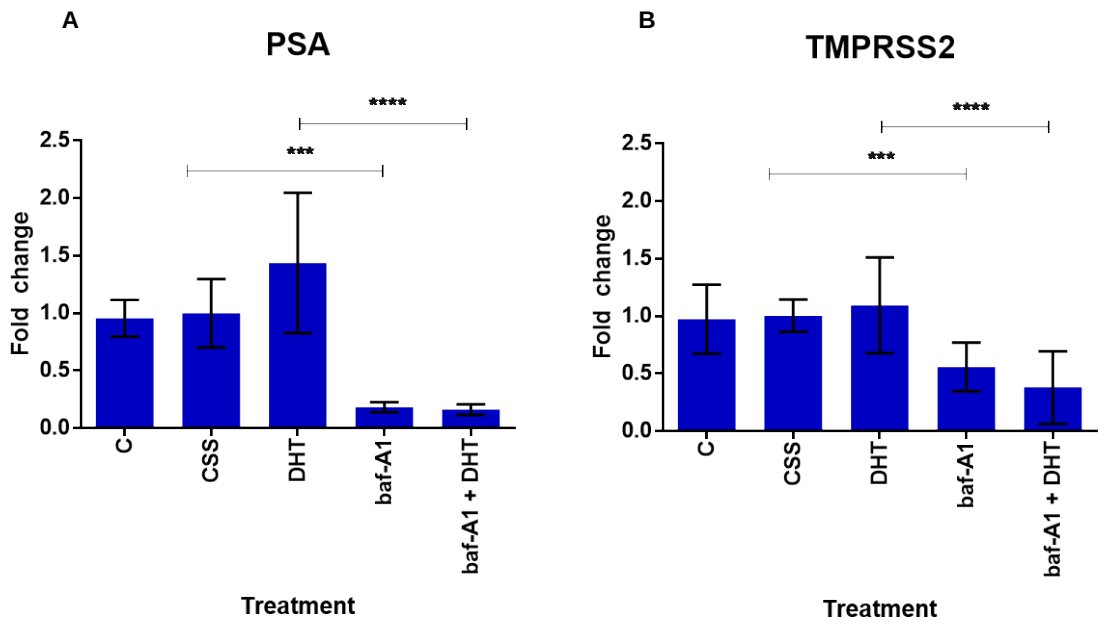

Figure 4-13. Expression of AR downstream target genes in 22Rv1 cells following treatment with 1 nM DHT and/or 10 nM bafilomycin-A1

22Rv1 cells were treated for 24 hours with either 1 nM DHT, 10 nM baf-A1 or both. RT-qPCR analysis was undertaken to assess mRNA levels of (A) *PSA* and (B) *TMPRSS2* and were normalised to *GAPDH*, relative to DMSO treated control CSS cells set to 1. Values were then plotted using GraphPad Prism 7 and are displayed as mean values ± standard deviation. Two-way ANOVA with Tukey's multiple comparison post-hoc test was used to generate P values and detect the statistical significance of the indicated differences: *** = p≤ 0.001, **** = p≤ 0.0001. Data shown represents three independent biological replicates completed in triplicate. C, control; CSS, charcoal stripped serum; DHT, dihydrotestosterone; baf-A1, bafilomycin-A1; PSA, prostate specific antigen.

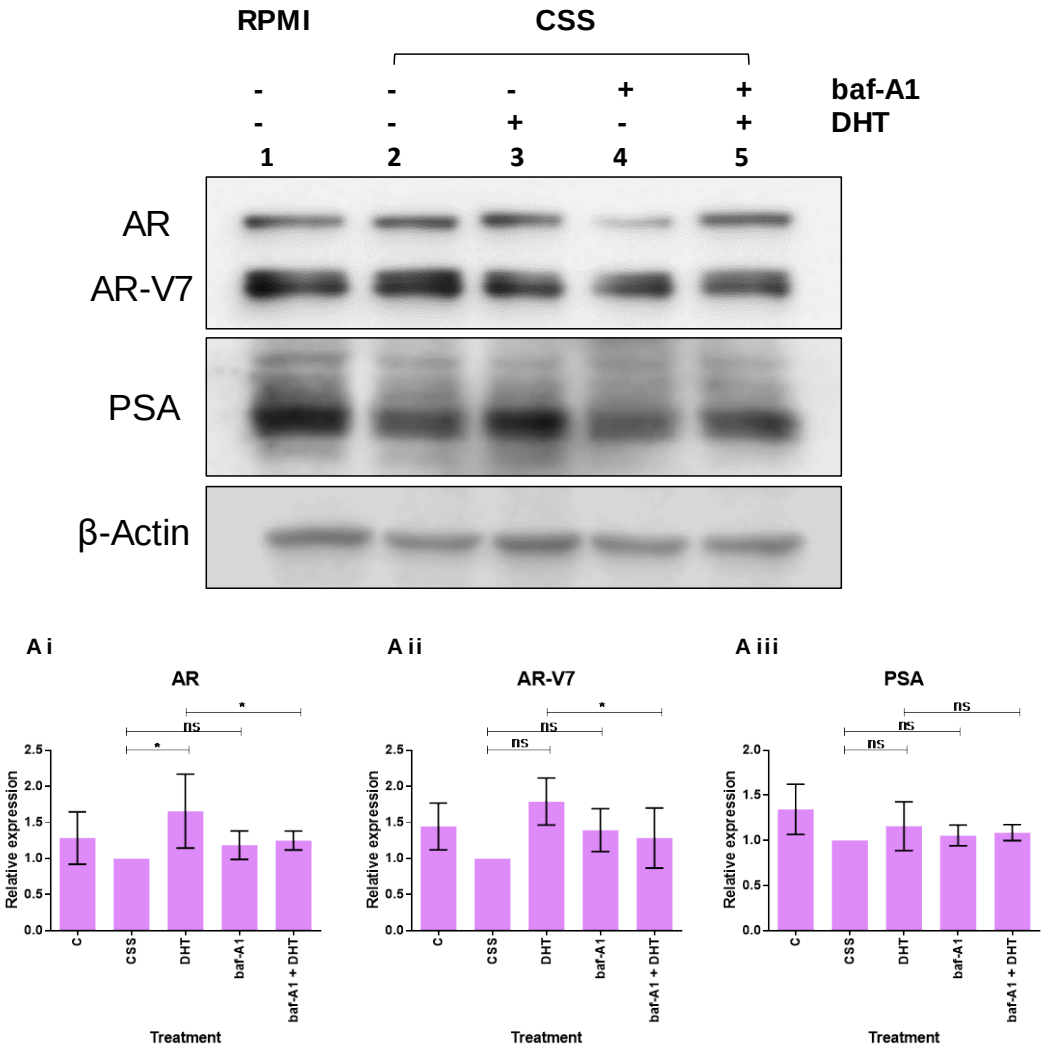

Figure 4-14. PSA and AR expression in 22Rv1 cells following treatment with 10 nM bafilomycin-A1

22Rv1 cells were treated for 24 hours with 1 nM DHT, 10 nM baf-A1 or both. A control 22Rv1 sample was included and was maintained in RPMI. Protein expression was measured using western blotting and cells were probed against AR, PSA and β-Actin. Blot is representative of three individual experiments. Densitometry data of AR (Ai), AR-V7 (Aii) and PSA (Aiii) normalised to β-Actin, relative to DMSO treated control CSS cells set to 1. Values were plotted using GraphPad Prism 7 and are displayed as mean values ± standard deviation. Student's T-Tests were used to generate P values and detect the statistical significance of the indicated differences: ns = non-significant, * = p≤ 0.05. C, control; CSS, charcoal stripped serum; DHT, dihydrotestosterone; baf-A1, bafilomycin-A1; PSA, prostate specific antigen; AR, androgen receptor; AR-V7, variant 7.

4.3.3 Determining the effect of V-ATPase inhibition on AR signalling in cells with AR point mutations

4.3.3.1 Using the reporter assay system to investigate the impact of V-ATPase inhibition on AR-F877L activity

Androgen receptor splice variants are not the only clinically relevant AR aberrations found in prostate cancer. Point mutations have been found to alter the characteristics of the AR leading to a range of different clinical consequences including acquired drug resistance. One such point mutation is the AR-F877L mutation in which phenylalanine is substituted for leucine at position 877 in the ligand binding domain of the AR. This is a mutational hotspot found in a number of different primary tumours and confers an antagonist to agonist switch of enzalutamide (344, 345).

Using the reporter system previously described in 4.3.1.2, HeK-293 cells were transfected with an AR DNA expression vector containing the AR-F877L mutation or the AR-WT as a control (Figure S 8-12). To test that the mutation did confer an enzalutamide antagonist to agonist switch, the transfected cells were treated with DMSO (solvent control), 1 nM DHT, 10 μM enzalutamide or both DHT and enzalutamide for 24 hours (Figure S 8-13). As expected, the AR-WT cells did not have an increase in ARE activation with the enzalutamide only treatment. However, the cells containing the AR-F877L mutant expression vector did have a statistically significant increase with enzalutamide treatment compared to the DMSO negative control.

Having demonstrated that the mutation did confer the enzalutamide antagonist to agonist switch, the reporter system was used with baf-A1 and con-A. HeK-293 cells were again transfected with the AR-F877L expression vector or the AR-WT vector along with ARE and *Renilla* vectors. After 24 hours post-transfection the cells were treated with DMSO, 1 nM DHT and a range of concentrations of either baf-A1 (Figure 4-15 A) or con-A (Figure 4-15 B) for 24 hours.

DHT treatment significantly increased ARE activity in both the AR-WT transfected cells and the AR-F877L cells to a similar level compared to the negative control (DMSO) (Figure 4-15). Baf-A1 treatment led to a significant reduction in ARE activity at 20 and 10 nM in the F877L cells (Figure 4-15 A). In agreement with the AR-WT results (Figure 4-2) 5, 2.5 and 1.25 nM con-A was sufficient to significantly reduce F877L transactivation (Figure 4-15 B).

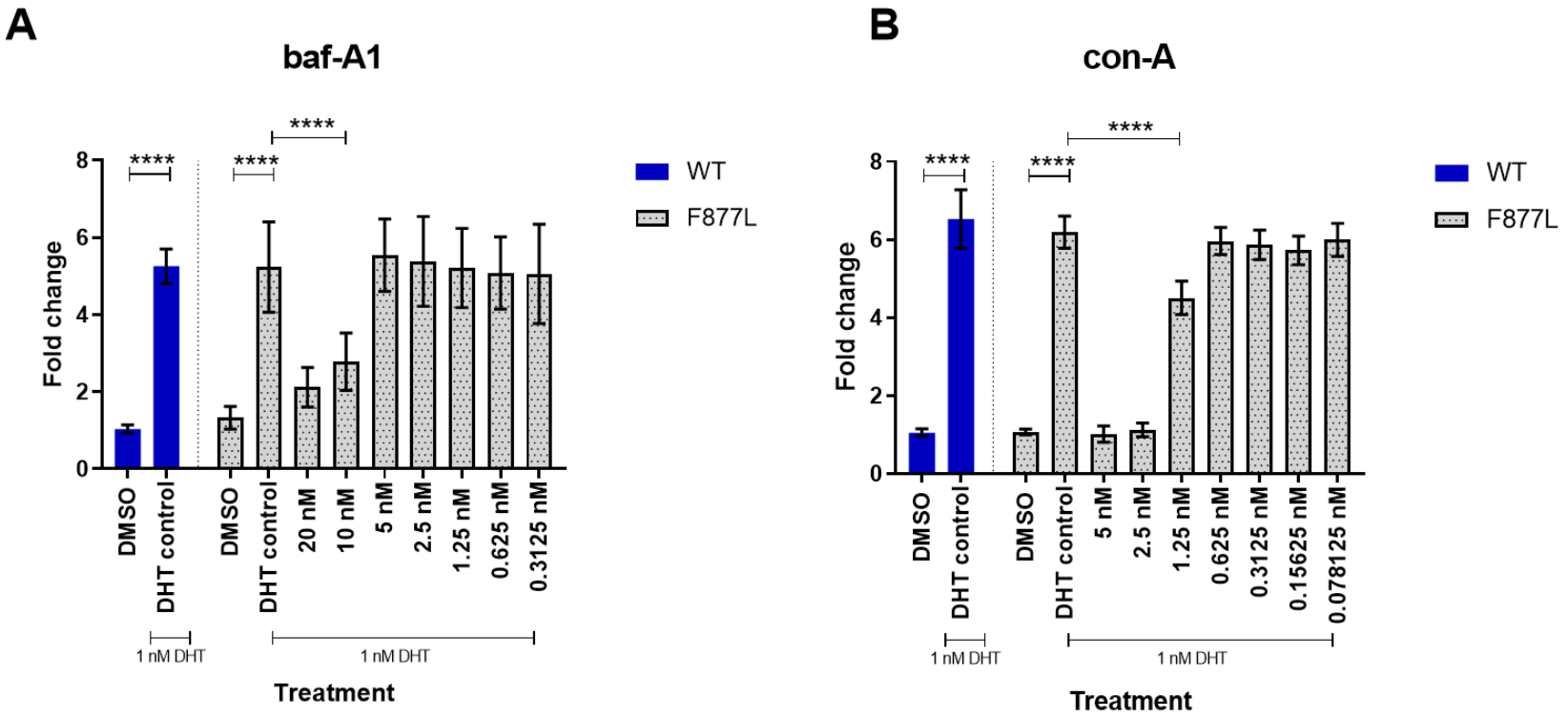

Figure 4-15. Measuring the effect of bafilomycin-A1 and concanamycin-A on AR-F877L activity using firefly luciferase

HeK-293 cells were transfected with the androgen response element (ARE) reporter plasmid and wild-type AR or AR-F877L expression vectors along with a *Renilla* luciferase vector. The cells were cultured in CSS media and treated with 1 nM DHT and indicated concentrations of (A) baf-A1 or (B) con-A for 24 hours. Luciferase activity was determined and firefly luciferase values were normalised to negative DMSO control cells set to 1. Values were then plotted using GraphPad Prism 7 and are displayed as mean values ± standard deviation. Two-way ANOVA with Tukey's multiple comparison post-hoc test was used to generate P values and detect the statistical significance of the indicated differences: **** = p≤ 0.0001. Data shown represents three independent replicates completed in triplicate. AR, androgen receptor; WT, wild-type; DMSO, solvent control; DHT, dihydrotestosterone; baf-A1, bafilomycin-A1; con-A, concanamycin-A.

4.3.3.2 Effect of V-ATPase inhibition on expression of downstream AR target genes in in LNCaP cells with inducible F877L/T878A mutations

The data collected from the reporter assays indicated that V-ATPase inhibition effectively reduced AR activity in the mutant AR-F877L HeK-293 cells. As with the splice variants in 4.3.2, the reporter system needed further validation in cell lines. To model the AR-F877L mutation, LNCaP cells containing the AR-F877L/T878A double mutant and vector only control LNCaP cells were kindly donated from Jocelyn Ceraline, University of Strasbourg (277). The AR-F877L/T878A mutation could be induced in the cells using doxycycline as part of the Tet-On gene expression system (277, 346). Vector only control cells were included in experiments as a comparison for the AR-F877L/T878A double mutant cells. The AR-F877L/T878A inducible double mutant LNCaP cell line was selected to model the AR-F877L mutation as the results could be directly compared to LNCaP vector only control cells, which only expressed the AR-T878A mutant.

Both the AR-F877L/T878A and LNCaP vector control cells were cultured in tetracycline-free RPMI for 24 hours before a further 96 hours in CSS media. This was to ensure that induction of the mutation could be controlled without endogenous interference. Furthermore, to effectively induce the AR mutation, cells were treated with 2 μM doxycycline for 72 hours. After 72 hours, 1 nM DHT, 10 μM enzalutamide, 10 nM baf-A1 or a combination of each was added to cells for 24 hours. RNA expression levels were then measured using RT-qPCR.

In the LNCaP vector only control cells, PSA expression was not significantly increased at the transcript level after enzalutamide only treatment compared to CSS control cells (Figure 4-16 A). As with non-mutant LNCaP cells (Figure 4-3), enzalutamide with DHT effectively reduced PSA and TMPRSS2 expression compared to DHT only cells, indicating that enzalutamide was antagonising AR activity. Furthermore, baf-A1 and DHT treatment significantly reduced PSA and TMPRSS2 mRNA levels compared to DHT only treated cells, which was further reduced with the addition of enzalutamide (Figure 4-16).

LNCaP cells with induced AR-F877L/T878A mutations had a significant increase in *PSA* (Figure 4-17 A) and *TMPRSS2* (Figure 4-17 B) expression following treatment with enzalutamide compared to CSS only control cells This showed that enzalutamide was acting as an agonist at the transcript level and that the AR-F877L mutation had been sufficiently induced by the doxycycline treatment. Baf-A1 treatment resulted in a statistically significant reduction of *PSA* and *TMPRSS2* expression compared to DHT only cells. The reduction of *PSA* mRNA with baf-A1 treatment again provides evidence for AR signalling disruption due to V-ATPase inhibition. Interestingly, when baf-A1 was combined

with enzalutamide in the presence of DHT, *PSA* levels were significantly reduced to a similar level of DHT only treated cells. Thus indicating baf-A1 could negate the increase in *PSA* expression due to enzalutamide-induced AR-F877L AR activity.

Compared to CSS only treated cells, baf-A1 treatment alone led to a decrease in both *PSA* and *TMPRSS2* expression in the AR-F877L mutant cells (Figure 4-17). Additionally, without androgenic stimulation, the combination of enzalutamide and baf-A1 substantially reduced *PSA* and *TMPRSS2* expression compared to enzalutamide only cells, again providing evidence that baf-A1 could potentially re-sensitize patients with enzalutamide resistance.

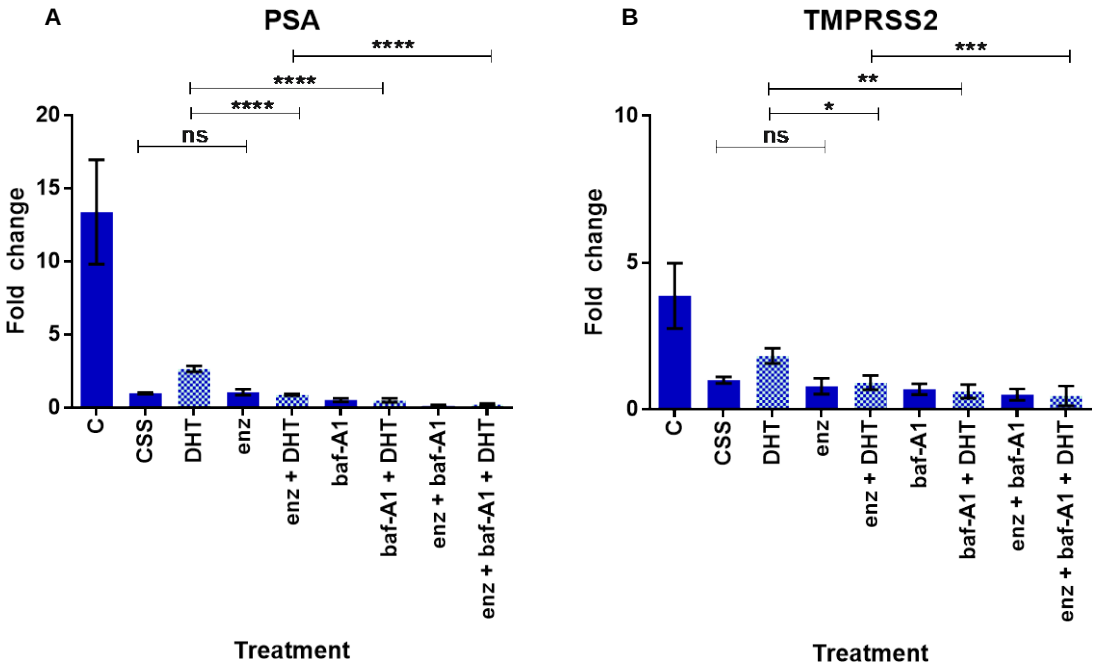

Figure 4-16. Expression of downstream AR target genes in LNCaP vector only control cells following treatment with 1 nM DHT, 10 nM bafilomycin-A1, 10 μM enzalutamide or a combination of each

LNCaP vector control cells were treated with 2 μM doxycycline for 72 hours to allow sufficient AR gene expression. A control sample was also included, which was maintained in RPMI and treated with an equivalent concentration of DMSO for 24 hours prior to cell harvest. The cells were treated for 24 hours with either 1 nM DHT, 10 nM baf-A1, 10 μM enz or a combination of each. RT-qPCR analysis was undertaken to assess mRNA levels of (A) *PSA* and (B) *TMPRSS2* and were normalised to *GAPDH*, relative to DMSO treated control CSS cells set to 1. Values were then plotted using GraphPad Prism 7 and are displayed as mean values ± standard deviation. Two-way ANOVA with Tukey's multiple comparison post-hoc test was used to generate P values and detect the statistical significance of the indicated differences: ns = non-significant, * = p≤ 0.05, ** = p≤ 0.01, *** = p≤ 0.001, **** = p≤ 0.0001, Two-way ANOVA. Data shown represents two independent biological replicates completed in triplicate. C, control; CSS, charcoal stripped serum; DHT, dihydrotestosterone; enz, enzalutamide; baf-A1, bafilomycin-A1; PSA, prostate specific antigen.

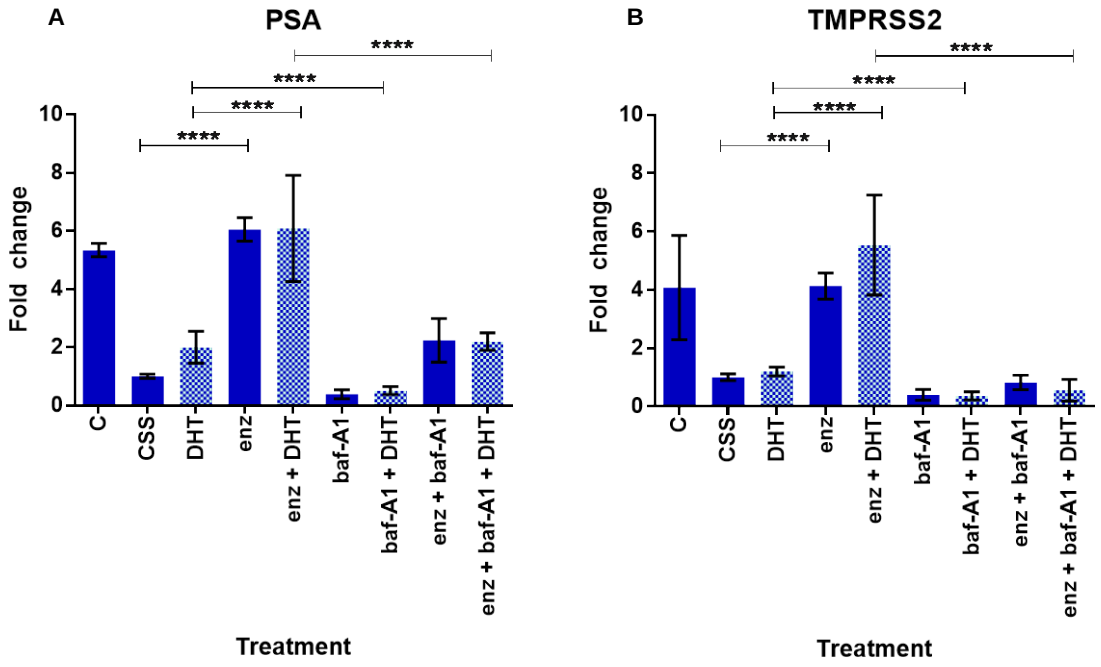

Figure 4-17. Expression of downstream AR target genes in LNCaP F877L/T878A double mutant cells following treatment with 1 nM DHT, 10 nM bafilomycin-A1, 10 μM enzalutamide or a combination of each

LNCaP cells containing the F877L/T878A double AR mutations were treated with 2 μM doxycycline for 72 hours to allow sufficient mutant AR gene expression. A control sample was also included, which was maintained in RPMI and treated with an equivalent concentration of DMSO for 24 hours prior to cell harvest. The cells were treated for 24 hours with either 1 nM DHT, 10 nM baf-A1, 10 μM enz or a combination of each. RT-qPCR analysis was undertaken to assess mRNA levels of (A) *PSA* and (B) *TMPRSS2* and were normalised to *GAPDH*, relative to DMSO treated control CSS cells set to 1. Values were then plotted using GraphPad Prism 7 and are displayed as mean values ± standard deviation. Two-way ANOVA with Tukey's multiple comparison post-hoc test was used to generate P values and detect the statistical significance of the indicated differences: **** = p≤ 0.0001, Two-way ANOVA. Data shown represents two independent biological replicates completed in triplicate. C, control; CSS, charcoal stripped serum; DHT, dihydrotestosterone; enz, enzalutamide; baf-A1, bafilomycin-A1; PSA, prostate specific antigen.

4.3.3.3 Effect of V-ATPase inhibition on AR signalling associated proteins in LNCaP cells with inducible F877L/T878A mutations

Similarly to 4.3.3.2, both the AR-F877L/T878A and vector LNCaP cells were cultured in tetracycline-free RPMI for 24 hours before a further 96 hours in CSS media, and were treated with 2 μM doxycycline for 72 hours. After 72 hours, 1 nM DHT, 10 μM enzalutamide, 10 nM baf-A1 or a combination of each was added to cells for 24 hours (Figure 4-18).

Figure 4-18 (A) shows that in the LNCaP vector only control cells, enzalutamide did not increase AR or PSA expression compared to CSS control cells (lane 4 vs lane 2). Additionally, as expected, enzalutamide did reduce AR and PSA expression in the presence of DHT (lane 5 vs lane 3). Baf-A1 treatment reduced AR expression with DHT co-treatment (lane 7 vs lane 3) and had the greatest reduction in both AR and PSA expression when combined with enzalutamide (lane 9 vs lane 3). This data is supportive of what was observed previously in LNCaP cells (4.3.1.8).

In comparison, Figure 4-18 (B) shows that the AR-F877L/T878A mutant cells had the same response to androgen as the vector only control cells, as the CSS media reduced AR and PSA expression, whilst DHT stimulation increased AR and PSA expression (Figure 4-18 A vs B lanes 1 – 3). Enzalutamide only treatment led to an increase in both AR and PSA levels compared to the CSS control cells (lane 4 vs lane 2). This demonstrated that the AR-F877L mutation was effectively switching enzalutamide from an antagonist to an agonist, supporting what was observed in the reporter assay (Figure 4-15).

Baf-A1 and DHT treated cells had lower AR expression than DHT alone treated cells (lane 7 vs lane 3) but had an increase in PSA expression, accompanied by a blurring of the PSA band. Furthermore, AR expression was lowest when baf-A1 and enzalutamide were added with DHT, resulting in lower expression levels than in cells cultured in CSS only (lane 9 vs lane 2). The PSA expression in cells treated with both baf-A1 and enzalutamide with DHT was greater than that of DHT or baf-A1 and DHT treated cells (lane 9 vs lanes 3 and 7). This shows that enzalutamide was acting as an agonist to stimulate AR signalling, increasing the downstream production of PSA.

When baf-A1 was used without DHT, there was no substantial change in AR expression and a slight increase in PSA expression compared to the CSS only cells (lane 6 vs lane 2). Combining baf-A1 with enzalutamide without androgenic induction, led to a slight reduction in AR expression compared to enzalutamide only treated cells, but an increase in PSA expression (lane 8 vs lane 4).

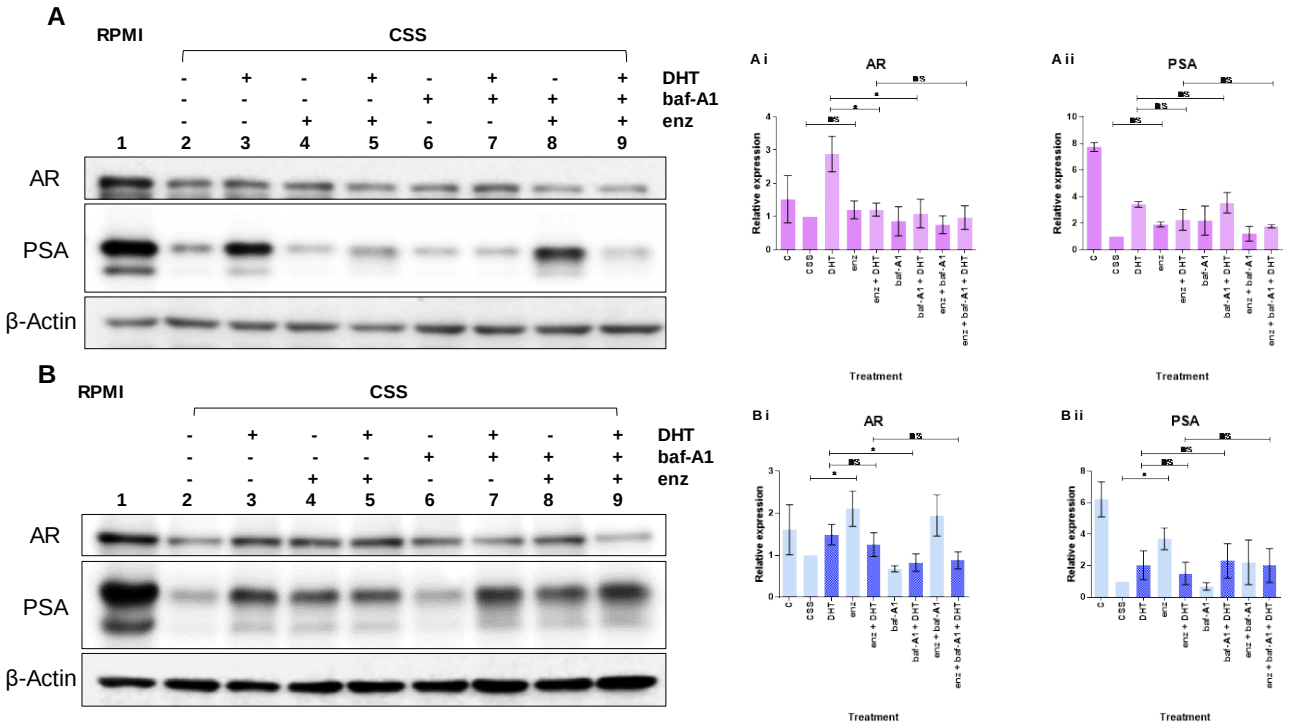

Figure 4-18. AR and PSA expression in LNCaP vector only cells and LNCaP F877L/T878A cells following treatment with 1 nM DHT, 10 nM bafilomycin-A1, 10 μM enzalutamide or a combination of each

LNCaP cells containing (A) the empty vector only or (B) the F877L/T878A double AR mutation were grown in tetracycline-free RPMI media for 24 hours, followed by a further 96 hours of growth in CSS media, and were treated with 2 μM doxycycline for 72 hours. The cells were treated for 24 hours with either 1 nM DHT, 10 nM baf-A1, 10 μM enz or a combination of each. A control LNCaP sample was included and was maintained in RPMI. Protein expression was measured using western blotting and cells were probed against AR, PSA and β-Actin. Blot is representative of three individual experiments. Densitometry data of AR (Ai and Bi) and PSA (Aii and Bii) normalised to β-Actin, relative to DMSO treated control CSS cells set to 1. Values were plotted using GraphPad Prism 7 and are displayed as mean values ± standard deviation. Student's T-Tests were used to generate P values and detect the statistical significance of the indicated differences: ns = non-significant, * = p≤ 0.05. C, control; CSS, charcoal stripped serum; DHT, dihydrotestosterone; enz, enzalutamide; baf-A1, bafilomycin-A1; PSA, prostate specific antigen; AR, androgen receptor.

4.4 Summary of findings

The primary aim of this section was to investigate whether chemical V-ATPase inhibition dysregulates AR activity regardless of AR mutational status. The key findings were as follows:

- V-ATPase inhibition using baf-A1 and con-A reduced wild-type AR transactivation in the reporter assay model at concentrations that were not cytotoxic
- V-ATPase inhibition reduced downstream AR target expression at the transcript level in hormone sensitive LNCaP and DuCaP cell lines.
- Combining baf-A1 with enzalutamide led to a greater reduction in AR target expression than enzalutamide alone
- AR-V7 and AR-Q641X splice variant activity was significantly reduced with V-ATPase inhibition despite androgenic independence
- Baf-A1 and con-A treatment resulted in a reduction in *PSA* and *TMPRSS2* mRNA levels and PSA and AR protein levels in 22Rv1 cells
- V-ATPase inhibition caused a reduction in AR-F877L mutant AR transactivation
- V-ATPase inhibition also reduced AR target expression at the transcript and protein level in AR-F877L/T878A double mutant LNCaP cells

Overall, the results support the hypothesis that V-ATPase is relevant to the AR in models of clinically relevant CRPC states as well as the prior evidence that it impacts on AR WT.

4.5 Discussion

4.5.1 V-ATPase inhibition in androgen sensitive PCa models

One of the key aims of the project was to first establish the effect of chemical V-ATPase inhibition on AR signalling in androgen sensitive PCa cells. Androgen sensitivity is a characteristic of early stage PCa as the AR is dependent on androgen for stimulation to drive cancer growth. The reporter assay system was an extremely useful tool for studying the effect of V-ATPase inhibition on AR activity due to the fact that it was an isolated system. By transfecting the wild-type AR into the AR negative HeK-293 cells I could measure the direct effect of chemical inhibition on AR transactivation, which had not been shown before. It was found that baf-A1 concentrations as low as 5 nM (Figure 4-2 A), and con-A as low as 1.25 nM (Figure 4-2 B), was sufficient to significantly reduce AR-WT activity. Previous research groups have demonstrated that AR expression could be

reduced with 10 nM con-A (313) but here I have shown concentrations as low as 1.25 nM could reduce AR activity without having a cytotoxic effect.

Building on the results from the reporter assay, I decided to use the V-ATPase inhibitors in more complex androgen dependent cell line systems with endogenous AR expression. The LNCaP cell line is one of the most well characterised androgen sensitive prostate cancer cell lines and was therefore an ideal model to investigate the effects of V-ATPase inhibition. I found that V-ATPase inhibition using baf-A1 and con-A at 10 nM reduced the expression of downstream AR targets at the transcript level (Figure 4-3 and Figure 4-4). At the protein level, V-ATPase inhibition also reduced AR expression (Figure 4-5). This is in agreement with recently published data which showed that in LNCaP cells, and another hormone sensitive line known as LAPC4, concanamycin-A treatment led to a significant reduction in AR expression at both protein and RNA level (313). One curious result that both I and *Michel et al.* found was that despite reducing AR protein expression, V-ATPase inhibition actually increased protein expression of the downstream target PSA, despite the fact that expression was reduced at the transcript level (2). To investigate whether this was a cell line specific phenomenon we used the AR-WT DuCaP cell line to validate the results. The DuCaP cells were treated with both V-ATPase inhibitors and stimulated with DHT to activate AR signalling (Figure 4-6 , Figure 4-7 and Figure 4-8). It was shown that AR protein expression was decreased, and that PSA protein expression was again increased. This confirmed that the increase in PSA protein expression was not cell line specific but that there was a disruption in AR signalling due to V-ATPase inhibition.

One of the primary functions of V-ATPase is to acidify intracellular vesicles to enable functions such as receptor endocytosis and vesicular transport (14, 347). For example, in endosomes a V-ATPase controlled reduction in pH causes the release of a ligand and recycles it to the plasma membrane. Additionally, the low pH maintained by V-ATPase is crucial for the transportation of acid hydrolases to the lysosomes from the Golgi (69). Given that this effect was only occurring at the protein level and not at the transcript level, it is logical to assume that the increase in PSA protein may be due to the inhibition of these key processes. Moreover, as PSA is secreted and TMPRSS2 is not, it is probable that this effect may be linked to protein secretion, which occurs via the ER/Golgi pathway. V-ATPase inhibition likely disrupts this secretory pathway and causes alkalinisation of transport vesicles leading to an accumulation of intracellular PSA. This accumulation of PSA might then mask the downregulation of *PSA* mRNA resulting from V-ATPase inhibition.

Furthermore, many proteins undergo glycosylation in the Golgi, which is an important post-translational modification, and mutations in V-ATPase subunits have been linked to defective glycosylation resulting in a wrinkly skin disease known as cutis laxia (71). The

fact that a reduction in V-ATPase activity and function results in defective protein glycosylation may explain why in LNCaP cells the increase in PSA protein expression was accompanied by a blurring of the PSA band on the western blot (Figure 4-5 and Figure 4-10). Glycosylation is important for protein folding due to the attachment of polysaccharide chains, and increases protein stability through kinetic and thermodynamic stabilizations (348, 349). Therefore if V-ATPase inhibition impairs PSA glycosylation then the protein would be less stable, potentially resulting in an altered molecular weight.

Research published by *Michel et al.* supports the idea that V-ATPase inhibition impairs PSA vesicular transport. They found that baf-A1 treatment resulted in an accumulation of PSA loaded vesicles which stained positive for LAMP1 and LAMP2, indicating they were of lysosomal nature (2). The absence of acridine orange staining, which is a fluorescent dye used to stain acidic vesicles, in baf-A1 treated cells, provides further evidence of defective lysosomal acidification (2).

To further investigate the potential link between V-ATPase and AR signalling I used the antiandrogen treatment enzalutamide to antagonize the AR in LNCaP cells. Enzalutamide is currently the most widely used antiandrogen treatment for metastatic prostate cancer, acting as an AR antagonist by binding to the ligand binding domain (350). It was therefore interesting to consider what effect combining V-ATPase inhibition with AR antagonism would have on AR signalling. In fact, both AR downstream transcript expression (Figure 4-9) and AR protein expression (Figure 4-10) were substantially reduced when the two treatments were given together in the presence of DHT. Although enzalutamide is generally used in metastatic and later-stage PCa, combining it with V-ATPase inhibition showed an additive effect with DHT stimulation in a hormone sensitive line. This provides some very early stage evidence for the use of a dual-combination therapy as a possible cancer treatment. Future work would need to be conducted to ascertain whether the effect is just additive or whether it is synergistic.

4.5.2 Investigating the effect of chemical V-ATPase inhibition on cells expressing AR splice variants

There is already a plethora of effective treatment options available for early stage and hormone responsive prostate cancer. However once the cancer become castrate resistant, and AR activity becomes independent of androgenic stimulation, treatment options become very limited (351), which is partly due to cross-resistance of AR directed drugs (352). For this reason it became important to investigate whether V-ATPase inhibition would be effective at reducing AR signalling in cells with mutant AR's. The AR-V7 splice variant has been detected in over 75% of cases post ADT and had an even higher expression following treatment with enzalutamide (288). It is associated with a

poorer prognosis and results in a significant survival disadvantage compared to AR-V7 negative disease (74.3 vs 25.2 months) (288). Using our reporter assay system, it was found that V-ATPase inhibition led to a significant reduction in AR-V7 activity, reducing ARE activation to DHT stimulated wild-type levels (Figure 4-11). The AR activity observed with AR-V7 was substantially higher than that of the AR-WT, which is important to consider when assessing the effectiveness of V-ATPase inhibition on AR activity. For example, inhibition was only as effective at reducing AR activity as AR-WT cells that had been stimulated with DHT, showing that AR activation was still occurring. However, it is important to stress that this is a model system and in reality it is likely that AR-V7 is highly heterogeneous with differing ratios of AR-WT to AR-V7 (288). Despite this, to show that this was not just AR-V7 specific, the same assay was repeated with the AR-Q641X splice variant and similar results were obtained (Figure 4-12). The main advantage of using this system is that because HeK-293 cells do not express the AR the direct effect of V-ATPase inhibition on AR transactivation can be studied without the presence of endogenous AR. An obvious limitation of this model is that it may not reflect what occurs naturally in cancerous cells. Therefore, we were also able to demonstrate that AR signalling is reduced with V-ATPase inhibition in the AR-V7-expressing 22Rv1 cell line (Figure 4-13 and Figure 4-14). This finding was significant due to the fact that AR-V7 expression is highly heterogeneous and even shows different expression levels in metastases from a single patient (288). Additionally, only knockdown of AR-V, not full-length AR, was able to restore the ability of enzalutamide to reduce cell proliferation in 22Rv1 cells (334), which highlights the importance of finding a compound that targets splice variant AR. Therefore, not only may V-ATPase represent a novel target that would be effective at reducing AR activity in patients expressing AR splice variants, but inhibition may overcome resistance to enzalutamide and re-sensitize patients with AR-V's.

4.5.3 Effect of V-ATPase inhibition on AR signalling in cells with AR point mutations

As mentioned, AR splice variants are not the only AR alterations found in PCa patients. Many AR point mutations have now been characterised in patients with different stages of PCa across each of the AR functional domains. To understand the impact of these point mutations relevant to my results, they have been characterised on the basis of transactivational activity as either loss of function, gain of function or no change from AR-WT activity with or without DHT binding. Interestingly, loss of function mutations have been shown to be more common than gain of function mutations (62% vs 16% respectively) and were found to be mainly localised in the ligand-binding domain (353). One of the most common and well-studied AR alterations is the AR-T878A mutation in the ligand binding domain. The threonine residue is primarily involved in hydrogen bonding to

the D-ring of a ligand and mutation results in ligand promiscuity (337). In one study, the mutation to an alanine residue was found to have the largest increase in AR transcriptional activity compared to any other AR mutation investigated (625%) (353). The AR-T878A mutation is also found in LNCaP cells, which is important to consider when thinking about how V-ATPase inhibition impacts on AR signalling, and it is why early experiments were validated in the AR-WT DuCaP cell line (Figure 4-6, Figure 4-7 and Figure 4-8).

Focusing on CRPC, another AR point mutation of interest was the AR-F877L mutation. This mutation was one of the first to emerge after repeated enzalutamide treatment (277). As previously discussed, not only does it result in resistance to enzalutamide but also confers an antagonist to agonist switch, making it an extremely important mutation for CRPC patients (274). It is localised to the ligand binding domain and is adjacent to the AR-T878A mutation found in LNCaP cells. The mutation is clinically relevant and was found to be present in 3 out of 4 enzalutamide resistant tumours in an *in vivo* xenograft model (277). After characterising the mutation in the reporter system (Figure S 8-13), baf-A1 and con-A were used to chemically inhibit the V-ATPase. It was found that at nanomolar concentrations both inhibitors could reduce AR-F877L transactivational activity in the same manner as the AR-WT (Figure 4-15). Furthermore, when LNCaP cells containing the AR-F877L/T878A double mutant were treated with both enzalutamide and baf-A1, AR signalling was significantly reduced compared to controls, indicating V-ATPase inhibition could overcome enzalutamide resistance (Figure 4-15, Figure 4-16, Figure 4-17 and Figure 4-18). This supports what was found with the AR-V splice variants (4.3.2) and again demonstrates the V-ATPase inhibition can overcome, and even reverse, increased AR transactivation as a result of a mutated AR.

Considering that mutations such as AR-T878A and AR-F877L have emerged and confer resistance to second-generation treatments, it was encouraging to find that V-ATPase inhibition reduced AR activity regardless of AR functionality. This provides more evidence that V-ATPase may represent a target for CRPC as patients may become re-sensitized to existing treatments.

Chapter Five

Chapter 5 Investigating the effect of genetic silencing of V-ATPase subunits on AR signalling

Investigating the effect of genetic silencing of V-ATPase subunits on AR signalling

5.1 Introduction

The results from Chapter 4 showed that chemically inhibiting V-ATPase reduced AR signalling in hormone sensitive prostate cancer cell lines (LNCaP and DuCaP), AR splice variant expressing cell lines (22Rv1) and AR mutant cell lines (LNCaP F877L/T878A). The inhibitors used, bafilomycin-A1 and concanamycin-A, both inhibit V-ATPase activity by binding to the V_Oc subunit ring structure. However, despite the fact that V-ATPase inhibition had a profound effect on reducing AR activity in prostate cancer cells, the inevitable toxicity to non-cancerous cells would prevent their use as anti-cancer treatments, which is primarily due to the high potential for toxic off-target effects.

As previously discussed, the V-ATPase complex is made up of different subunits, many of which have tissue specific isoforms (Figure 1-1). Additionally, it was found that some V-ATPase subunits function independently of the complete complex to regulate various signalling pathways (354). More recently it has been shown that a variety of subunit isoforms are overexpressed in different cancer types compared to non-cancerous healthy tissue (1). Therefore, the fact that cancerous cells have an increased expression of specific isoforms led me to question whether targeting these overexpressed isoforms could lead to a non-toxic reduction in V-ATPase activity, and a reduction in the potential for toxic off-target effects. Furthermore, as current V-ATPase inhibitors only target the V_Oc subunit ring, there is an obvious limitation in the pharmacological approaches being used, and consequently genetic methods are required to directly test the role of individual V-ATPase subunits. Thus, perhaps targeting an alternative subunit may improve the toxicity profile of future inhibitory compounds.

Remaining focussed on the link between V-ATPase and AR signalling in prostate cancer, I first wanted to establish which subunits might be of interest to silence in prostate cancer cell lines. After selecting a subunit for further investigation, the plan was to transiently knockdown the subunit using siRNA and measure the effect on AR signalling in LNCaP and 22Rv1 cells. Following on from this, I planned to use the CRISPR-Cas9 system as an additional genetic silencing tool to study the effect of subunit knockout on AR signalling.

5.2 Hypothesis and Aims

5.2.1 Hypothesis

The genetic silencing of a single V-ATPase subunit isoform results in dysregulated AR signalling.

5.2.2 Aims

The aim of this component of the project was to assess the effect of genetically silencing a single V-ATPase subunit isoform on AR signalling in prostate cancer cell lines. This aim was investigated by:

- Combining bioinformatics data with functional information to select a V-ATPase subunit isoform for genetic silencing experiments
- Measuring AR and AR-V7 expression after using siRNA to transiently knockdown subunit isoform expression in hormone sensitive (LNCaP) and AR-V7 (22Rv1) cell lines
- Assessing the effect of CRISPR mediated isoform knockdown on AR expression in LNCaP cells
- Combining CRISPR mediated isoform knockdown with siRNA mediated knockdown of an additional isoform to investigate the impact of dual isoform silencing on AR signalling in LNCaP cells
- Measuring the effect of CRISPR mediated single isoform knockout on AR downstream signalling target expression in 22Rv1 cells
- Assessing the effect of CRISPR mediated single isoform knockout on AR and AR-V7 expression in 22Rv1 cells
- Combining CRISPR mediated isoform knockdown with siRNA mediated knockdown of an additional isoform to investigate the impact of dual isoform silencing on AR signalling in 22Rv1 cells

5.3 Results

5.3.1 Selection of V-ATPase subunits for genetic silencing experiments

Although there is a lot of emerging data surrounding V-ATPase overexpression in different cancer types, very little is known about individual subunit overexpression in PCa. A literature search indicated that there is no data for V-ATPase subunit expression in PCa cell lines or patient tumour tissue. Thus, to gain an insight into subunit expression in PCa, publicly available data was analysed using cBioPortal as a platform (355). The cBioPortal is an open-access online tool for investigating multidimensional cancer genomics data sets. Although there are currently 18 PCa cohorts publicly available on cBioPortal, many of these cohorts have varying levels of data. For example, most cohorts have extensive genetic mutation information but lack RNA-sequencing expression data. Therefore, the TCGA (provisional) PCa dataset of 499 samples was selected for further meta-analysis (356). The reason for selecting this cohort was that it contains reliable and robust multi-level data including mutation, copy number, clinical and expression data.

The oncoplot in Figure 5-1 shows the copy number, RNA expression and mutation data for all of the mammalian V-ATPase subunits including the two accessory genes *ATP6AP1* and *ATP6AP2*. Each of the subunits are altered to varying degrees across the cohort. The subunit isoforms that are altered in the highest number of patients are *ATP6V1B2* and *ATP6V1C1*. *ATP6V1B2* encodes the V_1B2 isoform, which has enriched expression in the kidney and forms the catalytic hexamer with V_1A. Figure 5-1 shows that *ATP6V1B2* has low mRNA expression, many deep copy number deletions and is altered in 23% of patient samples. In contrast to this, *ATP6V1C1*, which encodes the V_1C1 mammalian subunit, has increased mRNA expression, copy number amplifications and is altered in 22% of patient samples. However, similarly to Chapter 3, it is important to note that the high number of copy number amplifications observed was due to an amplification of the long arm of chromosome 8. As a result, *ATP6V1C1* amplification could be the result of co-amplification with other genes. Despite this, *ATP6V1C1* also had increased mRNA expression, and therefore I hypothesized that as this could be related to V-ATPase function and silencing it would be more informative than silencing a subunit that is commonly downregulated in PCa. Furthermore, the V_1B2 subunit forms the catalytic hexamer which is essential for V-ATPase function (Figure 1-1), and therefore silencing *ATP6V1B2* gene expression may lead to a non-functional V-ATPase complex. V_1C1 is ubiquitously expressed in mammalian cells (34) and functions to regulate the assembly of

the V_1 and V_O domains to form the V-ATPase complex (Figure 1-2). Due to the fact that V_1C1 plays a regulatory role, rather than functioning as a catalytic subunit, it made for a more attractive target than V_1B2.

More recently V_1C1 has been shown to be overexpressed in different cancer types, which has been linked to functional defects. For example, in *Drosophila melanogaster*, Vha44 (the fruit fly equivalent of mammalian V_1C1) overexpression increased cellular invasion, increased V-ATPase activity, lowered endosomal pH and altered other V-ATPase subunit levels. The authors suggested that this was due to decreased endolysosomal degradation, and that the induction of tumorigenesis was dependent on JNK signalling (357). Additionally, in oral squamous cell carcinoma (OSCC) patients, *ATPV1C1* mRNA levels were found to be significantly higher compared to healthy tissue and had a direct correlation with tumour stage (99). Further research using immunohistochemistry (IHC) showed more intense staining in OSCC tissues compared to healthy tissue indicating V_1C1 is important for epithelial functioning and is involved in cancer progression (92). In cervical cancer patients, IHC analysis showed V_1C1 expression was significantly increased and was correlated with poor disease-free survival (358).

Taken together, the data from Figure 5-1, the regulatory function of the subunit and the fact that there is evidence for dysregulation in other cancer types, makes V_1C1 an attractive candidate for further investigation.

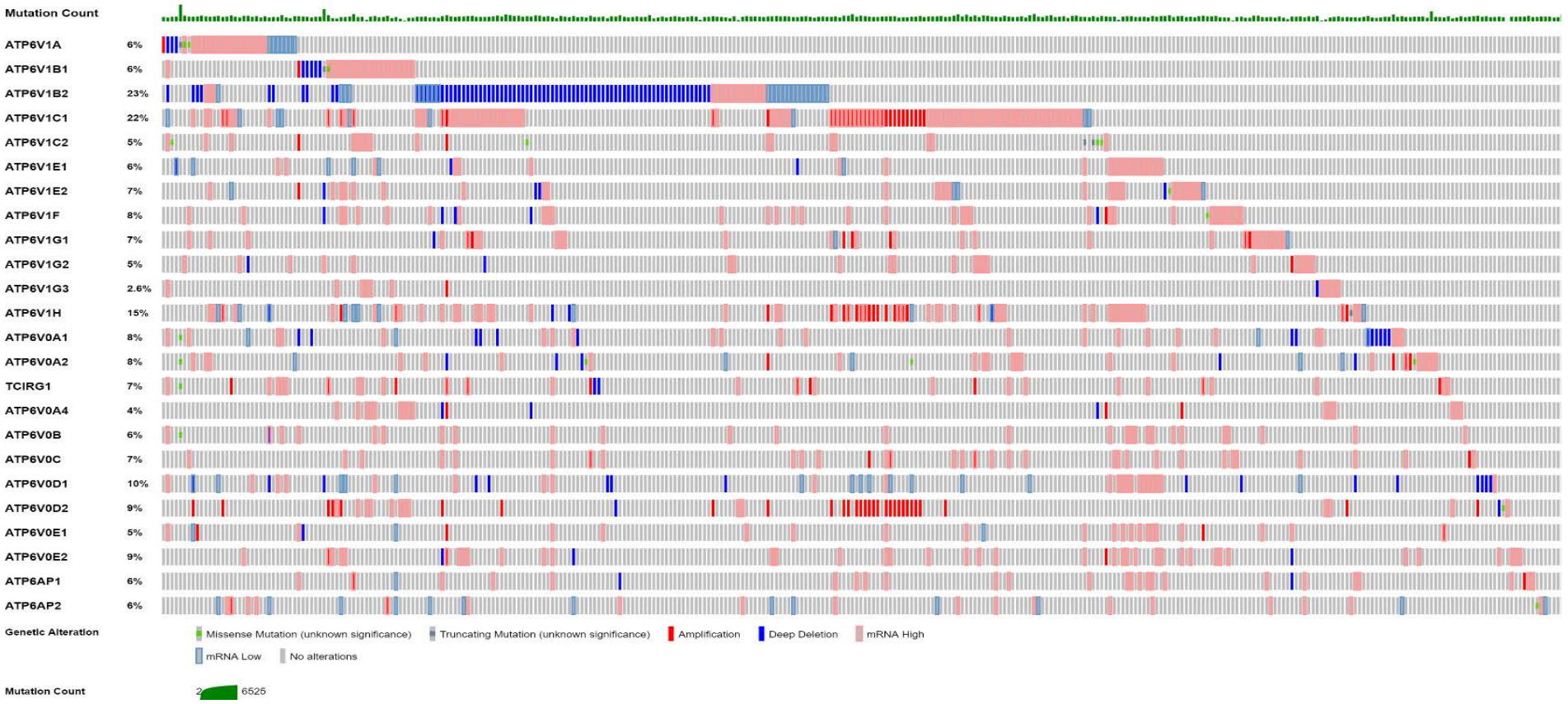

Figure 5-1. Oncoplot showing V-ATPase subunit copy number and mutations in prostate cancer

Using data from Prostate Adenocarcinoma cohort (TCGA, provisional) and cBioPortal, V-ATPase genes are plotted as an Oncoplot displaying genetic alterations and mRNA expression per patient sample. The differences in mRNA expression levels for each gene were calculated using mRNA expression z-Scores (RNA Seq V2 RSEM) with a z-score threshold of ±2.0. Mutation count (%) is representative of the number of patients with a selected gene alteration compared to the total number of patients sampled. The mutational burden (Mutation count) of each patient is also plotted along the top of the Oncoplot.

5.3.2 Effect of siRNA mediated knockdown of V-ATPase V_1C subunits on AR signalling in hormone sensitive LNCaP cells

After selecting the ubiquitously expressed V_1C1 subunit for further investigation, the first aim was to use siRNA to knockdown subunit expression and measure the effect on AR and PSA protein levels in LNCaP cells. To assess whether potential effects were due to the specific knockdown of V_1C1, expression of the V_1A subunit was also knocked-down using siRNA. The reason for this is because the V_1A subunit has no other isoforms and is an essential catalytic component of the V-ATPase complex (359). Therefore knocking down V_1A expression should reduce overall V-ATPase complex expression and activity. In addition, measuring V_1A protein levels in response to V_1C1 knockdown was used to assess how V_1C1 knockdown would affect overall complex expression. Finally, as the V_1C1 subunit has an alternative isoform known as V_1C2, the expression of V_1C2 was also measured in response to V_1C1 knockdown.

The amino acid sequence of the V_1C2 subunit isoform is 62% identical and 83% similar to V_1C1 (34). Furthermore, in comparison to the ubiquitously expressed V_1C1 isoform, V_1C2 is found to have tissue enriched expression in the kidney, lung and testis (360). This tissue specific expression has been further characterised in mice as V_1C2a and V_1C2b, which are products of alternative mRNA splicing (42). V_1C2a expression was found to be restricted to lamellar bodies of type 2 alveolar cells, whereas V_1C2b was found to be expressed in the plasma membrane of renal α and β-intercalated cells (42). Interestingly, the V_1C2 subunit isoform was found to form a unique V-ATPase complex expressed in the kidneys, which contained many kidney specific isoforms such as V_1B2, V_1G3, V_Od2 and V_Oa4, whereas the ubiquitously expressed V_1C1, V_1G1 and V_1B1 were found in a different V-ATPase complex (42). Using a similar yeast chimeric system to the one used in Chapter 3, it was also shown that chimeric V-ATPase complexes containing mouse V_1C2a or V_1C2b had a lower *Km* and proton transport rate than complexes with V_1C1 (42). These findings suggest selective V-ATPase subunit assembly *in vivo*, which might be related to the activity of cells with specialised functions, such as renal intercalated cells. A literature search indicated that there is currently no published evidence of V_1C2 cancer specific overexpression.

To knockdown the expression of V_1C1 or V_1A subunits, an siRNA pool (Dharmacon) was used, which contained 4 siRNAs targeting 4 separate regions of the V_1C1 or V_1A subunit transcripts. Furthermore, to ensure reliable conclusions could be made regarding the effect of V_1C1 or V_1A knockdown on AR signalling, cells were also transfected with a non-

specific siRNA pool (Dharmacon). LNCaP cells were reverse transfected with 25 nmol ATP6V1C1, ATP6V1A or non-specific siRNA and grown in RPMI media for either 48 or 72 hours. The reason for reverse transfecting the cells was to improve the relatively poor transfection efficiency of LNCaP cells (around 50-60%), and the siRNA concentration of 25 nmol was selected based on the manufacturers recommendations. After 48 or 72 hours, the cells were harvested and protein levels were measured using western blotting.

After both 48 and 72 hours of ATP6V1C1 siRNA transfection, V_1C1 protein levels were reduced by approximately 60% and 50% compared to the respective non-specific controls, which was statistically significant (Figure 5-2 Ai and Bi respectively). Additionally, the ATP6V1A siRNA significantly reduced levels of V_1A expression after 48 hours by approximately 40% (Figure 5-2 Aiii), which was further reduced to 50% after 72 hours of siRNA treatment (Figure 5-2 Biii). This shows that the siRNA transfections were effectively reducing V-ATPase subunit expression in LNCaP cells. The non-specific siRNA had no significant effect on the protein levels of any of the proteins investigated compared to the non-transfected control. Therefore the changes in protein expression were not due to a non-specific effect of the siRNA transfection. It is interesting to note that ATP6V1C1 siRNA transfection did not alter V_1A expression at either 48 or 72 hours, but ATP6V1A siRNA did reduce V_1C1 expression after 72 hours of treatment. This highlights the importance of the V_1A catalytic subunit in V-ATPase complex expression and shows that reduced V_1A expression leads to a reduction in the expression of other subunits.

The expression of AR was relatively unaffected by V_1C1 and V_1A knockdown after transfection with siRNA for 48 (Figure 5-2 Aiv) or 72 hours (Figure 5-2 Biv) compared to the non-specific siRNA and non-transfected controls. Additionally, PSA protein levels were also unaffected by V_1C1 and V_1A knockdown, suggesting that AR signalling was not reduced as a result of subunit knockdown, at least in the absence of hormone stimulation.

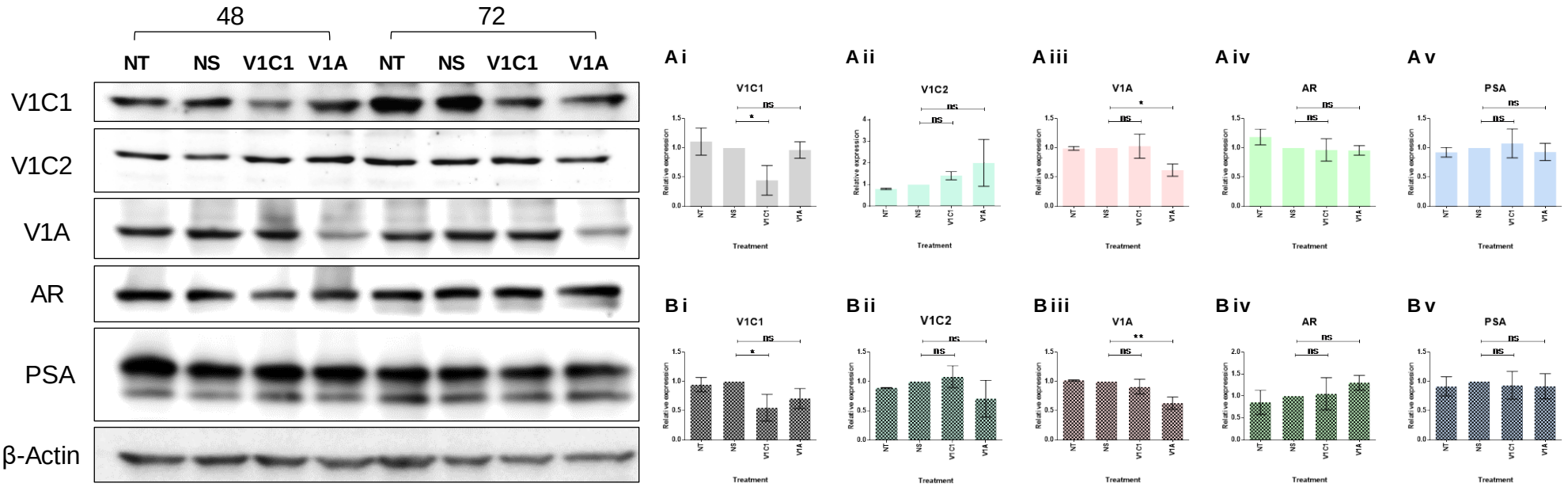

Figure 5-2. Effect of siRNA mediated knockdown of V_1C1 and V_1A on AR signalling in LNCaP cells

LNCaP cells were reverse transfected with either 25 nmol of ATP6V1C1, ATP6V1A or non-specific siRNA for either 48 or 72 hours. Control non-transfected cells were treated with equivalent concentrations of Dharmafect 1 reagent. Protein expression was measured using western blotting and cells were probed against ATP6V1C1, ATP6V1C2, ATP6V1A, AR, PSA and β-Actin. Blot is representative of three individual experiments. Densitometry data of 48 hour (Ai – Av) and 72 hour (Bi – Bv) siRNA treated cells normalised to β-Actin, relative to either 48 or 72hr NS set to 1. Values were plotted using GraphPad Prism 7 and are displayed as mean values ± standard deviation. Student's T-Tests were used to generate P values and detect the statistical significance of the indicated differences: ns = non-significant, * = p≤ 0.05, ** = p≤ 0.01. NT, non-transfected; NS, non-specific; AR, androgen receptor; PSA, prostate specific antigen.

Although there was no significant effect of V_1C1 or V_1A knockdown on AR and PSA expression after 48 or 72 hours post-transfection with siRNA, it was important to investigate whether this was due to differences in the exposure to different androgens. Therefore, I wanted to investigate the effect of V_1C1 and V_1A subunit knockdown on AR and PSA expression in a controlled androgenic environment, in which cells were grown in CSS media and treated with 1 nM DHT. In this instance, the LNCaP cells were seeded in RPMI media 24 hours prior to transfection, which reduced transfection efficiency compared to a reverse transfection. This was due to the fact that the LNCaP cells would not grow well if they were cultured in a hormone depleted environment. After a media change to CSS, LNCaP cells were transfected with 25 nmol ATP6V1C1, ATP6V1A or non-specific siRNA for 72 hours, and were then treated for 24 hours with either DMSO or 1 nM DHT. The cells were then collected and western blotting was used to measure the levels of the indicated proteins.

Similarly to Figure 5-2, ATP6V1C1 siRNA transfection for 72 hours was sufficient to significantly reduce V_1C1 protein levels, independent of androgenic stimulation (Figure 5-3 Ai). The addition of 1 nM DHT did not affect V_1C1 expression in any of the investigated conditions compared to the DMSO controls. This suggests androgen is not required for V_1C1 expression in prostate cancer. Furthermore, ATP6V1A siRNA transfected cells had a reduction of approximately 40% in V_1A subunit levels compared to the non-specific transfected cells, but only around 30% in the DHT treated cells compared to DMSO (Figure 5-3 Aiii). Again, there was not a significant difference in V_1A expression for any of the transfection conditions after androgenic stimulation. As with Figure 5-2, the non-specific siRNA had no significant effect on the levels of any of the proteins investigated compared to the non-transfected controls.

AR levels were increased overall in DHT treated cells compared to DMSO cells (Figure 5-3 Aiv), which was expected due to the androgenic activation of the AR signalling pathway. ATP6V1C1 siRNA transfection did not significantly affect AR levels with or without DHT treatment. PSA expression follows a similar pattern to the AR as DHT treatment increased expression compared to the DMSO controls and V_1C1 and V_1A knockdown did not significantly alter PSA expression. These results suggest that despite the results being statistically non-significant, a siRNA mediated reduction in V_1C1 might lead to a reduction DHT-dependent AR signalling activation.

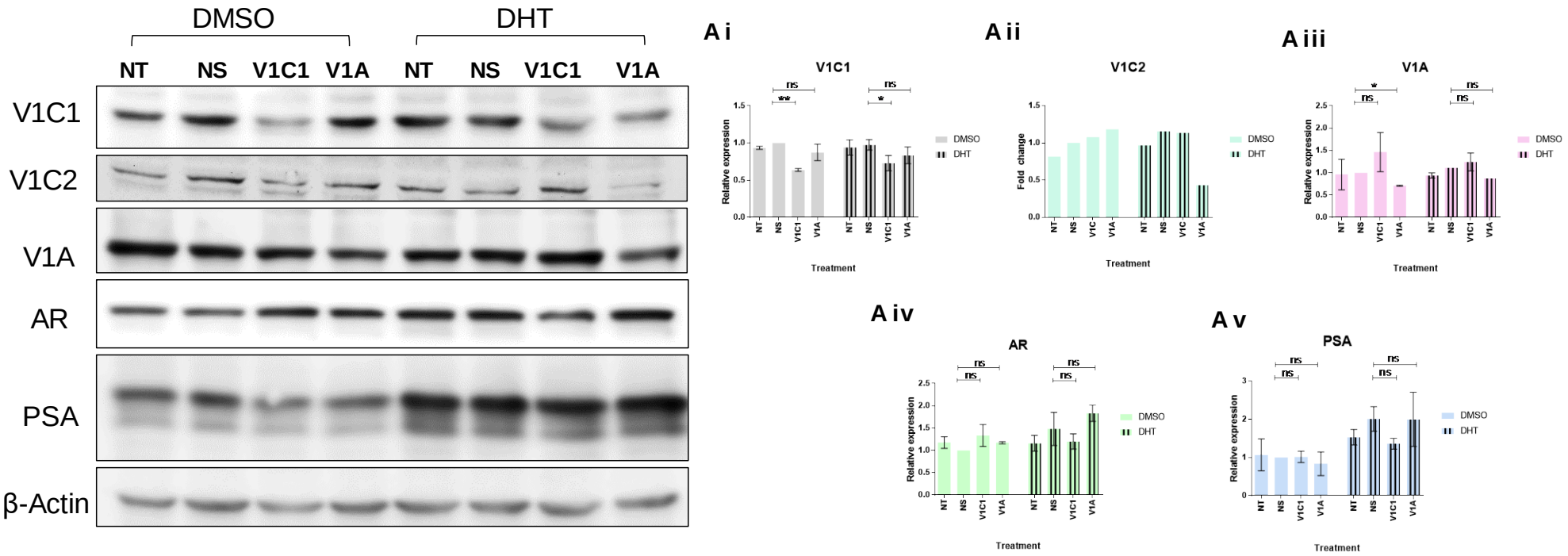

Figure 5-3. Effect of siRNA mediated knockdown of V_1C1 and V_1A with hormonal stimulation on AR signalling in LNCaP cells

LNCaP cells were transfected with either 25 nmol of ATP6V1C1, ATP6V1A or non-specific siRNA for 72 hours. Control non-transfected cells were treated with equivalent concentrations of Dharmafect 1 reagent. After 48 hours post-transfection, cells were treated with either 1 nM DHT or DMSO for a further 24 hours. Protein expression was measured using western blotting and cells were probed against ATP6V1C1, ATP6V1C2, ATP6V1A, AR, PSA and β-Actin. Blot is representative of three individual experiments. Densitometry data of V_1C1 (Ai), V_1C2 (Aii), V_1A (Aiii), AR (Aiv) and PSA (Av) normalised to β-Actin, relative to DMSO NS set to 1. Values were plotted using GraphPad Prism 7 and are displayed as mean values ± standard deviation. Student's T-Tests were used to generate P values and detect the statistical significance of the indicated differences: ns = non-significant, * = p≤ 0.05, ** = p≤ 0.01. NT, non-transfected; NS, non-specific; AR, androgen receptor; PSA, prostate specific antigen; DMSO, solvent control; DHT, dihydrotesosterone.

5.3.3 Effect of siRNA mediated knockdown of V-ATPase V_1C subunits on AR signalling in 22Rv1 cells

The results from 5.3.1 indicated that V_1C1 and V_1A subunit knockdown did not significantly reduce AR signalling in prostate cancer cells. However, as only the hormone sensitive LNCaP cells had been investigated, it was interesting to consider what effect the knockdown of these subunits would have on AR-WT and AR-V7 expression in 22Rv1 cells. Therefore, 22Rv1 cells were cultured in RPMI media and were reverse transfected with either 25 nmol of ATP6V1C1, ATP6V1A or non-specific siRNA for 48 or 72 hours. After siRNA treatment the cells were harvested and western blotting was used to measure the levels of the indicated proteins of interest.

ATP6V1C1 siRNA transfection led to a significant reduction in V_1C1 subunit levels by approximately 50% after 48 hours (Figure 5-4 Ai), which was further reduced after 72 hours to around 60% (Figure 5-4 Bi). This reduction of V_1C1 expression did not affect V_1A levels at either time point. The fact that the ATP6V1C1 transfection led to a greater reduction in V_1C1 expression in the 22Rv1 cells (~60%) than the LNCaP cells (~40%) is reflective of the increased transfection efficiency of 22Rv1 cells compared to LNCaP cells. Transfection with ATP6V1A siRNA significantly reduced V_1A expression by 50% after 48 hours (Figure 5-4 Aiii) and 72 (Figure 5-4 Biii) hours post transfection. The non-specific siRNA did not significantly alter the levels of any of the investigated proteins compared to the non-transfected control. After 48 hours of ATP6V1A siRNA transfection, V_1C2 protein levels were reduced compared to the non-specific siRNA transfected cells (Figure 5-4 Aii). Interestingly, after 48 hours of ATP6V1C1 siRNA transfection, the expression of V_1C2 was increased (Figure 5-4 Aii), which was further increased after 72 hours, and the difference was statistically significant (Figure 5-4 Bii), compared to the respective non-specific siRNA control cells. The fact that V_1C2 levels were increased to a greater extent after a longer period of V_1C1 knockdown suggests a surprising compensatory relationship between the two isoforms.

AR-WT protein levels were slightly reduced with ATP6V1C1 siRNA after 48 hours post-transfection but ATP6V1A siRNA had no effect (Figure 5-4 Aiv). After 72 hours, V_1C1 knockdown reduced AR-WT protein levels by ~50%, which was statistically significant, whereas V_1A knockdown again did not alter AR-WT protein expression (Figure 5-4 Biv). Additionally, neither V_1C1 nor V_1A knockdown led to a reduction of AR-V7 expression after 48 hours post-transfection (Figure 5-4 Av). However, after 72 hours ATP6V1C1 siRNA transfected cells had a reduction of ~40% in AR-V7 protein levels compared to the

non-specific transfected cells (Figure 5-4 Bv). The expression of PSA was not altered with V_1C1 or V_1A knockdown after either 48 (Figure 5-4 Avi) or 72 hours (Figure 5-4 Bvi).

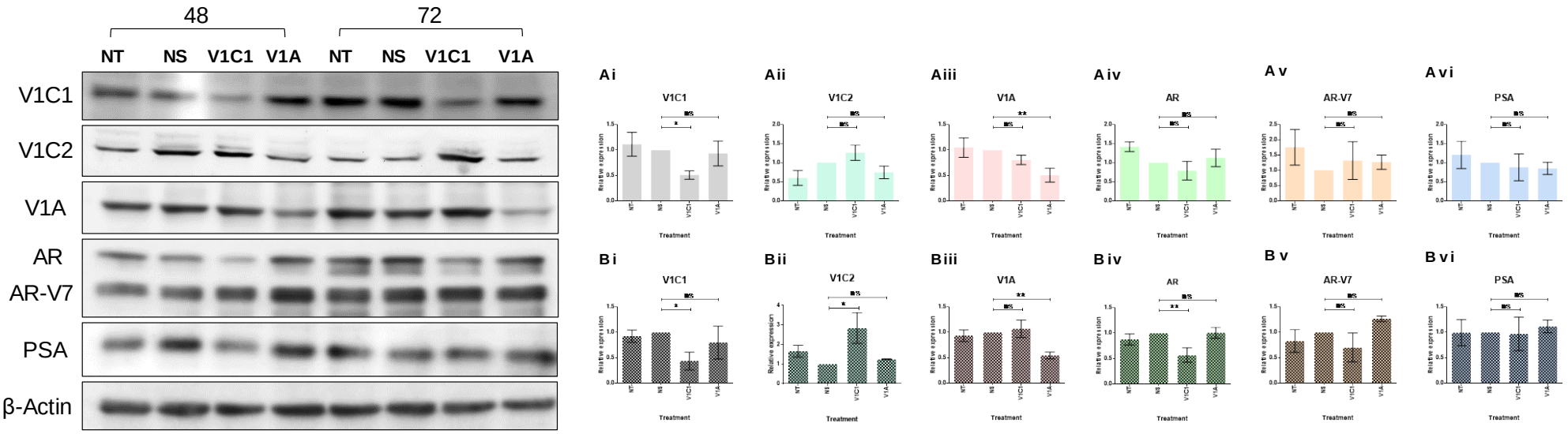

Figure 5-4. Effect of siRNA mediated knockdown of V_1C1 and V_1A on AR signalling in 22Rv1 cells

22Rv1 cells were reverse transfected with either 25 nmol of ATP6V1C1, ATP6V1A or non-specific siRNA for either 48 or 72 hours. Control non-transfected cells were treated with equivalent concentrations of Dharmafect 1 reagent. Protein expression was measured using western blotting and cells were probed against ATP6V1C1, ATP6V1C2, ATP6V1A, AR, PSA and β-Actin. Blot is representative of three individual experiments. Densitometry data of 48 hour (Ai – Avi) and 72 hour (Bi – Bvi) siRNA treated cells normalised to β-Actin, relative to either 48 or 72hr NS set to 1. Values were plotted using GraphPad Prism 7 and are displayed as mean values ± standard deviation. Student's T-Tests were used to generate P values and detect the statistical significance of the indicated differences: ns = non-significant, * = p≤ 0.05, ** = p≤ 0.01. NT, non-transfected; NS, non-specific; AR, androgen receptor; PSA, prostate specific antigen.

The results from Figure 5-4 indicated that V_1C1 subunit knockdown may have a direct effect on AR-WT and AR-V7 expression in 22Rv1 cells. Although 22Rv1 cells only have a minor sensitivity to androgen, it was important to replicate the results in hormone controlled conditions, similar to the results obtained with LNCaP cells (Figure 5-3). To keep the experimental conditions consistent across cell lines, 22Rv1 cells were cultured in RPMI for 24 hours prior to a media change to CSS media. The cells were then transfected with 25 nmol of either ATP6V1C1, ATP6V1A or non-specific siRNA for 72 hours. After 72 hours post-transfection, cells were treated with either 1 nM DHT or equivalent concentrations of DMSO to investigate whether V_1C1 and V_1A expression was androgen dependent in 22Rv1 cells.

ATP6V1C1 siRNA transfected cells had a reduction of ~75% in V_1C1 expression, which was independent of DHT, and was statistically significant (Figure 5-5 Ai). In agreement with previous results, 72 hours post-transfection with ATP6V1A siRNA led to a substantial decrease in V_1C1 expression (Figure 5-5 Ai). Furthermore, ATP6V1A siRNA transfection successfully reduced V_1A protein levels by around 70% independently of androgen (Figure 5-5 Aiii). Again, V_1A protein levels were not affected by ATP6V1C1 transfection (Figure 5-5 Aiii). Knockdown of the V_1A subunit also led to a reduction in V_1C2 protein levels, which was consistent with previous results (Figure 5-4).

The levels of AR-WT protein were reduced by ~60% after transfection with ATP6V1C1 siRNA without the addition of DHT, which was statistically significant (Figure 5-5 Aiv). Transfection with ATP6V1A siRNA did not alter AR-WT protein levels with or without DHT (Figure 5-5 Aiv). AR-WT levels did not have a statistically significant difference with DHT treatment compared to DMSO, which is supportive of the fact that 22Rv1 cells are only weakly sensitive to androgen. AR-V7 expression was lower in ATP6V1C1 transfected cells than the non-specific transfected cells (Figure 5-5 Av). Similarly to the AR-WT, AR-V7 levels were not altered after transfection with ATP6V1A siRNA (Figure 5-5 Av). In this instance PSA protein levels were reduced by 40% after V_1C1 knockdown, which was statistically significant, but PSA levels were not reduced after V_1A knockdown, in both DMSO and DHT treated cells (Figure 5-5 Avi).

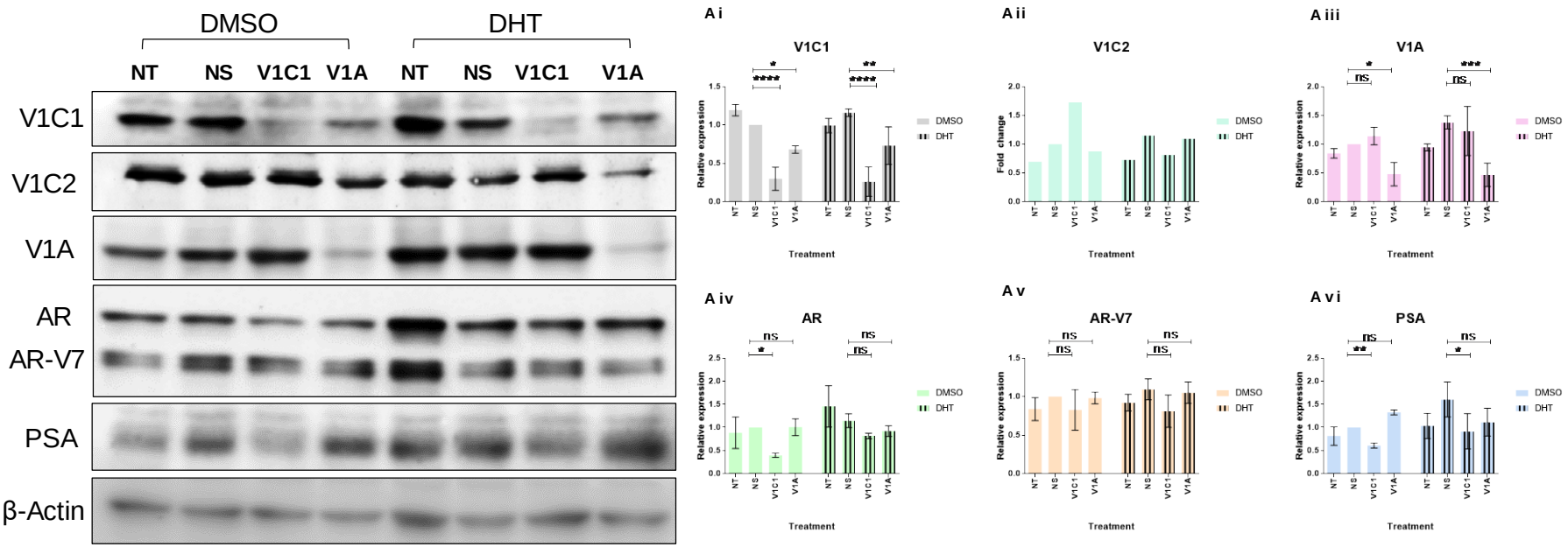

Figure 5-5. Effect of siRNA mediated knockdown of V_1C1 and V_1A with hormonal stimulation on AR signalling in 22Rv1 cells

22Rv1 cells were transfected with either 25 nmol of ATP6V1C1, ATP6V1A or non-specific siRNA for 72 hours. Control non-transfected cells were treated with equivalent concentrations of Dharmafect 1 reagent. After 48 hours post-transfection, cells were treated with either 1 nM DHT or DMSO for a further 24 hours. Protein expression was measured using western blotting and cells were probed against ATP6V1C1, ATP6V1C2, AR, ATP6V1A, PSA and β-Actin. Blot is representative of three individual experiments (except for ATP6V1C2 in which n=1). Densitometry data of V_1C1 (Ai), V_1C2 (Aii), V_1A (Aiii), AR (Aiv), AR-V7 (Av) and PSA (Avi) normalised to β-Actin, relative to DMSO NS set to 1. Values were plotted using GraphPad Prism 7 and are displayed as mean values ± standard deviation. Student's T-Tests were used to generate P values and detect the statistical significance of the indicated differences: ns = non-significant, * = p≤ 0.05, ** = p≤ 0.01, *** = p≤ 0.001. NT, non-transfected; NS, non-specific; AR, androgen receptor; PSA, prostate specific antigen; DMSO, solvent control; DHT, dihydrotesosterone.

5.3.4 Investigating the effect of CRISPR mediated knockdown of V_1C1 on AR signalling in LNCaP cells

The genetic silencing results in LNCaP cells indicated that transient V_1C1 subunit knockdown using siRNA did not reduce AR protein levels or impact upon AR signalling. Conversely, in 22Rv1 cells V_1C1 knockdown reduced AR expression but the knockdown of V_1A did not, suggesting a subunit specific effect. The key question then became whether the lack of a reduction in AR expression in LNCaP cells was due to a lower V_1C1 knockdown efficiency. To answer this it was decided that the CRISPR-Cas9 system would be used to achieve a complete gene knockout, or at least achieve a better subunit knockdown efficiency. Using the CRISPR-Cas9 system LNCaP cells were engineered with a V_1C1 knockdown and the experimental procedures are detailed in 2.10.2. To echo the methodology, one potential clone was confirmed as lacking V_1C1 protein expression by western blotting, which was referred to as a knockdown due to the appearance of three alleles in the sequence analysis (Figure S 8-8).

5.3.4.1 Measuring AR protein expression in V_1C1 knockdown LNCaP cells in response to enzalutamide treatment

To investigate the effect of V_1C1 knockdown on AR signalling, the LNCaP V_1C1 knockdown cells and LNCaP vector only control cells were cultured in CSS media and treated with 1 nM DHT, 10 μM enzalutamide or both for 24 hours. LNCaP vector only control cells were transfected with an empty Cas9 vector without the sgRNA. This was to control for any Cas9 mediated non-specific secondary effects. Additionally, the reason for including enzalutamide is because it was important to assess whether there would be a combinatorial effect of AR antagonism with V_1C1 knockdown on AR signalling.

As shown in Figure 5-6 (Ai), the expression of V_1C1 was not visible in the V_1C1 knockdown cells, indicating a successful CRISPR knockdown. Interestingly, V_1C1 expression was decreased by ~70% in cells cultured in CSS media compared to those cultured in RPMI (lane 2), and was increased in cells treated with DHT by ~40% compared to the CSS only cells (lane 3). Additionally, enzalutamide treatment led to a small reduction in AR expression (lane 4 vs lane 2), which was further reduced in the presence of DHT (lane 5 vs lane 3). This indicates that V_1C1 expression was dependent on AR signalling. The overall expression of the V_1C2 subunit isoform was increased in the knockdown cells compared to the vector only control cells (Figure 5-6 Aii). Also, in the V_1C1 knockdown cells, V_1C2 expression was increased in CSS cultured cells by ~50%

and suggesting an inverse relationship with AR signalling. However, enzalutamide treatment in the presence of DHT led to the greatest reduction in V_1C2 expression in both the vector only and V_1C1 knockdown cells.

AR protein levels in the vector only cells (Figure 5-6 Aiii) increased as expected with DHT treatment (lane 3) and were reduced with enzalutamide and DHT treatment (lane 5). This shows that transfecting the empty CRISPR vector only into the cells did not dysregulate AR signalling. In the V_1C1 knockdown cells, AR expression followed a similar pattern and there were no substantial differences in expression between the vector only and V_1C1 knockdown cells for any of the treatments. This supports what was observed with the ATP6V1C1 siRNA and suggests that the silencing of V_1C1 has no statistically significant effect on AR signalling in hormone sensitive LNCaP cells.

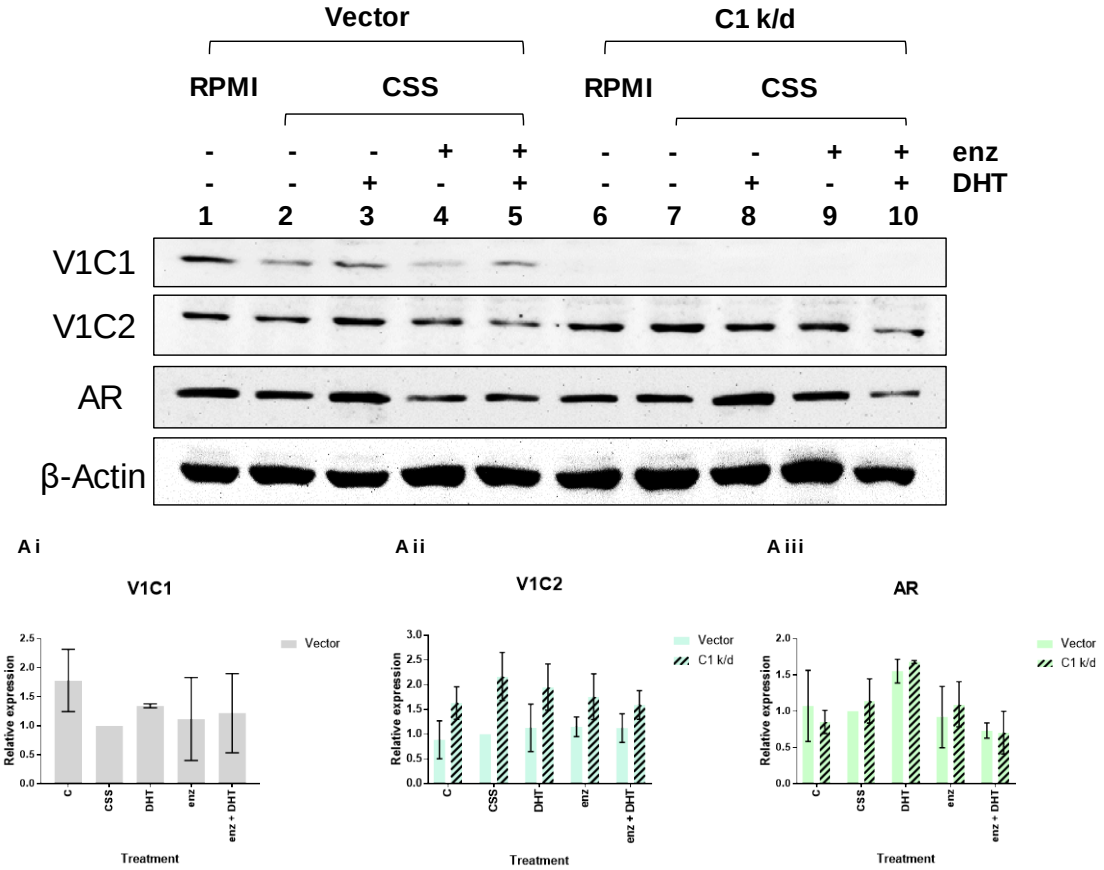

Figure 5-6. AR expression in LNCaP cells with CRISPR mediated V_1C1 knockdown

LNCaP vector only cells and V_1C1 CRISPR knockdown cells were treated for 24 hours with either 1 nM DHT, 10 μM enz or both. Control LNCaP samples were also included, which were maintained in RPMI only. Protein expression was measured using western blotting and cells were probed against ATP6V1C1, ATP6V1C2, AR and β-Actin. Blot is representative of two individual experiments. Densitometry data of V_1C1 (Ai), V_1C2 (Aii), and AR (Aiii) normalised to β-Actin, relative to Vector CSS set to 1. Values were plotted using GraphPad Prism 7 and are displayed as mean values ± standard deviation. k/o, knockout; CSS, charcoal stripped serum; DHT, dihydrotestosterone; enz, enzalutamide; PSA, prostate specific antigen; AR, androgen receptor.

5.3.4.2 Using the MTS assay to measure cell toxicity in response to siRNA treatment in LNCaP V_1C1 k/d cells

One of the most surprising findings was that V_1C2 expression was increased when there was a reduction of V_1C1 levels, which was apparent with both siRNA (Figure 5-2) and CRISPR mediated knockdown (Figure 5-6) . This would indicate that perhaps V_1C2 is compensating for the loss of V_1C1 in the V-ATPase complex and therefore countered AR signalling dysregulation. It was hypothesized that the V-ATPase complex could withstand a reduction in one isoform and still function, but silencing both subunit isoforms may cause significant cell death due to a functional loss of enzyme activity. The MTS assay was used to measure the potential toxicity of siRNA transfection in the LNCaP V_1C1 knockdown and vector only control cells. The cells were reverse transfected with 25 nmol ATP6V1C2, ATP6V1A and non-specific siRNA for 48 hours.

There was no obvious toxicity as a result of ATP6V1C2, ATP6V1A or non-specific siRNA transfection in the LNCaP vector only cells after 48 hours (Figure 5-7). On the other hand, the V_1C1 knockdown cells had a reduction of MTS signal when transfected with the non-specific siRNA compared to the non-transfected control. This suggests that the cells were already partially stressed and that the transfection resulted in substantial cell death. There was no statistically significant differences in toxicity observed in the ATP6V1A siRNA transfected cells compared to the non-specific siRNA cells, indicating generalised transfection induced cell death as opposed to a V-ATPase subunit specific effect. Interestingly, there was a small drop in MTS signal in the ATP6V1C2 transfected cells compared to the non-specific cells, which was statistically significant (Figure 5-7). The fact that there was a significant drop in MTS signal with ATP6V1C2 but not ATP6V1A siRNA suggests that V_1C2 knockdown induces a subunit specific increase in toxicity. It should also be noted that this was repeated at 72 hours but the toxicity was too high for the V_1C1 knockdown cells and there was substantial cell death for all siRNA transfected cells.

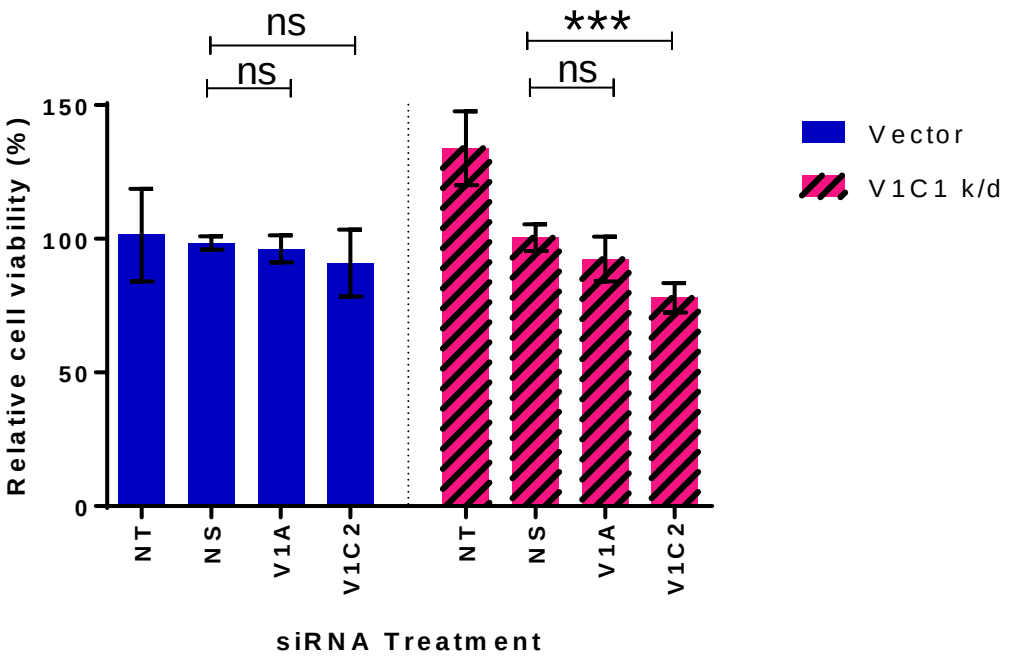

Figure 5-7. Using the MTS assay to determine LNCaP V_1C1 k/d cell line toxicity in response to siRNA treatment after 48 hours

LNCaP vector only and V_1C1 CRISPR knockdown cells were reverse transfected with either 25 nmol of ATP6V1C2, ATP6V1A or non-specific siRNA for 48 hours. Control non-transfected cells were treated with equivalent concentrations of Dharmafect 1 reagent. Data is presented relative to the respective non-specific treated cells set to 100% viability. Values were plotted using GraphPad Prism 7 and are displayed as mean values ± standard deviation. Two-way ANOVA with Tukey's multiple comparison post-hoc test was used to generate P values and detect the statistical significance of the indicated differences: ns = non-significant, *** = p≤ 0.001. Data shown represents three independent biological replicates completed in triplicate. k/d, knockdown; NT, non-transfected; NS, non-specific.

5.3.4.3 Measuring AR and PSA protein expression in LNCaP V_1C1 k/d cells in response to ATP6V1C2 siRNA mediated knockdown

Despite the toxicity induced by ATP6V1C2 siRNA mediated knockdown in LNCaP V_1C1 knockdown cells, it was still important to investigate whether the dual silencing of the V_1C subunit isoforms reduced AR expression. Similarly to Figure 5-7, LNCaP V_1C1 knockdown and vector only control cells were cultured in RPMI media and reverse transfected with either 25 nmol ATP6V1C2, ATP6V1A or non-specific siRNA for 48 hours.

Firstly, in the vector only control cells the reduction of AR protein levels after V_1A knockdown agrees with previous results in non-modified LNCaP cells (Figure 5-2). V_1C2 protein levels were only increased by a small amount overall in the V_1C1 knockdown cells compared to the vector only control cells, which was not statistically significant. Furthermore, the expression of V_1C2 after transfection with ATP6V1C2 siRNA was comparable to the non-specific siRNA, suggesting the knockdown had not been completely successful (Figure 5-8 Aii). The likely reason for this is because LNCaP cells have a poor transfection efficiency and as the knockdown cells were already stressed, the transfection conditions could not be extended without inducing significant cell death. Although the V_1C2 subunit knockdown was not effective, the ATP6V1A transfected cells significantly reduced V1A expression in both V_1C1 knockdown cells and vector only control cells (Figure 5-8 Aiii). There was also no visible difference in V_1A protein levels between the vector only and V_1C1 knockdown cells.

The expression of AR was unaffected in ATP6V1C2, ATP6V1A or non-specific siRNA transfected V_1C1 knockdown cells compared to vector only control cells, which was not statistically significant (Figure 5-8 Aiv). Furthermore, there was no statistically significant difference in PSA levels between the siRNA treatments. There were also no substantial differences in PSA expression between the V_1C1 knockdown cells and the vector only control cells (Figure 5-8 Av).

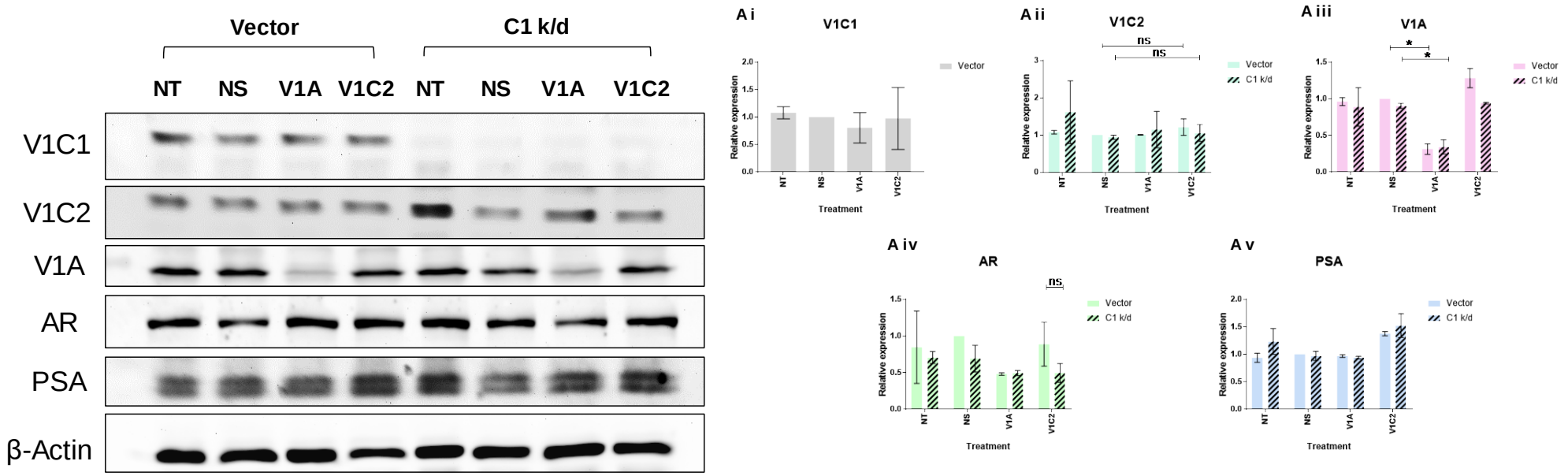

Figure 5-8. Effect of combined knockdown of V_1C1 and V_1C2 on AR and PSA expression in LNCaP V_1C1 k/d cells

Vector only and V_1C1 CRISPR knockdown LNCaP cells were reverse transfected with either 25 nmol of ATP6V1C2, ATP6V1A or non-specific siRNA for 48 hours. Control non-transfected cells were treated with equivalent concentrations of Dharmafect 1 reagent. Protein expression was measured using western blotting and cells were probed against ATP6V1C1, ATP6V1C2, ATP6V1A, AR, PSA and β-Actin. Blot is representative of three individual experiments. Densitometry data of V_1C1 (Ai), V_1C2 (Aii), V_1A (Aiii), AR (Aiv) and PSA (Av) normalised to β-Actin, relative to Vector NS set to 1. Values were plotted using GraphPad Prism 7 and are displayed as mean values ± standard deviation. Student's T-Tests were used to generate P values and detect the statistical significance of the indicated differences: ns = non-significant, * = p≤ 0.05. k/d, knockdown; NT, non-transfected; NS, non-specific; AR, androgen receptor; PSA, prostate specific antigen.

5.3.5 Investigating the effect of CRISPR mediated knockdown of V_1C1 on AR signalling in 22Rv1 cells

The LNCaP V_1C1 CRISPR mediated knockdown cells appeared to have similar protein levels of AR and PSA compared to LNCaP vector only controls, suggesting the V_1C1 subunit was not critical for AR expression (Figure 5-6 and Figure 5-8). However, the siRNA mediated knockdown of V_1C1 in 22Rv1 cells did reduce AR-WT and AR-V7 expression compared to non-specific siRNA controls (Figure 5-4). Therefore, to investigate this further the CRISPR-Cas9 system was used as described in 2.10.2, but this time two individual 22Rv1 clones emerged with complete V_1C1 protein knockout, which were referred to as V1C1-14 and V1C1-18. These clones were verified using western blotting and Sanger sequencing. As with the LNCaP CRISPR clone, throughout all investigations the 22Rv1 clones were compared to 22Rv1 empty Cas9 vector control cells, which did not include the CRISPR sgRNA sequence.

5.3.5.1 Effect of V_1C1 knockout on downstream AR targets at the transcript level

Before investigating the protein levels of AR-WT and AR-V7 in the 22Rv1 V_1C1 clones, I decided to measure the transcript levels of AR downstream signalling markers, *PSA* and *TMPRSS2*, in comparison to the 22Rv1 vector control cells. To do this, V1C1-14, V1C1-18 and 22Rv1 vector control cells were cultured in CSS media and treated with either DMSO, 1 nM DHT, 10 μM enzalutamide or both DHT and enzalutamide for 24 hours. After 24 hours, cells were harvested and transcript levels were analysed using RT-qPCR. As the siRNA results suggested that V_1C2 levels might be upregulated in response to V_1C1 knockout (Figure 5-4), it was important to compare *ATP6V1C2* transcript levels to the vector only control cells. The data was normalised to the internal housekeeping gene *GAPDH* and was analysed relative to the ΔCt values for DMSO treated vector only control cells cultured in CSS media. To make the results comparable between the two clones, both were analysed relative to the same vector only control ΔCt values.

5.3.5.1.1 22Rv1 V1C1 V1C1-14 results

Firstly, *PSA* expression in vector only 22Rv1 control cells did not have a statistically significant difference in CSS cultured cells compared to the RPMI cultured cells (Figure 5-9 A). Furthermore, DHT treatment did not increase *PSA* expression compared to the CSS control cells, and enzalutamide treated cells did not have lower *PSA* levels. This

supports the well characterised limited sensitivity of 22Rv1 cells to androgen and enzalutamide, indicating that the vector only control cells do not have different AR signalling characteristics to non-modified 22Rv1 cells. Interestingly, in the V1C1-14 cells *PSA* expression was increased in the DHT treated cells compared to the CSS cultured cells, which was statistically significant compared to DHT treated vector only cells. Additionally, enzalutamide treatment in the presence of DHT reduced *PSA* expression in the V1C1-14 cells, which was statistically significant. These surprising results suggested that the V_1C1 knockout cells were more sensitive to androgen and AR antagonism that the vector only control cells.

TMPRSS2 expression in the vector only control cells (Figure 5-9 B) was similar to that of *PSA* and shows that the expression of AR downstream targets were not significantly altered in response to androgen and AR antagonism. Again, the addition of DHT increased *TMPRSS2* expression in the V_1C1 knockout cells compared to the CSS cells, and enzalutamide with DHT treated cells had a lower *TMPRSS2* expression than DHT only treated cells, which was statistically significant. The expression of *TMPRSS2* was not significantly different for any of the treatments in the V1C1-14 cells compared to the vector only controls cells except after enzalutamide and DHT treatment.

In the vector only control cells *ATP6V1C1* expression did not appear to be altered in response to growth in CSS media or DHT stimulation (Figure 5-9 C). Despite the V_1C1 protein being knocked-out, there were still detectable levels of *ATP6V1C1* transcript, although the Ct values were higher than in the vector only control cells. The sgRNA:Cas9 complex was targeted at exon 5, whereas, the RT-qPCR probe binding site was located on the exon 11-12 boundary, which is downstream of the sgRNA target site (Figure S 8-14).

The expression of *ATP6V1C2* was increased in the CSS cultured cells compared to those cultured in RPMI (Figure 5-9 D). Furthermore, the addition of DHT resulted in a decrease in *ATP6V1C2* expression compared to the cells cultured in CSS media. Enzalutamide treated cells had increased *ATP6V1C2* expression compared to the CSS cells, and enzalutamide with DHT treatment increased *ATP6V1C2* expression compared to the DHT only treated cells. This indicates that there is an inverse relationship of *ATP6V1C2* expression and androgen in 22Rv1 cells, which is supportive of what was observed in LNCaP cells (Figure 5-6). The expression of *ATP6V1C2* was increased for all treatments in V_1C1 knockdown cells compared to the vector only cells, which was statistically significant. This pattern of expression was similar to that of the vector only control cells as CSS cultured cells had higher *ATP6V1C2* levels than the DHT treated cells. Enzalutamide

with DHT treatment also significantly increased *ATP6V1C2* expression compared to DHT only treated V1C1-14 cells.

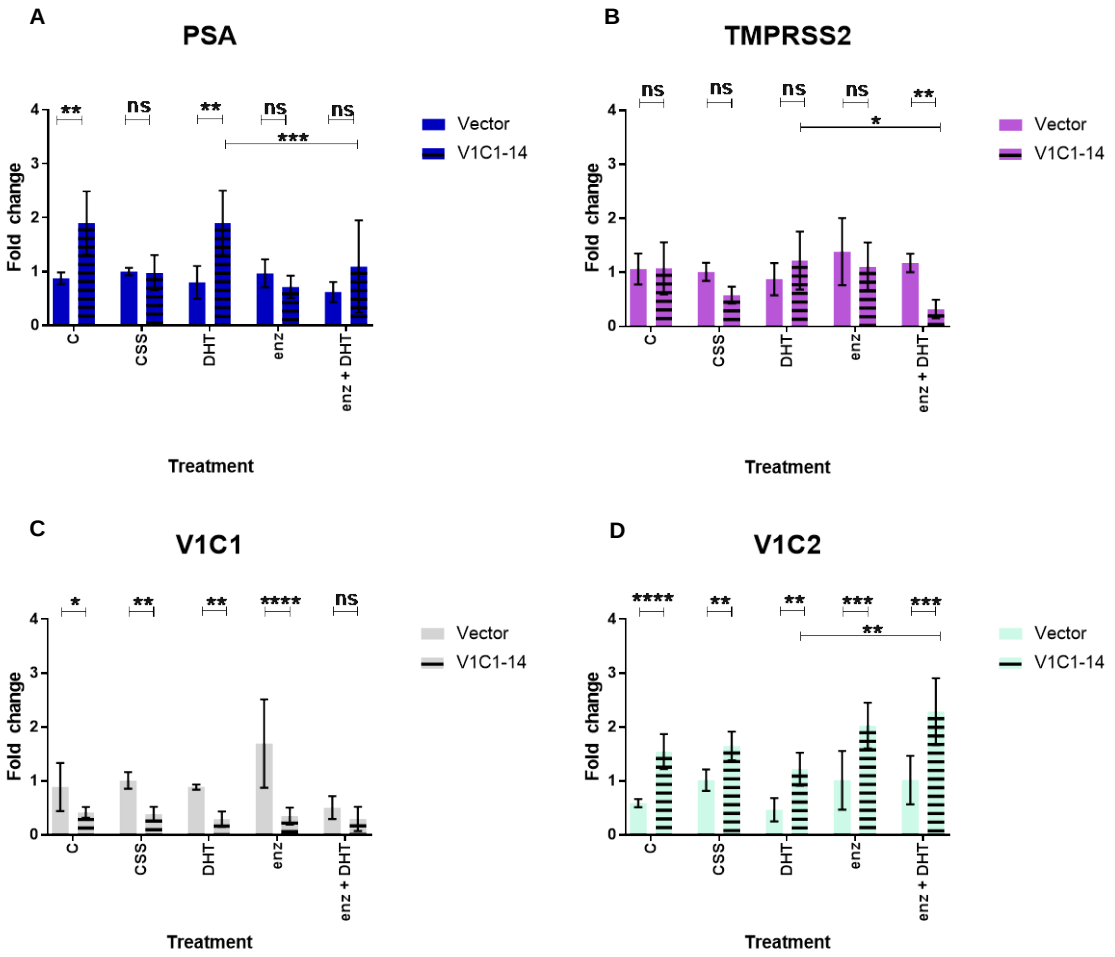

Figure 5-9. AR signalling expression in 22Rv1 V$_1$C1 CRISPR knockout cells (V1C1-14) following treatment with 1 nM DHT and/or 10 μM enzalutamide

22Rv1 vector only and V$_1$C1 CRISPR knockout (V1C1-14) 22Rv1 cells were treated for 24 hours with either 1 nM DHT, 10 μM enz or both. RT-qPCR analysis was undertaken to assess levels of (A) *PSA*, (B) *TMPRSS2*, (C) *ATP6V1C1*, (D) *ATP6V1C2* and were normalised to *GAPDH*, relative to Vector Control CSS set to 1. Values were then plotted using GraphPad Prism 7 and are displayed as mean values ± standard deviation. Two-way ANOVA with Tukey's multiple comparison post-hoc test was used to generate P values and detect the statistical significance of the indicated differences: ns = non-significant, *= p≤ 0.05, **= p≤ 0.01, *** = p≤ 0.001, **** = p≤ 0.0001. Data shown represents three independent biological replicates completed in triplicate. C, control; CSS, charcoal stripped serum; DHT, dihydrotestosterone; enz, enzalutamide; PSA, prostate specific antigen.

5.3.5.1.2 22Rv1 V_1C1 V1C1-18 results

The reason for including a second V_1C1 knockout clone was to eliminate the possibility of a non-specific mutational effect induced by CRISPR. It was important to validate that the results to increase reliability and reproducibility.

As with V1C1-14, *PSA* expression was significantly increased in the V1C1-18 V_1C1 knockout 22Rv1 cells compared to the vector only cells (Figure 5-10 A). Again, knockout V1C1-18 cells cultured in CSS had a lower expression of *PSA* than those in RPMI, and treatment with DHT increased *PSA* levels compared to the CSS cultured cells. *PSA* expression was significantly reduced when enzalutamide was combined with DHT compared to the DHT only treated cells. This increased sensitivity of *PSA* expression to androgen mirrors what was found in V1C1-14 cells (Figure 5-9 A).

The levels of *TMPRSS2* followed a similar pattern to *PSA* in the V1C1-18 cells as they were decreased in CSS media, compared to the RPMI cultured cells, and increased with DHT treatment (Figure 5-10 B). Similarly, enzalutamide with DHT treatment significantly reduced *TMPRSS2* expression compared to DHT alone treated cells. Compared to the vector control cells, the increase in expression of *TMPRSS2* was only statistically significant in the RPMI cultured V_1C1 knockout cells, which is supportive of the increase in hormone sensitivity observed in the V_1C1 knockout clones.

ATP6V1C1 expression did not significantly differ in the knockout cells compared to the vector only control cells (Figure 5-10 C). It is again very interesting that despite a CRISPR induced knockout, the levels of *ATP6V1C1* transcript were comparable to control cells. The only statistically significant difference between the vector control cells and the V_1C1 knockout cells was after enzalutamide treatment, but this looks to be due to an unexpected increase in expression in the control cells rather than a significant decrease in the knockout cells. Furthermore, the different treatments did not alter *ATP6V1C1* expression in the knockout cells.

Similarly to the V1C1-14 knockout cells, the V1C1-18 cells had a statistically significant increase in *ATP6V1C2* expression compared to the vector only control cells (Figure 5-10 D). Additionally, there appeared to be an inverse relationship of *ATP6V1C2* expression with hormone. The *ATP6V1C2* levels were increased in CSS cells, compared to RPMI cultured cells, and levels were further decreased with DHT treatment. Enzalutamide with DHT treatment again significantly increased *ATP6V1C2* levels compared to DHT alone treatment, supportive of what was found in the V1C1-14 knockout cells (Figure 5-9 D).

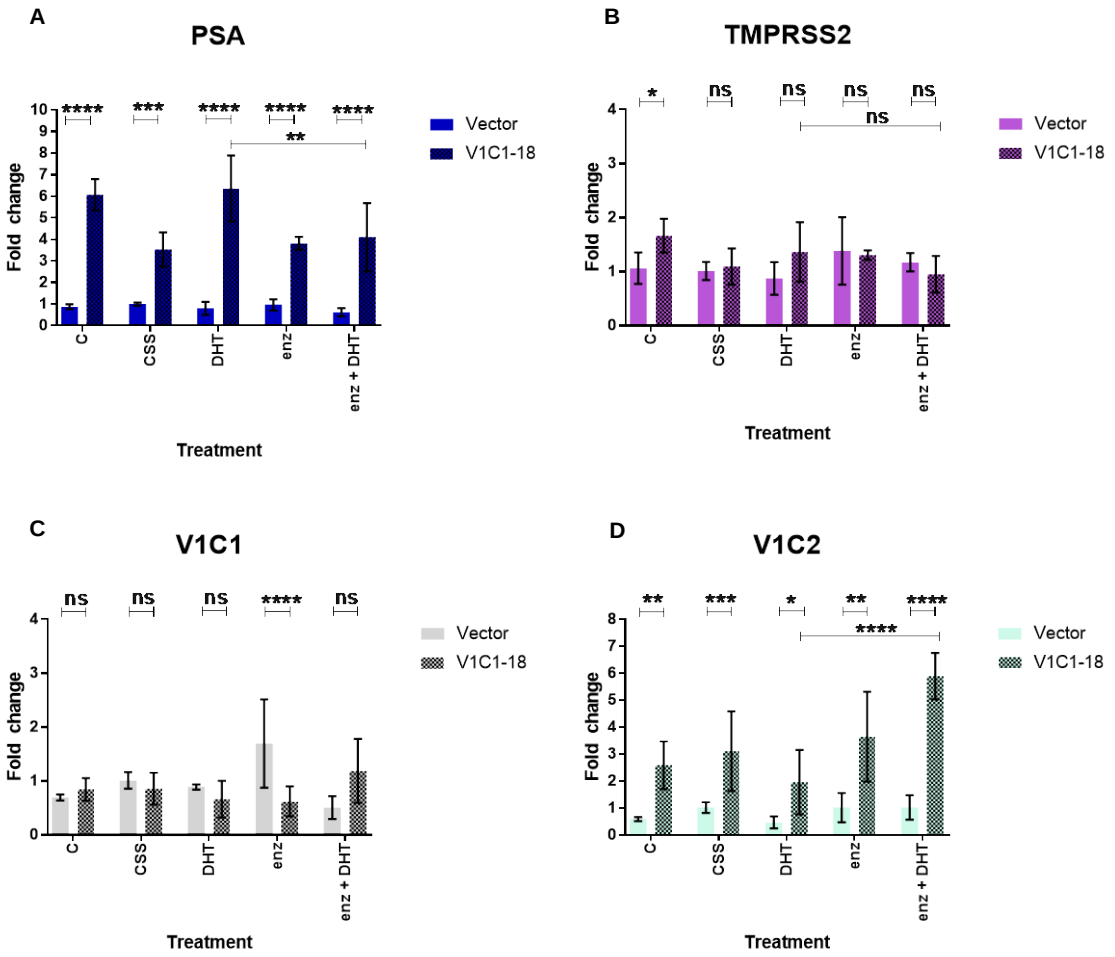

Figure 5-10. AR signalling expression in 22Rv1 V_1C1 CRISPR knockout cells (V1C1-18) following treatment with 1 nM DHT and/or 10 μM enzalutamide

22Rv1 vector only and V_1C1 CRISPR knockout (V1C1-18) 22Rv1 cells were treated for 24 hours with either 1 nM DHT, 10 μM enz or both. RT-qPCR analysis was undertaken to assess levels of (A) *PSA*, (B) *TMPRSS2*, (C) *ATP6V1C1*, (D) *ATP6V1C2* and were normalised to *GAPDH*, relative to Vector Control CSS set to 1. Values were then plotted using GraphPad Prism 7 and are displayed as mean values ± standard deviation. Two-way ANOVA with Tukey's multiple comparison post-hoc test was used to generate P values and detect the statistical significance of the indicated differences: ns = non-significant, *= p≤ 0.05, **= p≤ 0.01, *** = p≤ 0.001, **** = p≤ 0.0001. Data shown represents three independent biological replicates completed in triplicate. C, control; CSS, charcoal stripped serum; DHT, dihydrotestosterone; enz, enzalutamide; PSA, prostate specific antigen.

5.3.5.2 Effect of V_1C1 knockout on AR-WT and AR-V7 protein expression

Building on the results from 5.3.5.1, the next step was to investigate the effect of the V_1C1 knockout on AR-WT and AR-V7 protein expression in 22Rv1 cells. 22Rv1 vector control cells, V1C1-14 and V1C1-18 V_1C1 knockout cells were cultured in CSS media for 24 hours. The cells were then treated with either DMSO, 1 nM DHT, 10 μM enzalutamide or both DHT and enzalutamide for 24 hours. After treatment, cells were harvested and protein levels were measured using western blotting.

In the vector control cells, V_1C1 protein levels were similar in the CSS cultured cells compared to the RPMI cultured cells (Figure 5-11 Ai). There was a slight increase with DHT treatment compared to CSS only cells, which was reduced with the addition of enzalutamide. As shown in the western blot images, V_1C1 protein expression was not detectable in the V1C1-14 (Figure 5-11) or V1C1-18 knockout cells (Figure 5-12), suggesting a complete protein knockout in both clones.

Levels of V_1C2 were higher in the CSS cultured vector only control cells compared to the RPMI cells (Figure 5-11 Aii), which is supportive of the transcript data (Figure 5-9 B). DHT treatment slightly lowered V_1C2 expression compared to the CSS cells. The V1C1-14 knockout cells had increased levels of V_1C2 compared to the vector only control. Again, there appeared to be an inverse relationship with hormone in the knockout cells, as CSS cultured cells had substantially higher levels of V_1C2 than RPMI, which was lowered with the addition of DHT. Interestingly, the expression of V_1C2 protein was lowest with enzalutamide and DHT treatment compared to the rest of the treatments, which is the opposite of what was observed at the transcript level (Figure 5-9 B). Furthermore, this pattern of V_1C2 expression was observed in the V1C1-18 knockout cells, with the only key difference being that the RPMI treated cells had higher V_1C2 expression than the vector control cells (Figure 5-12 Aii).

The expression of AR-WT in the vector only cells was increased by with DHT treatment, and enzalutamide did not reduce AR-WT expression compared to the CSS control cells (Figure 5-11 Aiii). In the V1C1-14 knockout cells, AR-WT had a 2-fold increase in expression in RPMI cultured cells compared to the vector only control cells. The V1C1-14 cells cultured in CSS media had a similar AR-WT expression to the vector control cells, which was increased after DHT treatment. AR-WT expression was also greater in the enzalutamide with DHT treated knockout cells compared to the vector only. Furthermore, the levels of AR-WT in the V1C1-18 cells (Figure 5-12 Aiii) were almost identical to the V1C1-14 cells and the same pattern of expression was observed.

AR-V7 levels were higher for all treatments in the V1C1-14 than the vector control cells (Figure 5-11 Aiv). There was a slight increase in expression of AR-V7 in the V1C1-14 cells after treatment with DHT compared to the vector control cells. Surprisingly, except for the RPMI cultured cells, the levels of AR-V7 were lower for all treatments in the V1C1-18 cells than in the vector only control cells (Figure 5-12 Aiv). Despite the lower levels of AR-V7, the response to the treatments was the same in both knockout clones i.e. higher levels in DHT treated cells compared to the CSS cells, and lower levels after treatment with enzalutamide and DHT compared to DHT only treated cells.

Taken together, these results suggest that AR-WT and AR-V7 expression was increased in 22Rv1 V_1C1 knockout cells compared to vector only control cells. Additionally, V_1C2 expression was increased in cells that do not express V_1C1, and this expression appears to be inversely correlated with hormone.

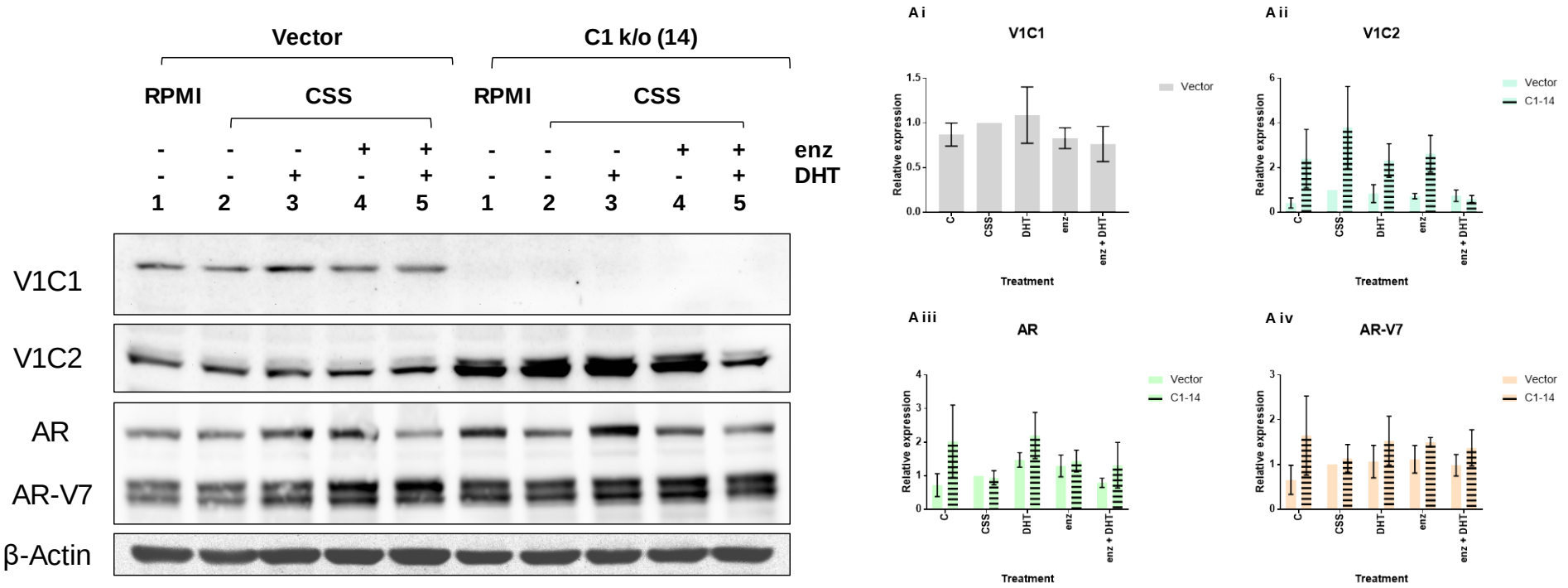

Figure 5-11. AR expression in 22Rv1 cells with CRISPR mediated V_1C1 knockout (V1C1-14)

22Rv1 vector only control cells and V_1C1 CRISPR knockout cells (V1C1-14) were treated for 24 hours with either 1 nM DHT, 10 μM enz or both. Additional LNCaP samples were also included, which were maintained in RPMI only. Protein expression was measured using western blotting and cells were probed against ATP6V1C1, ATP6V1C2, AR and β-Actin. Blot is representative of two individual experiments. Densitometry data of V_1C1 (Ai), V_1C2 (Aii), AR (Aiii) and AR-V7 (Aiv) normalised to β-Actin, relative to Vector CSS set to 1. Values were plotted using GraphPad Prism 7 and are displayed as mean values ± standard deviation. k/o, knockout; CSS, charcoal stripped serum; DHT, dihydrotestosterone; enz, enzalutamide; PSA, prostate specific antigen; AR, androgen receptor.

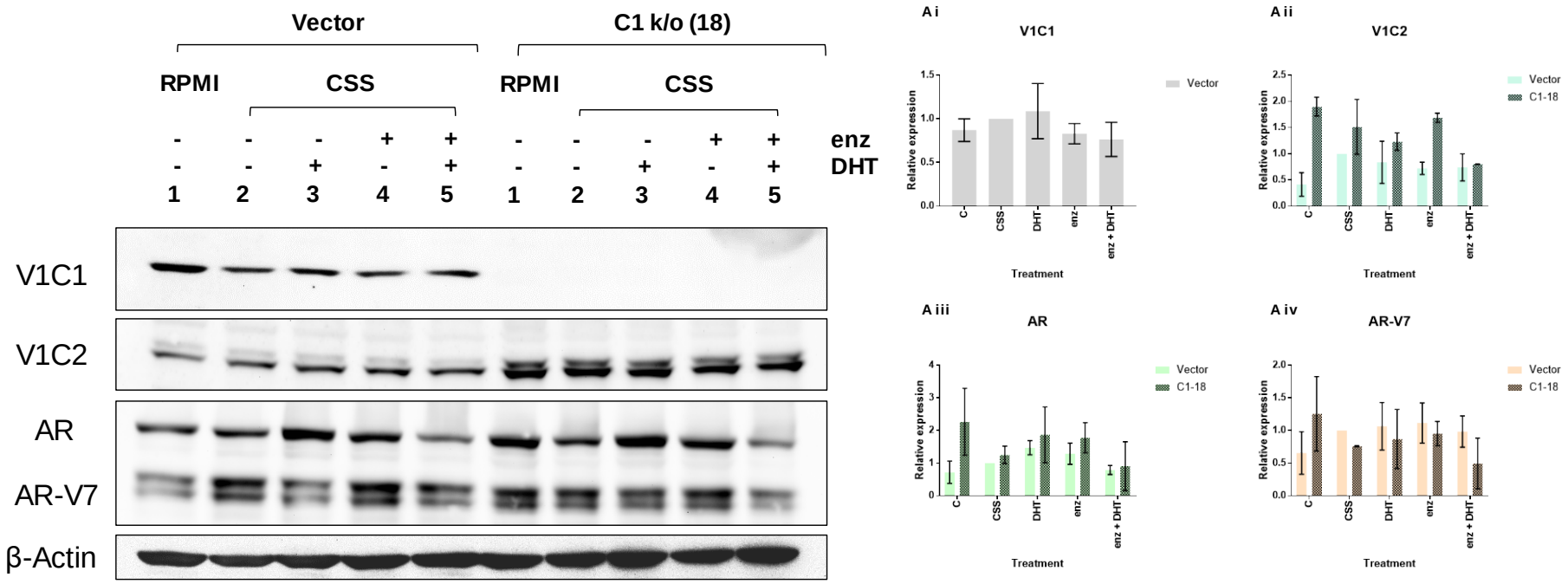

Figure 5-12. AR expression in 22Rv1 cells with CRISPR mediated V_1C1 knockout (V1C1-18)

22Rv1 vector only control cells and V_1C1 CRISPR knockout cells (V1C1-18) were treated for 24 hours with either 1 nM DHT, 10 μM enz or both. Additional LNCaP samples were also included, which were maintained in RPMI only. Protein expression was measured using western blotting and cells were probed against ATP6V1C1, ATP6V1C2, AR and β-Actin. Blot is representative of two individual experiments. Densitometry data of V_1C1 (Ai), V_1C2 (Aii), AR (Aiii) and AR-V7 (Aiv) normalised to β-Actin, relative to Vector CSS set to 1. Values were plotted using GraphPad Prism 7 and are displayed as mean values ± standard deviation. k/o, knockout; CSS, charcoal stripped serum; DHT, dihydrotestosterone; enz, enzalutamide; PSA, prostate specific antigen; AR, androgen receptor.

5.3.6 Determining the effect of V_1C1 knockout on AR signalling in 22Rv1 cells with siRNA mediated V_1C2 knockdown

5.3.6.1 Using the MTS assay to measure cell toxicity in response to siRNA treatment in 22Rv1 V_1C1 k/o cells

Given that the expression of V_1C2 was increased at the transcript and protein level of both V_1C1 22Rv1 knockout clones compared to the vector only control cells, it was important to investigate whether silencing V_1C2 would affect AR signalling in 22Rv1 V_1C1 knockout cells. As with the LNCaP V_1C1 knockdown cells (Figure 5-7), the MTS assay was first used to measure potential cell toxicity in response to siRNA treatment. V1C1-14, V1C1-18 and vector only control 22Rv1 cells were reverse transfected with either 25 nmol ATP6V1C2, ATP6V1A or non-specific siRNA for 48 or 72 hours. Non-transfected cells were included to account for any generalised siRNA induced toxicity.

There was no statistically significant toxicity measured in the vector control cells after transfection with ATP6V1C2 or ATP6V1A after 48 (Figure 5-13 Ai and Bi) or 72 hours (Figure 5-13 Aii and Bii). Additionally, transfection with non-specific siRNA did not induce substantial cell toxicity compared to the non-transfected vector only control cells. In the V1C1-14 cells, there was no significant toxicity recorded after transfection with ATP6V1A siRNA for 48 (Figure 5-13 Ai) and 72 hours (Figure 5-13 Aii) compared to the non-specific control. However, there was a reduction in the MTS signal in the non-specific siRNA transfected cells, compared to the non-transfected V1C1-14 cells at both time points. This suggests that there is a generalised toxic effect of siRNA treatment on the knockout cells. Furthermore, the lower MTS signal recorded for the ATP6V1C2 transfected V1C1-14 cells was statistically significant compared to the non-transfected cells after 48 hours (Figure 5-13 Ai), which was further reduced after 72 hours (Figure 5-13 Aii). This indicates that there was a degree of subunit specific induced toxicity because compared to the non-specific siRNA, the ATP6V1C2 transfection increased cellular toxicity, but the ATP6V1A transfection did not.

The V1C1-18 cells appeared to be less sensitive to siRNA induced toxicity than the V1C1-14 cells. After 48 hours of transfection, neither the ATP6V1A nor ATP6V1C2 siRNA significantly increased toxicity compared to the non-specific siRNA (Figure 5-13 Bi). However, there was an increase in toxicity in the non-specific siRNA transfected cells compared to the non-transfected cells. Furthermore, after 72 hours there was a statistically significant reduction in MTS signal for ATP6V1C2 transfected cells but not

ATP6V1A (Figure 5-13 Bii). This supports what was found in the V1C1-14 cells and suggests that silencing both V_1C isoforms was toxic to the 22Rv1 cells.

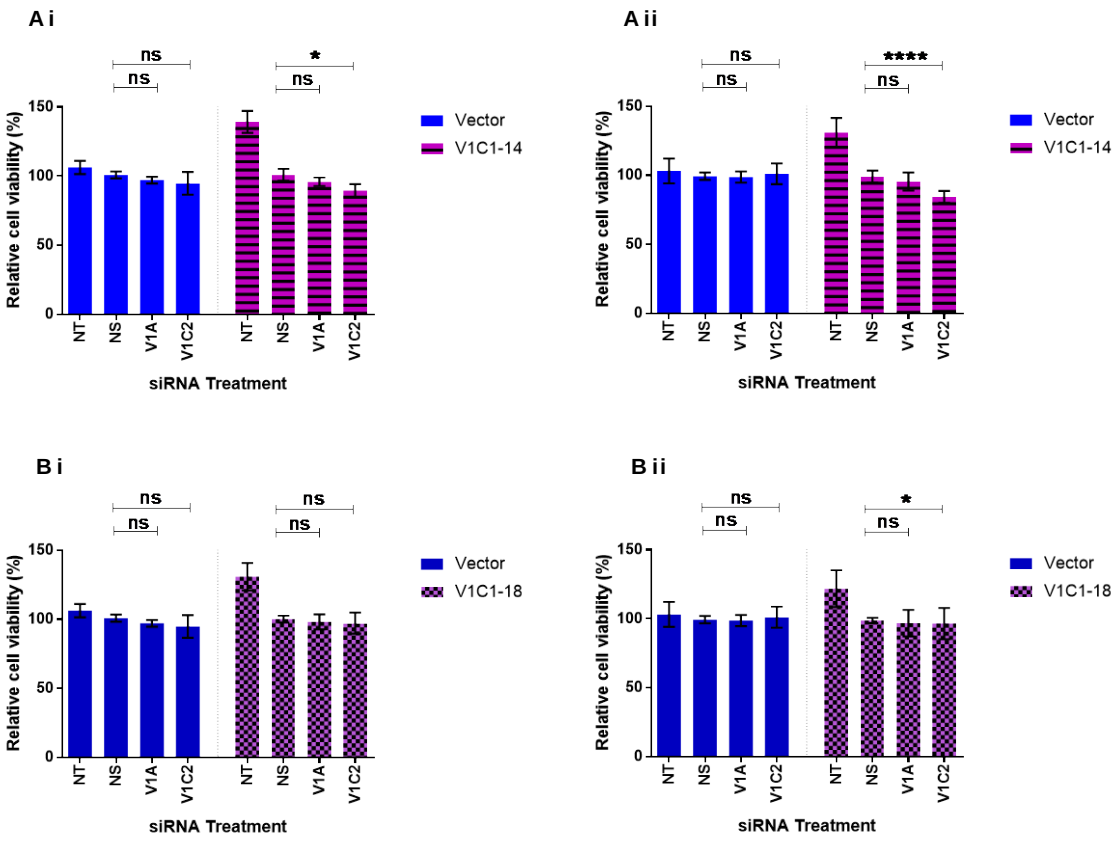

Figure 5-13. Using the MTS assay to determine 22Rv1 V_1C1 k/o cell line toxicity in response to siRNA treatment after 48 and 72 hours

22Rv1 vector only and V1C1-14 (A) and V1C1-18 (B) V_1C1 CRISPR knockout cells were reverse transfected with either 25 nmol of ATP6V1C2, ATP6V1A or non-specific siRNA for 48 (i) or 72 (ii) hours. Control non-transfected cells were treated with equivalent concentrations of Dharmafect 1 reagent. Data is presented relative to the respective non-specific treated cells set to 100% viability. Values were plotted using GraphPad Prism 7 and are displayed as mean values ± standard deviation. Two-way ANOVA with Tukey's multiple comparison post-hoc test was used to generate P values and detect the statistical significance of the indicated differences: ns = non-significant, * = p≤ 0.05, **** = p≤ 0.0001. Data shown represents three independent biological replicates completed in triplicate. k/o, knockout; NT, non-transfected; NS, non-specific.

5.3.6.2 Measuring AR-WT and AR-V7 protein expression in 22Rv1 V_1C1 k/o cells in response to ATP6V1C2 siRNA mediated knockdown

The results from the MTS assay indicated that transfection with ATP6V1C2, but not ATP6V1A, resulted in significant toxicity in 22Rv1 V_1C1 knockdown cells after 72 hours (Figure 5-13). Despite the increase in toxicity, 72 hours of siRNA treatment results in a greater subunit knockdown than 48 hours in 22Rv1 cells (Figure 5-4). Therefore, as the 22Rv1 V_1C1 knockout clones were able to tolerate a longer siRNA transfection time than LNCaP cells, both 48 and 72 hour transfection time points were investigated.

V1C1-14, V1C1-18 and 22Rv1 vector only control cells were reverse transfected with either 25 nmol ATP6V1C2, ATP6V1A or non-specific siRNA for 48 or 72 hours. As with the MTS assay, non-transfected cells were included to account for any generalised siRNA induced toxicity. The cells were then harvested and protein levels were measured using western blotting.

5.3.6.2.1 Results for 22Rv1 V1C1-14

Firstly, in the vector only cells protein levels of V_1C1 were largely unaltered with ATP6V1C2 and ATP6V1A siRNA transfection after 48 (Figure 5-14) or 72 hours (Figure 5-15). Transfection with ATP6V1C2 reduced V_1C2 expression in the V1C1-14 vector only cells after 48 hours, which was statistically significant compared to the respective non-specific siRNA control cells (Figure 5-14 Aii). Additionally, after 72 hours of ATP6V1C2 siRNA transfection, V_1C2 expression was reduced in the V1C1-14 vector only control cells, which was again statistically significant (Figure 5-15 Aii).

V_1C2 protein levels were slightly reduced with ATP6V1A siRNA transfection in V_1C1 knockdown cells after 48 hours compared to the non-specific siRNA control. Furthermore, V_1C2 expression was significantly increased in non-transfected and non-specific siRNA transfected V1C1-14 cells compared to vector only control cells after 48 hours (Figure 5-14 Aii). In the 72 hour transfected V1C1-14 cells, there was a statistically significant increase in V_1C2 expression for the non-transfected cells compared the vector control cells.

V_1A protein levels were significantly reduced after ATP6V1A siRNA transfection for 48 (Figure 5-14 Aiii) and 72 hours (Figure 5-15 Aiii) in both V_1C1 knockdown and vector only control cells. V_1A expression was reduced in the ATP6V1C2 transfected V1C1-14 cells after 48 hours, but not in the vector only control cells, relative to the respective non-specific siRNA transfected cells (Figure 5-14 Aiii). After 72 hours of ATP6V1C2

transfection, the levels of V_1A in V1C1-14 cells was similar to that of vector only control cells (Figure 5-15 Aiii).

The expression of AR-WT was higher in the V1C1-14 cells compared to the vector only control cells in all siRNA transfected cells after 48 hours (Figure 5-14 Aiv). . Additionally, the overall expression of AR-WT was higher in the V1C1-14 cells than the vector only control cells after 48 (Figure 5-14 Aiv) and 72 hours (Figure 5-15 Aiv) of transfection. Furthermore, after 72 hours of transfection, AR-WT expression was reduced in the ATP6V1A transfected vector only control cells compared to the non-specific siRNA transfected cells. This was not the case for the V1C1-14 cells as transfection of ATP6V1A for 72 hours resulted in an increase in AR-WT expression compared to the non-specific siRNA transfected cells (Figure 5-15 Aiv). Interestingly, after 72 hours, AR-WT expression was reduced in ATP6V1C2 transfected V1C1-14 cells compared to the non-specific siRNA cells.

AR-V7 levels were higher in the non-transfected, non-specific and ATP6V1A siRNA transfected vector only control cells than the V1C1-14 cells after 48 hours (Figure 5-14 Av). In the vector only control cells, ATP6V1C2 siRNA transfected cells had increased level of AR-V7 protein compared to the non-specific siRNA transfected cells. However, in the V1C1-14 cells, ATP6V1C2 siRNA transfected cells had a reduction in AR-V7 protein levels compared to the non-specific siRNA cells. After 72 hours of siRNA transfection, ATP6V1A transfected vector control cells had reduced AR-V7 levels compared to the non-specific control (Figure 5-15 Av). The reverse was observed in the V1C1-14 cells as after 72 hours, ATP6V1A transfected cells had higher levels of AR-V7 compared to the non-specific siRNA cells, and AR-V7 levels were lower in ATP6V1C2 siRNA transfected cells. This interesting finding agrees with the AR data and suggests that silencing both V_1C isoforms reduces AR-WT and AR-V7 expression.

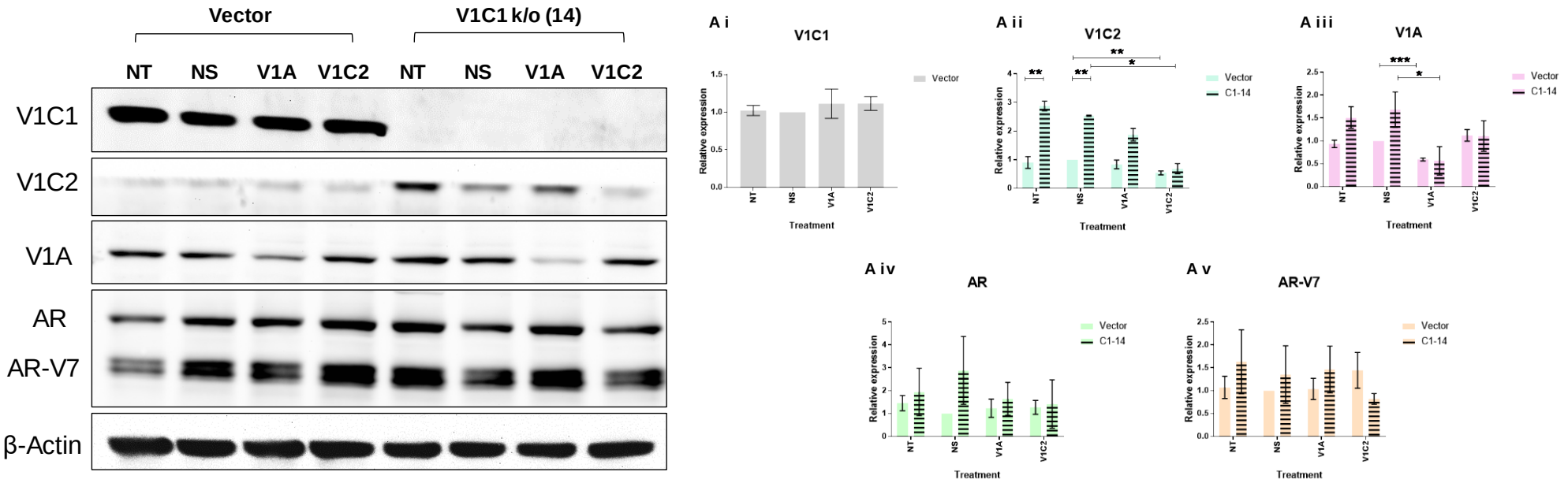

Figure 5-14. Combined knockdown of V_1C1 and V_1C2 in 22Rv1 cells (V1C1-14) for 48 hours

Vector only and V_1C1 CRISPR knockout (V1C1-14) 22Rv1 cells were reverse transfected with either 25 nmol of ATP6V1C2, ATP6V1A or non-specific siRNA for 48 hours. Control non-transfected cells were treated with equivalent concentrations of Dharmafect 1 reagent. Protein expression was measured using western blotting and cells were probed against ATP6V1C1, ATP6V1C2, ATP6V1A, AR, PSA and β-Actin. Blot is representative of three individual experiments. Densitometry data of V_1C1 (Ai), V_1C2 (Aii), V_1A (Aiii), AR (Aiv) and AR-V7 (Av) normalised to β-Actin, relative to Vector NS set to 1. Values were plotted using GraphPad Prism 7 and are displayed as mean values ± standard deviation. Student's T-Tests were used to generate P values and detect the statistical significance of the indicated differences: ns = non-significant, * = p≤ 0.05, ** = p≤ 0.01, *** = p≤ 0.001. NT, non-transfected; NS, non-specific; AR, androgen receptor; PSA, prostate specific antigen.

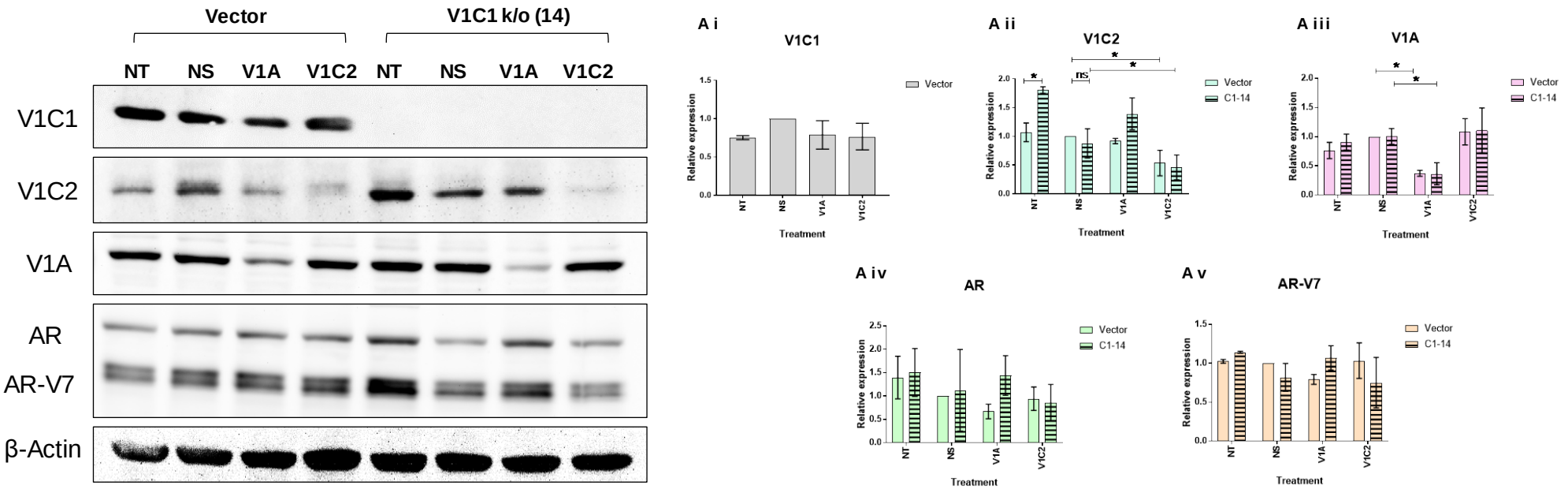

Figure 5-15. Combined knockdown of V_1C1 and V_1C2 in 22Rv1 cells (V1C1-14) for 72 hours

Vector only and V_1C1 CRISPR knockout (V1C1-14) 22Rv1 cells were reverse transfected with either 25 nmol of ATP6V1C2, ATP6V1A or non-specific siRNA for 72 hours. Control non-transfected cells were treated with equivalent concentrations of Dharmafect 1 reagent. Protein expression was measured using western blotting and cells were probed against ATP6V1C1, ATP6V1C2, ATP6V1A, AR, PSA and β-Actin. Blot is representative of three individual experiments. Densitometry data of V_1C1 (Ai), V_1C2 (Aii), V_1A (Aiii), AR (Aiv) and AR-V7 (Av) normalised to β-Actin, relative to Vector NS set to 1. Values were plotted using GraphPad Prism 7 and are displayed as mean values ± standard deviation. Student's T-Tests were used to generate P values and detect the statistical significance of the indicated differences: ns = non-significant, * = p≤ 0.05. NT, non-transfected; NS, non-specific; AR, androgen receptor; PSA, prostate specific antigen.

5.3.6.2.2 Results for 22Rv1 V1C1-18

Firstly, the densitometry data for all of the vector only control cells is the same as in 5.3.6.2.1. This was to keep consistency across the two clones and to ensure reliable comparisons could be made between the two. Also, in agreement with previously shown data (Figure 5-12), there were no detectable levels of V_1C1 protein in the V1C1-18 knockout cells (Figure 5-16 and Figure 5-17).

Similarly to the V1C1-14 cells, the levels of V_1C2 in the V1C1-18 cells were overall higher than in the vector only control cells after 48 hours post-transfection (Figure 5-16 Aii). There was a statistically significant reduction in V_1C2 expression after transfection with ATP6V1C2 siRNA for 48 hours compared to the non-specific siRNA transfected cells, indicating the siRNA was effective at reducing subunit expression in the V1C1-18 cells. After 72 hours post-transfection with siRNA, V_1C2 expression in the V1C1-18 cells was further increased compared to the vector only control cells (Figure 5-17 Aii). There were statistically significant differences in V_1C2 expression between the vector only control cells and the V1C1-18 cells after 72 hours of transfection with non-specific and ATP6V1A siRNA. Again, after 72 hours of transfection with ATP6V1C2 siRNA, the expression of V_1C2 was significantly reduced compared to the non-specific siRNA treated cells.

Levels of V_1A were slightly higher in the V1C1-18 cells than in the vector only control cells after 48 hours post transfection (Figure 5-16 Aiii). ATP6V1A siRNA transfection for 48 hours was sufficient to significantly reduce V_1A expression by 1 fold in the V1C1-18 cells compared to non-specific siRNA treated cells. Transfection with ATP6V1C2 siRNA did not alter V_1A expression compared to the non-specific siRNA control in the knockout cells (Figure 5-16 Aiii). After 72 hours of siRNA transfection, levels of V_1A were similar to that of 48 hour transfected cells, although ATP6V1C2 siRNA transfected cells had sufficiently higher levels of V_1A compared to non-specific siRNA transfected cells (Figure 5-17 Aiii).

The expression of AR-WT was lower in ATP6V1A transfected V1C1-18 cells compared to the non-specific siRNA transfected cells after 48 hours (Figure 5-16 Aiv). Overall, AR-WT expression appeared to be slightly increased in the V1C1-18 cells than the vector only control cells after 48 hours of transfection. In the V1C1-18 cells transfected for 72 hours, levels of AR-WT were increased with ATP6V1A siRNA, and there was a very small decrease in AR-WT expression in ATP6V1C2 transfected cells compared to the non-specific transfected cells (Figure 5-17 Aiv).

Finally, AR-V7 levels after 48 hours of siRNA transfection were higher in the V1C1-18 cells than in the vector only control cells (Figure 5-16 Av). Transfection with ATP6V1A siRNA reduced AR-V7 expression compared to the non-specific siRNA transfected cells. After 72 hours of transfection, AR-V7 levels were lower in the non-transfected, non-specific and ATP6V1C2 transfected V1C1-18 cells compared to the vector only control cells (Figure 5-17 Av). Additionally, in the V1C1-18 cells ATP6V1C2 transfection led to a small visible decrease in AR-V7 expression compared to the non-specific siRNA treated cells.

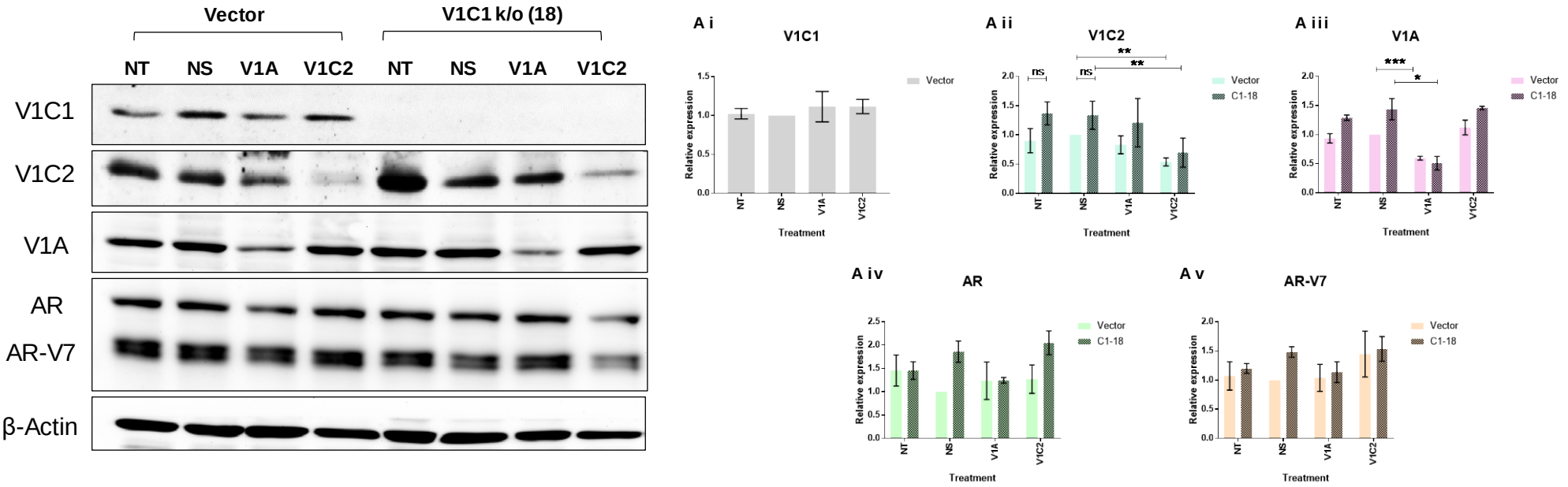

Figure 5-16. Combined knockdown of V_1C1 and V_1C2 in 22Rv1 cells (V1C1-18) for 48 hours

Vector only and V_1C1 CRISPR knockout (V1C1-18) 22Rv1 cells were reverse transfected with either 25 nmol of ATP6V1C2, ATP6V1A or non-specific siRNA for 48 hours. Control non-transfected cells were treated with equivalent concentrations of Dharmafect 1 reagent. Protein expression was measured using western blotting and cells were probed against ATP6V1C1, ATP6V1C2, ATP6V1A, AR, PSA and β-Actin. Blot is representative of three individual experiments. Densitometry data of V_1C1 (Ai), V_1C2 (Aii), V_1A (Aiii), AR (Aiv) and AR-V7 (Av) normalised to β-Actin, relative to Vector NS set to 1. Values were plotted using GraphPad Prism 7 and are displayed as mean values ± standard deviation. Student's T-Tests were used to generate P values and detect the statistical significance of the indicated differences: ns = non-significant, * = p≤ 0.05, ** = p≤ 0.01, *** = p≤ 0.001. NT, non-transfected; NS, non-specific; AR, androgen receptor; PSA, prostate specific antigen.

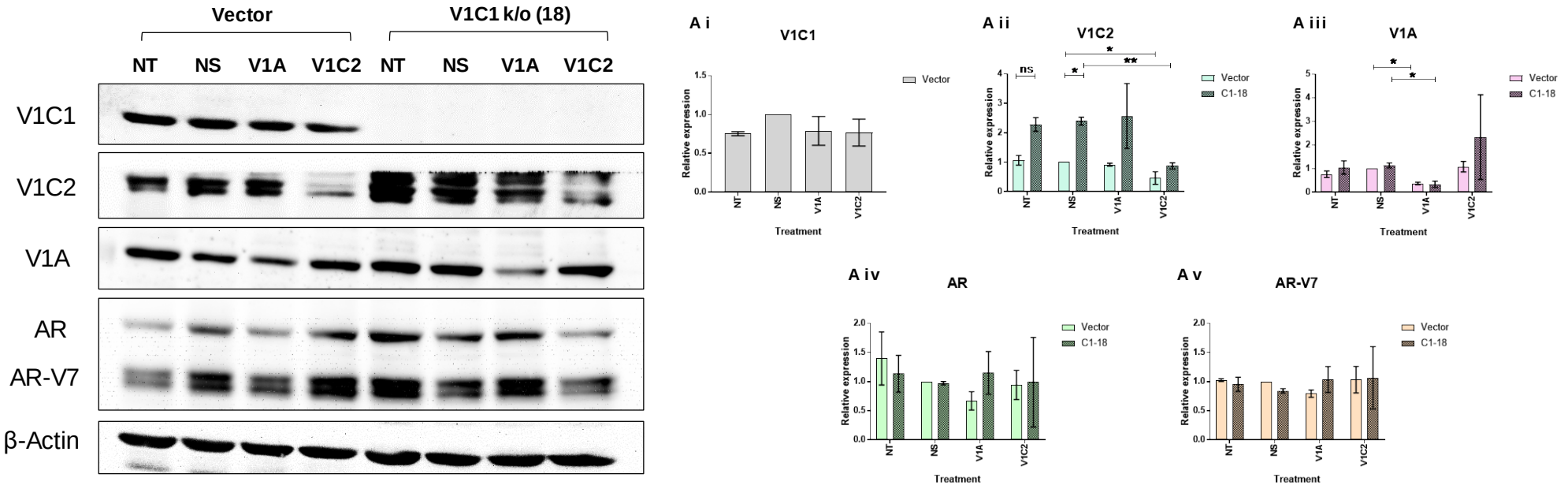

Figure 5-17. Combined knockdown of V_1C1 and V_1C2 in 22Rv1 cells (V1C1-18) for 72 hours

Vector only and V_1C1 CRISPR knockout (V1C1-18) 22Rv1 cells were reverse transfected with either 25 nmol of ATP6V1C2, ATP6V1A or non-specific siRNA for 72 hours. Control non-transfected cells were treated with equivalent concentrations of Dharmafect 1 reagent. Protein expression was measured using western blotting and cells were probed against ATP6V1C1, ATP6V1C2, ATP6V1A, AR, PSA and β-Actin. Blot is representative of three individual experiments. Densitometry data of V_1C1 (Ai), V_1C2 (Aii), V_1A (Aiii), AR (Aiv) and AR-V7 (Av) normalised to β-Actin, relative to Vector NS set to 1. Values were plotted using GraphPad Prism 7 and are displayed as mean values ± standard deviation. Student's T-Tests were used to generate P values and detect the statistical significance of the indicated differences: ns = non-significant, * = p≤ 0.05, ** = p≤ 0.01. NT, non-transfected; NS, non-specific; AR, androgen receptor; PSA, prostate specific antigen.

5.4 Summary of findings

The primary aim was to investigate the effect of genetically silencing a single V-ATPase subunit isoform on AR signalling in prostate cancer cell lines. The key findings were as follows:

- *ATP6V1C1* was found to be altered in 22% of prostate adenocarcinoma patients in a TCGA cohort, which included a high number of copy number amplifications
- ATP6V1C1 siRNA mediated knockdown of the V_1C1 subunit in LNCaP cells had no statistically significant effect on AR protein expression after 48 or 72 hours, with or without androgenic stimulation
- In 22Rv1 cells, ATP6V1C1 siRNA mediated knockdown did significantly reduce AR-WT protein levels after 72 hours post-transfection
- V_1C1 expression was androgen sensitive in LNCaP cells
- V_1C2 expression was increased in V_1C1 knockdown LNCaP cells compared to vector only control cells
- Both LNCaP and 22Rv1 V_1C1 deficient cell lines were viable
- Expression of downstream AR targets (*PSA* and *TMPRSS2*) were increased at the transcript level in 22Rv1 V_1C1 knockout cells compared to vector only controls
- Transcript levels of *ATP6V1C2* were higher in V_1C1 knockout 22Rv1 cells than vector only controls
- V_1C2 expression appeared to have an inverse relationship with hormone in 22Rv1 cells at both transcript and protein level
- Silencing the V_1C1 subunit in 22Rv1 cells increased AR signalling sensitivity to androgen
- AR-WT and AR-V7 protein levels were slightly higher in 22Rv1 V_1C1 knockout cells compared to vector only control cells
- AR-WT expression was reduced with combined V_1C1 knockout and V_1C2 knockdown compared to vector only control cells

Overall, this data supports the hypothesis that the genetic silencing of a single V-ATPase subunit isoform results in dysregulated AR signalling.

5.5 Discussion

Due to the high number of *ATP6V1C1* alterations in prostate adenocarcinoma patients, including increased mRNA expression, I hypothesised that silencing the V_1C1 subunit would result in dysregulated AR signalling. This hypothesis was based on the knowledge that AR signalling contributes to prostate cancer growth and therefore an increase in V-ATPase subunit expression, and perhaps function, might increase AR signalling in prostate cancer. Combining functional knowledge with the expression data, the V_1C1 subunit became an attractive subunit to investigate whether there was a potential link with AR signalling in both hormone sensitive (LNCaP) and constitutively active (22Rv1) models of prostate cancer.

5.5.1 Effect of V_1C1 knockdown on AR signalling in hormone sensitive LNCaP cells

5.5.1.1 siRNA mediated V_1C1 knockdown

To test the role of the V_1C1 subunit in the hormone sensitive LNCaP cell line, siRNA was first used to see whether a transient knockdown would alter AR activity. *McConnell et al.* have previously shown that a shRNA mediated 90% knockdown of *ATP6V1C1* in a breast cancer mouse model resulted in a significant reduction of orthotropic and intraosseous tumour growth. This genetic silencing also reduced V-ATPase activity, cell proliferation and mTORC1 activation *in vitro* (361). Therefore, silencing the V_1C1 subunit had a direct effect on cancer cell proliferation. As the AR signalling pathway is the dominant driver of cancer cell growth in hormone sensitive prostate cancer, silencing of the V_1C1 subunit was expected to reduce AR signalling. However, in LNCaP cells siRNA mediated V_1C1 knockdown did not significantly reduce AR or PSA protein expression after 48 or 72 hours (Figure 5-2). As previously mentioned DHT is the main physiological ligand for AR signalling activation and therefore it was important to investigate the effect of V_1C1 knockdown on DHT-induced AR activation. Interestingly V_1C1 knockdown reduced AR and PSA expression by approximately 20% and 40% in the DHT stimulated LNCaP cells, but not the androgen deprived CSS LNCaP cells (Figure 5-3). This phenomenon may be due to the reduction in V_1C1 levels partially blocking DHT-dependent AR activation. Optimal binding of DHT to the AR occurs in a very narrow pH range, with optimal binding occurring at pH 8.0 (362). Perhaps a reduction in V_1C1 expression results in a reduction of V-ATPase complex formation, and consequently the cell becomes more alkaline, reducing

the binding efficiency of DHT to the AR, so AR and PSA expression are decreased. Although not directly relevant to this model, it is also interesting to consider that 5α-reductase type 2, which is the enzyme responsible for producing 70-80% of the DHT found circulating in blood, also has a narrow pH range and an optimal pH of 5.5 (363). If the V-ATPase is dysregulated, and the intracellular pH becomes too high, then maybe there is an overall reduction in circulating DHT in humans.

Although there was a slight reduction in AR and PSA expression, it was not statistically significant. One of the reasons for this could be due to the slight increase seen in the expression of the V_1C2 isoform when only the V_1C1 isoform, and not the V_1A subunit, was reduced. Despite there only being a minor increase in V_1C2, it led me to hypothesize whether the isoform could be compensating for the loss of V_1C1. Another explanation as to why AR and PSA expression was only marginally reduced is because *McConnell et al*. demonstrated that a knockdown of 90% was necessary to reduce cell proliferation and reduce V-ATPase activity (361), and the best efficiency I was able to achieve in LNCaP cells was 60%. This was due to the poor transfection efficiency of the LNCaP cell line. Therefore, to address both of these concerns, I went on to utilize the CRISPR-Cas9 system to improve the knockdown efficiency and to gain an insight into the apparent V_1C2 compensation.

5.5.1.2 CRISPR-Cas9 mediated V_1C1 knockdown

The V_1C1 knockdown was successful and no V_1C1 protein was visible on a western blot (Figure 5-6). I first investigated whether AR expression in the V_1C1 knockdown cells was altered in response to AR stimulation with DHT, AR antagonism with enzalutamide or a combination of both. The results from these experiments were compared to LNCaP cells which had been transfected with an empty Cas9 vector to control for any non-specific Cas9 mediated effects. An interesting observation was that in the vector control cells V_1C1 expression appeared to be linked to AR signalling, whereby expression decreased in CSS media, increased with DHT treatment and was decreased again with enzalutamide treatment (Figure 5-6). The increase in expression in response to DHT treatment was more prominent than what was seen in the previous siRNA experiments (Figure 5-3), hinting at a direct link between V-ATPase and AR signalling. Despite this potential link, AR expression was similar in both vector only control cells and the V_1C1 knockdown cells, suggesting that perhaps the loss of V_1C1 does not affect AR signalling. However, the levels of V_1C2 protein were substantially higher in the V_1C1 knockdown cells than the vector only control cells (Figure 5-6). This finding indicates that V_1C2 is upregulated to compensate for the loss of V_1C1.

5.5.2 The V_1C2 subunit isoform compensates for loss of V_1C1

A literature search suggests that this is the first time V_1C2 compensation for V_1C1 has been shown, although this is not the first time a subunit isoform has been found to compensate for another. *Kawamura et al.* generated a mouse model that lacked the neuronal specific V_1G2 isoform, but had no obvious detrimental changes to brain architecture or mouse behaviour. In this model, the V_1G1 ubiquitously expressed isoform was found to accumulate to larger amounts than in a wild-type mouse model. Interestingly, despite an increase in V_1G1 protein, there was no increase in V_1G1 mRNA, indicating that a loss of function of V_1G1 was compensated by V_1G2 without mRNA upregulation (364). In addition to this research, *Păunescu et al.* demonstrated that the ubiquitously expressed V_1B2 isoform can compensate for the loss of the kidney specific V_1B1 isoform in medullary A intercalated cells. They found that apical V_1B2 immunostaining was two-fold higher in a V_1B1 null mouse model compared to one positively expressing V_1B1. However, this increase in staining was not accompanied by an upregulation of V_1B2 mRNA or protein. They concluded that the increase in staining was due to the relocalisation of V_1B2 V-ATPase complexes to the plasma membrane. The compensated V_1B2 complexes were also able to maintain 28-40% of normal V-ATPase activity, which was sufficient to maintain acid-base homeostasis in mice deficient in V_1B1 (365). Another study investigating the role of V_Oa3 in phagosome acidification found that mice deficient in V_Oa3 still exhibit V-ATPase dependent acidification, albeit to a lesser degree than in wild-type mice (366). This indicates that the V_Oa1 and V_Oa2 isoforms could at least partially rescue V-ATPase function.

Taken together, all of these studies demonstrate that despite the loss of a particular subunit isoform, another isoform is able to compensate and maintain V-ATPase function. Therefore, it is plausible that the loss of the V_1C1 subunit is compensated by the upregulation of the V_1C2 isoform, which is why AR signalling is unaffected by a permanent loss of V_1C1. This does not necessarily mean that that a transient inhibition or reduction of the V_1C1 subunit would not lead to a reduction in AR activity.

To address whether the V_1C2 compensation was responsible for maintaining AR expression, I transfected V_1C1 knockout LNCaP cells with ATP6V1C2 siRNA (Figure 5-8). Unfortunately this combined knockdown approach was not effective and I could not achieve an efficient V_1C2 knockdown. This was partly because of the poor transfection efficiency of LNCaP cells and the significant cellular toxicity observed in response to the transfection itself (Figure 5-7). However, it was interesting that there was a significant increase in toxicity in the ATP6V1C2 transfected cells compared to the non-specific siRNA

control cells, which was not observed in ATP6V1A siRNA transfected cells. This suggests that the cells can cope with the loss of one V_1C subunit isoform but a reduction in both results in cellular toxicity, and therefore probably a loss of V-ATPase function.

Additionally, even though the V_1C2 subunit appears to compensate for the permanent reduction of V_1C1, I cannot rule out the possibility that other signalling pathways have been upregulated to maintain efficient AR expression. As discussed previously, there are a plethora of alternative pathways that have been directly and indirectly linked to AR regulation including AKT, JAK/STAT etc. that act to bypass the 'classical' AR signalling pathway. Also, I cannot rule out the possibility of positive clonal selection and that the reason this particular LNCaP clone survived the V_1C1 CRISPR-Cas9 knockdown was because of the upregulation of other mechanisms, which have given it a survival advantage.

5.5.3 Effect of V_1C1 knockdown on AR signalling in AR-V7 expressing 22Rv1 cells

5.5.3.1 siRNA mediated V_1C1 knockdown

Transiently silencing the V_1C1 subunit appeared to slightly reduce AR expression in LNCaP cells in the presence of DHT, but a permanent reduction of V_1C1 had no obvious effect on AR signalling. Another interesting finding by *McConnell et al.* was that *ATP6V1C1* mRNA expression was significantly higher in breast cancer cell lines than in the untransformed C3H10T1/2 cell line, and *ATP6V1C1* knockdown reduced proliferation in the cancer cell lines but not the C3H10T1/2 line. In addition to this, *ATP6V1C1* mRNA expression was higher in breast cancer cell lines with a higher metastatic potential than those with a low metastatic potential (361). The 22Rv1 cell line is often used to model metastatic CRPC due to the expression of AR splice variants and that it can form metastatic bone lesions in mice (367). Therefore, I hypothesized that perhaps targeting the V_1C1 subunit in 22Rv1 cells would result in a reduction of AR signalling.

Similarly to the LNCaP cell line, I started by first transiently reducing V_1C1 expression in 22Rv1 cells using siRNA (Figure 5-4). The 22Rv1 cells have a better transfection efficiency and I achieved a greater transfection efficiency of up to ~75%. After 48 hours of ATP6V1C1 siRNA transfection, AR-WT and PSA protein levels were slightly reduced, but AR-V7 levels were increased. Moreover, after 72 hours, AR-WT levels were significantly reduced by ~50%, AR-V7 levels were reduced by ~40% compared to the non-specific siRNA transfected controls. Interestingly, this significant reduction in AR-WT expression

was accompanied by an increase of V_1C2 expression by 2.5 fold. This suggests that V_1C2 is upregulated to compensate for the loss of V_1C1 but AR-WT expression is still reduced, either suggesting V_1C2 has not been upregulated enough to efficiently compensate or the mechanism is independent of V_1C2 expression. Furthermore, although 22Rv1 cells are used as a model for CRPC and are largely insensitive to androgen, I still wanted to test the effect of V_1C1 knockdown on DHT-induced AR signalling. Without DHT stimulation, V_1C1 knockdown resulted in a significant reduction of AR-WT and PSA, plus a smaller reduction of AR-V7.There was also an accompanying increase in V_1C2 expression by around 50%. These results are supportive of the earlier siRNA experiments and indicate that V_1C1 knockdown does reduce AR-WT and AR-V7 mediated AR signalling. When the cells were stimulated with DHT, the extent of V_1C1 knockdown was comparable to the non-DHT stimulated cells, but the reduction in AR-WT and PSA levels was much smaller.AR-V7 expression in response to V_1C1 knockdown was similar to that of the non-DHT stimulated cells. Furthermore, V_1C2 levels were lower overall in the DHT stimulated cells, with the V_1C1 knockdown actually reducing V_1C2 levels. These results contrast with what was observed in LNCaP cells and one explanation for this is because 22Rv1 cells are less reliant on DHT for AR signalling than LNCaP cells, and they have expression of a constitutively active AR variant that can bypass the requirement of DHT. Regardless of the results from the DHT treated cells, the transient knockdown of V_1C1 reduced AR signalling in 22Rv1 cells.

5.5.3.2 CRISPR-Cas9 mediated V_1C1 knockout

To investigate this further, the CRISPR-Cas9 system was again used to reduce V_1C1 expression. Two clones, V1C1-14 and V1C1-18, emerged as complete V_1C1 knockouts. Interestingly, compared to the vector only control cells, *ATP6V1C1* mRNA expression was significantly reduced in the V1C1-14 cells, but was *ATP6V1C1* levels were comparable to levels in the vector only control cells. In both of the knockout cells *ATP6V1C2* mRNA expression was significantly increased for every treatment compared to the vector only control cells, indicating that *ATP6V1C2* compensation occurs at the transcript level, which was not detected in any of the previous studies investigating V-ATPase subunit isoform compensation (364-366). Another interesting finding was that there appeared to be an inverse relationship with androgen as *ATP6V1C2* levels were higher in CSS cultured cells than DHT treated cells and cells cultured in RPMI.

Control 22Rv1 cells are largely insensitive to androgen, but both of the V1C1-14 and -18 knockouts had increased androgenic sensitivity. This is evident as the mRNA expression of *PSA* and *TMPRSS2* was increased in response to DHT treatment compared to cells

cultured in CSS media. Compared to the vector only control cells, *PSA* mRNA expression was increased by a maximum of 2-fold in the V1C1-14 cells and up to 6-fold in the V1C1-18 cells indicating an increase in AR signalling at the transcript level. The fact that V_1C1 knockout cells appear to have an increased sensitivity to androgen and enzalutamide is an interesting finding. In the presence of DHT, enzalutamide treatment had the greatest reduction in *PSA* mRNA, and *TMPRSS2* mRNA expression was reduced to lower levels than the vector only control cells. This provides some evidence for combining AR antagonists with targeted V-ATPase subunit therapies.

Moving on from measuring mRNA levels, I went on to assess AR-WT and AR-V7 protein expression changes in the 22Rv1 V_1C1 knockout cells. Firstly, in the vector only control cells, V_1C1 protein expression displayed some sensitivity to androgen as levels were slightly increased in response to DHT treatment compared to CSS cultured cells, which could be reduced by treating the cells with enzalutamide. Again, V_1C2 protein levels were increased in the knockout cells compared to the vector only control cells. They decreased with DHT treatment and increased with enzalutamide treatment, complimenting what was observed at the transcript level. In both V1C1-14 and -18 cells AR-WT expression was increased for every treatment in the knockout cells compared to the vector only control cells. Furthermore, AR-V7 protein levels were increased in V1C1-14, and were comparable in V1C1-18 cells, compared to the vector control cells. This is supportive of the LNCaP V_1C1 CRISPR-Cas9 data and suggests that a permanent knockdown/out of V_1C1 actually results in an increase in AR signalling.

Similarly to the LNCaP cells, I wanted to investigate whether V_1C2 compensation was responsible for this increase in AR expression. Therefore, I transfected the V1C1-14 and V1C1-18 cells with ATP6V1C2 siRNA for 48 and 72 hours. Due to the improved transfection efficiency and reduced toxicity compared to the LNCaP cells, I was able to achieve a statistically significant knockdown of V_1C2 protein compared to the non-specific siRNA control cells. It is interesting to note that once again the transfection with ATP6V1C2 siRNA resulted in the greatest level of cellular toxicity compared to the non-specific control and ATP6V1A siRNA transfected cells (Figure 5-13). This suggests that knockdown of both V_1C isoforms results in substantial cell death, probably due to a reduction in V-ATPase complex assembly. After 48 hours of ATP6V1C2 transfection in the vector only control cells there were comparable levels of V_1C1 protein to the non-specific siRNA control cells, which was reduced after 72 hours. This indicates that V_1C1 does not compensate for the loss of V_1C2, which is probably because V_1C1 is the dominant V_1C isoform and V_1C2 protein levels are endogenously low in 22Rv1 cells. In agreement with previous data, V_1C2 protein levels were higher overall in both of the V_1C1 knockdown

clones, but after 48 and 72 hours of ATP6V1C2 transfection, V_1C2 levels were comparable to the vector only control cells. Most importantly, AR-WT and AR-V7 protein levels in both V_1C1 knockout clones were visibly lower on a western blot compared to the vector only controls after ATP6V1C2 siRNA transfection. These protein levels were also lower than the respective non-specific and ATP6V1A siRNA transfected cells. Although this is not represented in the densitometry data, I believe more repeats would show this effect more clearly. Therefore, perhaps a transient dual knockdown of both V_1C isoforms would be required to effectively reduce AR-WT and AR-V7 mediated AR signalling.

The fact that a transient reduction of V_1C1 was more effective in reducing AR expression in LNCaP cells than 22Rv1 cells may be due to differences in the transfection efficiency, or it could be due to differences in the metastatic potential of the cell lines. For example, *McConnell et al.* proposed that reducing V_1C1 expression may reduce V-ATPase assembly and prevent mTORC1 mediated cancer cell growth due to a failure of mTORC1 to receive amino acid signals. The mTORC1 pathway is hyper-activated in prostate cancer tumour compared to benign tissue (368). Additionally, mTOR is phosphorylated during the development of prostate cancer and there is a correlation between a high expression of phosphorylated mTOR and a worse prognosis (369). It is interesting to speculate that if the mTORC1 pathway is more dominant in 22Rv1 cells than LNCaP cells, and the cells are more dependent on mTORC1 for survival, then they would also be more reliant on V-ATPase expression and function.

Overall, I believe the V_1C2 subunit is likely compensating for the permanent loss of V_1C1, and expression of V_1C2 can maintain AR signalling in LNCaP and 22Rv1 cells. The transient reduction of V_1C1 may result in an upregulation of V_1C2 but perhaps it might not be enough to functionally compensate for the reduction of V_1C1 over a short period of time. However, as previously discussed the differences in AR signalling observed between transient and complete V_1C1 knockdown might be due to the upregulation of adaptive mechanisms, which are able to maintain AR signalling. An increase in mTORC1 signalling may be one of the adaptive changes and it would interesting to investigate this further.

Chapter Six

Chapter 6 Final Discussion

Final Discussion

At the beginning of this thesis my primary hypothesis stated that V-ATPase dysregulation is directly linked to cancer via alterations in activity. The secondary hypothesis stated that V-ATPase inhibition influences androgen receptor signalling in prostate cancer, and therefore makes an attractive therapeutic target. Listed below are the key findings related to each aim.

Aim: Measure the effect of selected somatic missense mutations on V-ATPase activity and function.

Key findings:

- There is a potential mutational hotspot at position 61 corresponding to a glutamic acid residue in the N-Terminal alpha helix of the mammalian V_1E2 subunit isoform, which is mutated to a lysine, valine or glutamine residue in different cancer samples.
- The mammalian V_1E1 and V_1E2 subunit isoforms complement ΔE null mutant yeast cells and form an active V-ATPase complex, and the selected mutations do not affect V-ATPase localisation.
- In the V_1E2 isoform, both the E61V and E61Q mutant complexes had significantly higher catalytic rates compared to the WT, and E61Q also had the highest rate of proton transport compared to all of the mutant and WT V_1E2 complexes.
- In the V_1E1 isoform, the E61Q mutant complex had a significantly higher catalytic rate compared to the WT, but the rate of proton transport was highest in the V_1E1 WT complex compared to all of the mutant V_1E1 complexes.

Aim: Investigate the effect of V-ATPase inhibition on AR signalling in prostate cancer cell lines with AR splice variants and point mutations.

Key findings:

- V-ATPase inhibition using baf-A1 and con-A reduced AR protein levels, and levels of AR downstream transcriptional targets, in the hormone sensitive LNCaP and DuCaP cell lines, as well as in the splice variant expressing 22Rv1 cell line
- Combining baf-A1 with the AR antagonist enzalutamide led to a greater reduction in AR downstream target expression than enzalutamide alone in LNCaP cells
- V-ATPase inhibition caused a reduction in cancer associated AR splice variant and mutant AR transactivation, AR mRNA and AR protein levels

Aim: Investigate the effect of genetically silencing V-ATPase subunits on AR signalling in prostate cancer cell lines.

Key findings:

- *ATP6V1C1* was found to be altered in 22% of prostate adenocarcinoma patients in a TCGA cohort, which included a high number of copy number amplifications
- ATP6V1C1 siRNA mediated knockdown of the V_1C1 subunit in LNCaP cells had no significant effect on AR protein expression, with or without androgenic stimulation
- In 22Rv1 cells, ATP6V1C1 siRNA mediated knockdown significantly reduced AR-WT protein levels, and reduced the levels of AR-V7
- Expression of downstream AR target genes were increased in 22Rv1 V_1C1 knockout cells compared to vector only controls
- Levels of V_1C2 mRNA and protein were upregulated in response to a downregulation of V_1C1, indicating isoform compensation
- AR-WT expression was reduced when V_1C1 22Rv1 knockout cells were transfected with ATP6V1C2 siRNA compared to vector only control cells

The data presented in this thesis supports the hypothesis that V-ATPase dysregulation is directly linked to cancer via alterations in activity. Some somatic mutations in V-ATPase subunit isoforms identified in the COSMIC database altered V-ATPase catalytic activity and proton flux independent of changes in expression, although determining the effects of these mutations *in vivo* would require further investigation. In prostate cancer cell lines with functional mutations and splice variants, inhibition of V-ATPase reduced the expression of AR signalling, supporting the secondary hypothesis that V-ATPase inhibition influences AR signalling in prostate cancer. A transient reduction of the V_1C1 subunit resulted in a reduction in AR signalling in 22Rv1 cells, suggesting targeting this isoform might represent a novel target for reducing AR signalling in CRPC. An unexpected compensation of the V_1C2 subunit isoform for the V_1C1 isoform may be responsible for maintaining AR signalling in V_1C1 deficient cells, but determining the exact mechanism requires further research. Overall the results revealed the following three important findings for the first time: (1) Somatic mutations in V-ATPase subunit isoforms can have a functional effect on V-ATPase catalytic activity (2) V-ATPase inhibition alters AR signalling regardless of AR mutational status, and (3) Silencing the V_1C subunit isoforms alters AR signalling in both hormone sensitive and CRPC models of prostate cancer.

6.1 Importance of V-ATPase somatic mutations in cancer

The majority of previously published research investigating the role of V-ATPase in cancer has been centred upon expression rather than alterations in V-ATPase activity. Somatic mutations have been identified in multiple subunit isoforms but the functional effect of most of these mutations is unknown. Recently, research into somatic mutations in the V_1B2 subunit found that specific amino acid substitutions are linked to lymphoma progression via increased mTORC1 signalling (323), whereas others can result in a loss of V-ATPase activity (324). A literature search indicated that somatic mutations in other subunit isoforms had not been published, and therefore I sought to investigate this further. Chapter 3 addressed the impact of selected somatic mutations in the N-terminal alpha helix of the V_1E2 subunit isoform that were identified in the COSMIC database. Position 61 corresponding to a glutamic acid residue appeared to be a hotspot for mutations in this N-terminal alpha helix (Figure 3-3) and so I hypothesised that these amino acid substitutions would affect V-ATPase catalytic activity and function. The three substitutions that were studied were glutamic acid (E) to lysine (K), valine (V) or glutamine (Q). Although these mutations were identified in the V_1E2 subunit isoform, it was important to study the same mutations in the alternative ubiquitously expressed V_1E1 isoform. As these mutations were re-created in a human/yeast chimeric model, the selected mutations were also created in the yeast V_1E subunit to act as a comparator. All of the human mutations complemented the yeast model system (Figure 3-5) and they did not affect V-ATPase localisation (Figure 3-6). The catalytic activity of the enzyme was then measured using an ADP+Pi detection assay in purified vacuolar membranes, and V-ATPase function was assessed by measuring the rate of proton flux in an acridine orange quenching assay.

It is known that the V-ATPase complex is composed of different subunit isoforms depending on tissue localisation and specialised cell function (1). It was therefore interesting that the biochemical catalytic activity of the wild-type V_1E2 subunit was likely higher than that of the V_1E1 isoform (Figure 3-7 and Figure 3-8). However, without knowing the relative expression of each isoform, this cannot be firmly concluded. Despite this, the apparent increase in catalytic activity suggests that there may be a functional relationship between V_1E2 activity and its tissue specific expression in the acrosome of spermatids (44). These specialised acidifying cells might require increased V-ATPase activity to function efficiently, and therefore V_1E2 expression would provide this enhanced functional capacity. Furthermore, the wild-type V_1E2 isoform displayed greater temperature sensitivity than the V_1E1 isoform, as an increase in temperature from 30°C to 37°C greatly increased the V-ATPase catalytic rate. This data supports what was found in the mouse V-ATPase complex, as V_1E2 was more sensitive to temperature than V_1E1

(44). Again, this increase in temperature sensitivity may be related to the tissue specific expression of V_1E2.

It is important to discuss that although the mutations complemented the Vma4 subunit in the yeast model system, the Michealis-Menten kinetics could not be calculated. The fact that the Vma4 mutants complemented the model system suggests that the V-ATPase was functional, as the yeast cells were able to grow at pH 7.5 (Figure 3-5). Although Pi was detectable, the rate of production was comparable to the membranes incubated with or without baf-A1. This meant that the Michealis-Menten curves could not be subtracted from each other to produce a non-linear curve representing V-ATPase activity, which suggests that V-ATPase activity was extremely low or that other proton transporters were compensating for the loss of V-ATPase activity. This is not the first example of substitutions in a yeast V-ATPase subunit leading to a reduction or loss of enzyme activity (324), but it is interesting that these mutations did not have the same functional defects in the human V_1E isoforms.

The selected mutations demonstrated a similar pattern of activity in both the V_1E1 and V_1E2 isoforms, which is summarized in Table 6-1. Glutamic acid to lysine resulted in a small increase in V-ATPase catalytic activity, whereas valine leads to an even higher rate, and the glutamine substitution caused the greatest increase in V-ATPase catalysis. Interestingly, although there were slight increases in the activity of the complexes containing the V_1E1 isoform, the E61 valine and glutamine mutations in the V_1E2 isoform resulted in ~10 fold increase in catalytic activity.

Table 6-1. Summary table of changes in V-ATPase enzyme kinetics as a result of selected V_1E mutations

Table representing changes in V-ATPase V_{max}, *Km* and proton coupling efficiency (H^+) with either E61 K, V or Q amino acid substitutions in V_1E1 or V_1E2 subunits. Upward arrows indicate an increase and downward arrows indicate a decrease compared to their respective subunit wild-types. E, glutamic acid; K, lysine; V, valine; Q, glutamine.

		V_1E1			V_1E2		
E61		K	V	Q	K	V	Q
30°C	V_{max}	↑	↑	↑	↑	↑	↑
	Km	↑	↑	↑	↓	↓	↓
37°C	V_{max}	↑	↑	↑	↑	↑	↑
	Km	↑	↑	↑	↑	↑	↓
	H^+	↓	↓	↓	↓	↓	↑

The fact that these mutations were identified in the V_1E2 isoform suggests that perhaps these mutations exert subunit specificity and that they have a functional consequence. In an attempt to explain this significant increase in activity, I considered the biochemical properties of the amino acids. The one defining difference in the characteristics of the glutamic acid, lysine, valine and glutamine residues was charge. It is also entirely plausible that a change in amino acid structure may affect protein folding locally, and over distance, altering interactions within the V-ATPase complex resulting in a weaker subunit structure. As the V_1E subunit forms a peripheral stalk with the V_1G subunit, the loss of a charged residue or change in protein structure may also affect the stability of the stalk, which consequently may result in an increase in the flexibility of the hydrolytic complex, allowing for a greater rate of V_1 rotation. Unfortunately, due to the lack of a crystal structure for the human V-ATPase, I can only use sequencing data to speculate about the characteristics of surrounding amino acids. Furthermore, despite these mutations increasing the rate of ATP hydrolysis, many of them did not increase the proton flux. In the V_1E1 isoform all of the substitutions resulted in a reduction in the proton coupling efficiency compared to the wild-type. This was similar to what was found in the V_1E2 isoform and the E61Q mutation was the only one to increase the proton coupling efficiency. It is interesting to speculate that this increase in proton coupling might lead to a reduction in intracellular pH, consequently resulting in the activation of proteases such as MMP's, which may increase the invasive and metastatic capabilities of cancer cells as

demonstrated in expression studies (75). It was surprising that although two of the substitutions (K and V) resulted in an increase in ATP hydrolysis, the acidifying function of V-ATPase was reduced. It is difficult to know why only the E61Q mutation resulted in an increase in both catalytic rate and proton flux, which also appeared to be isoform specific, and so requires further investigation. Despite this, the key finding was that there are somatic mutations found in V-ATPase subunit isoforms that have a functional impact on V-ATPase activity. Therefore, although the frequency of somatic mutations is low in individual subunits, they might have functional importance and result in detrimental effects such as an increase in cancer cell invasion and metastasis.

6.2 Suggestions for future work to analyse the functional impact of V-ATPase somatic mutations in cancer

Firstly, since I started this research several versions of COSMIC have been released. The most recent release (v89) revealed another mutation at the E61 hotspot corresponding to a glycine residue. Glycine has similar biochemical properties to valine but is smaller and non-polar, and it would be interesting to consider how residue size would impact upon the activity and function of V-ATPase complexes containing the V_1E1 and V_1E2 isoforms. Furthermore, glycine is a unique amino acid as it has a hydrogen as its side chain, which means that there is more conformational flexibility and it can reside in specific areas of protein structures. Additionally, all of the V-ATPase subunits have distinct functions and only the selected mutations in the V_1E2 subunit were investigated. It is also worth considering how somatic mutations in other V-ATPase subunits might alter V-ATPase activity.

Mutational hotspots could be identified in alternative subunit isoforms using large data sets and interesting mutations could be re-created. Comparisons could then be made between different cancer cohorts, such as non-metastatic vs metastatic, to improve our understanding of the clinical relevance of V-ATPase somatic mutations, and how they contribute to disease progression. Also, the databases I used to select the mutations (TCGA and COSMIC) only contained information from tumour samples, so it would be useful to know the frequency of mutations in non-cancerous ‘normal’ tissue samples. As V-ATPase mutations may occur in normal samples but might not have been selected for, single cell analysis would need to be undertaken. This would provide evidence as to whether the substitutions are driven by cancer selection or the result of random mutations.

To further assess the impact of the selected somatic mutations they could be re-created in cancer cell lines using the CRISPR-Cas9 system. The V_1E2 E61V and E61Q mutations were identified in lung adenocarcinoma cancer samples, whereas V_1E2 E61K was

identified in a melanoma sample, so cell lines could be used to represent the different cancer types. For example, the mutations could be created in both the V_1E1 and V_1E2 subunits in common human lung adenocarcinoma cell lines such as SK LU 1. In addition, they could be created in squamous cell carcinoma and small-cell lung cancer cell lines to assess the effect of these mutations in different cancer subtypes. As E61K was identified in a different cancer type, all of the mutations could be created in lung cancer and melanoma cell lines to determine whether the mutations result in differences in activity depending on the cancer type. If these mutations were to be created in cell lines, a greater variety of informative outputs could be measured. Matrigel and cell motility assays could be used to assess whether these single mutations alter the invasive and metastatic potential of cancer cells. Alterations in cellular pH could be measured using acridine orange and Lysosensor probes, providing an alternative functional output to proton flux. Western blotting and RT-qPCR could be used to measure whether the mutations affect endogenous isoform expression. Perhaps if somatic mutations were driving V-ATPase activity, V-ATPase complex expression might be lower compared to complexes without somatic mutations.

6.3 The interactions between V-ATPase and AR signalling in prostate cancer

Previous work had shown that inhibiting the V-ATPase in prostate cancer cell lines resulted in a reduction in the mRNA levels of downstream AR targets such as *PSA*, which was accompanied by a surprising increase in PSA protein levels. A mechanism involving defective secretory vesicle trafficking was suggested to explain this curious result (2). My own results in reported in Chapter 4 support this finding, and I agree that it is likely due to defective vesicular trafficking, resulting in an accumulation of PSA protein. This early work indicated that there was a link between V-ATPase and AR signalling in prostate cancer. To investigate the link further I used chemical V-ATPase inhibitors in PCa cell lines and found that V-ATPase inhibition resulted in a reduction in wild-type AR transactivation (Figure 4-2). This finding was supported by a reduction in AR protein and mRNA levels of downstream AR targets (Figure 4-3 and Figure 4-4). Moving on from this, I investigated whether V-ATPase inhibition would cause the same reduction in AR signalling in cells that expressed AR splice variants and activating mutations. This is a critical question, since AR splice variants, such as AR-V7 and AR-Q641X, are associated with progression to CRPC as the AR function becomes constitutively active. Functional AR activating mutations such as F877L and T878A result in a broadening of the ligand-binding domain and resistance to many important antiandrogens including enzalutamide. These are, therefore, clinically relevant model systems. I demonstrated that V-ATPase inhibition

reduced AR-V7 (Figure 4-11), AR-Q641X (Figure 4-12) and AR-F877L (Figure 4-15) transactivation. To support this finding I inhibited the V-ATPase in AR-V7 expressing 22Rv1 cells (Figure 4-13 and Figure 4-14) and LNCaP cells expressing the inducible F877L/T878A double mutant (Figure 4-17 and Figure 4-18). Again, there was a reduction in AR protein expression and a decrease in the mRNA levels of AR downstream targets. Together, these data provide more evidence of a link between V-ATPase and AR signalling. Most importantly, it shows that V-ATPase inhibition results in a reduction of AR signalling, which is independent of AR aberration expression.

In support of my findings, *Licon-Munoz et al.* published a similar reduction in AR expression in hormone sensitive cell lines, and presented a mechanism responsible for this downregulation (313), which is summarised in Figure 6-1. The proposed mechanism suggests V-ATPase inhibition results in defective transferrin receptor recycling due to alkalization of endo-lysosomal compartments. This in turn blocks iron uptake and reduces HIF-1α hydroxylation, resulting in an increase in HIF-1α stability. HIF-1α is then free to translocate to the nucleus and downregulate AR expression. Although I did not investigate the mechanism linking the AR and V-ATPase, I believe this transcriptional AR regulatory mechanism is, in part, likely responsible for a V-ATPase mediated reduction in AR activation (313). In line with the proposed mechanism involving HIF-1 α, baf-A1 inhibition has previously been shown to induce HIF-1α in AR negative PCa cells (370). It is also interesting that knockdown of Ac45, as well as V_Oa1 and V_Oa3, reduced transferrin receptor recycling to the plasma membrane (311). Hence targeting these subunits might reduce AR activity via a decrease in intracellular iron concentration and a reduction in HIF-1α hydroxylation. However, an unexpected result published by *Licon-Munoz et al.* was that co-incubation of con-A with iron significantly reduced HIF-1α protein levels (313), which conflicts with their suggested mechanism. I therefore believe the interactions between V-ATPase and the AR are multifaceted, involving several signalling pathways.

Firstly, results published by *Fernandez et al.* show that the expression of AR target genes such as *TMPRSS2* were suppressed by HIF-signalling, and that specific HIF-1α target expression was induced by DHT (371). This induction of HIF-1α by DHT is supported by research conducted by *Mabjeesh et al.* who demonstrated that DHT could indirectly influence HIF-1α activation. DHT activation of HIF-1α is translation dependent as the mRNA levels of *HIF-1α* are unchanged after DHT treatment. This androgen mediated activation of HIF-1α and HIF-1α regulated gene expression, occurs via an autocrine PI3K/AKT-dependent pathway. The proposed model involves the binding of DHT to the AR, which activates the AR and results in an increase in the secretion of specific proteins including EGF. Activation of EGF then drives the synthesis of HIF-1α protein, which can then bind to HIF-response elements (HRE) (372). This binding to HRE would

downregulate AR gene expression, representing a negative feedback mechanism of DHT induced AR expression. Therefore, the involvement of androgen cannot be underestimated when considering the V-ATPase/AR axis.

Adding to the complexity of the AR/HIF-1α interaction, one study investigating the dual inhibition of both HIF-1α and the AR found that HIF-1α inhibition resulted in a downregulation of AR target gene expression. This inhibition of HIF-1α conversely caused an increase in AR transcriptional activity, which was greater than in cells treated with DHT. Additionally, siRNA mediated knockdown of HIF-1α resulted in a reduction of DHT enhanced AR transactivation and, when combined with enzalutamide treatment, it had a synergistic effect on reducing DHT mediated AR activity in both hormone sensitive LNCaP cells and AR-V7 expressing 22Rv1 cells. HIF-1α siRNA treatment also reduced LNCaP and 22Rv1 cell growth (371). This suggests that the repressive effect on the expression of specific genes surpasses its ability to increase ARE–mediated transactivation, and that cross talk between the two pathways involves gene specific regulation.

Another pathway that might be involved in the AR/V-ATPase axis is the mTOR signalling pathway. Although the primary function of the V-ATPase is to regulate intracellular pH, research published by *Zoncu et al.* revealed that the V-ATPase complex can directly regulate mTORC1 activity though its amino acid sensing capabilities (76). This indicates that the V-ATPase is more versatile than a simple proton pump and may actually play a direct role in various signalling pathways. In addition to this, there is a possible link between the AR and mTOR signalling pathways via a reciprocal AR/mTOR loop. Knockdown of AR in LNCaP cells resulted in an upregulation of TSC1 and TSC2, which are negative regulators of mTOR activity. Additionally, a decrease in mTOR activity consequently increased AR protein levels, but only in an androgen depleted environment (373). In support of this, PI3K/AKT activation of mTORC1/2 was shown to repress receptor tyrosine kinase (HER2/3) activation, leading to a repression of AR activation and a reduction of AR target gene expression. Additionally, PI3K pathway inhibition stimulated HER2/3 and activated the AR (198). Data presented by *McConnell et al.* suggested that *ATP6V1C1* knockdown resulted in a reduction in V-ATPase complex assembly in breast cancer cell lines, causing a reduction in mTORC1 activity (361). Therefore, a reduction in V-ATPase activity might reduce mTORC1 signalling and consequently increase AR activation in prostate cancer.

My own investigations inhibiting *ATP6V1C1* reported in Chapter 5 gave mixed results depending on the percentage of subunit knockdown and the cell line investigated. Transient knockdown of *ATP6V1C1* reduced AR expression in 22Rv1 cells (Figure 5-4), but a CRSIPR-Cas9 induced knockout actually increased AR expression (Figure 5-11 and Figure 5-12). The mTORC1 signalling pathway was not investigated but it is possible it

might contribute to this compensatory effect on AR expression after *ATP6V1C1* knockout. It could be that there is a physical interaction between the V_1C1 subunit and components of the mTORC1 signalling pathway. *Zoncu et al.* showed that the V_1C subunit co-precipitated with the p14 component of the Ragulator complex, which is involved in regulating mTORC1 activity. Alternatively, as V_1C1 is involved in V-ATPase regulation, it is plausible that a transient reduction of the V_1C1 subunit causes aberrant V-ATPase regulation, consequently impacting upon other signalling pathways such as mTORC. This transcriptional cross-talk with AR remains poorly understood but might represent another way the V-ATPase is linked to AR signalling. Due to the interactions between V-ATPase and mTORC, it also cannot be ruled out that the V-ATPase complex, or at least its components, contribute directly to the AR signalling pathway.

Based on the available literature, I agree with *Lincon-Munoz et al*. that the V-ATPase is likely acting upstream of the AR, and is indirectly impacting upon AR regulation, potentially through vesicular trafficking. However, given the intricacy of the AR/HIF-1α with DHT interaction, and the possible involvement of other pathways such as mTORC, it is difficult to determine the exact mechanism, especially considering the complexity, and multi-factorial mechanisms, of hormonal regulation in the progression of PCa to CRPC. Given the importance of V-ATPase in normal physiology, it is more likely that V-ATPase inhibition interferes with a number of different signalling pathways, both directly and indirectly, which may involve gene specific regulation.

Importantly, my results demonstrate that V-ATPase inhibition can reduce AR signalling in prostate cancer cells regardless of mutant AR expression. This suggests that V-ATPase could be targeted as a way to overcome AR signalling in patients with AR aberrations, providing additional treatment options to those where current treatments have failed, or patients with CRPC. Although targeting the complex as a whole would potentially be highly toxic due to off target effects, evidence is starting to emerge that targeting specific V-ATPase subunits might be an efficient method of reducing AR signalling, without the toxic non-specific effects observed with chemical V-ATPase inhibitors. For example, subunits such as Ac45 and the V_Oa isoforms may represent the best targets to prevent V-ATPase mediated trafficking to downstream effector proteins, whereas perhaps transiently reducing the V_1C1 subunit would reduce AR signalling via alternative pathways such as mTORC. It is therefore essential that we completely understand these complex interactions between the V-ATPase subunits and the AR.

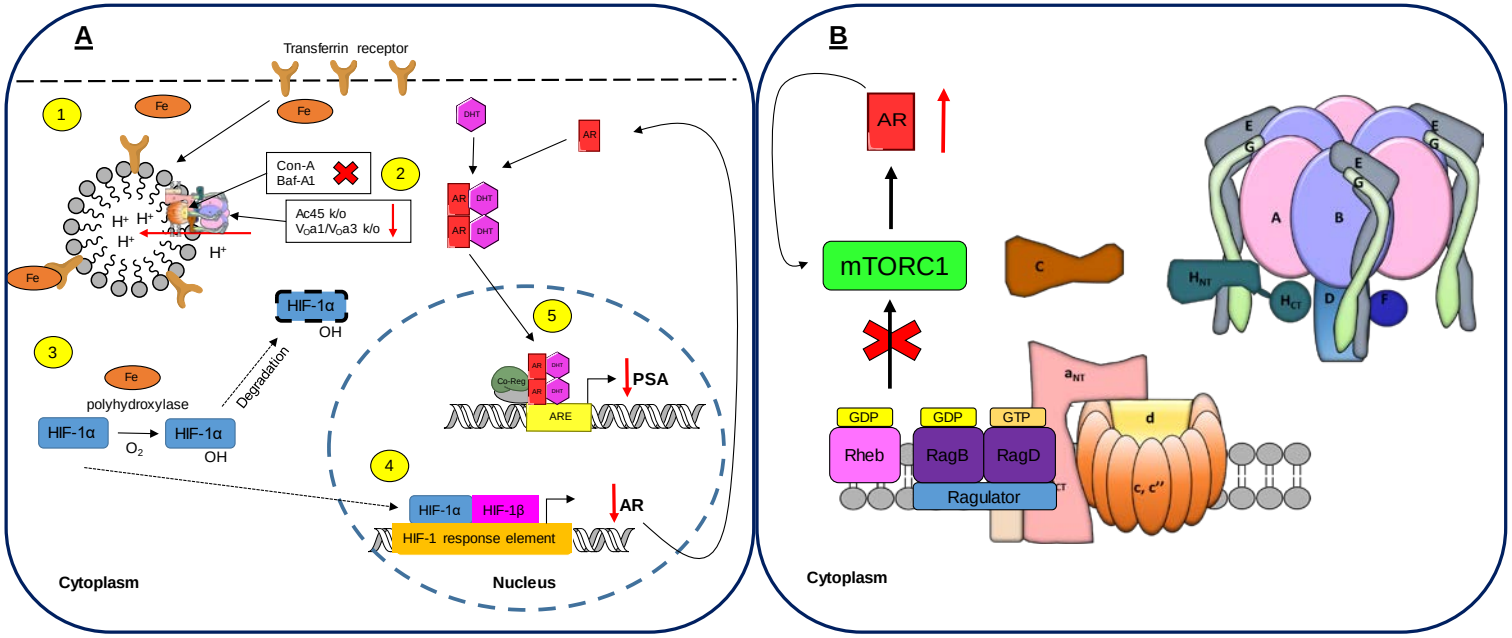

Figure 6-1. Proposed mechanisms of V-ATPase interactions with the AR

(A) V-ATPase inhibition reduces AR activation via HIF-1α. Following the diagram: (1) The transferrin receptor transports iron into cells and requires V-ATPase mediated endocytosis to traffic intracellular iron. (2) V-ATPase inhibition due to con-A or baf-A1 results in defective transferrin receptor recycling due to alkalization of endo-lysosomal compartments. Knockout of Ac45 or V_Oa1/a3 subunits also reduces transferrin receptor recycling by reducing V-ATPase targeting to the plasma membrane. (3) This in turn blocks iron uptake and reduces HIF-1α hydroxylation, which prevents HIF-1α degradation and results in an increase in HIF-1α stability. (4) HIF-1α is then free to translocate to the nucleus and bind to HIF-1 response elements that downregulate AR expression. (5) The reduction in AR expression results in a reduction of ARE mediated downstream signalling, leading to reduced expression of AR target genes such as *PSA*. (B) Absence of the V_1C subunit from the V-ATPase complex results in an increase in V-ATPase complex disassembly, which in turn reduces mTORC1 formation on LAMP1$^+$ lysosomes to receive amino acid signalling. The reduction in mTORC1 activity may result in an increase in HER2/3, which activates the AR, forming a reciprocal AR/mTOR loop. Fe, iron; con-A, concanamycin-A; baf-A1, bafilomycin-A1; k/o, knockout; AR, androgen receptor; DHT, dihydrotestosterone; PSA, prostate specific antigen; co-reg; co-regulatory proteins; ARE, androgen response element.

6.4 Suggestions for future work to understand the interactions between V-ATPase and AR signalling in prostate cancer

Having demonstrated that V-ATPase inhibition can reduce AR signalling in cells with AR mutations and splice variants, the next steps would be to; (1) further investigate the biological mechanism behind V-ATPase and AR interactions and (2) investigate the role of individual V-ATPase subunits in PCa progression. Of course, these two stages are interconnected and it would be important to investigate how individual subunits alter the mechanism behind the V-ATPase/AR axis. It is also possible that the V-ATPase has non-AR linked effects in PCa, and it would be worth investigating these potential effects.

Firstly, my results showed an additive effect on AR expression when combining chemical V-ATPase inhibition using baf-A1 with AR antagonism using enzalutamide in LNCaP cells (Figure 4-10). It would be interesting to examine whether this effect was additive or whether it was synergistic. A number of different quantitative methods are available to determine synergy, where the combinatorial effect is greater than the expected effects of the individual compounds potencies (374). The most common method for synergy assessment is the method of isoboles. In brief, dose pairs are plotted on the isobole (solid line for a specified effect), which represents combination doses that are additive when the 2 compounds have a ratio of constant potency. If the specified outcome is achieved (e.g., 50% Emax) with lower doses, such as one point below the isobole, then the dose combination is synergistic (374). Calculating synergy between V-ATPase inhibitors and AR antagonists may be one way to reduce the concentration of each drug, and therefore the toxicity level, making V-ATPase a more attractive therapeutic target.

To further understand the mechanism relating V-ATPase to the AR, it would be essential to explore the mechanisms already suggested. The proposed involvement of iron and HIF-1α could be investigated in cell lines that express AR splice variants, such as 22Rv1, and cell lines that are AR negative, such as PC-3. This would give an insight into whether the role of HIF-1α changes during PCa progression. Additionally, glucose is another key regulator of V-ATPase activity. Glucose starvation induces V-ATPase assembly and activity though AMPK and PI3K/AMPK signalling (375), and the increase in AMPK in response to glucose deprivation results in mTORC1 inhibition both indirectly and directly (376). Therefore, it would be interesting to explore the V-ATPase/mTORC1/AR axis in response to glucose starvation. To do this, PCa cell lines could be cultured in glucose positive or glucose negative media. Alternatively, if the cells grew poorly in the glucose negative media, the media could be supplemented with fructose instead. Furthermore, although an effect of V-ATPase inhibition on the AR has been demonstrated, given the

evidence it is unlikely that this effect is specific to the AR. This could be further investigated by measuring the expression of other nuclear receptors such as the glucocorticoid receptor.

To investigate the role of particular V-ATPase subunit isoforms, immunohistochemical staining of FFPE tumour tissue representing various stage of disease progression would indicate which subunits might be particularly important in PCa development. Sequential samples from the same patient would be ideal to monitor V-ATPase subunit expression in PCa, although realistically it is difficult to get these samples in high numbers. Tumour tissue microarrays (TMA) could be used for effective high-throughput screening of tumour samples for individual V-ATPase subunit isoforms. Once defined, genetic silencing experiments could be used to measure the effect of the overexpressed subunits. Conversely, subunits that are under-expressed could be overexpressed in cell lines to ascertain the clinical relevance of subunit loss. Biological outputs such as cell toxicity, pH regulation, invasion and metastatic potential could all be measured in response to changes in subunit expression to understand more about the functionality of individual isoform expression. Additionally, as my own results indicated a difference in AR signalling based on whether a subunit was transiently knocked down or completely knocked out, future experiments investigating alternative subunits would have to consider additional techniques. Due to the toxicity observed when combining CRISPR-Cas9 with siRNA, CRISPR-Cas9 could be used to silence more than one isoform. This would overcome the apparent V_1C2 subunit isoform compensation observed in response to V_1C1 knockout. Ideally, chemical compounds targeting different V-ATPase subunits with various half-lives could be used to explore what period of specific subunit inhibition would produce a maximal reduction in AR activity with minimal toxicity. If a particular subunit of interest showed promising results *in vitro* with regards to expression and genetic experiments, and a highly selective compound was developed for that particular isoform, then perhaps patient derived xenograft mouse models could be used to further determine the potential biological effects of selective V-ATPase subunit inhibition.

V-ATPase subunit silencing experiments could include the measurement of other signalling pathways such as PI3K, AKT and mTORC. Western blotting and RT-qPCR could be used to measure the expression of specific signalling markers, which would demonstrate the involvement of a particular pathway in response to V-ATPase subunit loss. It is likely that effects would differ depending on the cell line, so several cell lines modelling PCa progression would have to be used. To uncover the true effect of subunit knockouts, the subunits could be re-introduced into the V-ATPase complex to observe whether this would rescue the knockout effects. As DHT influences HIF-1α and mTORC activity, subunit-silencing experiments could be completed in hormone-depleted

conditions and the expression of HIF-1α and mTORC could be measured in response to DHT treatment. Alternatively, the expression of the AR and downstream targets could be measured in response to CRISPR-Cas9 silencing of components of the HIF-1α and mTORC1 pathways.

Chapter Seven

Chapter 7 References

References

1. Whitton B, Okamoto H, Packham G, Crabb SJ. Vacuolar ATPase as a potential therapeutic target and mediator of treatment resistance in cancer. Cancer Med. 2018;7(8):3800-11.

2. Michel V, Licon-Munoz Y, Trujillo K, Bisoffi M, Parra KJ. Inhibitors of vacuolar ATPase proton pumps inhibit human prostate cancer cell invasion and prostate-specific antigen expression and secretion. Int J Cancer. 2013;132(2):E1-10.

3. Marshansky V, Futai M. The V-type H+-ATPase in vesicular trafficking: targeting, regulation and function. Curr Opin Cell Biol. 2008;20(4):415-26.

4. Hinton A, Bond S, Forgac M. V-ATPase functions in normal and disease processes. Pflugers Arch. 2009;457(3):589-98.

5. Breton S, Brown D. Regulation of Luminal Acidification by the V-ATPase. Phys. 2013;28(5):318-29.

6. Hennings JC, Picard N, Huebner AK, Stauber T, Maier H, Brown D, et al. A mouse model for distal renal tubular acidosis reveals a previously unrecognized role of the V-ATPase a4 subunit in the proximal tubule. EMBO Mol Med. 2012;4(10):1057-71.

7. Păunescu TG, Rodriguez S, Benz E, McKee M, Tyszkowski R, Albers MW, et al. Loss of the V-ATPase B1 Subunit Isoform Expressed in Non-Neuronal Cells of the Mouse Olfactory Epithelium Impairs Olfactory Function. PLoS One. 2012;7(9):e45395.

8. Qin A, Cheng TS, Pavlos NJ, Lin Z, Dai KR, Zheng MH. V-ATPases in osteoclasts: structure, function and potential inhibitors of bone resorption. Int J Biochem Cell Biol. 2012;44(9):1422-35.

9. Wagner CA. When proton pumps go sour: Urinary acidification and kidney stones. Kidney Int. 2008;73(10):1103-5.

10. Pietrement C, Sun-Wada GH, Silva ND, McKee M, Marshansky V, Brown D, et al. Distinct expression patterns of different subunit isoforms of the V-ATPase in the rat epididymis. Biol Reprod. 2006;74(1):185-94.

11. Hinton A, Sennoune SR, Bond S, Fang M, Reuveni M, Sahagian GG, et al. Function of a Subunit Isoforms of the V-ATPase in pH Homeostasis and in Vitro Invasion of MDA-MB231 Human Breast Cancer Cells. J Biol Chem. 2009;284(24):16400-8.

12. Okamoto-Terry H, Umeki K, Nakanishi-Matsui M, Futai M. Glu-44 in the Amino-terminal α-Helix of Yeast Vacuolar ATPase E Subunit (Vma4p) Has a Role for V(o)V(1) Assembly. J Biol Chem. 2013;288(51):36236-43.

13. Fethiere J, Venzke D, Diepholz M, Seybert A, Geerlof A, Gentzel M, et al. Building the stator of the yeast vacuolar-ATPase: specific interaction between subunits E and G. J Biol Chem. 2004;279(39):40670-6.

14. Cotter K, Stransky L, McGuire C, Forgac M. Recent Insights into the Structure, Regulation, and Function of the V-ATPases. Trends Biochem Sci. 2015;40(10):611-22.

15. Zhao J, Benlekbir S, Rubinstein JL. Electron cryomicroscopy observation of rotational states in a eukaryotic V-ATPase. Nature. 2015;521(7551):241-5.

16. Kawasaki-Nishi S, Nishi T, Forgac M. Arg-735 of the 100-kDa subunit a of the yeast V-ATPase is essential for proton translocation. PNAS. 2001;98(22):12397-402.

17. Jefferies KC, Cipriano DJ, Forgac M. Function, structure and regulation of the vacuolar (H(+))-ATPases. Arch Biochem Biophys. 2008;476(1):33-42.

18. Bowman BJ, Bowman EJ. Mutations in subunit C of the vacuolar ATPase confer resistance to bafilomycin and identify a conserved antibiotic binding site. J Biol Chem. 2002;277(6):3965-72.

19. Huss M, Ingenhorst G, Konig S, Gassel M, Drose S, Zeeck A, et al. Concanamycin A, the specific inhibitor of V-ATPases, binds to the V(o) subunit c. J Biol Chem. 2002;277(43):40544-8.

20. Bockelmann S, Menche D, Rudolph S, Bender T, Grond S, von Zezschwitz P, et al. Archazolid A binds to the equatorial region of the c-ring of the vacuolar H+-ATPase. J Biol Chem. 2010;285(49):38304-14.

21. Arata Y, Baleja JD, Forgac M. Localization of subunits D, E, and G in the yeast V-ATPase complex using cysteine-mediated cross-linking to subunit B. Biochemistry. 2002;41(37):11301-7.

22. Zhang Z, Zheng Y, Mazon H, Milgrom E, Kitagawa N, Kish-Trier E, et al. Structure of the Yeast Vacuolar ATPase. J Biol Chem. 2008;283(51):35983-95.

23. Kitagawa N, Mazon H, Heck AJR, Wilkens S. Stoichiometry of the Peripheral Stalk Subunits E and G of Yeast V1-ATPase Determined by Mass Spectrometry. JBC. 2008;283(6):3329-37.

24. Esteban O, Bernal RA, Donohoe M, Videler H, Sharon M, Robinson CV, et al. Stoichiometry and Localization of the Stator Subunits E and Gin Thermus thermophilus H+-ATPase/Synthase. JBC. 2008;283(5):2595-603.

25. Dunn SD, McLachlin DT, Revington M. The second stalk of Escherichia coli ATP synthase. Biochim Biophys Acta. 2000;1458(2-3):356-63.

26. Kawasaki-Nishi S, Bowers K, Nishi T, Forgac M, Stevens TH. The amino-terminal domain of the vacuolar proton-translocating ATPase a subunit controls targeting and in vivo dissociation, and the carboxyl-terminal domain affects coupling of proton transport and ATP hydrolysis. J Biol Chem. 2001;276(50):47411-20.

27. Nelson H, Nelson N. Disruption of genes encoding subunits of yeast vacuolar H(+)-ATPase causes conditional lethality. PNAS. 1990;87(9):3503-7.

28. Morel N, Dedieu JC, Philippe JM. Specific sorting of the a1 isoform of the V-H+ATPase a subunit to nerve terminals where it associates with both synaptic vesicles and the presynaptic plasma membrane. J Cell Sci. 2003;116(Pt 23):4751-62.

29. Peri F, Nusslein-Volhard C. Live imaging of neuronal degradation by microglia reveals a role for v0-ATPase a1 in phagosomal fusion in vivo. Cell. 2008;133(5):916-27.

30. Hurtado-Lorenzo A, Skinner M, El Annan J, Futai M, Sun-Wada GH, Bourgoin S, et al. V-ATPase interacts with ARNO and Arf6 in early endosomes and regulates the protein degradative pathway. Nat Cell Biol. 2006;8(2):124-36.

31. Toyomura T, Murata Y, Yamamoto A, Oka T, Sun-Wada GH, Wada Y, et al. From lysosomes to the plasma membrane: localization of vacuolar-type H+ -ATPase with the a3 isoform during osteoclast differentiation. J Biol Chem. 2003;278(24):22023-30.

32. Wagner CA, Finberg KE, Breton S, Marshansky V, Brown D, Geibel JP. Renal vacuolar H+-ATPase. Physiol Rev. 2004;84(4):1263-314.

33. Bartkiewicz M, Hernando N, Reddy SV, Roodman GD, Baron R. Characterization of the osteoclast vacuolar H(+)-ATPase B-subunit. Gene. 1995;160(2):157-64.

34. Smith AN, Borthwick KJ, Karet FE. Molecular cloning and characterization of novel tissue-specific isoforms of the human vacuolar H+-ATPase C, G and d subunits, and their evaluation in autosomal recessive distal renal tubular acidosis. Gene. 2002;297(1):169-77.

35. Imai-Senga Y, Sun-Wada GH, Wada Y, Futai M. A human gene, ATP6E1, encoding a testis-specific isoform of H(+)-ATPase subunit E. Gene. 2002;289(1-2):7-12.

36. Paunescu TG, Da Silva N, Marshansky V, McKee M, Breton S, Brown D. Expression of the 56-kDa B2 subunit isoform of the vacuolar H(+)-ATPase in proton-secreting cells of the kidney and epididymis. Am J Physiol Cell Physiol. 2004;287(1):C149-62.

37. Da Silva N, Shum WW, El-Annan J, Paunescu TG, McKee M, Smith PJ, et al. Relocalization of the V-ATPase B2 subunit to the apical membrane of epididymal clear cells of mice deficient in the B1 subunit. Am J Physiol Cell Physiol. 2007;293(1):C199-210.

38. Yuan Y, Zhang J, Chang Q, Zeng J, Xin F, Wang J, et al. De novo mutation in ATP6V1B2 impairs lysosome acidification and causes dominant deafness-onychodystrophy syndrome. Cell Res. 2014;24(11):1370-3.

39. Menendez I, Carranza C, Herrera M, Marroquin N, Foster J, 2nd, Cengiz FB, et al. Dominant deafness-onychodystrophy syndrome caused by an ATP6V1B2 mutation. Clin Case Rep. 2017;5(4):376-9.

40. Wang F, Gatica D, Ying ZX, Peterson LF, Kim P, Bernard D, et al. Follicular lymphoma-associated mutations in vacuolar ATPase ATP6V1B2 activate autophagic flux and mTOR. J Clin Invest. 2019;130:1626-40.

41. Feng S, Deng L, Chen W, Shao J, Xu G, Li YP. Atp6v1c1 is an essential component of the osteoclast proton pump and in F-actin ring formation in osteoclasts. Biochem J. 2009;417(1):195-203.

42. Sun-Wada GH, Murata Y, Namba M, Yamamoto A, Wada Y, Futai M. Mouse proton pump ATPase C subunit isoforms (C2-a and C2-b) specifically expressed in kidney and lung. J Biol Chem. 2003;278(45):44843-51.

43. Wang Y, Chen W, Hao L, McVicar A, Wu J, Gao N, et al. C1 Silencing Attenuates Inflammation and Alveolar Bone Resorption in Endodontic Disease. J Endod. 2019;45(7):898-906.

44. Sun-Wada G-H, Imai-Senga Y, Yamamoto A, Murata Y, Hirata T, Wada Y, et al. A Proton Pump ATPase with Testis-specific E1-Subunit Isoform Required for Acrosome Acidification. JBC. 2002;277(20):18098-105.

45. Smith AN, Jouret F, Bord S, Borthwick KJ, Al-Lamki RS, Wagner CA, et al. Vacuolar H+-ATPase d2 subunit: molecular characterization, developmental regulation, and localization to specialized proton pumps in kidney and bone. J Am Soc Nephrol. 2005;16(5):1245-56.

46. Sun-Wada GH, Yoshimizu T, Imai-Senga Y, Wada Y, Futai M. Diversity of mouse proton-translocating ATPase: presence of multiple isoforms of the C, d and G subunits. Gene. 2003;302(1-2):147-53.

47. Smith AN, Borthwick KJ, Karet FE. Molecular cloning and characterization of novel tissue-specific isoforms of the human vacuolar H(+)-ATPase C, G and d subunits, and

their evaluation in autosomal recessive distal renal tubular acidosis. Gene. 2002;297(1-2):169-77.

48. Lee SH, Rho J, Jeong D, Sul JY, Kim T, Kim N, et al. v-ATPase V0 subunit d2-deficient mice exhibit impaired osteoclast fusion and increased bone formation. Nat Med. 2006;12(12):1403-9.

49. Shinmura K, Igarashi H, Kato H, Koda K, Ogawa H, Takahashi S, et al. BSND and ATP6V1G3: Novel Immunohistochemical Markers for Chromophobe Renal Cell Carcinoma. Medicine. 2015;94(24):e989-e.

50. Oot RA, Huang L-S, Berry EA, Wilkens S. Crystal structure of the yeast vacuolar ATPase heterotrimeric EGC(head) peripheral stalk complex. Structure (London, England : 1993). 2012;20(11):1881-92.

51. Parra KJ, Chan CY, Chen J. Saccharomyces cerevisiae vacuolar H+-ATPase regulation by disassembly and reassembly: one structure and multiple signals. Eukaryotic cell. 2014;13(6):706-14.

52. Diab H, Ohira M, Liu M, Cobb E, Kane PM. Subunit Interactions and Requirements for Inhibition of the Yeast V(1)-ATPase. J Biol Chem. 2009;284(20):13316-25.

53. Jefferies KC, Forgac M. Subunit H of the V-ATPase Inhibits ATP Hydrolysis by the Free V(1) Domain by Interaction with the Rotary Subunit F. J Biol Chem. 2008;283(8):4512-9.

54. Balakrishna AM, Basak S, Manimekalai MSS, Grüber G. Crystal Structure of Subunits D and F in Complex Gives Insight into Energy Transmission of the Eukaryotic V-ATPase from Saccharomyces cerevisiae. JBC. 2015;290(6):3183-96.

55. Smardon AM, Tarsio M, Kane PM. The RAVE complex is essential for stable assembly of the yeast V-ATPase. J Biol Chem. 2002;277(16):13831-9.

56. Smardon AM, Kane PM. RAVE is essential for the efficient assembly of the C subunit with the vacuolar H(+)-ATPase. J Biol Chem. 2007;282(36):26185-94.

57. Kawasaki-Nishi S, Nishi T, Forgac M. Yeast V-ATPase complexes containing different isoforms of the 100-kDa a-subunit differ in coupling efficiency and in vivo dissociation. J Biol Chem. 2001;276(21):17941-8.

58. Smardon AM, Diab HI, Tarsio M, Diakov TT, Nasab ND, West RW, et al. The RAVE complex is an isoform-specific V-ATPase assembly factor in yeast. Mol Biol Cell. 2014;25(3):356-67.

59. Sethi N, Yan Y, Quek D, Schupbach T, Kang Y. Rabconnectin-3 is a functional regulator of mammalian Notch signaling. J Biol Chem. 2010;285(45):34757-64.

60. Sautin YY, Lu M, Gaugler A, Zhang L, Gluck SL. Phosphatidylinositol 3-Kinase-Mediated Effects of Glucose on Vacuolar H(+)-ATPase Assembly, Translocation, and Acidification of Intracellular Compartments in Renal Epithelial Cells. Mol Cell Biol. 2005;25(2):575-89.

61. Xu Y, Parmar A, Roux E, Balbis A, Dumas V, Chevalier S, et al. Epidermal growth factor-induced vacuolar (H+)-atpase assembly: a role in signaling via mTORC1 activation. J Biol Chem. 2012;287(31):26409-22.

62. Pastor-Soler N, Beaulieu V, Litvin TN, Silva ND, Chen Y, Brown D, et al. Bicarbonate-regulated Adenylyl Cyclase (sAC) Is a Sensor That Regulates pH-dependent V-ATPase Recycling. J Biol Chem. 2003;278(49):49523-9.

63. Alzamora R, Al-Bataineh MM, Liu W, Gong F, Li H, Thali RF, et al. AMP-activated protein kinase regulates the vacuolar H+-ATPase via direct phosphorylation of the A subunit (ATP6V1A) in the kidney. Am J Physiol Renal Physiol. 2013;305(7):F943-56.

64. Hallows KR, Alzamora R, Li H, Gong F, Smolak C, Neumann D, et al. AMP-activated protein kinase inhibits alkaline pH- and PKA-induced apical vacuolar H(+)-ATPase accumulation in epididymal clear cells. Am J Physiol Cell Physiol. 2009;296(4):C672-C81.

65. Gong F, Alzamora R, Smolak C, Li H, Naveed S, Neumann D, et al. Vacuolar H(+)-ATPase apical accumulation in kidney intercalated cells is regulated by PKA and AMP-activated protein kinase. Am J Physiol Cell Physiol. 2010;298(5):F1162-F9.

66. O'Callaghan KM, Ayllon V, O'Keeffe J, Wang Y, Cox OT, Loughran G, et al. Heme-binding protein HRG-1 is induced by insulin-like growth factor I and associates with the vacuolar H+-ATPase to control endosomal pH and receptor trafficking. J Biol Chem. 2010;285(1):381-91.

67. Jansen EJ, Hafmans TG, Martens GJ. V-ATPase-mediated granular acidification is regulated by the V-ATPase accessory subunit Ac45 in POMC-producing cells. Mol Biol Cell. 2010;21(19):3330-9.

68. Pena-Llopis S, Vega-Rubin-de-Celis S, Schwartz JC, Wolff NC, Tran TA, Zou L, et al. Regulation of TFEB and V-ATPases by mTORC1. Embo J. 2011;30(16):3242-58.

69. Maxfield FR, McGraw TE. Endocytic recycling. Nat Rev Mol Cell Biol. 2004;5(2):121-32.

70. Poea-Guyon S, Ammar MR, Erard M, Amar M, Moreau AW, Fossier P, et al. The V-ATPase membrane domain is a sensor of granular pH that controls the exocytotic machinery. J Cell Biol. 2013;203(2):283-98.

71. Kornak U, Reynders E, Dimopoulou A, van Reeuwijk J, Fischer B, Rajab A, et al. Impaired glycosylation and cutis laxa caused by mutations in the vesicular H+-ATPase subunit ATP6V0A2. Nat Genet. 2007;40:32.

72. Saftig P, Klumperman J. Lysosome biogenesis and lysosomal membrane proteins: trafficking meets function. Nat Rev Mol Cell Biol. 2009;10(9):623-35.

73. Williamson WR, Hiesinger PR. On the role of v-ATPase V0a1-dependent degradation in Alzheimer disease. Commun Integr Biol. 2010;3(6):604-7.

74. Strasser B, Iwaszkiewicz J, Michielin O, Mayer A. The V-ATPase proteolipid cylinder promotes the lipid-mixing stage of SNARE-dependent fusion of yeast vacuoles. Embo J. 2011;30(20):4126-41.

75. Stransky L, Cotter K, Forgac M. The Function of V-ATPases in Cancer. Physiol Rev. 2016;96(3):1071-91.

76. Zoncu R, Bar-Peled L, Efeyan A, Wang S, Sancak Y, Sabatini DM. mTORC1 senses lysosomal amino acids through an inside-out mechanism that requires the vacuolar H(+)-ATPase. Science. 2011;334(6056):678-83.

77. Maranda B, Brown D, Bourgoin S, Casanova JE, Vinay P, Ausiello DA, et al. Intra-endosomal pH-sensitive recruitment of the Arf-nucleotide exchange factor ARNO and Arf6 from cytoplasm to proximal tubule endosomes. J Biol Chem. 2001;276(21):18540-50.

78. Marshansky V. The V-ATPase a2-subunit as a putative endosomal pH-sensor. Biochem Soc Trans. 2007;35(Pt 5):1092-9.

79. Merkulova M, Hurtado-Lorenzo A, Hosokawa H, Zhuang Z, Brown D, Ausiello DA, et al. Aldolase directly interacts with ARNO and modulates cell morphology and acidic vesicle distribution. Am J Physiol Cell Physiol. 2011;300(6):C1442-C55.

80. Marshansky V, Rubinstein JL, Grüber G. Eukaryotic V-ATPase: Novel structural findings and functional insights. Biochimica et Biophysica Acta (BBA) - Bioenergetics. 2014;1837(6):857-79.

81. Yan Y, Denef N, Schüpbach T. The vacuolar proton pump (V-ATPase) is required for Notch signaling and endosomal trafficking in Drosophila. Dev Cell. 2009;17(3):387-402.

82. Roy M, Pear WS, Aster JC. The multifaceted role of Notch in cancer. Curr Opin Genet Dev. 2007;17(1):52-9.

83. Vaccari T, Duchi S, Cortese K, Tacchetti C, Bilder D. The vacuolar ATPase is required for physiological as well as pathological activation of the Notch receptor. Development (Cambridge, England). 2010;137(11):1825-32.

84. Kobia F, Duchi S, Deflorian G, Vaccari T. Pharmacologic inhibition of vacuolar H+ ATPase reduces physiologic and oncogenic Notch signaling. Mol Oncol. 2014;8(2):207-20.

85. George A, Leahy H, Zhou J, Morin PJ. The vacuolar-ATPase inhibitor bafilomycin and mutant VPS35 inhibit canonical Wnt signaling. Neurobiol Dis. 2007;26(1):125-33.

86. Cruciat CM, Ohkawara B, Acebron SP, Karaulanov E, Reinhard C, Ingelfinger D, et al. Requirement of prorenin receptor and vacuolar H+-ATPase-mediated acidification for Wnt signaling. Science. 2010;327(5964):459-63.

87. Liu P, Chen H, Han L, Zou X, Shen W. Expression and role of V1A subunit of V-ATPases in gastric cancer cells. Int J Clin Oncol. 2015;20(4):725-35.

88. Chung C, Mader CC, Schmitz JC, Atladottir J, Fitchev P, Cornwell ML, et al. The vacuolar-ATPase modulates matrix metalloproteinase isoforms in human pancreatic cancer. Lab Invest. 2011;91(5):732-43.

89. Feng S, Zhu G, McConnell M, Deng L, Zhao Q, Wu M, et al. Silencing of atp6v1c1 prevents breast cancer growth and bone metastasis. Int J Biol Sci. 2013;9(8):853-62.

90. Lu Q, Lu S, Huang L, Wang T, Wan Y, Zhou CX, et al. The expression of V-ATPase is associated with drug resistance and pathology of non-small-cell lung cancer. Diagn Pathol. 2013;8:145-.

91. Xu J, Xie R, Liu X, Wen G, Jin H, Yu Z, et al. Expression and functional role of vacuolar H(+)-ATPase in human hepatocellular carcinoma. Carcinogenesis. 2012;33(12):2432-40.

92. Garcia-Garcia A, Perez-Sayans Garcia M, Rodriguez MJ, Antunez-Lopez J, Barros-Angueira F, Somoza-Martin M, et al. Immunohistochemical localization of C1 subunit of V-ATPase (ATPase C1) in oral squamous cell cancer and normal oral mucosa. Biotech Histochem. 2012;87(2):133-9.

93. Capecci J, Forgac M. The function of vacuolar ATPase (V-ATPase) a subunit isoforms in invasiveness of MCF10a and MCF10CA1a human breast cancer cells. J Biol Chem. 2013;288(45):32731-41.

94. McConnell M, Feng S, Chen W, Zhu G, Shen D, Ponnazhagan S, et al. Osteoclast proton pump regulator Atp6v1c1 enhances breast cancer growth by activating the

mTORC1 pathway and bone metastasis by increasing V-ATPase activity. Oncotarget. 2017.

95. Chueca E, Apostolova N, Esplugues JV, García-González MA, Lanas Á, Piazuelo E. Proton Pump Inhibitors Display Antitumor Effects in Barrett's Adenocarcinoma Cells. Front Pharmacol. 2016;7:452.

96. Huang L, Lu Q, Han Y, Li Z, Zhang Z, Li X. ABCG2/V-ATPase was associated with the drug resistance and tumor metastasis of esophageal squamous cancer cells. Diagn Pathol. 2012;7:180-.

97. Son SW, Kim S-H, Moon E-Y, Kim D-H, Pyo S, Um SH. Prognostic significance and function of the vacuolar H(+)-ATPase subunit V1E1 in esophageal squamous cell carcinoma. Oncotarget. 2016;7(31):49334-48.

98. Ohta T, Numata M, Yagishita H, Futagami F, Tsukioka Y, Kitagawa H, et al. Expression of 16 kDa proteolipid of vacuolar-type H(+)-ATPase in human pancreatic cancer. British Journal of Cancer. 1996;73(12):1511-7.

99. Perez-Sayans M, Reboiras-Lopez MD, Somoza-Martin JM, Barros-Angueira F, Diz PG, Rey JM, et al. Measurement of ATP6V1C1 expression in brush cytology samples as a diagnostic and prognostic marker in oral squamous cell carcinoma. Cancer Biol Ther. 2010;9(12):1057-64.

100. Kulshrestha A, Katara GK, Ibrahim S, Pamarthy S, Jaiswal MK, Sachs AG, et al. Vacuolar ATPase ‘a2’ isoform exhibits distinct cell surface accumulation and modulates matrix metalloproteinase activity in ovarian cancer. Oncotarget. 2015;6(6):3797-810.

101. Song T, Jeon HK, Hong JE, Choi JJ, Kim TJ, Choi CH, et al. Proton Pump Inhibition Enhances the Cytotoxicity of Paclitaxel in Cervical Cancer. Cancer Res Treat. 2017;49(3):595-606.

102. Cotter K, Liberman R, Sun-Wada G, Wada Y, Sgroi D, Naber S, et al. The a3 isoform of subunit a of the vacuolar ATPase localizes to the plasma membrane of invasive breast tumor cells and is overexpressed in human breast cancer. Oncotarget. 2016;7(29):46142-57.

103. Katara GK, Jaiswal MK, Kulshrestha A, Kolli B, Gilman-Sachs A, Beaman KD. Tumor-associated vacuolar ATPase subunit promotes tumorigenic characteristics in macrophages. Oncogene. 2014;33(49):5649-54.

104. Gleize V, Boisselier B, Marie Y, Poea-Guyon S, Sanson M, Morel N. The renal v-ATPase a4 subunit is expressed in specific subtypes of human gliomas. Glia. 2012;60(6):1004-12.

105. Green MR, Kihira S, Liu CL, Nair RV, Salari R, Gentles AJ, et al. Mutations in early follicular lymphoma progenitors are associated with suppressed antigen presentation. Proc Natl Acad Sci U S A. 2015;112(10):E1116-E25.

106. Okosun J, Wolfson RL, Wang J, Araf S, Wilkins L, Castellano BM, et al. Recurrent mTORC1-activating RRAGC mutations in follicular lymphoma. Nat Genet. 2016;48(2):183-8.

107. Forbes SA, Beare D, Boutselakis H, Bamford S, Bindal N, Tate J, et al. COSMIC: somatic cancer genetics at high-resolution. Nucleic Acids Res. 2017;45(D1):D777-D83.

108. Avnet S, Di Pompo G, Lemma S, Salerno M, Perut F, Bonuccelli G, et al. V-ATPase is a candidate therapeutic target for Ewing sarcoma. Biochim Biophys Acta. 2013;1832(8):1105-16.

109. Cotter K, Capecci J, Sennoune S, Huss M, Maier M, Martinez-Zaguilan R, et al. Activity of Plasma Membrane V-ATPases Is Critical for the Invasion of MDA-MB231 Breast Cancer Cells. J Biol Chem. 2015;290(6):3680-92.

110. Nishisho T, Hata K, Nakanishi M, Morita Y, Sun-Wada G-H, Wada Y, et al. The a3 Isoform Vacuolar Type H+-ATPase Promotes Distant Metastasis in the Mouse B16 Melanoma Cells. Molecular Cancer Research. 2011;9(7):845-55.

111. Zou P, Yang Y, Xu X, Liu B, Mei F, You J, et al. Silencing of vacuolar ATPase c subunit ATP6V0C inhibits the invasion of prostate cancer cells through a LASS2/TMSG1-independent manner. Oncol Rep. 2018;39(1):298-306.

112. Uhlman A, Folkers K, Liston J, Pancholi H, Hinton A. Effects of Vacuolar H(+)-ATPase Inhibition on Activation of Cathepsin B and Cathepsin L Secreted from MDA-MB231 Breast Cancer Cells. Cancer Microenviron. 2017;10(1-3):49-56.

113. Gocheva V, Joyce JA. Cysteine Cathepsins and the Cutting Edge of Cancer Invasion. Cell Cycle. 2007;6(1):60-4.

114. Lu X, Qin W, Li J, Tan N, Pan D, Zhang H, et al. The growth and metastasis of human hepatocellular carcinoma xenografts are inhibited by small interfering RNA targeting to the subunit ATP6L of proton pump. Cancer Res. 2005;65(15):6843-9.

115. Hendrix A, Sormunen R, Westbroek W, Lambein K, Denys H, Sys G, et al. Vacuolar H+ ATPase expression and activity is required for Rab27B-dependent invasive growth and metastasis of breast cancer. Int J Cancer. 2013;133(4):843-54.

116. Kubisch R, Fröhlich T, Arnold GJ, Schreiner L, Schwarzenberg K, Roidl A, et al. V-ATPase inhibition by archazolid leads to lysosomal dysfunction resulting in impaired cathepsin B activation in vivo. Int J Cancer. 2014;134(10):2478-88.

117. Lin H-H, Lin H-K, Lin IH, Chiou Y-W, Chen H-W, Liu C-Y, et al. Mechanical phenotype of cancer cells: cell softening and loss of stiffness sensing. Oncotarget. 2015;6(25):20946-58.

118. Bartel K, Winzi M, Ulrich M, Koeberle A, Menche D, Werz O, et al. V-ATPase inhibition increases cancer cell stiffness and blocks membrane related Ras signaling - a new option for HCC therapy. Oncotarget. 2017;8(6):9476-87.

119. Katara GK, Kulshrestha A, Mao L, Wang X, Sahoo M, Ibrahim S, et al. Mammary epithelium-specific inactivation of V-ATPase reduces stiffness of extracellular matrix and enhances metastasis of breast cancer. Mol Oncol. 2018;12(2):208-23.

120. Feng S, Cai M, Liu P, Wei L, Wang J, Qi J, et al. Atp6v1c1 May Regulate Filament Actin Arrangement in Breast Cancer Cells. PloS one. 2014;9(1):e84833.

121. Licon-Munoz Y, Michel V, Fordyce CA, Parra KJ. F-actin reorganization by V-ATPase inhibition in prostate cancer. Biol Open. 2017;6(11):1734-44.

122. Wiedmann RM, von Schwarzenberg K, Palamidessi A, Schreiner L, Kubisch R, Liebl J, et al. The V-ATPase-Inhibitor Archazolid Abrogates Tumor Metastasis via Inhibition of Endocytic Activation of the Rho-GTPase Rac1. Cancer Res. 2012;72(22):5976-87.

123. Tarrado-Castellarnau M, de Atauri P, Cascante M. Oncogenic regulation of tumor metabolic reprogramming. Oncotarget. 2016;7(38):62726-53.

124. Cairns RA, Harris IS, Mak TW. Regulation of cancer cell metabolism. Nature Reviews Cancer. 2011;11:85.

125. Liberti MV, Locasale JW. The Warburg Effect: How Does it Benefit Cancer Cells? Trends Biochem Sci. 2016;41(3):211-8.

126. Fogarty FM, O'Keeffe J, Zhadanov A, Papkovsky D, Ayllon V, O'Connor R. HRG-1 enhances cancer cell invasive potential and couples glucose metabolism to cytosolic/extracellular pH gradient regulation by the vacuolar-H+ ATPase. Oncogene. 2013;33:4653.

127. Zhang CS, Hawley SA, Zong Y, Li M, Wang Z, Gray A, et al. Fructose-1,6-bisphosphate and aldolase mediate glucose sensing by AMPK. Nature. 2017;548(7665):112-6.

128. Katara GK, Kulshrestha A, Jaiswal MK, Pamarthy S, Gilman-Sachs A, Beaman KD. Inhibition of vacuolar ATPase subunit in tumor cells delays tumor growth by decreasing the essential macrophage population in the tumor microenvironment. Oncogene. 2015;35:1058.

129. Bowman EJ, Siebers A, Altendorf K. Bafilomycins: a class of inhibitors of membrane ATPases from microorganisms, animal cells, and plant cells. Proc Natl Acad Sci U S A. 1988;85(21):7972-6.

130. Huss M, Wieczorek H. Inhibitors of V-ATPases: old and new players. J Exp Biol. 2009;212(Pt 3):341-6.

131. Morimura T, Fujita K, Akita M, Nagashima M, Satomi A. The proton pump inhibitor inhibits cell growth and induces apoptosis in human hepatoblastoma. Pediatr Surg Int. 2008;24(10):1087-94.

132. Lebreton S, Jaunbergs J, Roth MG, Ferguson DA, De Brabander JK. Evaluating the potential of vacuolar ATPase inhibitors as anticancer agents and multigram synthesis of the potent salicylihalamide analog saliphenylhalamide. Bioorg Med Chem Lett. 2008;18(22):5879-83.

133. Whitehurst AW, Bodemann BO, Cardenas J, Ferguson D, Girard L, Peyton M, et al. Synthetic lethal screen identification of chemosensitizer loci in cancer cells. Nature. 2007;446(7137):815-9.

134. von Schwarzenberg K, Wiedmann RM, Oak P, Schulz S, Zischka H, Wanner G, et al. Mode of Cell Death Induction by Pharmacological Vacuolar H(+)-ATPase (V-ATPase) Inhibition. J Biol Chem. 2013;288(2):1385-96.

135. Hong J, Nakano Y, Yokomakura A, Ishihara K, Kim S, Kang Y-S, et al. Nitric Oxide Production by the Vacuolar-Type (H⁺)-ATPase Inhibitors Bafilomycin A1 and Concanamycin A and Its Possible Role in Apoptosis in RAW 264.7 Cells. J Pharmacol Exp Ther. 2006;319(2):672-81.

136. Schempp CM, von Schwarzenberg K, Schreiner L, Kubisch R, Müller R, Wagner E, et al. V-ATPase Inhibition Regulates Anoikis Resistance and Metastasis of Cancer Cells. Mol Cancer Ther. 2014;13(4):926-37.

137. McHenry P, Wang WLW, Devitt E, Kluesner N, Davisson VJ, McKee E, et al. Iejimalides A and B inhibit lysosomal vacuolar H+-ATPase (V-ATPase) activity and induce S-phase arrest and apoptosis in MCF-7 cells. J Cell Biochem. 2010;109(4):634-42.

138. Wu YC, Wu WK, Li Y, Yu L, Li ZJ, Wong CC, et al. Inhibition of macroautophagy by bafilomycin A1 lowers proliferation and induces apoptosis in colon cancer cells. Biochem Biophys Res Commun. 2009;382(2):451-6.

139. Schneider LS, von Schwarzenberg K, Lehr T, Ulrich M, Kubisch-Dohmen R, Liebl J, et al. Vacuolar-ATPase Inhibition Blocks Iron Metabolism to Mediate Therapeutic Effects in Breast Cancer. Cancer Res. 2015;75(14):2863-74.

140. McGuire C, Cotter K, Stransky L, Forgac M. Regulation of V-ATPase Assembly and Function of V-ATPases in Tumor Cell Invasiveness. Biochim Biophys Acta. 2016;1857(8):1213-8.

141. Mauvezin C, Nagy P, Juhász G, Neufeld TP. Autophagosome–lysosome fusion is independent of V-ATPase-mediated acidification. Nature Communications. 2015;6:7007.

142. Mijaljica D, Prescott M, Devenish RJ. V-ATPase engagement in autophagic processes. Autophagy. 2011;7(6):666-8.

143. Gao Y, Liu Y, Hong L, Yang Z, Cai X, Chen X, et al. Golgi-associated LC3 lipidation requires V-ATPase in noncanonical autophagy. Cell Death Dis. 2016;7(8):e2330.

144. Guo H, Chitiprolu M, Roncevic L, Javalet C, Hemming FJ, Trung MT, et al. Atg5 Disassociates the V1V0-ATPase to Promote Exosome Production and Tumor Metastasis Independent of Canonical Macroautophagy. Dev Cell. 2017;43(6):716-30.e7.

145. Santana-Codina N, Mancias JD, Kimmelman AC. The Role of Autophagy in Cancer. Annual Review of Cancer Biology. 2017;1(1):19-39.

146. Graham RM, Thompson JW, Webster KA. Inhibition of the vacuolar ATPase induces Bnip3-dependent death of cancer cells and a reduction in tumor burden and metastasis. Oncotarget. 2014;5(5):1162-73.

147. Straud S, Zubovych I, De Brabander JK, Roth MG. Inhibition of Iron Uptake Is Responsible for Differential Sensitivity to V-ATPase Inhibitors in Several Cancer Cell Lines. PloS one. 2010;5(7):e11629.

148. Ikemura K, Hiramatsu S, Okuda M. Drug Repositioning of Proton Pump Inhibitors for Enhanced Efficacy and Safety of Cancer Chemotherapy. Front Pharmacol. 2017;8:911.

149. Luciani F, Spada M, De Milito A, Molinari A, Rivoltini L, Montinaro A, et al. Effect of proton pump inhibitor pretreatment on resistance of solid tumors to cytotoxic drugs. J Natl Cancer Inst. 2004;96(22):1702-13.

150. De Milito A, Canese R, Marino ML, Borghi M, Iero M, Villa A, et al. pH-dependent antitumor activity of proton pump inhibitors against human melanoma is mediated by inhibition of tumor acidity. Int J Cancer. 2010;127(1):207-19.

151. Sabolic I, Brown D, Verbavatz JM, Kleinman J. H(+)-ATPases of renal cortical and medullary endosomes are differentially sensitive to Sch-28080 and omeprazole. American Journal of Physiology-Renal Physiology. 1994;266(6):F868-F77.

152. von Schwarzenberg K, Lajtos T, Simon L, Müller R, Vereb G, Vollmar AM. V-ATPase inhibition overcomes trastuzumab resistance in breast cancer. Mol Oncol. 2014;8(1):9-19.

153. Sasazawa Y, Futamura Y, Tashiro E, Imoto M. Vacuolar H+-ATPase inhibitors overcome Bcl-xL-mediated chemoresistance through restoration of a caspase-independent apoptotic pathway. Cancer Sci. 2009;100(8):1460-7.

154. Murakami T, Shibuya I, Ise T, Chen ZS, Akiyama S, Nakagawa M, et al. Elevated expression of vacuolar proton pump genes and cellular PH in cisplatin resistance. Int J Cancer. 2001;93(6):869-74.

155. You H, Jin J, Shu H, Yu B, Milito AD, Lozupone F, et al. Small interfering RNA targeting the subunit ATP6L of proton pump V-ATPase overcomes chemoresistance of breast cancer cells. Cancer Lett. 2009;280(1):110-9.

156. Xu X, Liu B, Zou P, Zhang Y, You J, Pei F. Silencing of LASS2/TMSG1 enhances invasion and metastasis capacity of prostate cancer cell. J Cell Biochem. 2014;115(4):731-43.

157. Fan S, Niu Y, Tan N, Wu Z, Wang Y, You H, et al. LASS2 enhances chemosensitivity of breast cancer by counteracting acidic tumor microenvironment through inhibiting activity of V-ATPase proton pump. Oncogene. 2013;32(13):1682-90.

158. Lozupone F, Borghi M, Marzoli F, Azzarito T, Matarrese P, Iessi E, et al. TM9SF4 is a novel V-ATPase-interacting protein that modulates tumor pH alterations associated with drug resistance and invasiveness of colon cancer cells. Oncogene. 2015;34(40):5163-74.

159. UK CR. Prostate cancer incidence statistics [Available from: https://www.cancerresearchuk.org/health-professional/cancer-statistics/statistics-by-cancer-type/prostate-cancer.

160. Welty CJ, Cowan JE, Nguyen H, Shinohara K, Perez N, Greene KL, et al. Extended Followup and Risk Factors for Disease Reclassification in a Large Active Surveillance Cohort for Localized Prostate Cancer. J Urol. 2015;193(3):807-11.

161. Kirby M, Hirst C, Crawford ED. Characterising the castration-resistant prostate cancer population: a systematic review. Int J Clin Prac. 2011;65(11):1180-92.

162. Huggins C, Hodges CV. Studies on Prostatic Cancer. I. The Effect of Castration, of Estrogen and of Androgen Injection on Serum Phosphatases in Metastatic Carcinoma of the Prostate. Cancer Res. 1941;1(4):293-7.

163. Thomas C, Bogemann M, Konig F, Machtens S, Schostak M, Steuber T, et al. [Advanced Prostate Cancer Consensus Conference (APCCC) 2015 in St. Gallen : Critical review of the recommendations on diagnosis and therapy of metastatic prostate cancer by a German expert panel]. Urologe A. 2016;55(6):772-82.

164. Nelson PS, Clegg N, Arnold H, Ferguson C, Bonham M, White J, et al. The program of androgen-responsive genes in neoplastic prostate epithelium. PNAS. 2002;99(18):11890-5.

165. Viger RS, Silversides DW, Tremblay JJ. New Insights into the Regulation of Mammalian Sex Determination and Male Sex Differentiation. Vitamins & Hormones. 70: Academic Press; 2005. p. 387-413.

166. Russell DW, Wilson JD. STEROID 5α-REDUCTASE: TWO GENES/TWO ENZYMES. Annu Rev Biochem. 1994;63(1):25-61.

167. Brinkmann AO. Molecular mechanisms of androgen action--a historical perspective. Methods Mol Biol. 2011;776:3-24.

168. Robinson-Rechavi M, Carpentier A-S, Duffraisse M, Laudet V. How many nuclear hormone receptors are there in the human genome? Trends Genet. 2001;17(10):554-6.

169. Chmelar R, Buchanan G, Need EF, Tilley W, Greenberg NM. Androgen receptor coregulators and their involvement in the development and progression of prostate cancer. Int J Cancer. 2007;120(4):719-33.

170. Lee Y-F, Shyr C-R, Thin TH, Lin W-J, Chang C. Convergence of two repressors through heterodimer formation of androgen receptor and testicular orphan receptor-4: A

unique signaling pathway in the steroid receptor superfamily. PNAS. 1999;96(26):14724-9.

171. Lubahn DB, Joseph DR, Sar M, Tan J, Higgs HN, Larson RE, et al. The human androgen receptor: complementary deoxyribonucleic acid cloning, sequence analysis and gene expression in prostate. Mol Endocrinol. 1988;2(12):1265-75.

172. Hay CW, Hunter I, MacKenzie A, McEwan IJ. An Sp1 Modulated Regulatory Region Unique to Higher Primates Regulates Human Androgen Receptor Promoter Activity in Prostate Cancer Cells. PLoS One. 2015;10(10):e0139990.

173. Burnstein KL. Regulation of androgen receptor levels: implications for prostate cancer progression and therapy. J Cell Biochem. 2005;95(4):657-69.

174. Hay CW, Watt K, Hunter I, Lavery DN, MacKenzie A, McEwan IJ. Negative regulation of the androgen receptor gene through a primate-specific androgen response element present in the 5' UTR. Horm Cancer. 2014;5(5):299-311.

175. Huang P, Chandra V, Rastinejad F. Structural overview of the nuclear receptor superfamily: insights into physiology and therapeutics. Annu Rev Physiol. 2010;72:247-72.

176. Nance MA. Clinical aspects of CAG repeat diseases. Brain Pathol. 1997;7(3):881-900.

177. Cude KJ, Montgomery JS, Price DK, Dixon SC, Kincaid RL, Kovacs KF, et al. The role of an androgen receptor polymorphism in the clinical outcome of patients with metastatic prostate cancer. Urol Int. 2002;68(1):16-23.

178. Freedman ML, Pearce CL, Penney KL, Hirschhorn JN, Kolonel LN, Henderson BE, et al. Systematic evaluation of genetic variation at the androgen receptor locus and risk of prostate cancer in a multiethnic cohort study. Am J Hum Genet. 2005;76(1):82-90.

179. La Spada AR, Wilson EM, Lubahn DB, Harding AE, Fischbeck KH. Androgen receptor gene mutations in X-linked spinal and bulbar muscular atrophy. Nature. 1991;352(6330):77-9.

180. Coffey K, Robson CN. Regulation of the androgen receptor by post-translational modifications. J Endocrinol. 2012;215(2):221-37.

181. Gioeli D, Paschal BM. Post-translational modification of the androgen receptor. Mol Cell Endocrinol. 2012;352(1-2):70-8.

182. Gaughan L, Stockley J, Wang N, McCracken SRC, Treumann A, Armstrong K, et al. Regulation of the androgen receptor by SET9-mediated methylation. Nucleic Acids Res. 2011;39(4):1266-79.

183. Fu M, Rao M, Wang C, Sakamaki T, Wang J, Di Vizio D, et al. Acetylation of androgen receptor enhances coactivator binding and promotes prostate cancer cell growth. Mol Cell Biol. 2003;23(23):8563-75.

184. Xu K, Shimelis H, Linn DE, Jiang R, Yang X, Sun F, et al. Regulation of androgen receptor transcriptional activity and specificity by RNF6-induced ubiquitination. Cancer Cell. 2009;15(4):270-82.

185. Jenster G, de Ruiter PE, van der Korput HA, Kuiper GG, Trapman J, Brinkmann AO. Changes in the abundance of androgen receptor isotypes: effects of ligand treatment, glutamine-stretch variation, and mutation of putative phosphorylation sites. Biochemistry. 1994;33(47):14064-72.

186. Chen S, Gulla S, Cai C, Balk SP. Androgen receptor serine 81 phosphorylation mediates chromatin binding and transcriptional activation. J Biol Chem. 2012;287(11):8571-83.

187. Guo Z, Dai B, Jiang T, Xu K, Xie Y, Kim O, et al. Regulation of androgen receptor activity by tyrosine phosphorylation. Cancer Cell. 2006;10(4):309-19.

188. Liu Y, Karaca M, Zhang Z, Gioeli D, Earp HS, Whang YE. Dasatinib inhibits site-specific tyrosine phosphorylation of androgen receptor by Ack1 and Src kinases. Oncogene. 2010;29(22):3208-16.

189. Bennett NC, Gardiner RA, Hooper JD, Johnson DW, Gobe GC. Molecular cell biology of androgen receptor signalling. Int J Biochem Cell Biol. 2010;42(6):813-27.

190. Kim J, Coetzee GA. Prostate specific antigen gene regulation by androgen receptor. J Cell Biochem. 2004;93(2):233-41.

191. Tyagi RK, Lavrovsky Y, Ahn SC, Song CS, Chatterjee B, Roy AK. Dynamics of intracellular movement and nucleocytoplasmic recycling of the ligand-activated androgen receptor in living cells. Mol Endocrinol. 2000;14(8):1162-74.

192. Chen Y-W, Lee M-S, Lucht A, Chou F-P, Huang W, Havighurst TC, et al. TMPRSS2, a Serine Protease Expressed in the Prostate on the Apical Surface of Luminal Epithelial Cells and Released into Semen in Prostasomes, Is Misregulated in Prostate Cancer Cells. Am J Pathol. 2010;176(6):2986-96.

193. Lin B, Ferguson C, White JT, Wang S, Vessella R, True LD, et al. Prostate-localized and Androgen-regulated Expression of the Membrane-bound Serine Protease TMPRSS2. Cancer Res. 1999;59(17):4180-4.

194. Tomlins SA, Laxman B, Varambally S, Cao X, Yu J, Helgeson BE, et al. Role of the TMPRSS2-ERG Gene Fusion in Prostate Cancer. Neoplasia. 2008;10(2):177-88.

195. Foradori CD, Weiser MJ, Handa RJ. Non-genomic actions of androgens. Front Neuroendocrinol. 2008;29(2):169-81.

196. Taylor BS, Schultz N, Hieronymus H, Gopalan A, Xiao Y, Carver BS, et al. Integrative genomic profiling of human prostate cancer. Cancer Cell. 2010;18(1):11-22.

197. Bitting RL, Armstrong AJ. Targeting the PI3K/Akt/mTOR pathway in castration-resistant prostate cancer. Endocr Relat Cancer. 2013;20(3):R83-99.

198. Carver BS, Chapinski C, Wongvipat J, Hieronymus H, Chen Y, Chandarlapaty S, et al. Reciprocal feedback regulation of PI3K and androgen receptor signaling in PTEN-deficient prostate cancer. Cancer Cell. 2011;19(5):575-86.

199. Schweizer MT, Yu EY. Persistent androgen receptor addiction in castration-resistant prostate cancer. J Hematol Oncol. 2015;8:128.

200. Lu W, Tinsley HN, Keeton A, Qu Z, Piazza GA, Li Y. Suppression of Wnt/β-catenin signaling inhibits prostate cancer cell proliferation. Eur J Pharmacol. 2009;602(1):8-14.

201. Clevers H. Wnt/beta-catenin signaling in development and disease. Cell. 2006;127(3):469-80.

202. Yang F, Li X, Sharma M, Sasaki CY, Longo DL, Lim B, et al. Linking beta-catenin to androgen-signaling pathway. J Biol Chem. 2002;277(13):11336-44.

203. Unni E, Sun S, Nan B, McPhaul MJ, Cheskis B, Mancini MA, et al. Changes in androgen receptor nongenotropic signaling correlate with transition of LNCaP cells to androgen independence. Cancer Res. 2004;64(19):7156-68.

204. Bonaccorsi L, Muratori M, Carloni V, Marchiani S, Formigli L, Forti G, et al. The androgen receptor associates with the epidermal growth factor receptor in androgen-sensitive prostate cancer cells. Steroids. 2004;69(8-9):549-52.

205. Heidenreich A, Bastian PJ, Bellmunt J, Bolla M, Joniau S, van der Kwast T, et al. EAU Guidelines on Prostate Cancer. Part 1: Screening, Diagnosis, and Local Treatment with Curative Intent—Update 2013. Eur Urol. 2014;65(1):124-37.

206. Shen MM, Abate-Shen C. Molecular genetics of prostate cancer: new prospects for old challenges. Genes & development. 2010;24(18):1967-2000.

207. Lavery A, Kirby RS, Chowdhury S. Prostate cancer. Medicine. 2016;44(1):47-51.

208. Mateo J, Boysen G, Barbieri CE, Bryant HE, Castro E, Nelson PS, et al. DNA Repair in Prostate Cancer: Biology and Clinical Implications. Eur Urol. 2017;71(3):417-25.

209. Pritchard CC, Mateo J, Walsh MF, De Sarkar N, Abida W, Beltran H, et al. Inherited DNA-Repair Gene Mutations in Men with Metastatic Prostate Cancer. NEJM. 2016;375(5):443-53.

210. Gelmann EP, Steadman DJ, Ma J, Ahronovitz N, Voeller HJ, Swope S, et al. Occurrence of NKX3.1 C154T Polymorphism in Men with and without Prostate Cancer and Studies of Its Effect on Protein Function. Cancer Res. 2002;62(9):2654-9.

211. Chen H, Tu S-w, Hsieh J-T. Down-regulation of Human DAB2IP Gene Expression Mediated by Polycomb Ezh2 Complex and Histone Deacetylase in Prostate Cancer. JBC. 2005;280(23):22437-44.

212. Cuzick J, Thorat MA, Andriole G, Brawley OW, Brown PH, Culig Z, et al. Prevention and Early Detection of Prostate Cancer. Lancet Oncol. 2014;15(11):e484-e92.

213. Cantarutti A, Bonn SE, Adami HO, Gronberg H, Bellocco R, Balter K. Body mass index and mortality in men with prostate cancer. Prostate. 2015;75(11):1129-36.

214. Mottet N, van den Bergh RCN, Briers E, Bourke L, Cornford P, De Santis M, et al. EAU - ESTRO - ESUR - SIOG Guidelines on Prostate Cancer 2018. European Association of Urology Guidelines 2018 Edition. presented at the EAU Annual Congress Copenhagen 2018. Arnhem, The Netherlands: European Association of Urology Guidelines Office; 2018.

215. Hamdy FC, Donovan JL, Lane JA, Mason M, Metcalfe C, Holding P, et al. 10-Year Outcomes after Monitoring, Surgery, or Radiotherapy for Localized Prostate Cancer. NEJM. 2016;375(15):1415-24.

216. Heidenreich A, Bastian PJ, Bellmunt J, Bolla M, Joniau S, van der Kwast T, et al. EAU Guidelines on Prostate Cancer. Part II: Treatment of Advanced, Relapsing, and Castration-Resistant Prostate Cancer. Eur Urol. 2014;65(2):467-79.

217. Schmitt B, Wilt TJ, Schellhammer PF, DeMasi V, Sartor O, Crawford ED, et al. Combined androgen blockade with nonsteroidal antiandrogens for advanced prostate cancer: a systematic review. Urology. 2001;57(4):727-32.

218. Moul JW. Twenty years of controversy surrounding combined androgen blockade for advanced prostate cancer. Cancer. 2009;115(15):3376-8.

219. Sweeney CJ, Chen Y-H, Carducci M, Liu G, Jarrard DF, Eisenberger M, et al. Chemohormonal Therapy in Metastatic Hormone-Sensitive Prostate Cancer. NEJM. 2015;373(8):737-46.

220. James ND, Sydes MR, Clarke NW, Mason MD, Dearnaley DP, Spears MR, et al. Addition of docetaxel, zoledronic acid, or both to first-line long-term hormone therapy in prostate cancer (STAMPEDE): survival results from an adaptive, multiarm, multistage, platform randomised controlled trial. Lancet.387(10024):1163-77.

221. Tannock IF, de Wit R, Berry WR, Horti J, Pluzanska A, Chi KN, et al. Docetaxel plus Prednisone or Mitoxantrone plus Prednisone for Advanced Prostate Cancer. NEJM. 2004;351(15):1502-12.

222. Berthold DR, Pond GR, Soban F, Wit Rd, Eisenberger M, Tannock IF. Docetaxel Plus Prednisone or Mitoxantrone Plus Prednisone for Advanced Prostate Cancer: Updated Survival in the TAX 327 Study. J Clin Oncol. 2008;26(2):242-5.

223. Ramaswamy B, Puhalla S. Docetaxel: a tubulin-stabilizing agent approved for the management of several solid tumors. Drugs Today (Barc). 2006;42(4):265-79.

224. Seruga B, Tannock IF. Chemotherapy-Based Treatment for Castration-Resistant Prostate Cancer. J Clin Oncol. 2011;29(27):3686-94.

225. Vrignaud P, Semiond D, Benning V, Beys E, Bouchard H, Gupta S. Preclinical profile of cabazitaxel. Drug Des Devel Ther. 2014;8:1851-67.

226. de Bono JS, Oudard S, Ozguroglu M, Hansen S, Machiels JP, Kocak I, et al. Prednisone plus cabazitaxel or mitoxantrone for metastatic castration-resistant prostate cancer progressing after docetaxel treatment: a randomised open-label trial. Lancet. 2010;376(9747):1147-54.

227. Oudard S, Fizazi K, Sengelov L, Daugaard G, Saad F, Hansen S, et al. Cabazitaxel Versus Docetaxel As First-Line Therapy for Patients With Metastatic Castration-Resistant Prostate Cancer: A Randomized Phase III Trial-FIRSTANA. J Clin Oncol. 2017;35(28):3189-97.

228. Eisenberger M, Hardy-Bessard AC, Kim CS, Geczi L, Ford D, Mourey L, et al. Phase III Study Comparing a Reduced Dose of Cabazitaxel (20 mg/m(2)) and the Currently Approved Dose (25 mg/m(2)) in Postdocetaxel Patients With Metastatic Castration-Resistant Prostate Cancer-PROSELICA. J Clin Oncol. 2017;35(28):3198-206.

229. Attard G, Belldegrun AS, de Bono JS. Selective blockade of androgenic steroid synthesis by novel lyase inhibitors as a therapeutic strategy for treating metastatic prostate cancer. BJU Int. 2005;96(9):1241-6.

230. Fizazi K, Scher HI, Molina A, Logothetis CJ, Chi KN, Jones RJ, et al. Abiraterone acetate for treatment of metastatic castration-resistant prostate cancer: final overall survival analysis of the COU-AA-301 randomised, double-blind, placebo-controlled phase 3 study. Lancet Oncol. 2012;13(10):983-92.

231. Ryan CJ, Smith MR, de Bono JS, Molina A, Logothetis CJ, de Souza P, et al. Randomized Phase 3 Trial of Abiraterone Acetate in Men with Metastatic Castration-Resistant Prostate Cancer and No Prior Chemotherapy. NEJM. 2013;368(2):138-48.

232. Fizazi K, Scher HI, Molina A, Logothetis CJ, Chi KN, Jones RJ, et al. Abiraterone acetate for treatment of metastatic castration-resistant prostate cancer: final overall survival analysis of the COU-AA-301 randomised, double-blind, placebo-controlled phase 3 study. Lancet Oncol. 2012;13(10):983-92.

233. Li Z, Alyamani M, Li J, Rogacki K, Abazeed M, Upadhyay SK, et al. Redirecting abiraterone metabolism to fine-tune prostate cancer anti-androgen therapy. Nature. 2016;533(7604):547-51.

234. Tran C, Ouk S, Clegg NJ, Chen Y, Watson PA, Arora V, et al. Development of a Second-Generation Antiandrogen for Treatment of Advanced Prostate Cancer. Science (New York, NY). 2009;324(5928):787-90.

235. Scher HI, Fizazi K, Saad F, Taplin M-E, Sternberg CN, Miller K, et al. Increased Survival with Enzalutamide in Prostate Cancer after Chemotherapy. NEJM. 2012;367(13):1187-97.

236. Beer TM, Armstrong AJ, Rathkopf DE, Loriot Y, Sternberg CN, Higano CS, et al. Enzalutamide in Metastatic Prostate Cancer before Chemotherapy. NEJM. 2014;371(5):424-33.

237. Sumanasuriya S, De Bono J. Treatment of Advanced Prostate Cancer—A Review of Current Therapies and Future Promise. Cold Spring Harb Perspect Med. 2018;8(6).

238. Schrader AJ, Boegemann M, Ohlmann CH, Schnoeller TJ, Krabbe LM, Hajili T, et al. Enzalutamide in castration-resistant prostate cancer patients progressing after docetaxel and abiraterone. Eur Urol. 2014;65(1):30-6.

239. Mostaghel EA, Marck BT, Plymate SR, Vessella RL, Balk S, Matsumoto AM, et al. Resistance to CYP17A1 Inhibition with Abiraterone in Castration-Resistant Prostate Cancer: Induction of Steroidogenesis and Androgen Receptor Splice Variants. Clin Cancer Res. 2011;17(18):5913-25.

240. Rathkopf DE, Morris MJ, Fox JJ, Danila DC, Slovin SF, Hager JH, et al. Phase I study of ARN-509, a novel antiandrogen, in the treatment of castration-resistant prostate cancer. J Clin Oncol. 2013;31(28):3525-30.

241. Smith MR, Antonarakis ES, Ryan CJ, Berry WR, Shore ND, Liu G, et al. Phase 2 Study of the Safety and Antitumor Activity of Apalutamide (ARN-509), a Potent Androgen Receptor Antagonist, in the High-risk Nonmetastatic Castration-resistant Prostate Cancer Cohort. Eur Urol. 2016;70(6):963-70.

242. Smith MR, Saad F, Chowdhury S, Oudard S, Hadaschik BA, Graff JN, et al. Apalutamide Treatment and Metastasis-free Survival in Prostate Cancer. NEJM. 2018;378(15):1408-18.

243. Chi KN, Agarwal N, Bjartell A, Chung BH, Gomes AJPdS, Given RW, et al. First results from TITAN: A phase III double-blind, randomized study of apalutamide (APA) versus placebo (PBO) in patients (pts) with metastatic castration-sensitive prostate cancer (mCSPC) receiving androgen deprivation therapy (ADT). J Clin Oncol. 2019;37(15_suppl):5006-.

244. Fizazi K, Massard C, Bono P, Jones R, Kataja V, James N, et al. Activity and safety of ODM-201 in patients with progressive metastatic castration-resistant prostate cancer (ARADES): an open-label phase 1 dose-escalation and randomised phase 2 dose expansion trial. Lancet Oncol. 2014;15(9):975-85.

245. Fizazi K, Shore N, Tammela TL, Ulys A, Vjaters E, Polyakov S, et al. Darolutamide in Nonmetastatic, Castration-Resistant Prostate Cancer. NEJM. 2019;380(13):1235-46.

246. Smith MR, Saad F, Hussain M, Sternberg CN, Fizazi K, Yamada KS, et al. ARASENS: A phase 3 trial of darolutamide in combination with docetaxel for men with metastatic hormone-sensitive prostate cancer (mHSPC). J Clin Oncol. 2018;36(6_suppl):TPS383-TPS.

247. Parker C, Nilsson S, Heinrich D, Helle SI, O'Sullivan JM, Fosså SD, et al. Alpha Emitter Radium-223 and Survival in Metastatic Prostate Cancer. NEJM. 2013;369(3):213-23.

248. Di Lorenzo G, Ferro M, Buonerba C. Sipuleucel-T (Provenge(R)) for castration-resistant prostate cancer. BJU Int. 2012;110(2 Pt 2):E99-104.

249. Kantoff PW, Higano CS, Shore ND, Berger ER, Small EJ, Penson DF, et al. Sipuleucel-T immunotherapy for castration-resistant prostate cancer. N Engl J Med. 2010;363(5):411-22.

250. Simpson EL, Davis S, Thokala P, Breeze PR, Bryden P, Wong R. Sipuleucel-T for the Treatment of Metastatic Hormone-Relapsed Prostate Cancer: A NICE Single Technology Appraisal; An Evidence Review Group Perspective. PharmacoEconomics. 2015;33(11):1187-94.

251. Fizazi K, Carducci M, Smith M, Damião R, Brown J, Karsh L, et al. Denosumab versus zoledronic acid for treatment of bone metastases in men with castration-resistant prostate cancer: a randomised, double-blind study. Lancet. 2011;377(9768):813-22.

252. Nakazawa M, Antonarakis ES, Luo J. Androgen Receptor Splice Variants in the Era of Enzalutamide and Abiraterone. Horm Cancer. 2014;5(5):265-73.

253. Koivisto P, Visakorpi T, Kallioniemi OP. Androgen receptor gene amplification: a novel molecular mechanism for endocrine therapy resistance in human prostate cancer. Scand J Clin Lab Invest Suppl. 1996;226:57-63.

254. Visakorpi T, Hyytinen E, Koivisto P, Tanner M, Keinanen R, Palmberg C, et al. In vivo amplification of the androgen receptor gene and progression of human prostate cancer. Nat Genet. 1995;9(4):401-6.

255. Grad JM, Dai JL, Wu S, Burnstein KL. Multiple androgen response elements and a Myc consensus site in the androgen receptor (AR) coding region are involved in androgen-mediated up-regulation of AR messenger RNA. Mol Endocrinol. 1999;13(11):1896-911.

256. Yeap BB, Voon DC, Vivian JP, McCulloch RK, Thomson AM, Giles KM, et al. Novel binding of HuR and poly(C)-binding protein to a conserved UC-rich motif within the 3'-untranslated region of the androgen receptor messenger RNA. J Biol Chem. 2002;277(30):27183-92.

257. Cloke B, Shah K, Kaneda H, Lavery S, Trew G, Fusi L, et al. The poly(c)-binding protein-1 regulates expression of the androgen receptor. Endocrinology. 2010;151(8):3954-64.

258. Zhou H, Mazan-Mamczarz K, Martindale JL, Barker A, Liu Z, Gorospe M, et al. Post-transcriptional regulation of androgen receptor mRNA by an ErbB3 binding protein 1 in prostate cancer. Nucleic Acids Res. 2010;38(11):3619-31.

259. Zhang Y, Linn D, Liu Z, Melamed J, Tavora F, Young CY, et al. EBP1, an ErbB3-binding protein, is decreased in prostate cancer and implicated in hormone resistance. Mol Cancer Ther. 2008;7(10):3176-86.

260. Zhang Y, Fondell JD, Wang Q, Xia X, Cheng A, Lu ML, et al. Repression of androgen receptor mediated transcription by the ErbB-3 binding protein, Ebp1. Oncogene. 2002;21(36):5609-18.

261. Köhler A, Demir U, Kickstein E, Krauss S, Aigner J, Aranda-Orgillés B, et al. A hormone-dependent feedback-loop controls androgen receptor levels by limiting MID1, a novel translation enhancer and promoter of oncogenic signaling. Mol Cancer. 2014;13:146-.

262. Jernberg E, Bergh A, Wikström P. Clinical relevance of androgen receptor alterations in prostate cancer. 2017;6(8):R146.

263. Koochekpour S. Androgen receptor signaling and mutations in prostate cancer. Asian J Androl. 2010;12(5):639-57.

264. Veldscholte J, Ris-Stalpers C, Kuiper GG, Jenster G, Berrevoets C, Claassen E, et al. A mutation in the ligand binding domain of the androgen receptor of human LNCaP cells affects steroid binding characteristics and response to anti-androgens. Biochem Biophys Res Commun. 1990;173(2):534-40.

265. Fenton MA, Shuster TD, Fertig AM, Taplin ME, Kolvenbag G, Bubley GJ, et al. Functional characterization of mutant androgen receptors from androgen-independent prostate cancer. Clin Cancer Res. 1997;3(8):1383-8.

266. Taplin M-E, Bubley GJ, Ko Y-J, Small EJ, Upton M, Rajeshkumar B, et al. Selection for Androgen Receptor Mutations in Prostate Cancers Treated with Androgen Antagonist. Cancer Res. 1999;59(11):2511-5.

267. Culig Z, Hobisch A, Cronauer MV, Cato AC, Hittmair A, Radmayr C, et al. Mutant androgen receptor detected in an advanced-stage prostatic carcinoma is activated by adrenal androgens and progesterone. Mol Endocrinol. 1993;7(12):1541-50.

268. Steketee K, Timmerman L, Ziel-van der Made AC, Doesburg P, Brinkmann AO, Trapman J. Broadened ligand responsiveness of androgen receptor mutants obtained by random amino acid substitution of H874 and mutation hot spot T877 in prostate cancer. Int J Cancer. 2002;100(3):309-17.

269. Gaddipati JP, McLeod DG, Heidenberg HB, Sesterhenn IA, Finger MJ, Moul JW, et al. Frequent detection of codon 877 mutation in the androgen receptor gene in advanced prostate cancers. Cancer Res. 1994;54(11):2861-4.

270. Suzuki H, Akakura K, Komiya A, Aida S, Akimoto S, Shimazaki J. Codon 877 mutation in the androgen receptor gene in advanced prostate cancer: relation to antiandrogen withdrawal syndrome. Prostate. 1996;29(3):153-8.

271. Chen EJ, Sowalsky AG, Gao S, Cai C, Voznesensky O, Schaefer R, et al. Abiraterone treatment in castration-resistant prostate cancer selects for progesterone responsive mutant androgen receptors. Clin Cancer Res. 2015;21(6):1273-80.

272. Shi X-B, Ma A-H, Xia L, Kung H-J, de Vere White RW. Functional Analysis of 44 Mutant Androgen Receptors from Human Prostate Cancer. Cancer Res. 2002;62(5):1496-502.

273. Romanel A, Gasi Tandefelt D, Conteduca V, Jayaram A, Casiraghi N, Wetterskog D, et al. Plasma AR and abiraterone-resistant prostate cancer. Sci Transl Med. 2015;7(312):312re10-re10.

274. Wyatt AW, Azad AA, Volik SV, Annala M, Beja K, McConeghy B, et al. Genomic Alterations in Cell-Free DNA and Enzalutamide Resistance in Castration-Resistant Prostate Cancer. JAMA Oncol. 2016;2(12):1598-606.

275. Steinestel J, Luedeke M, Arndt A, Schnoeller TJ, Lennerz JK, Wurm C, et al. Detecting predictive androgen receptor modifications in circulating prostate cancer cells. Oncotarget. 2015;10(41):4213-23.

276. Joseph JD, Lu N, Qian J, Sensintaffar J, Shao G, Brigham D, et al. A clinically relevant androgen receptor mutation confers resistance to second-generation antiandrogens enzalutamide and ARN-509. Cancer Discov. 2013;3(9):1020-9.

277. Korpal M, Korn JM, Gao X, Rakiec DP, Ruddy DA, Doshi S, et al. An F876L Mutation in Androgen Receptor Confers Genetic and Phenotypic Resistance to MDV3100 (Enzalutamide). Cancer Discov. 2013;3(9):1030-43.

278. Balbas MD, Evans MJ, Hosfield DJ, Wongvipat J, Arora VK, Watson PA, et al. Overcoming mutation-based resistance to antiandrogens with rational drug design. eLife. 2013;2:e00499.

279. Hara T, Miyazaki J-i, Araki H, Yamaoka M, Kanzaki N, Kusaka M, et al. Novel Mutations of Androgen Receptor. A Possible Mechanism of Bicalutamide Withdrawal Syndrome. 2003;63(1):149-53.

280. Rathkopf DE, Smith MR, Ryan CJ, Berry WR, Shore ND, Liu G, et al. Androgen receptor mutations in patients with castration-resistant prostate cancer treated with apalutamide. Ann Oncol. 2017;28(9):2264-71.

281. Tepper CG, Boucher DL, Ryan PE, Ma AH, Xia L, Lee LF, et al. Characterization of a novel androgen receptor mutation in a relapsed CWR22 prostate cancer xenograft and cell line. Cancer Res. 2002;62(22):6606-14.

282. Sun S, Sprenger CCT, Vessella RL, Haugk K, Soriano K, Mostaghel EA, et al. Castration resistance in human prostate cancer is conferred by a frequently occurring androgen receptor splice variant. J Clin Invest. 2010;120(8):2715-30.

283. Zhu Y, Sharp A, Anderson CM, Silberstein JL, Taylor M, Lu C, et al. Novel Junction-specific and Quantifiable In Situ Detection of AR-V7 and its Clinical Correlates in Metastatic Castration-resistant Prostate Cancer. Eur Urol. 2018;73(5):727-35.

284. Welti J, Sharp A, Yuan W, Dolling D, Nava Rodrigues D, Figueiredo I, et al. Targeting Bromodomain and Extra-Terminal (BET) Family Proteins in Castration-Resistant Prostate Cancer (CRPC). Clin Cancer Res. 2018;24(13):3149-62.

285. Antonarakis ES, Lu C, Wang H, Luber B, Nakazawa M, Roeser JC, et al. AR-V7 and Resistance to Enzalutamide and Abiraterone in Prostate Cancer. NEJM. 2014;371(11):1028-38.

286. Hu R, Dunn TA, Wei S, Isharwal S, Veltri RW, Humphreys E, et al. Ligand-independent Androgen Receptor Variants Derived from Splicing of Cryptic Exons Signify Hormone Refractory Prostate Cancer. Cancer Res. 2009;69(1):16-22.

287. Qu Y, Dai B, Ye D, Kong Y, Chang K, Jia Z, et al. Constitutively active AR-V7 plays an essential role in the development and progression of castration-resistant prostate cancer. Sci Rep. 2015;5:7654-.

288. Sharp A, Coleman I, Yuan W, Sprenger C, Dolling D, Rodrigues DN, et al. Androgen receptor splice variant-7 expression emerges with castration resistance in prostate cancer. J Clin Invest. 2019;129(1):192-208.

289. Ceraline J, Cruchant MD, Erdmann E, Erbs P, Kurtz JE, Duclos B, et al. Constitutive activation of the androgen receptor by a point mutation in the hinge region: a new mechanism for androgen-independent growth in prostate cancer. Int J Cancer. 2004;108(1):152-7.

290. Armstrong CM, Gao AC. Current strategies for targeting the activity of androgen receptor variants. Asian J Urol. 2019;6(1):42-9.

291. Moigne RL, Zhou H-J, Mawji NR, Banuelos CA, Wang J, Jian K, et al. Next generation N-terminal domain androgen receptor inhibitors with improved potency and metabolic stability in castration-resistant prostate cancer models. J Clin Oncol. 2019;37(7_suppl):220-.

292. Bellacosa A, Kumar CC, Di Cristofano A, Testa JR. Activation of AKT kinases in cancer: implications for therapeutic targeting. Adv Cancer Res. 2005;94:29-86.

293. Yoshimoto M, Ludkovski O, DeGrace D, Williams JL, Evans A, Sircar K, et al. PTEN genomic deletions that characterize aggressive prostate cancer originate close to segmental duplications. Genes Chromosom Cancer. 2012;51(2):149-60.

294. Chee KG, Longmate J, Quinn DI, Chatta G, Pinski J, Twardowski P, et al. The AKT Inhibitor Perifosine in Biochemically Recurrent Prostate Cancer: A Phase II California/Pittsburgh Cancer Consortium Trial. Clin Genitourin Cancer.5(7):433-7.

295. Toren P, Kim S, Johnson F, Zoubeidi A. Combined AKT and MEK Pathway Blockade in Pre-Clinical Models of Enzalutamide-Resistant Prostate Cancer. PLoS One. 2016;11(4):e0152861.

296. ClinicalTrials.gov. A Study of Enzalutamide in Combination With AZD5363 in Patients With mCRPC (RE-AKT) 2015 [Available from: https://clinicaltrials.gov/ct2/show/NCT02525068.

297. Crabb SJ, Birtle AJ, Martin K, Downs N, Ratcliffe I, Maishman T, et al. ProCAID: a phase I clinical trial to combine the AKT inhibitor AZD5363 with docetaxel and prednisolone chemotherapy for metastatic castration resistant prostate cancer. Invest New Drugs. 2017;35(5):599-607.

298. Gallagher DJ, Gaudet MM, Pal P, Kirchhoff T, Balistreri L, Vora K, et al. Germline BRCA Mutations Denote a Clinicopathologic Subset of Prostate Cancer. Clin Cancer Res. 2010;16(7):2115-21.

299. Graff JN, Alumkal JJ, Drake CG, Thomas GV, Redmond WL, Farhad M, et al. Early evidence of anti-PD-1 activity in enzalutamide-resistant prostate cancer. Oncotarget. 2016;7(33):52810-7.

300. Slovin SF, Higano CS, Hamid O, Tejwani S, Harzstark A, Alumkal JJ, et al. Ipilimumab alone or in combination with radiotherapy in metastatic castration-resistant prostate cancer: results from an open-label, multicenter phase I/II study. Ann Oncol. 2013;24(7):1813-21.

301. Kwon ED, Drake CG, Scher HI, Fizazi K, Bossi A, van den Eertwegh AJM, et al. Ipilimumab versus placebo after radiotherapy in patients with metastatic castration-resistant prostate cancer that had progressed after docetaxel chemotherapy (CA184-043): a multicentre, randomised, double-blind, phase 3 trial. Lancet Oncol. 2014;15(7):700-12.

302. Haffner MC, Guner G, Taheri D, Netto GJ, Palsgrove DN, Zheng Q, et al. Comprehensive Evaluation of Programmed Death-Ligand 1 Expression in Primary and Metastatic Prostate Cancer. Am J Pathol. 2018;188(6):1478-85.

303. de Bono J, Goh J, Ojamaa K, Piulats J, Drake C, Hoimes C, et al. KEYNOTE-199: Pembrolizumab (pembro) for docetaxel-refractory metastatic castration-resistant prostate cancer (mCRPC). J Clin Oncol. 2018;36:5007-.

304. Manogue C, Cotogno P, Ledet E, Lewis B, Wyatt AW, Sartor O. Biomarkers for Programmed Death-1 Inhibition in Prostate Cancer. Oncologist. 2019;24(4):444-8.

305. Ledermann J, Harter P, Gourley C, Friedlander M, Vergote I, Rustin G, et al. Olaparib Maintenance Therapy in Platinum-Sensitive Relapsed Ovarian Cancer. NEJM. 2012;366(15):1382-92.

306. Mateo J, Carreira S, Sandhu S, Miranda S, Mossop H, Perez-Lopez R, et al. DNA-Repair Defects and Olaparib in Metastatic Prostate Cancer. NEJM. 2015;373(18):1697-708.

307. Goodall J, Mateo J, Yuan W, Mossop H, Porta N, Miranda S, et al. Circulating Cell-Free DNA to Guide Prostate Cancer Treatment with PARP Inhibition. Cancer Discov. 2017;7(9):1006-17.

308. Sella A, Yarom N, Zisman A, Kovel S. Paclitaxel, estramustine and carboplatin combination chemotherapy after initial docetaxel-based chemotherapy in castration-resistant prostate cancer. Oncology. 2009;76(6):442-6.

309. Ceccaldi R, O'Connor KW, Mouw KW, Li AY, Matulonis UA, D'Andrea AD, et al. A Unique Subset of Epithelial Ovarian Cancers with Platinum Sensitivity and PARP Inhibitor Resistance. Cancer Res. 2015;75(4):628-34.

310. Wang W-LW, McHenry P, Jeffrey R, Schweitzer D, Helquist P, Tenniswood M. Effects of Iejimalide B, a marine macrolide, on growth and apoptosis in prostate cancer cell lines. J Cell Biochem. 2008;105(4):998-1007.

311. Smith GA, Howell GJ, Phillips C, Muench SP, Ponnambalam S, Harrison MA. Extracellular and Luminal pH Regulation by Vacuolar H+-ATPase Isoform Expression and Targeting to the Plasma Membrane and Endosomes. J Biol Chem. 2016;291(16):8500-15.

312. Sennoune SR, Bermudez LE, Lees JC, Hirsch J, Filleur S, Martinez-Zaguilan R. Vacuolar H+-ATPase is down-regulated by the angiogenesis-inhibitory pigment epithelium-derived factor in metastatic prostate cancer cells. Cell Mol Biol (Noisy-le-grand). 2014;60(1):45-52.

313. Licon-Munoz Y, Fordyce CA, Hayek SR, Parra KJ. V-ATPase-dependent repression of androgen receptor in prostate cancer cells. Oncotarget. 2018;9(48):28921-34.

314. COSMIC. ATP6V1E2 Gene Analysis [Available from: http://cancer.sanger.ac.uk/cosmic/gene/analysis?ln=ATP6V1E2.

315. Mojica FJ, Juez G, Rodriguez-Valera F. Transcription at different salinities of Haloferax mediterranei sequences adjacent to partially modified PstI sites. Mol Microbiol. 1993;9(3):613-21.

316. Cong L, Ran FA, Cox D, Lin S, Barretto R, Habib N, et al. Multiplex genome engineering using CRISPR/Cas systems. Science. 2013;339(6121):819-23.

317. Ran FA, Hsu PD, Wright J, Agarwala V, Scott DA, Zhang F. Genome engineering using the CRISPR-Cas9 system. Nat Protoc. 2013;8:2281.

318. Bennardo N, Gunn A, Cheng A, Hasty P, Stark JM. Limiting the persistence of a chromosome break diminishes its mutagenic potential. PLoS Genet. 2009;5(10):e1000683-e.

319. Bétermier M, Bertrand P, Lopez BS. Is non-homologous end-joining really an inherently error-prone process? PLoS Genet. 2014;10(1):e1004086-e.

320. Ran FA, Hsu PD, Lin CY, Gootenberg JS, Konermann S, Trevino AE, et al. Double nicking by RNA-guided CRISPR Cas9 for enhanced genome editing specificity. Cell. 2013;154(6):1380-9.

321. Wakiuchi N, Tanimoto H, Harada H, Oji Y, Shiga H. Characterization of proton pumping and ATPase activities in microsomal fractions from barley roots. Soil Sci Plant Nutr. 1988;34(4):507-18.

322. Cox BE, Griffin EE, Ullery JC, Jerome WG. Effects of cellular cholesterol loading on macrophage foam cell lysosome acidification. J Lipid Res. 2007;48(5):1012-21.

323. Okosun J, Wolfson RL, Wang J, Araf S, Wilkins L, Castellano BM, et al. Recurrent mTORC1-activating RRAGC mutations in follicular lymphoma. Nat Genet. 2016;48(2):183-8.

324. Krysiak K, Gomez F, White BS, Matlock M, Miller CA, Trani L, et al. Recurrent somatic mutations affecting B-cell receptor signaling pathway genes in follicular lymphoma. Blood. 2017;129(4):473-83.

325. Wang F, Gatica D, Ying ZX, Peterson LF, Kim P, Bernard D, et al. Follicular lymphoma-associated mutations in vacuolar ATPase ATP6V1B2 activate autophagic flux and mTOR. J Clin Invest. 2019;130(4):1626-40.

326. Baykara O, Bakir B, Buyru N, Kaynak K, Dalay N. Amplification of chromosome 8 genes in lung cancer. J Cancer. 2015;6(3):270-5.

327. Kang JU. Chromosome 8q as the most frequent target for amplification in early gastric carcinoma. Oncol Lett. 2014;7(4):1139-43.

328. Tate JG, Bamford S, Jubb HC, Sondka Z, Beare DM, Bindal N, et al. COSMIC: the Catalogue Of Somatic Mutations In Cancer. Nucleic Acids Res. 2018;47(D1):D941-D7.

329. Zhao J, Benlekbir S, Rubinstein JL. Electron cryomicroscopy observation of rotational states in a eukaryotic V-ATPase. Nature. 2015;521(7551):241-5.

330. Kane PM. Disassembly and Reassembly of the Yeast Vacuolar H+-ATPase in Vivo. JBC. 1995;270(28):17025-32.

331. Parra KJ, Kane PM. Reversible Association between the V₁and V₀ Domains of Yeast Vacuolar H⁺-ATPase Is an Unconventional Glucose-Induced Effect. Mol Cell Biol. 1998;18(12):7064-74.

332. Yoshimori T, Yamamoto A, Moriyama Y, Futai M, Tashiro Y. Bafilomycin A1, a specific inhibitor of vacuolar-type H(+)-ATPase, inhibits acidification and protein degradation in lysosomes of cultured cells. J Biol Chem. 1991;266(26):17707-12.

333. Drose S, Bindseil KU, Bowman EJ, Siebers A, Zeeck A, Altendorf K. Inhibitory effect of modified bafilomycins and concanamycins on P- and V-type adenosinetriphosphatases. Biochemistry. 1993;32(15):3902-6.

334. Li Y, Chan SC, Brand LJ, Hwang TH, Silverstein KAT, Dehm SM. Androgen receptor splice variants mediate enzalutamide resistance in castration-resistant prostate cancer cell lines. Cancer Res. 2013;73(2):483-9.

335. Streicher W, Zengerling F, Laschak M, Weidemann W, Hopfner M, Schrader AJ, et al. AR-Q640X, a model to study the effects of constitutively active C-terminally truncated AR variants in prostate cancer cells. World J Urol. 2012;30(3):333-9.

336. Kallio HML, Hieta R, Latonen L, Brofeldt A, Annala M, Kivinummi K, et al. Constitutively active androgen receptor splice variants AR-V3, AR-V7 and AR-V9 are co-expressed in castration-resistant prostate cancer metastases. Br J Cancer. 2018;119(3):347-56.

337. Veldscholte J, Berrevoets CA, Ris-Stalpers C, Kuiper GG, Jenster G, Trapman J, et al. The androgen receptor in LNCaP cells contains a mutation in the ligand binding domain which affects steroid binding characteristics and response to antiandrogens. J Steroid Biochem Mol Biol. 1992;41(3-8):665-9.

338. Prekovic S, van Royen ME, Voet AR, Geverts B, Houtman R, Melchers D, et al. The Effect of F877L and T878A Mutations on Androgen Receptor Response to Enzalutamide. Mol Cancer Ther. 2016;15(7):1702-12.

339. Mwamukonda K, Chen Y, Ravindranath L, Furusato B, Hu Y, Sterbis J, et al. Quantitative expression of TMPRSS2 transcript in prostate tumor cells reflects TMPRSS2-ERG fusion status. Prostate Cancer Prostatic Dis. 2010;13(1):47-51.

340. Jin H-J, Kim J, Yu J. Androgen receptor genomic regulation. Transl Androl Urol. 2013;2(3):157-77.

341. Regufe da Mota S, Bailey S, Strivens RA, Hayden AL, Douglas LR, Duriez PJ, et al. LSD1 inhibition attenuates androgen receptor V7 splice variant activation in castration resistant prostate cancer models. Cancer Cell Int. 2018;18:71-.

342. Schalken J, Fitzpatrick JM. Enzalutamide: targeting the androgen signalling pathway in metastatic castration-resistant prostate cancer. BJU Int. 2016;117(2):215-25.

343. Wadosky KM, Koochekpour S. Androgen receptor splice variants and prostate cancer: From bench to bedside. Oncotarget. 2017;8(11):18550-76.

344. Lallous N, Volik SV, Awrey S, Leblanc E, Tse R, Murillo J, et al. Functional analysis of androgen receptor mutations that confer anti-androgen resistance identified in circulating cell-free DNA from prostate cancer patients. Genome Biol. 2016;17:10-.

345. Rathkopf DE, Smith MR, Ryan CJ, Berry WR, Shore ND, Liu G, et al. Androgen receptor mutations in patients with castration-resistant prostate cancer treated with apalutamide. Ann Oncol. 2017;28(9):2264-71.

346. Das AT, Tenenbaum L, Berkhout B. Tet-On Systems For Doxycycline-inducible Gene Expression. Curr Gene Ther. 2016;16(3):156-67.

347. Pamarthy S, Kulshrestha A, Katara GK, Beaman KD. The curious case of vacuolar ATPase: regulation of signaling pathways. Mol Cancer. 2018;17(1):41.

348. Lee HS, Qi Y, Im W. Effects of N-glycosylation on protein conformation and dynamics: Protein Data Bank analysis and molecular dynamics simulation study. Sci Rep. 2015;5:8926.

349. Shental-Bechor D, Levy Y. Effect of glycosylation on protein folding: A close look at thermodynamic stabilization. PNAS. 2008;105(24):8256-61.

350. Linder S, van der Poel HG, Bergman AM, Zwart W, Prekovic S. Enzalutamide therapy for advanced prostate cancer: efficacy, resistance and beyond. Endocr Relat Cancer. 2018;26(1):R31-R52.

351. Nevedomskaya E, Baumgart SJ, Haendler B. Recent Advances in Prostate Cancer Treatment and Drug Discovery. Int J Mol Sci. 2018;19(5):1359.

352. Nakazawa M, Paller C, Kyprianou N. Mechanisms of Therapeutic Resistance in Prostate Cancer. Curr Oncol Rep. 2017;19(2):13-.

353. Hay CW, McEwan IJ. The impact of point mutations in the human androgen receptor: classification of mutations on the basis of transcriptional activity. PLoS One. 2012;7(3):e32514-e.

354. Maxson ME, Grinstein S. The vacuolar-type H⁺-ATPase at a glance – more than a proton pump. J Cell Sci. 2014;127(23):4987-93.

355. Cerami E, Gao J, Dogrusoz U, Gross BE, Sumer SO, Aksoy BA, et al. The cBio cancer genomics portal: an open platform for exploring multidimensional cancer genomics data. Cancer Discov. 2012;2(5):401-4.

356. Network CGAR. The Molecular Taxonomy of Primary Prostate Cancer. Cell. 2015;163(4):1011-25.

357. Petzoldt AG, Gleixner EM, Fumagalli A, Vaccari T, Simons M. Elevated expression of the V-ATPase C subunit triggers JNK-dependent cell invasion and overgrowth in a Drosophila epithelium. Disease Models & Mechanisms. 2013;6(3):689.

358. Song T, Jeon H-K, Hong JE, Choi J-J, Kim T-J, Choi CH, et al. Proton Pump Inhibition Enhances the Cytotoxicity of Paclitaxel in Cervical Cancer. Cancer Res Treat. 2017;49(3):595-606.

359. Toei M, Saum R, Forgac M. Regulation and Isoform Function of the V-ATPases. Biochemistry. 2010;49(23):4715-23.

360. Feng N-H, Lin H-I, Wang J-S, Chou S-T, Ma H-K, Rooney SA, et al. Differential expression of a V-type ATPase C subunit gene, Atp6v1c2, during culture of rat lung type II pneumocytes. J Biomed Sci. 2005;12(6):899-911.

361. McConnell M, Feng S, Chen W, Zhu G, Shen D, Ponnazhagan S, et al. Osteoclast proton pump regulator Atp6v1c1 enhances breast cancer growth by activating the mTORC1 pathway and bone metastasis by increasing V-ATPase activity. Oncotarget. 2017;8(29):47675-90.

362. Wilson EM, French FS. Binding properties of androgen receptors. Evidence for identical receptors in rat testis, epididymis, and prostate. J Biol Chem. 1976;251(18):5620-9.

363. Marchetti PM, Barth JH. Clinical biochemistry of dihydrotestosterone. Ann Clin Biochem. 2013;50(Pt 2):95-107.

364. Kawamura N, Sun-Wada G-H, Wada Y. Loss of G2 subunit of vacuolar-type proton transporting ATPase leads to G1 subunit upregulation in the brain. Sci Rep. 2015;5:14027.

365. Păunescu TG, Russo LM, Silva ND, Kovacikova J, Mohebbi N, Hoek ANV, et al. Compensatory membrane expression of the V-ATPase B2 subunit isoform in renal medullary intercalated cells of B1-deficient mice. American Journal of Physiology-Renal Physiology. 2007;293(6):F1915-F26.

366. Sun-Wada GH, Tabata H, Kawamura N, Aoyama M, Wada Y. Direct recruitment of H+-ATPase from lysosomes for phagosomal acidification. J Cell Sci. 2009;122(Pt 14):2504-13.

367. Cunningham D, You Z. In vitro and in vivo model systems used in prostate cancer research. J Biol Methods. 2015;2(1):e17.

368. Evren S, Dermen A, Lockwood G, Fleshner N, Sweet J. Immunohistochemical examination of the mTORC1 pathway in high grade prostatic intraepithelial neoplasia (HGPIN) and prostatic adenocarcinomas (PCa): a tissue microarray study (TMA). Prostate. 2010;70(13):1429-36.

369. Sutherland SI, Pe Benito R, Henshall SM, Horvath LG, Kench JG. Expression of phosphorylated-mTOR during the development of prostate cancer. Prostate. 2014;74(12):1231-9.

370. Lim JH, Park JW, Kim MS, Park SK, Johnson RS, Chun YS. Bafilomycin induces the p21-mediated growth inhibition of cancer cells under hypoxic conditions by expressing hypoxia-inducible factor-1alpha. Mol Pharmacol. 2006;70(6):1856-65.

371. Fernandez EV, Reece KM, Ley AM, Troutman SM, Sissung TM, Price DK, et al. Dual targeting of the androgen receptor and hypoxia-inducible factor 1α pathways

synergistically inhibits castration-resistant prostate cancer cells. Mol Pharmacol. 2015;87(6):1006-12.

372. Mabjeesh NJ, Willard MT, Frederickson CE, Zhong H, Simons JW. Androgens stimulate hypoxia-inducible factor 1 activation via autocrine loop of tyrosine kinase receptor/phosphatidylinositol 3'-kinase/protein kinase B in prostate cancer cells. Clin Cancer Res. 2003;9(7):2416-25.

373. Wu Y, Chhipa RR, Cheng J, Zhang H, Mohler JL, Ip C. Androgen receptor-mTOR crosstalk is regulated by testosterone availability: implication for prostate cancer cell survival. Anticancer Res. 2010;30(10):3895-901.

374. Tallarida RJ. Quantitative methods for assessing drug synergism. Genes Cancer. 2011;2(11):1003-8.

375. McGuire CM, Forgac M. Glucose starvation increases V-ATPase assembly and activity in mammalian cells through AMP kinase and phosphatidylinositide 3-kinase/Akt signaling. J Biol Chem. 2018;293(23):9113-23.

376. Saxton RA, Sabatini DM. mTOR Signaling in Growth, Metabolism, and Disease. Cell. 2017;168(6):960-76.

Chapter Eight

Chapter 8 Supplementary Figures and Data

Supplementary Figures and Data

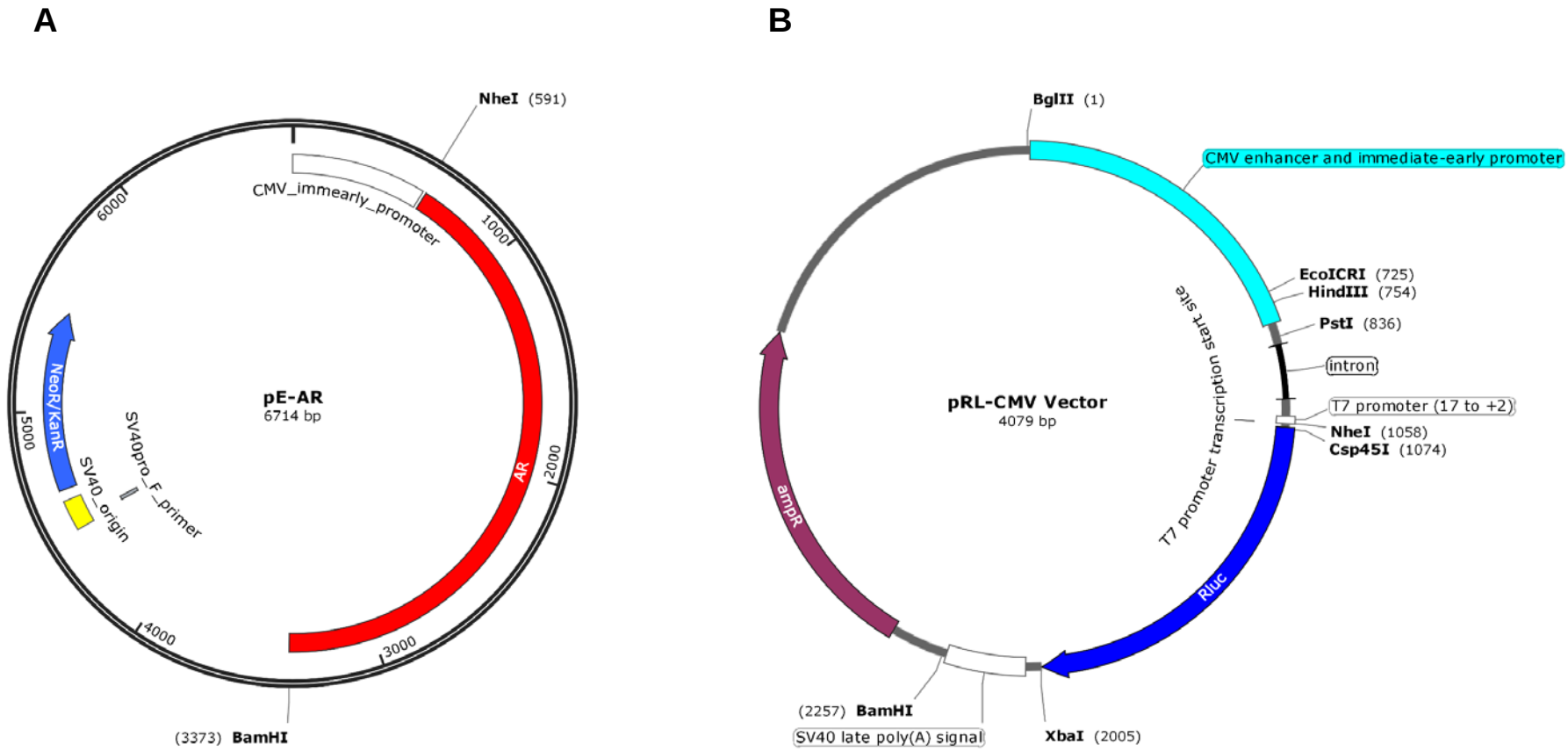

Figure S 8-1. Plasmid maps for pE-AR and pRL-CMV vector

The plasmid maps for (A) pE-AR and (B) pRL-CMV used in the luciferase experiments were constructed using SnapGene (version 4.3.10).

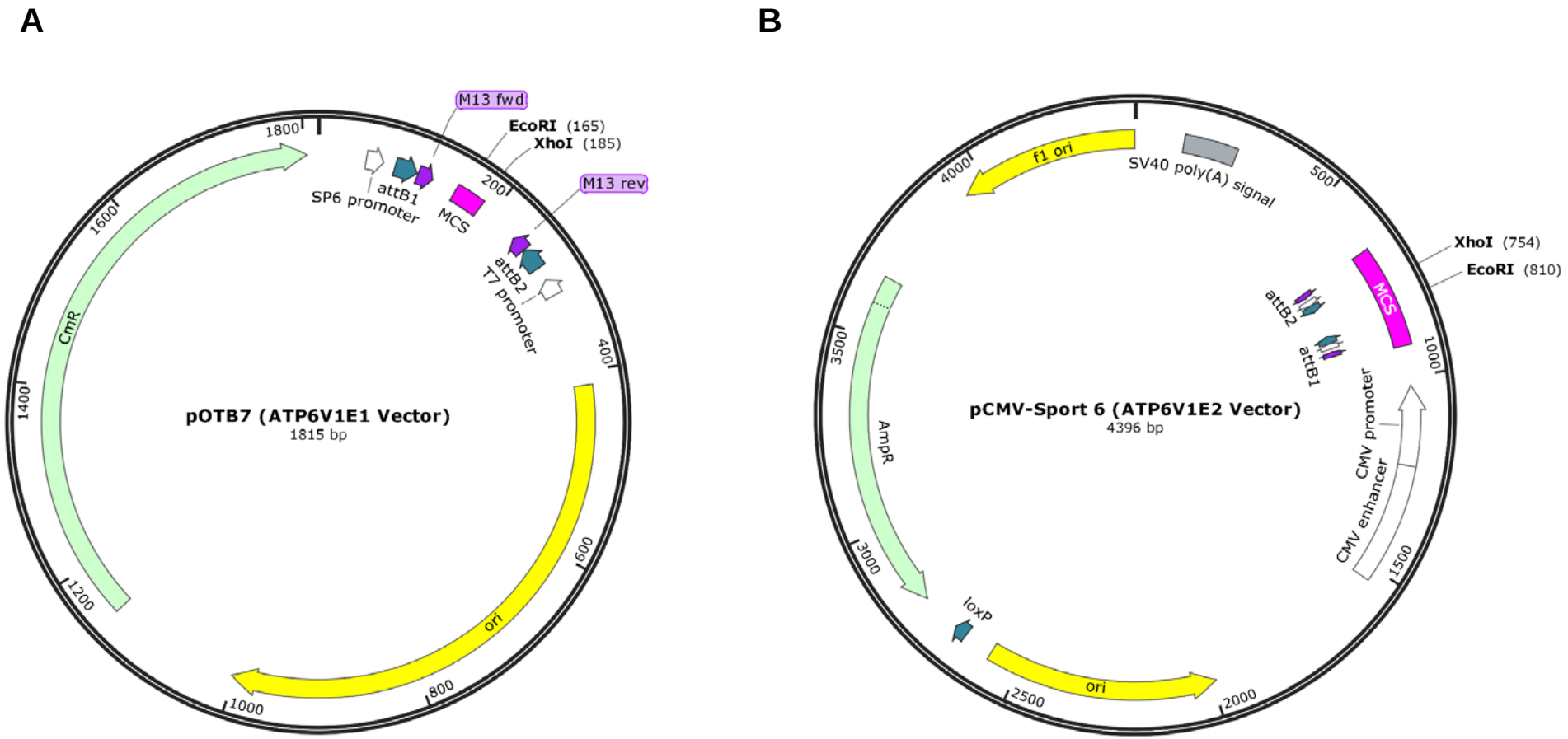

Figure S 8-2. ATP6V1E1 and ATP6V1E2 cloning plasmid maps

The plasmid maps for (A) pOTB7 and (B) pCMV-Sport 6 used for expressing human *ATP6V1E1* and *ATP6V1E2* respectively, were constructed using SnapGene (version 4.3.10).

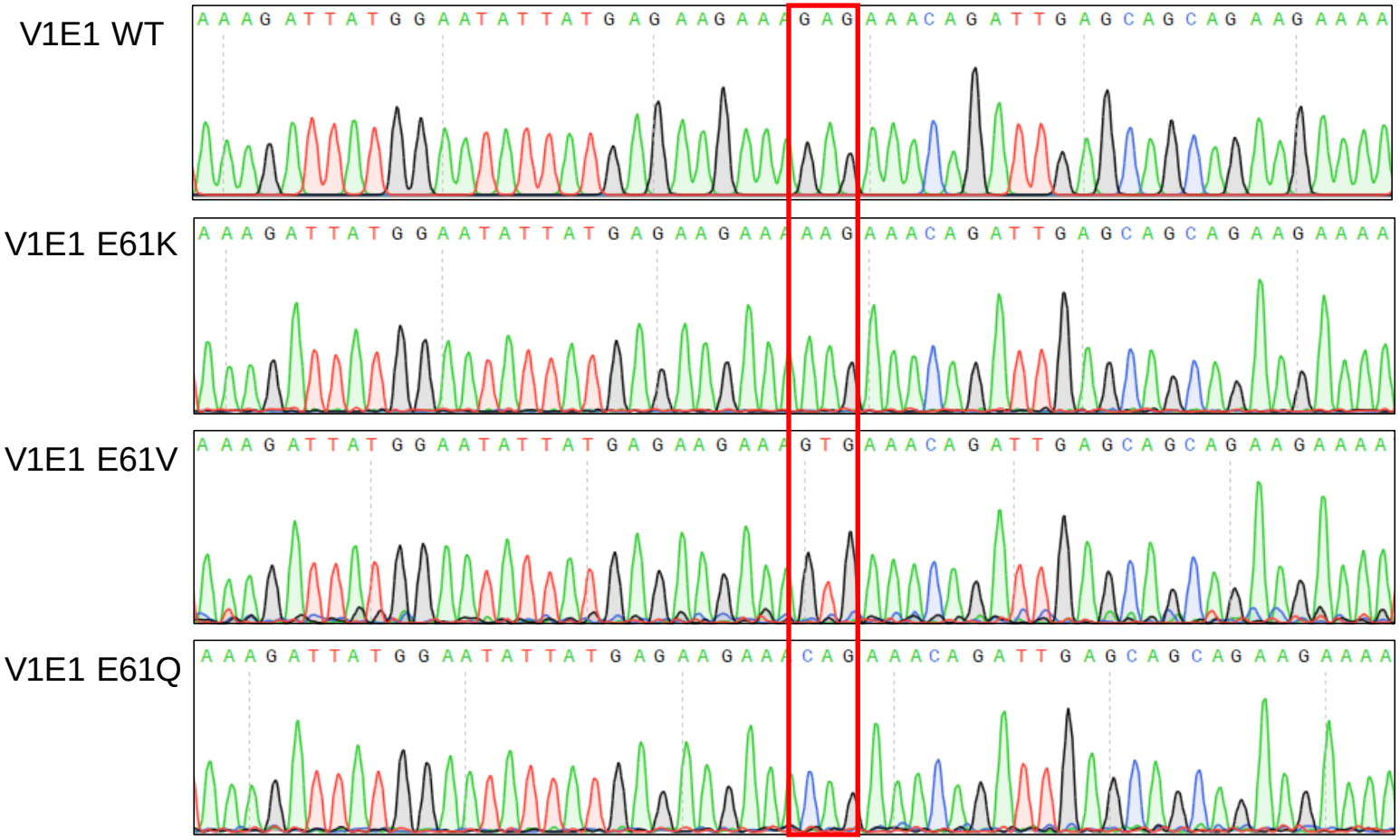

Figure S 8-3. Chromatogram trace data from the sequenced V_1E1 subunit mutations

Chromatogram sequencing data from Eurofins Genomics EU for human/yeast chimeric V_1E1 E61 WT and mutants was analysed and processed using SnapGene (version 4.3.10). WT; wild-type; E, glutamic acid; K, lysine; V, valine; Q, glutamine.

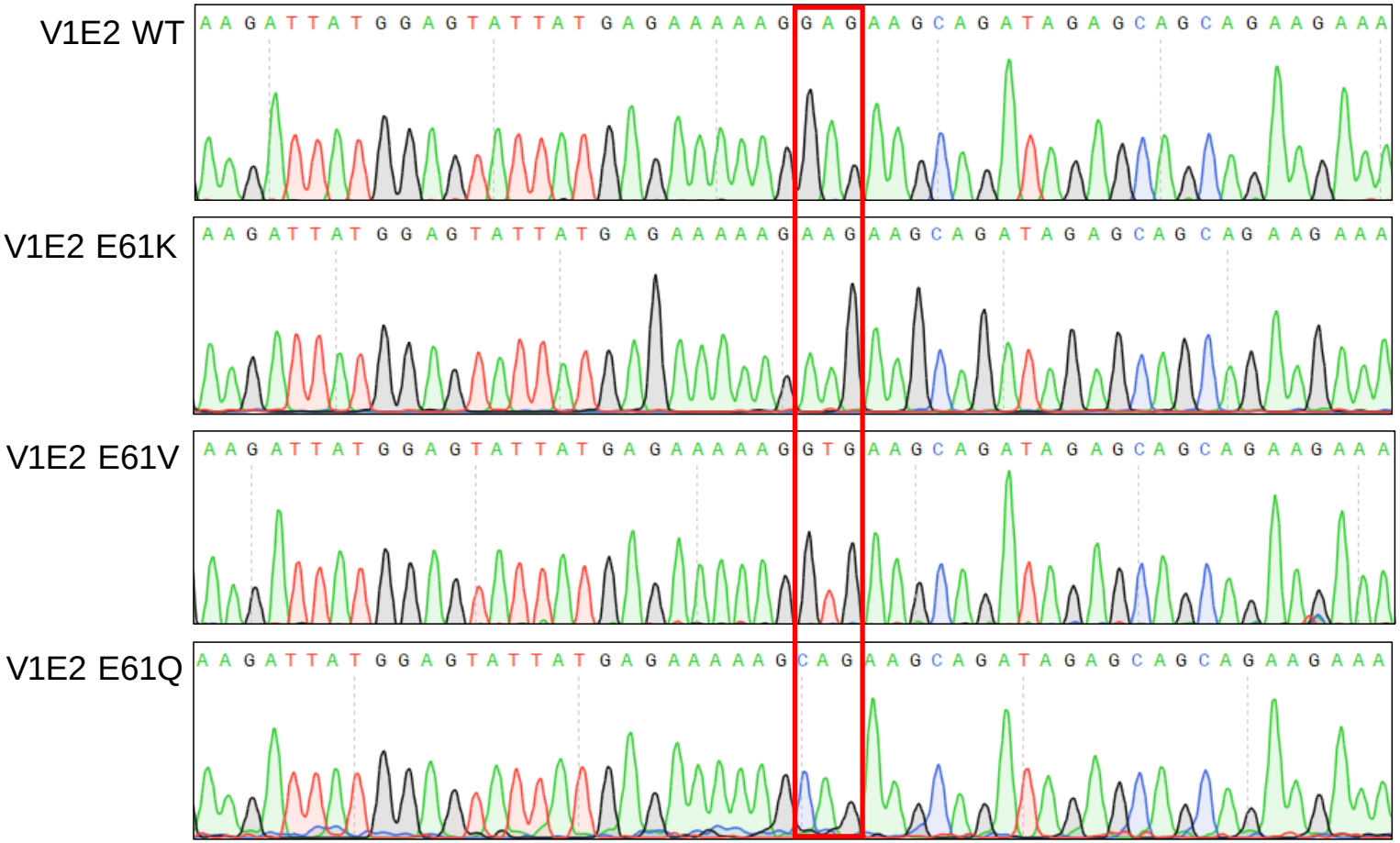

Figure S 8-4. Chromatogram trace data from the sequenced V_1E2 subunit mutations

Chromatogram sequencing data from Eurofins Genomics EU for human/yeast chimeric V_1E2 E61 WT and mutants was analysed and processed using SnapGene (version 4.3.10). WT; wild-type; E, glutamic acid; K, lysine; V, valine; Q, glutamine.

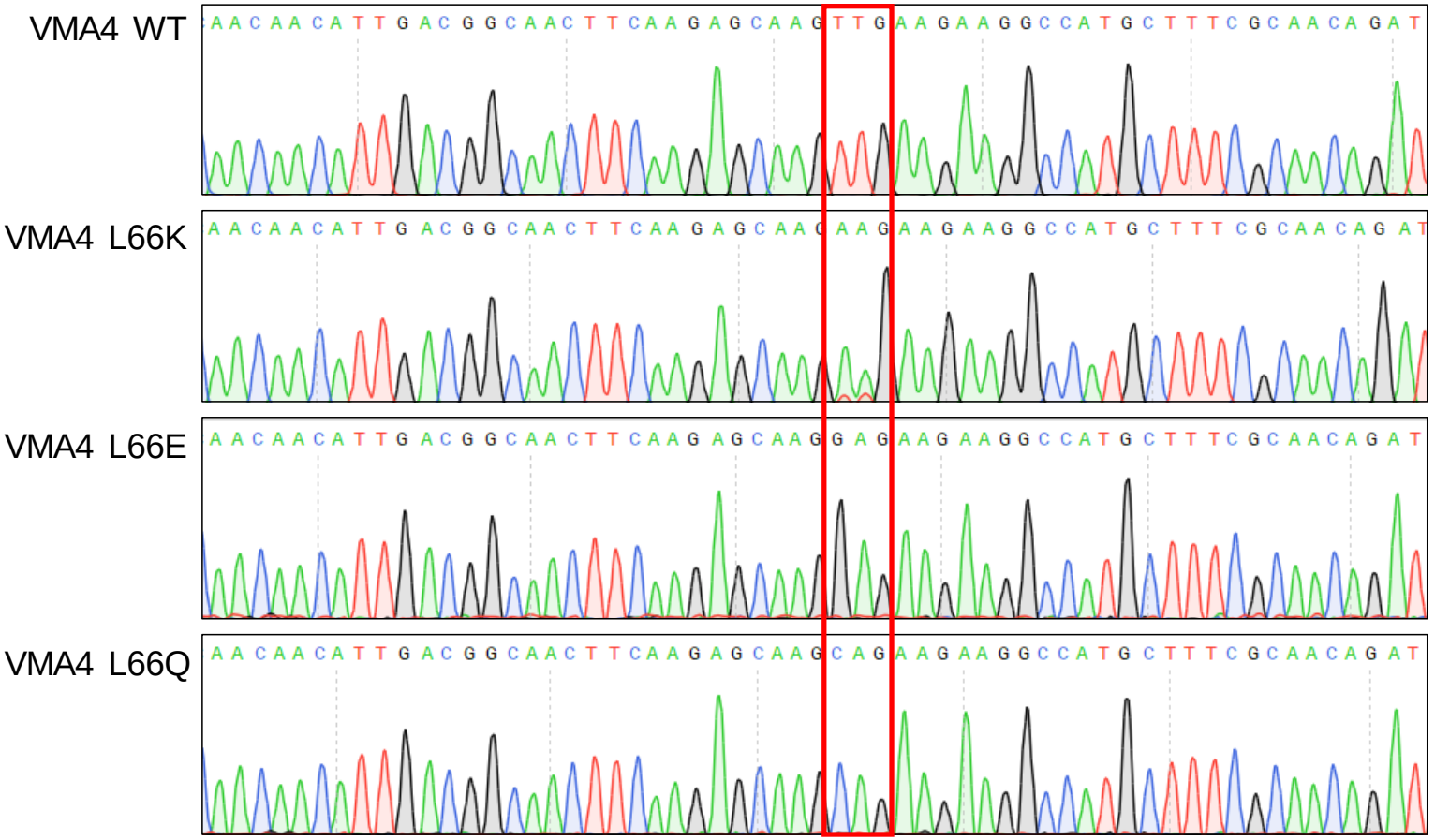

Figure S 8-5. Chromatogram trace data from the sequenced yeast E subunit (Vma4) mutations

Chromatogram sequencing data from Eurofins Genomics EU for human/yeast chimeric VMA4 E61 WT and mutants was analysed and processed using SnapGene (version 4.3.10). WT; wild-type; E, glutamic acid; K, lysine; L, leucine; Q, glutamine.

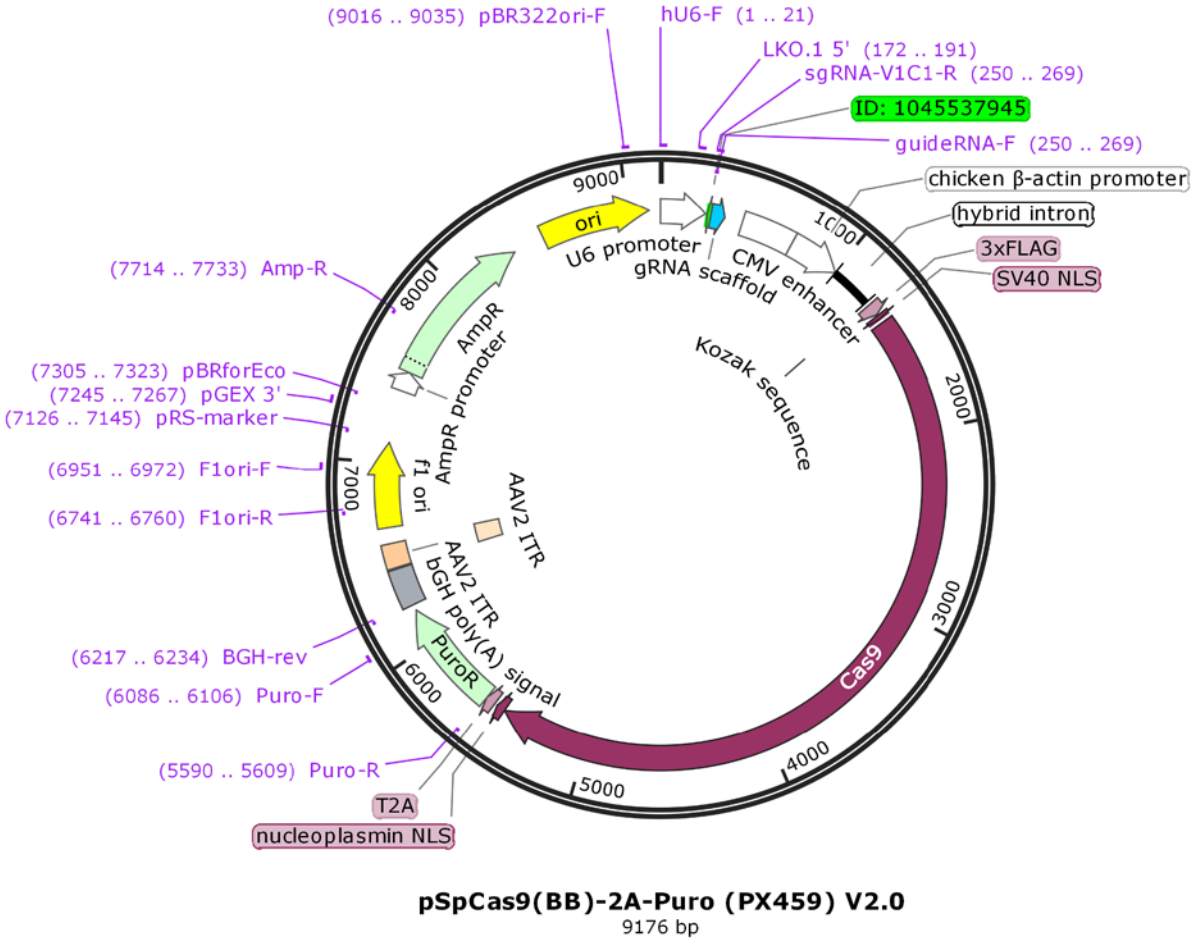

Figure S 8-6. CRISPR plasmid map with sgRNA insert

The V_1C1 sgRNA (Wellcome Sanger Institute Genome Editing ID: 1045537945) was inserted into a CRISPR plasmid containing the gRNA scaffold, Cas9 and puromycin selection sequence. Plasmid pSpCas9(BB)-2A-Puro (PX459) V2.0 was a gift from Feng Zhang (Addgene plasmid # 62988 ; http://n2t.net/addgene:62988 ; RRID:Addgene_62988). The plasmid map was constructed using SnapGene (version 4.3.10).

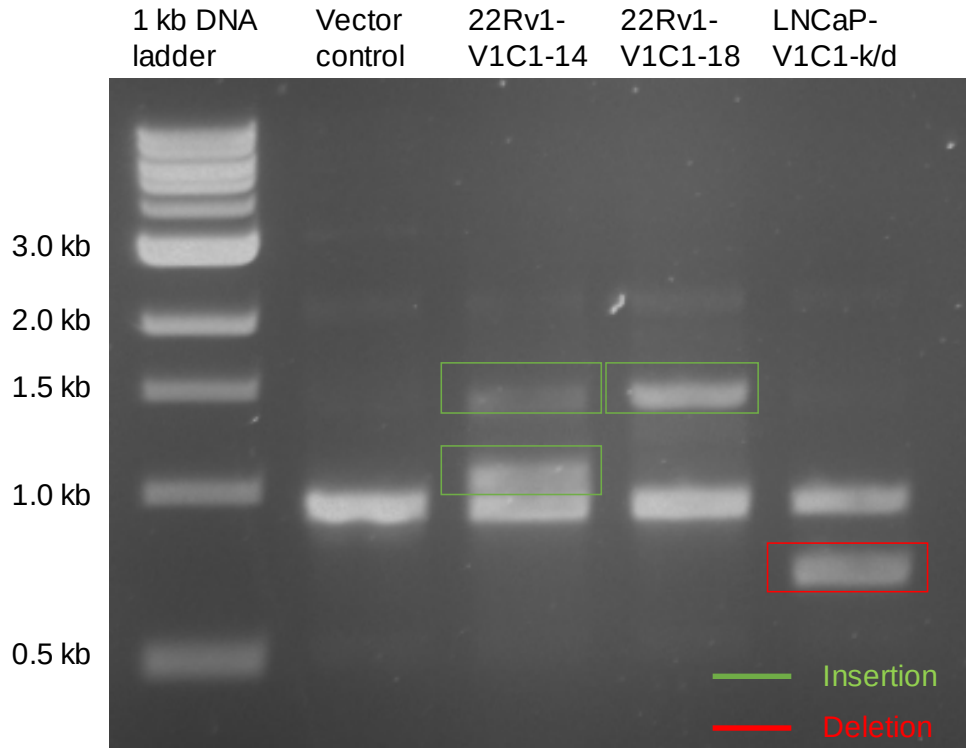

Figure S 8-7. DNA gel electrophoresis image of 22Rv1 and LNCaP V_1C1 CRISPR PCR products

Primers flanking upstream and downstream regions of the CRISPR sgRNA sequence were used to amplify 22Rv1 and LNCaP V_1C1 PCR products. These PCR products were separated and visualised using DNA gel electrophoresis. The 22Rv1 V1C1-14 clone contained three separate alleles including two insertions and another alteration. 22Rv1 V1C1-18 contained two alleles, one with an insertion and one with a two bp deletion. The LNCaP V_1C1 knockdown clone had three alleles, one of which contained a large ~238 bp deletion. Kb, kilobase; bp, base pair; k/d, knockdown.

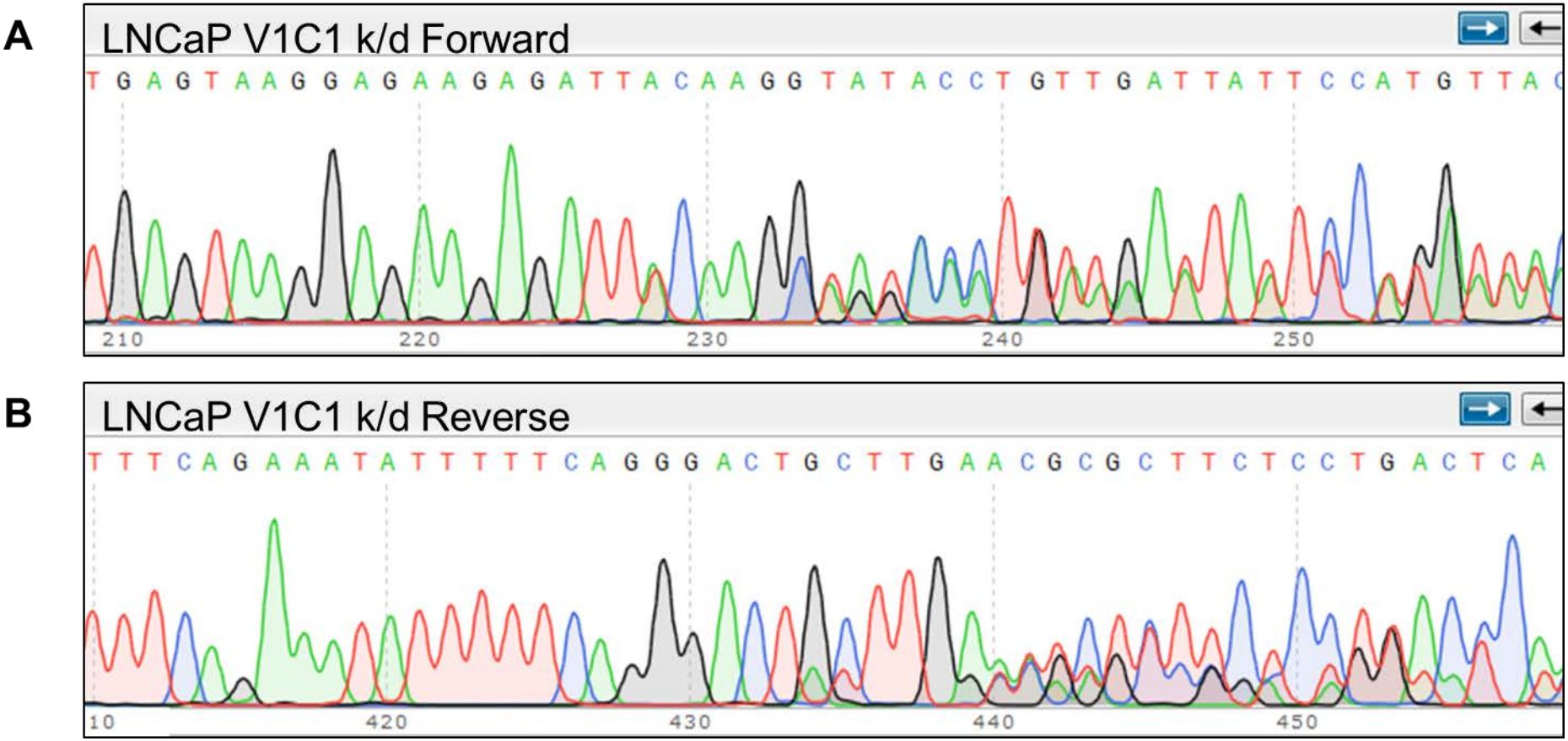

Figure S 8-8. Chromatogram of LNCaP V_1C1 k/d sequencing data

Forward and reverse primers flanking the CRISPR sgRNA sequence were used to amplify LNCaP V_1C1 k/d DNA. The resulting PCR product was sent for Sanger sequencing and the trace data was visualised using Snapgene (version 4.3.10). There were three traces visible on the chromatogram indicating three separate alleles were present. Bp, Base pair; k/d, knockdown.

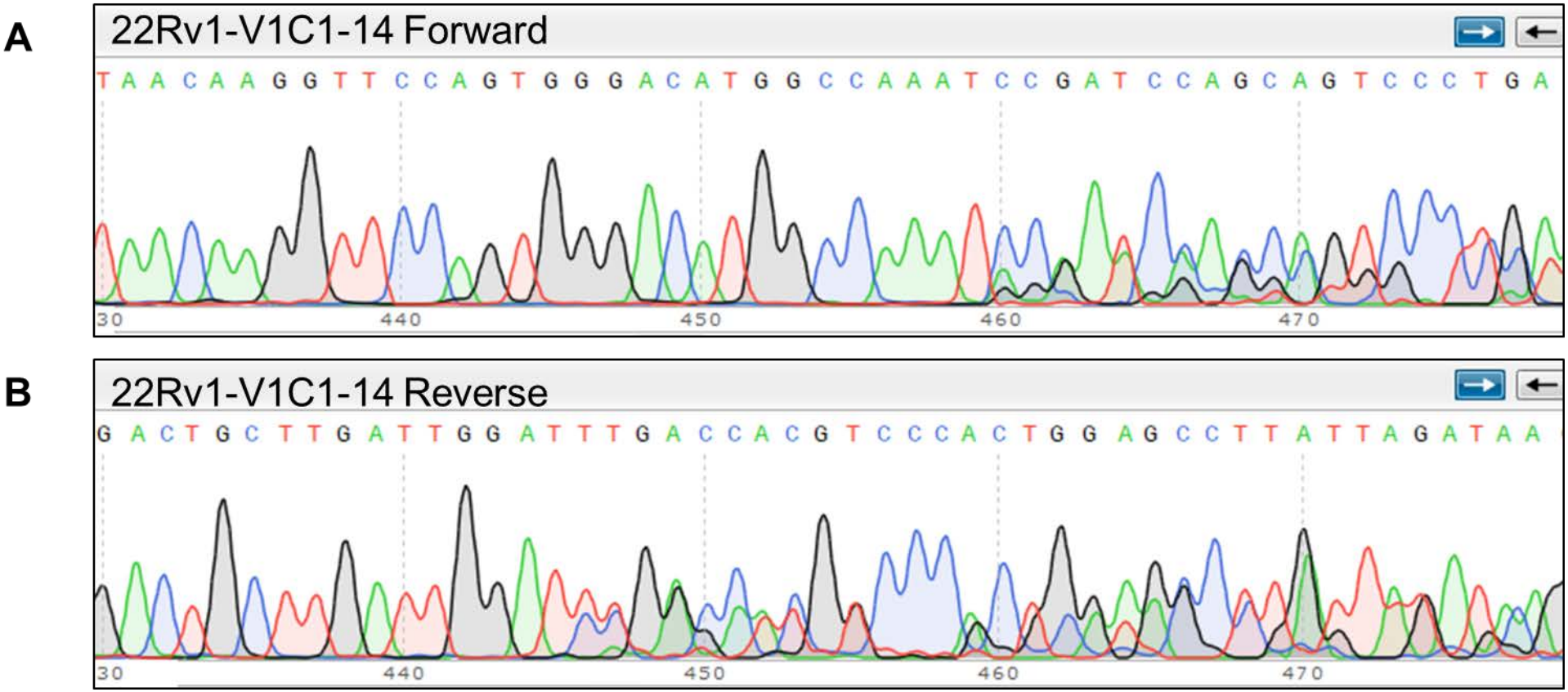

Figure S 8-9. Chromatogram images for 22Rv1 V1C1-14 CRISPR clones

Forward and reverse primers flanking the CRISPR sgRNA sequence were used to amplify 22Rv1 V1C1-14 clone DNA. The resulting PCR products were sent for Sanger sequencing and the forward (A) and reverse (B) trace data was visualised using Snapgene (version 4.3.10). There were two traces visible on the chromatogram for 22Rv1 V1C1-14 indicating a trans-heterozygous CRISPR induced event had occurred. Bp, Base pair.

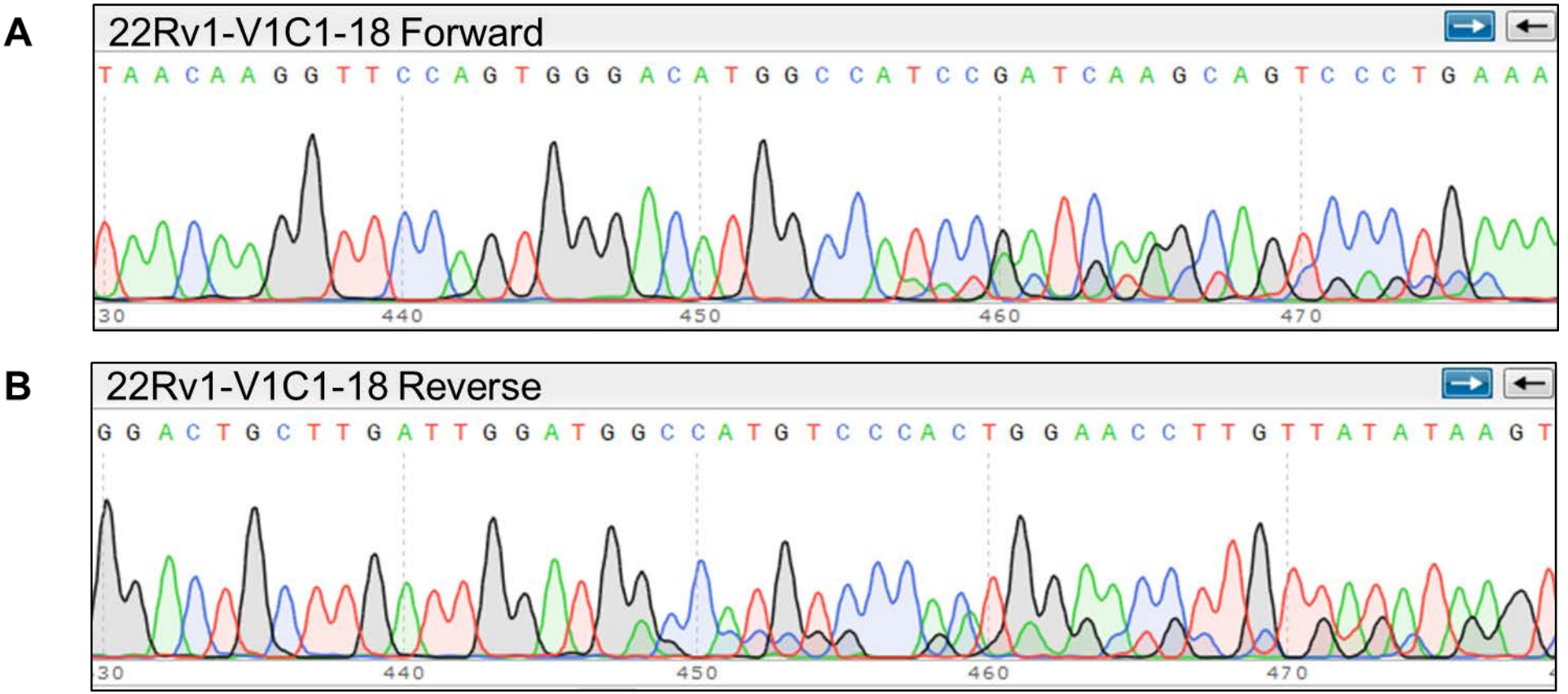

Figure S 8-10. Chromatogram images for 22Rv1 V1C1-18 CRISPR clones

Forward and reverse primers flanking the CRISPR sgRNA sequence were used to amplify the 22Rv1 V1C1-18 clone DNA. The resulting PCR products were sent for Sanger sequencing and the forward (A) and reverse (B) trace data was visualised using Snapgene (version 4.3.10). Two traces were visible for 22Rv1 V1C1-18 suggesting a trans-heterozygous CRISPR induced event had occurred. Two bp (AA) had been deleted in one allele and there was a large bp insertion in the other resulting in premature stop codons. Bp, Base pair.

Table S 8-1. Mutations identified in the N-terminal alpha helix of the V_1E2 subunit isoform

The Catalogue of Somatic Mutations in Cancer (COSMIC) database was used to identify somatic mutations within the 83 amino acid sequence comprising the N-terminal alpha helix of the mammalian V_1E2 subunit isoform.

Position (AA)	Mutation (CDS)	Mutation (Amino Acid)	Mutation count	Mutation type	Mutation ID (COSM)
3	c.9G>C	p.L3L	1	Silent	461019
5	c.15T>C	p.D5D	1	Silent	4664487
6	c.18C>T	p.V6V	1	Silent	1021190
9	c.26A>G	p.K9R	1	Missense	301344
11	c.32A>G	p.Q11R	2	Missense	1752572
16	c.46A>G	p.M16V	2	Missense	4664486
18	c.54C>A	p.F18L	1	Missense	4583530
22	c.66A>G	p.E22E	1	Silent	477450
25	c.74A>T	p.E25V	1	Missense	4392713
30	c.90C>T	p.I30I	2	Silent	1021189
32	c.96C>T	p.A32A	1	Silent	4514273
36	c.106G>A	p.E36K	1	Missense	4805537
36	c.107A>T	p.E36V	1	Missense	7357040
41	c.121G>C	p.E41Q	1	Missense	3839600
43	c.127G>A	p.G43R	2	Missense	3581840
44	c.131G>A	p.R44H	1	Missense	363539
47	c.141A>G	p.Q47Q	1	Silent	3581839
48	c.144C>T	p.T48T	1	Silent	4405770
55	c.163G>C	p.E55Q	1	Missense	7224012
61	**c.181G>A**	**p.E61K**	**1**	**Missense**	**3581838**
61	**c.181G>C**	**p.E61Q**	**1**	**Missense**	**345330**
61	**c.182A>G**	**p.E61G**	**1**	**Missense**	**6608148**
61	**c.182A>T**	**p.E61V**	**1**	**Missense**	**393133**
62	c.185A>C	p.K62T	2	Missense	3185685
63	c.189G>C	p.Q63H	1	Missense	6561043
67	c.199C>A	p.Q67K	1	Missense	6608149
67	c.201G>C	p.Q67H	1	Missense	7147724
68	c.204G>A	p.K68K	2	Silent	3714285
71	c.211C>T	p.L71L	1	Silent	107056
71	c.213G>A	p.L71L	1	Silent	6325057
76	c.227G>T	p.R76M	1	Missense	6608152

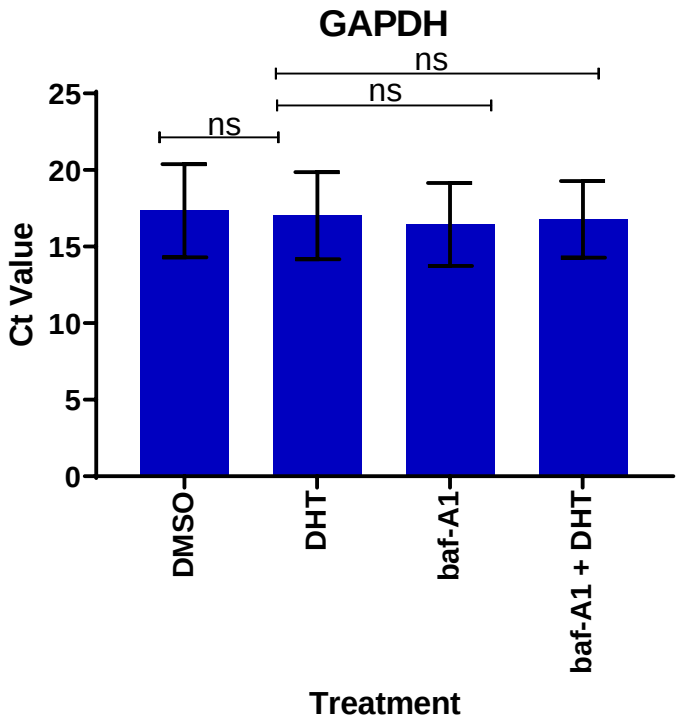

Figure S 8-11. GAPDH Ct values in response to baf-A1 treatment

LNCaP cells were cultured in CSS media for 24 hours and treated for 24 hours with either 1 nM DHT, 10 nM baf-A1 or both. RT-qPCR analysis was undertaken to assess levels of *GAPDH* mRNA. Ct values were then plotted using GraphPad Prism 7 and are displayed as mean values ± standard deviation. Two-way ANOVA with Tukey's multiple comparison post-hoc test was used to generate P values and detect the statistical significance of the indicated differences: ns = non-significant. Data shown represents three independent replicates completed in triplicate. CSS, charcoal stripped serum; DHT, dihydrotestosterone; baf-A1, bafilomycin-A1.

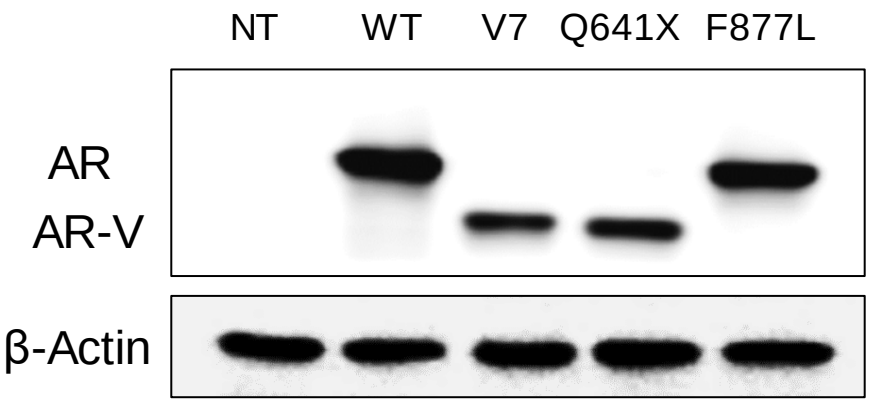

Figure S 8-12. HeK-293 cells expressing mutant AR plasmids

HeK-293 cells were reverse transfected with either wild-type AR, AR-V7 variant, AR-Q641X variant or AR-F877L expression plasmids. After 24 hours cells were collected and expression of AR and β-Actin was analysed by immunoblotting. NT, non-transfected; WT, wild-type; AR, androgen receptor; AR-V, androgen receptor variant.

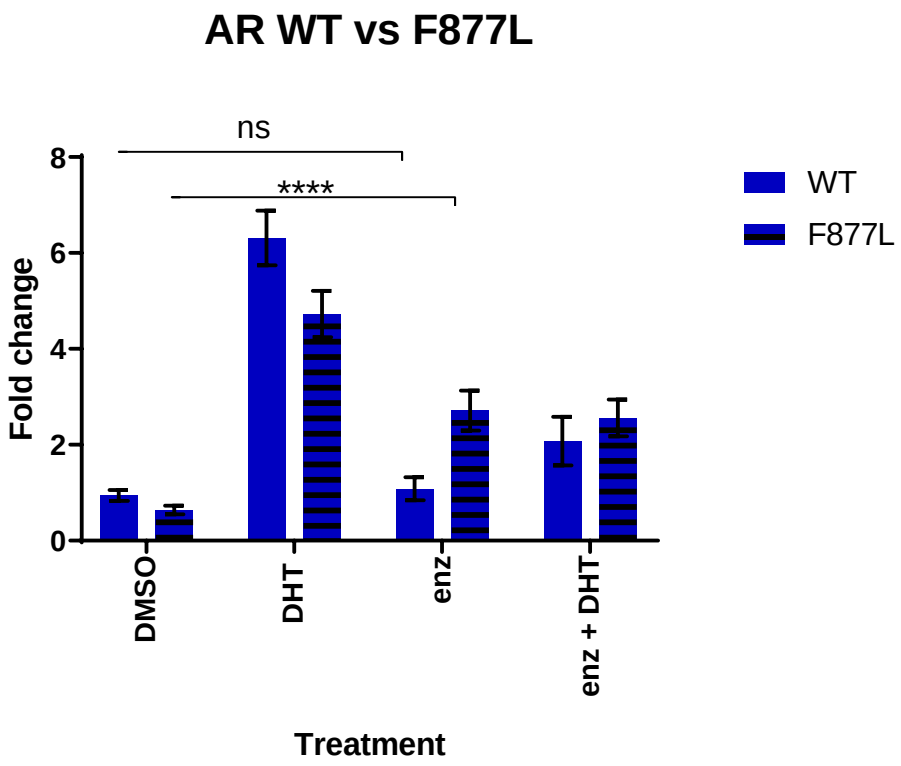

Figure S 8-13. Effect of enzalutamide on AR-F877L activity in HeK-293 cells
HeK-293 cells were transfected with the androgen response element (ARE) reporter plasmid and wild-type AR or AR-F877L expression plasmid along with a *Renilla* luciferase reporter plasmid. The cells were cultured in CSS media and treated with 1 nM DHT and/or 10 μM enzalutamide for 24 hours. Control cells were treated with equivalent concentrations of DMSO. Luciferase activity was determined and firefly luciferase values were normalised to AR-WT DMSO control cells set to 1. Values were then plotted using GraphPad Prism 7 and are displayed as mean values ± standard deviation. Two-way ANOVA with Tukey's multiple comparison post-hoc test was used to generate P values and to detect the statistical significance of the indicated differences: **** = p≤ 0.0001. Data shown is derived from three independent replicate experiments each completed in triplicate. AR, androgen receptor; WT, wild-type; DMSO, solvent control; DHT, dihydrotestosterone; enz, enzalutamide.

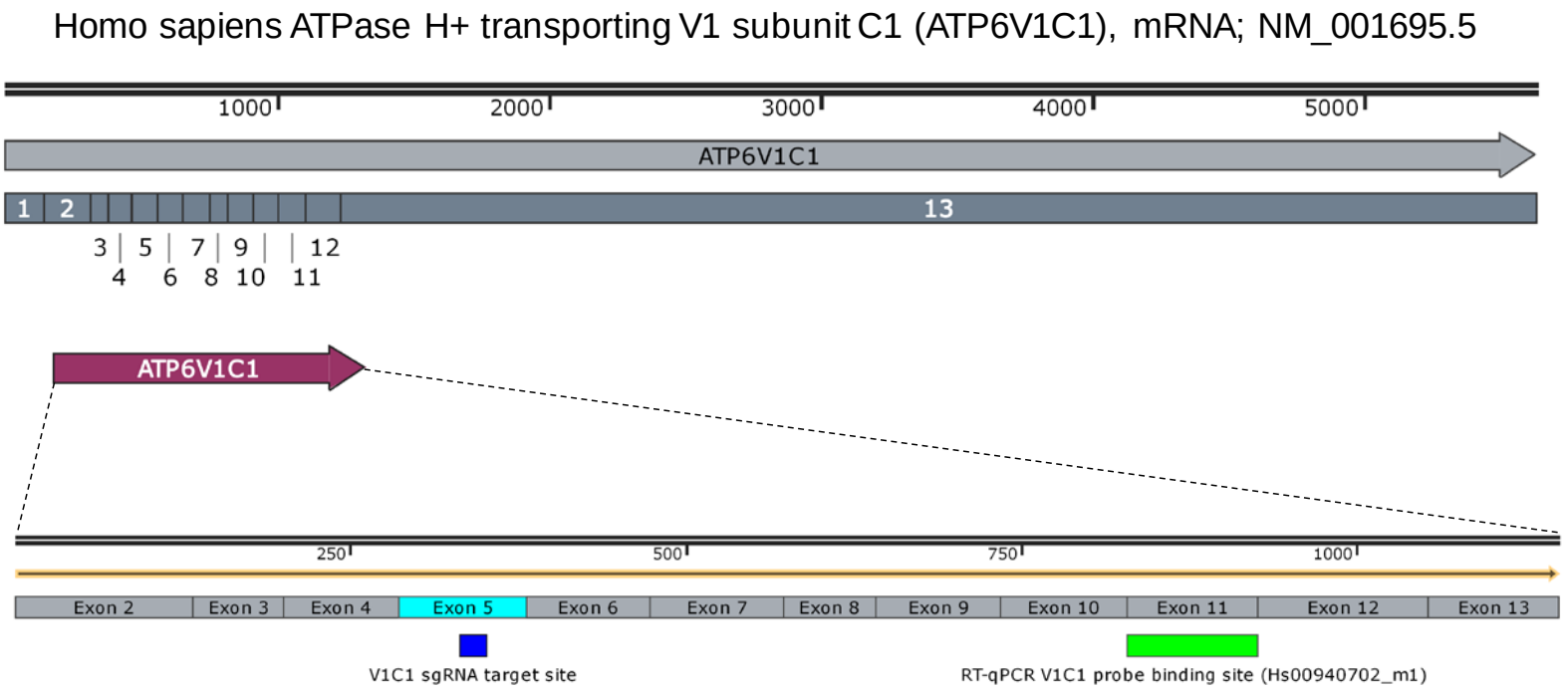

Figure S 8-14. Location of ATP6V1C1 sgRNA target site and RT-qPCR probe binding site

Exons 2-13 containing the protein coding sequence of the *ATP6V1C1* gene (Ref seq NM_001695.5), which is flanked by long untranslated regions in exon 1 and exon 13. The V_1C1 sgRNA target site is 20 nucleotides long and is located within exon 5. The RT-qPCR V_1C1 probe binding site spans the boundary of exons 11-12.